An investigation of ground based and aeromagnetic data over the Cairngorm and other Caledonian granites in the UK

Thesis

AN INVESTIGATION OF GROUND BASED AND AEROMAGNETIC DATA OVER THE CAIRNGORM AND OTHER CALEDONIAN GRANITES IN THE U.K.

T.M. STOKES

APRIL 1994

PhD

DEPARTMENT OF EARTH SCIENCES

THE OPEN UNIVERSITY

TEXT BOUND CLOSE TO THE SPINE IN THE ORIGINAL THESIS

TEXT CUT OFF IN THE ORIGINAL

An investigation of ground based and aeromagnetic data over the Cairngorm and other Caledonian granites in the U.K.

A thesis presented for the degree of

Doctor of Philosophy

by

Terence M. Stokes

(B.A.(Hons) The Open University)

(B.Sc.(Hons) Lancaster)

Department of Earth Sciences

The Open University

Milton Keynes

Buckinghamshire

England

December 1993

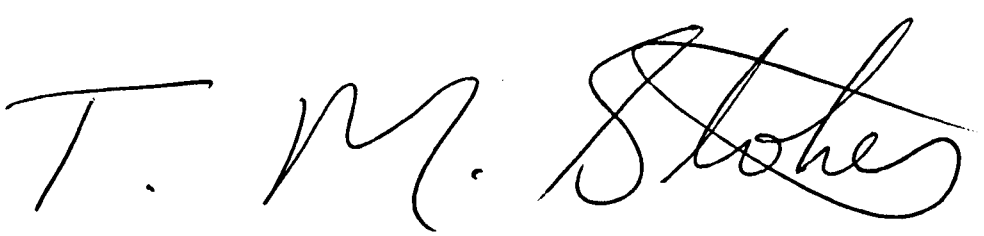

An investigation of ground based and aeromagnetic data over the Cairngorm and other Caledonian granites in the United Kingdom.

Abstract

The aeromagnetic map of Great Britain shows a number of granites associated with magnetic anomalies. One of the largest of these granites, the Cairngorm pluton, has a complex overlying aeromagnetic anomaly, yet measurements show that the surface rocks have a magnetic susceptibility too low to account for this aeromagnetic field.

The purpose of this investigation was to determine the likely reasons for this discrepancy employing a range of computer based techniques, and using new land-based data.

Potential field data for the Cairngorm area, together with a region of the Southern Uplands, was subjected to frequency domain reduction and filtering. Hand specimens from the granite and host rock were collected for susceptibility measurements. The results have been integrated with profile models to explain the variations observed in the aeromagnetic and ground based magnetic field.

The Cairngorm granites appear to be zoned at depth, with a variable thickness cap of low density, low magnetic susceptibility granite. The presence of intermediate composition rock in the upper reaches of the granite mass provides evidence for stoping, whilst the presence of intermediate composition rock at deeper levels is thought to be due to multiple magma pulses and/or differentiation.

The Loch Doon granite has a low magnetic susceptibility subsurface core extending off its eastern flank. A number of correlations between the geophysics and geochemistry of the granites investigated were noted.

The concept of gravmag space has been developed and applied as a framework in which to explore the relationships between the granites of Scotland and northern England. Relationships between the background geophysics and the geochemistry of granites in the area of the proposed Iapetus subduction zone have also been investigated.

This work is dedicated to the memory of

Geoff Brown

late Professor of Earth Sciences

The Open University

Contents

List of Contents

Chapter 2 Processing of magnetic data

Chapter 3 The Cairngorm granites

Figures

Acknowledgements

Grateful acknowledgement is made of the help of Geoff Brown and Sandy Smith for their discussions on the geology of the Cairngorm area, for their help in locating research papers, and for their encouragement. Thanks are extended to Hazel Rymer for organising the loan of equipment; to Roger Banks for making available computer programs and for discussions on the reduction to the pole of aeromagnetic data; to Dr. Tantrigoda for making available his program for pseudogravimetric reduction; to David Wright for help with the use of computing facilities; to the British Geological Survey for the provision of aeromagnetic and gravity data; to the University of Liverpool for measuring the magnetic susceptibility of rock samples; to the Universities of Cambridge and Leicester for the use of their computing facilities; to the Dumfries and Galloway Forestry Commission for permission to walk their land; to the staff of Lutterworth library for their patient and friendly assistance in ordering books and research papers; and to Kirsteen, Peter and Julia whose patience and cooperation allowed this research to be carried through. Finally thanks to John Hinde and the mountain rescue team of Royal Air Force Kinloss for teaching the principles of winter survival so well.

Chapter 1 The origin and measurement of the Earth's magnetic field

1.1 Introduction

A large body of geological, geochemical and geophysical data has been accumulated on the British Caledonian granites since Hutton first described the contact between the local rocks and the Cairnsmore of Fleet granite in 1790. A continuing interaction between field work, experimentation and theory has led to the development of a range of models to explain the origin and emplacement of granitic magmas. Development of the modern theory of plate tectonics has allowed earlier models to be refined and integrated in an attempt to relate the local development of granitic magmas to large scale tectonic events. Given the inherent variability of local events together with the weathered state of the near surface rocks, it comes as no surprise to find disagreement between geologists over possible explanations for their observations. Laboratory work such as that due to Tuttle and Bowen has given a firmer foundation to the models deployed to explain field based observations. Despite this, the complexity of the geological systems still gives rise to debate over every aspect of the origin and emplacement of granitic magmas.

In many respects, geophysics and geochemistry share similar problems. Events occurring at pressures and temperatures that are hard to reproduce for any length of time or reasonable volume in a laboratory environment have to be understood in order to maintain a foothold in the real world of geology. This understanding is essential to discriminate between possible models of the available data.

Of the many developments that have occurred in geophysics, the work of Baranov and of Bhattacharyya stand out as the most important in the context of this thesis. Baranov (1957) for developing the idea of reducing aeromagnetic data to a more useful form, and Bhattacharyya (1964,1966,1975) for developing the mathematical tool of harmonic analysis in a geophysical context.

Over the period during which this thesis has been completed, computer hardware and software has changed at an unprecedented rate. This has been a mixed blessing. Of necessity, the computer processing has been carried out on a range of mainframe computers and microcomputers. Graphical software and output devices have changed regularly. Although the software and hardware have improved, each change incorporates a time penalty in the learning curve of the software and devices. This is reflected in the different styles of data display used in the figures in this thesis.

This study investigates the reason for the presence of a positive aeromagnetic anomaly associated with the largest British Caledonian pluton, the Cairngorm granite(s). As with all such projects, initial ideas have been revised considerably as the work has progressed. Two themes have been used to guide the work. First, as much geological information as possible should be used to constrain the interpretation of the potential fields. Second, the models developed should be as simple as possible in keeping with the known facts. Possible relationships between magnetic and geological properties have been explored for a range of Caledonian granites and the relationship between gravity and magnetic properties of these granites has been investigated.

This first chapter summarises the origin and measurement of the Earth's magnetic field. Much has been omitted that appears not to be directly relevant to the present work. Chapter two describes the computer processing techniques employed to manipulate the data, together with some of the limitations inherent in these techniques. Chapter three applies these techniques to aeromagnetic data, and to data collected by myself during field trips to the Cairngorm area. Chapter four looks at two contrasting granites in the Southern Uplands of Scotland while chapter 5 explores some of the large scale relationships found during the course of this work.

1.2 The magnetic field of the Earth

The magnetic field of the earth, as measured at the ground, has contributions from the earth's core, the near surface rocks in the outer 30 kilometres of the lithosphere, and the ionosphere. The magnetic field of each source adds vectorially to produce the total field observed at the surface of the earth.

The contribution of the core is that of a relatively steady state dipolar field which appears to reverse polarity on a time scale of around 10^4 years. This dipolar field accounts for about 90% of the main field. The temperature of the core is assumed to be well in excess of the Curie temperature of all known minerals. Hence the source of the main field is thought to be the circulation of conductive materials in convection cells near the core-mantle boundary. A variety of configurations of charge movement can give rise to self-excited dynamos. For example Busse and Carrigan (1974) suggested a large number of small, circular convection-like cells. They suggested that the energy for the dynamo action could come from convection within the core itself. Other possibilities such as density gradient convection and the presence of torques due to the precession of the Earth have been suggested and the origin of the field remains the subject of lively debate.

The magnetic field arising from the lithosphere is mainly a reflection of the titanomagnetite content of the rocks. Basic igneous rocks with high magnetite levels tend to give large magnetic field variations, whilst acidic igneous and sedimentary rocks with low magnetite levels tend to give small magnetic field variations.

The other major contributor to the observed magnetic fields are ionospheric current systems. These are the magnetopause current, the plasma sheet current and the ring current. All can give rise to magnetic fields ranging from several nanotesla to several hundred nanotesla. In addition, current systems induced in the ground are effective in adding to the observed magnetic field effects. The most regular variation is due to ionospheric currents which can cause daily variations of 50 nanotesla. It is necessary to remove such variations from magnetic field data before interpretation is carried out.

Changes in declination of the Earth's magnetic field have been observed for over three hundred years. This secular variation is described by four main features. These are a decrease in the magnetic moment of the main field dipole; a westward drift of the non-dipole field; a northward movement of the dipolar axis and a continual secular variation.

The secular variation of the main geomagnetic field can be explained by a westward drift, particularly of areas where the rate of change of the field is a maximum, known as isoporic foci. The secular variation is not completely explained by a westward drift. Some field harmonics appear to move to the east, and changes in the magnitude of the field can be significant. Yukutake and Tachinaka (1969) described a field model with two sets of harmonics, one set of which is stationary and the other mobile along lines of latitude. They were able to show that the rate of change of the variable harmonic components depended upon the stationary component, and could reverse direction if the stationary dipole increased in magnitude. Denham (1974), in analysing lake sediments, was able to demonstrate eastward and westward drifts of the dipole field over the last 24000 years.

Variations in the period of rotation of the earth have been known for a long time. A steady increase in the length of day can be explained by tidal friction and the consequential transfer of angular momentum to the Moon and Sun. Vestine (1953) suggested that momentum transfer between the mantle and core should also occur. The spectrum of the variations in length of day show a peak at 57.5 years, in good agreement with the 58 year period of the secular variation. An alternative hypothesis, attributable to Hide (1966) suggests that a hydromagnetic wave motion is present within the core, and

that the westward motion of this wave causes the observed variations at the surface.

The net result of these variations at the surface of the Earth is twofold. At any given point, the amplitude of the observed magnetic field will vary with time. Given the vector nature of the magnetic field additions, and the likelihood that some of these fields will be near horizontal (as with ionospheric currents), the location and shape of a three dimensional magnetic anomaly over the surface of the Earth can change.

In conclusion the interpretation of magnetic field anomalies is complicated by a number of factors. These include temporal fluctuations in the magnetic field strength during each day, secular variations affecting the strength and direction of magnetisation by 10% over periods of 10^3 to 10^4 years, and major changes such as reversals and changes of magnetisation by ±50% over periods of 10^5 to 10^6 years.

1.3 Mineral magnetism

Ferromagnetic grains with diameters less than 10^{-6} metres have a uniform magnetization direction within them, usually along a crystallographic axis. Grains with diameters greater than 10^{-4} metres can develop individual elements of volume with a specific magnetic direction within the volume, but with directional differences between such volumes. These magnetic domains are separated from each other by areas known as Bloch walls, where electron spin directions change from that of one domain to that of the neighbouring domain, usually over a distance of 5 to 10 atoms. For small crystals, one single domain or two antiparallel domains can form. Larger crystals tend to have a large number of magnetic domains which normally form closure domains .

For a single domain, a large amount of magnetostatic energy is associated with the magnetic field coming from the surfaces. Two oppositely oriented domains reduce the magnetostatic energy by approximately one half. Continuing increases in the number of domains (or in the domain wall widths) reduces the magnetic energy to a minimum, after which the magnetostatic energy will start to rise again .

The behaviour of small, single domain crystals is different to that of the larger particles, which usually contain many domains. An increase in an external

magnetic field applied reversely along the axis of a single domain crystal will have no effect until, at some point, the domain changes direction to line up with the applied field. It will remain in that direction until a similar field is applied in the reverse direction. A change in the main axis of the domains magnetic field can be achieved with high strength (10^8 nT) magnetic fields, but removal of the field will allow the domain to go back to its previous orientation, usually along an 'easy' crystallographic axis. Multidomain particles immediately start to acquire domain magnetic components in the direction of any applied field, usually by growth of domains oriented along the applied field at the expense of other nearby domains.

The application of an external field causes the domains to line up with the external field, giving rise to a number of magnetic poles at the top and bottom surfaces of the mineral grain. The pole density is the number of such magnetic poles per square metre, and the magnetization of the block is the number of dipoles per unit volume. The magnetic poles within the top or bottom surface repel each other and, given the space, will move as far apart as possible.

Characterizing the magnetic response of a rock is done by measuring its magnetic susceptibility in low magnetic fields appropriate to the linear part of the magnetic hysteresis curve for such a sample (attempting

to measure the susceptibility in a high magnetic field will give low or zero values for the susceptibility). By applying a magnetic field of strength H, a magnetization intensity of M is induced within the rock, where

$$\chi = M/H \qquad 1.3.1$$

χ is the magnetic susceptibility of the rock per kilogram or per cubic metre, and is a dimensionless quantity. M, the magnetization, is also called the dipole moment per unit volume (or per unit mass).

The magnetic field measured outside the rock (B) is a combination of the applied field H and the magnetization intensity M. Thus

$$B = \mu_0(H + M) \qquad 1.3.2$$

M and H have units of Am^{-1} and B has units of Tesla.

Rock susceptibilites may be anisotropic for two reasons. First, the electron spins can usually align more readily along one particular crystallographic axis, known as the easy axis. The magnetization of such a crystal in an applied field is always along the easy direction. Second, the close location of the north and south magnetic poles on the opposite surfaces of a grain causes repulsion between like poles. The forces will be at a minimum with the surface poles as far away from each

other as possible. Variations in size and orientation of the opposite surfaces can cause asymmetric distribution of the poles, leading to an induced magnetization that is dependent upon the shape of the grain. The magnetization is usually directed along the long axis of asymmetric grains. Magnetic anisotropy will be at a maximum when both effects occur together. For other situations, as with magnetite, shape anisotropy will be dominant.

The major minerals causing the observed magnetic fields arising from rocks are the titanomagnetites. Figure 1.3.a shows a ternary diagram for iron-titanium oxides present in magmatic rocks. The end members of the titanomagnetite series ($Fe_{3-x}Ti_xO_4$ where $0<x<1$) are magnetite (Fe_3O_4) and ulvospinel (Fe_2TiO_4) which form this solid solution series. The mineral assemblage developing in an igneous rock ultimately depends upon the bulk composition of the magma from which the minerals crystallize.

The magnetism of materials arises mainly from the spin angular momentum of the electrons. This effectively gives a microscopically small magnet with a magnetic dipole moment of $9.277e^{-24}$ Am^2 or one Bohr magneton. In a solid with large concentrations of magnetic dipoles, co-operative action due to orbital overlap can occur, the so-called direct exchange. In oxides, orbital overlap with anions gives rise to the

indirect exchange. Both of these effects result in long range order within the magnetically active material.

Ferrimagnetic materials have two magnetic sublattices with opposite but unequal magnetization - giving a net observable magnetization.

Many rock forming minerals are classed as diamagnetic, since the magnetic susceptibility is about -10^{-6}. These materials have no unpaired electrons. The effect of the external field is to rotate the orbital paths of the outer few electrons, giving rise to a magnetic field in the opposite direction (hence the negative susceptibility).

Paramagnetic materials have incomplete outer electron shells and hence unpaired electrons. In an external field, the spin rotates, giving a field in the same direction as the applied field. Hence χ is positive and has a value of approximately 10^{-6} for paramagnetic substances.

Ferro and ferri magnetic materials have values for χ of about 0.1 to 100. They are the oxides and sulphides of iron. These materials contain several unpaired electrons, with dipole coupling between adjacent atoms giving rise to the long range order in magnetic domains. The magnetic susceptibility of a rock is usually proportional to the percentage of ferrimagnetic minerals

present (mainly magnetite but including ilmenite and pyrrhotite).

Antiferromagnetic materials such as haematite have equal numbers of dipoles pointing in opposite directions and cancelling out, although small crystal lattice defects may give some small net magnetization. By contrast ferromagnetic materials have all dipoles lined up in the same direction, giving rise to very strong magnetic fields. Such materials are rare in the Earths' crust. Ferrimagnetic materials such as magnetite have dipole coupling similar to antiferromagnetic materials, but with unequal numbers of dipoles in opposite directions. This gives a strong net magnetization and high magnetic susceptibilities of the order of 0.1 to 100. Most rock minerals that are strongly magnetically active are ferrimagnetic. These magnetic minerals mostly lie within the ternary system FeO-TiO-Fe_2O_3 and are mainly crystallization magnetic minerals (the titanomagnetites).

Beyond the Curie temperature the magnetization of ferro and ferri magnetic minerals disappears due to the increased random thermal motion and increased interatomic seperations. However, as the temperature falls the reverse effect ensues and any magnetic domains present in a crystal will grow if aligned with the external magnetic field. If aligned oppositely, they will reduce due to the movement of the Bloch walls in favour of individual aligned domains. If the Bloch wall moves

across crystal imperfections, the result is a permanent memory of the original magnetization characteristics, remanence.

A number of different physical effects have been found to give rise to remanence over the last thirty years. Thermal remanence (TRM) is described above. The growth of a crystal grain with magnetic domains may also occur at low temperatures, the grain acquiring an oriented permanent field via the magnetic domains. This chemical remanence is usually of less intensity than the thermal variety. Chemical changes can usually be responsible for loss of thermal remanence and loss of ferrimagnetic behavior. Weathering is a good example of such an effect.

Depositional remanence and post-depositional remanence are mainly of importance in sedimentary rocks, where minerals in suspension settle out, their dipole fields being aligned with the Earths main field at the time of settling. This type of remanence may take on significance in situations where fractionation has occurred from a magma, govong rise to a separation of minerals some of which have relatively high magnetic susceptibilities.

If enough energy is supplied to a ferromagnetic material, the magnetic dipoles can be moved away from their TRM directions and the growth of magnetic domains

will occur in the new field direction, together with a decay of TRM in the old direction. The relaxation time for such a change in a single crystal depends upon the ambient temperature and was given by Neel (1955) as

$$\tau = C.\ \exp(v.B_C.J_S/2.k.T_{abs}) \qquad 1.3.3$$

where C is a constant with a value of 10^{10} s^{-1}

v is the volume of the crystal

k is Boltzmann's constant

T_{abs} is the absolute temperature

J_S is the spontaeous magnetization

B_C is the coercivity

As the crystal cools below its Curie point, the relaxation time increases exponentially as a function of the temperature. The remanent magnetization becomes frozen into the crystal. A similar effect is present when the volume of the crystal is increased. For a crystal of diameter 0.8 mm at a temperature of 100°C the relaxation time is calculated to be of the order of 300 Ma.

For titanomagnetites, the Curie point rises approximately linearly with composition from -152°C to 575°C. This effect is due to a decreasing intergranular distance as the magnetite content rises. As the pressure rises so the Curie point temperature also rises at a rate of approximately 10^{-8} K/Pa. Pressure also has the effect of decreasing the intergranular distance. This is not a

significant effect and is normally discounted in geophysical applications.

1.4 Magnetic Surveying

Magnetic surveying exploits the magnetic susceptibility variations found in different rock units. Such susceptibility variations give rise to changes in the induced magnetic field arising from the rocks. These induced magnetic variations are sufficiently large to be measurable at the surface of the Earth, even when the rocks are buried at great depth in the lithosphere.

The measurement of magnetic field variations has a long history. Declination measurements were made systematically during the sixteenth century and were used to estimate longitude. Inclination measurements in England are recorded as early as 1581 by Robert Norman. Intensity measurements,however,are only traceable back to the eighteenth century, when early forms of the oscillation magnetometer were used to measure the horizontal component of the Earths main field.

The development of magnetic field measurement techniques for prospecting is recorded from the early nineteenth century. Since then rapid changes in instrumentation have improved the portability, accuracy and sensitivity of the equipment. Ship,aircraft and satellite based observations are now commonplace, giving global coverage, although at the loss of resolution as distance from the Earth and speed of the sensor are increased.

Green (1976) described the interpretation of aeromagnetic data sets obtained from long aeromagnetic profiles across central Africa. He was able to use two-dimensional spectral analysis to interpret the presence of magnetically active bodies at depths ranging from 0.2 km below the surface to 30 km below the surface. The causative bodies were related to local tectonics, particularly to exposed precambrian shields (shallow anomalies) and sedimentary basins (intermediate depth anomalies). Extensive, inductively magnetized bodies at depths of up to 30 km. were identified but not definitively interpreted.

McLeod (1983a) inverted POGO satellite data to obtain crustal magnetization estimates for the western United States. By utilising two-dimensional power spectra he was able to obtain crustal magnetization values consistent with some previous workers. In a related paper, McLeod(1983b), again using POGO satellite data, was able to show that the result of filtering out 'noise' from satellite data could be a loss of up to 50% of the actual magnetic anomaly field at satellite altitudes of about 100km.

The continued development of instrumentation has improved the ease of use, portability, accuracy and sensitivity of field equipment. The recent development of superconducting quantum interference device (SQUID) magnetometers allows the measurement of magnetic fields

to a resolution of 10^{-12} Tesla, 1000 times better than a standard proton precession magnetometer.

1.5 Survey design and field procedure

In designing a survey it is necessary to take into account a number of factors which may affect the accuracy of the readings taken and their usefulness.

1.5.1 Resolution

The resolution available along a single line is dependent upon the spacing of the readings. More readings give higher resolution but take a longer time. In addition, the spacing between lines has a major effect upon areal resolution. Anomalies of short wavelength may be picked up on a given line but may be missing completely from adjacent lines. Contouring such results is difficult. Given that the field work was carried out on granites of considerable surface area (400 km^2), field line spacing was a major restriction.

1.5.2 Positional accuracy

The positional accuracy of a set of readings can significantly affect the shape of any contoured data. To obtain good accuracy features which are clearly visible on both ground and map are selected along the route to be walked. These would include bends in a river, the southern tip of a loch, and bridges.

The distance between such features is kept to a minimum. Each feature is used to locate the next, for

example by following part of a river, or by a compass bearing. Accurate pacing allows intermediate points to be located on the map, with errors distributed evenly along the line between each pair of features.

1.5.3 Location

In some remote areas such as eastern and central Cairngorm, access is difficult. For these areas a centrally based campsite was used, although problems were still encountered in getting adequate coverage. In many instances a time consuming walk was necessary before useful results could be acquired. Widely spaced spot values were used to speed up coverage of such areas, although resolution is reduced by this process.

1.5.4 Weather

Readings were taken year round over a period of six years, both summer and winter. Given the unpredictable nature of British weather, a rucsack and compass were frequently necessary. The compass was always kept three metres away from the magnetometer when readings were taken. Electrical storms invariably prevented all field work.

1.5.5 Field procedure

Each line was broken into a series of short traverses. These were completed taking readings at

intervals of 100 metres. Errors were distributed along each traverse. Maximum positional errors were estimated to be ±20 metres, with most errors being ±5 metres, over distances of 0.5 to 1.0 kilometre. All results were noted at the time of taking a reading, except for those occasions when an OMNI IV magnetometer was available. Using an OMNI IV magnetometer allowed readings to be taken and stored in the magnetometer memory, the results being read out of memory at the end of each day. Repeatability of the readings was checked at regular intervals.

1.5.6 The effect of pipelines

Typical iron or steel objects have a magnetic moment of 10^2 to 10^3 Am^2. 100 kilograms of iron would give a magnetic anomaly of 7 nT at a distance of 10 metres. Such objects are particularly common in built up areas and by the side of roads.

For some areas such as Western Cairngorm, time was spent taking readings along roads. As far as was possible, all obvious sources of iron were avoided. However, the effect of locally buried pipelines can be substantial, causing anomalies of several hundred nT. When substantial variations were encountered, the values were checked by moving into local fields. The most repeatable value was then taken as the reading for that position. Noise levels on roads were estimated to be ±10

nT , with occasional values containing higher levels of noise.

1.5.7 Temporal variation

Correction for time variations is essential, as many of the anomalies are broad, and profile lines long. To carry out this correction, selected points were used to take readings at the beginning and end of each day. It was rarely possible to include a third reading at mid-day due to the size of the survey lines. Reduction of data for temporal variations is described in Chapter 2.1.

1.5.8 Magnetic effects of equipment

In order to reduce the noise level, the sensor was carried on a 2.2 metre aluminium staff. A back pack was used to carry the magnetometer head only on those occasions when high winds or very steep slopes made use of the staff difficult. The back pack was estimated to cause a reduction in reading of 14 nT, mainly due to the closer proximity of the magnetometer electronics. This value was added to those readings where the backpack was used. Checks were also carried out on the effect of the rucsack, boots and other equipment by taking readings in one place with and without the equipment present. Additions to the rucsack were checked in the same way. Variations no greater than 8 nT were noted and the day's results were corrected accordingly.

1.5.9 Repeatability of readings

Repeatability of the readings was checked at regular intervals during each day of field work. With one exception these gave no cause for concern, variations being 0 to 1 nT. Orientation of the arrow on the sensor was maintained in an approximately northerly direction. Directional sensitivity was estimated at 2 nT or less. All readings were taken with the operator in the same position with respect to the sensor head, with the exception of steep slopes. In those instances when a staff was used on a steep slope, the variations in distance between the sensor head and the ground produced variations in measured field values of up to 10 nT. Variations due to operator position were estimated at 2 nT or less.

1.6 The proton precession magnetometer

The proton precession magnetometer uses the precession of spinning protons in a hydrocarbon fluid to measure the total magnetic field strength. Electrically charged particles such as the proton have a spin which gives rise to a magnetic moment defined by

$$\mu = 2.7(q_p/m).L \qquad 1.6.1$$

where μ is the magnetic susceptibility

q_p is the charge on the proton

m is the mass of the proton

L is the angular momentum of the particle

When a strong magnetic field is applied to the volume of space occupied by the protons, the proton's magnetic moment will be forced to line up with the magnetic field lines passing through the local volume. On cutting off the external magnetic field, the proton's magnetic moment can only feel the effect of the Earths weak magnetic field. The axis of spin of the proton's will now rotate, or precesss, about the Earth's magnetic field lines with an angular velocity given by

$$\omega = \mu.B/L \qquad 1.6.2$$

where B is the applied magnetic field strength

The value of μ/L is known to an accuracy of 0.25%. With modern electronics, the measurement of ω to high precision is relatively straightforward, allowing the calculation of B. The value of μ/L is taken as 2.67513×10^{8} r s^{-1} T^{-1}.

Proton precession magnetometers require a source of protons, a strong polarizing magnetic field to line the protons up, and a means of measuring the frequency of precession of the protons.

The source of protons is usually an organic fluid such as decane or paraffin, both liquids rich in protons. The liquid is contained within an aluminium bottle and is surrounded by one or two coils of wire. Passing a strong electric current through the primary coil induces a relatively strong magnetic field of the order of 10^{-2} Tesla in the volume surrounded by the coil. This field is strong enough to line up a large proportion of the protons present against the effect of thermal collisions.

By cutting off the magnetic field generated by the coil very quickly (usually in about 50 microseconds), the aligned protons are left in the Earth's weak magnetic field with their magnetic moments pointing in a different direction to the field lines. The protons experience a net torque and will precess about the Earth's field lines at a frequency given by equation 1.6.2.

Thermal collisions eventually break up the alignment of the proton magnetic moments. During the time of alignment (1 to 2 seconds) the measurement of precessional frequency can be made.

The precessing protons induce a time varying voltage in either the primary coil, or in some magnetometers a secondary coil, of the order of 10^{-5} volts at a frequency of about 2.5 kHz in a field of 49000 nT. To get high resolution of the measured frequency several electronic tricks are employed. A digital counter is driven by an 85 kHz oscillator. After the counter has recorded 10000 oscillations it closes the logic gate. During this time each precessional oscillation is multiplied by a factor of 200 amd the results passed via the logic gate to counter 2. The precessional frequency is then calculated, followed by the magnetic field strength, the direct reading in nano Tesla being shown on the display.

There are a number of problems associated with the proton precession magnetometer. Electrical noise in the coils (induced for example by local A.C. power lines) can cause phase shifts in the signal being measured. This in turn can lead to a wrong calculation of the precessional frequency.

Very steep magnetic field gradients may be sufficient to cause a significant difference in the magnetic field at the two ends of the detector. The precessing protons at the two ends will have different frequencies which will add in the detector coil to give beats on the induced voltage. This will cause errors in the measured frequency. Consequently there is a maximum gradient in which a proton precession magnetometer may be reliably used.

The orientation of the sensor in theory should have no effect. In practice the signal amplitude does vary as $\sin^2(\phi)$, where ϕ is the angle between the Earth's main field and the field produced by the sensor coils. This variation averaged 2 nT in the present study.

Chapter 2 Processing of magnetic data

2.1 Corrections to the field data - temporal variations

Correction for diurnal or micropulsation time variations can be carried out for a variety of reasons. For example if the anomalies of interest are broad (several kilometres) and low amplitude (less than about 50 nT) diurnal time variations can mimic anomalies in amplitude across the area of interest. If the traverse lines are very long, uncorrected data can contain large variations from sources other than those actually present. This would prevent any detailed assessment of deep-seated anomalies, but would not necessarily have a significant effect upon smaller near-surface anomalies. However, micropulsations, which may be as high as 100 nT, can appear as high frequency, near-surface anomalies.

The reason for correcting the field data in the present case lies with the presence of long traverse lines. Since aeromagnetic data was already available for the area, it was used as a constraint for the correctness or otherwise of the field data during contouring. The corrected data was felt to represent the anomalies present on the ground along the survey lines with a good level of accuracy.

The correction of temporal variations usually

treats the magnetic field as a scalar quantity when in fact it is a vector, having both magnitude and direction. The cause of the temporal variations lies with variation in altitude, direction and intensity of ionospheric current systems. These current systems will usually produce magnetic field lines of varying intensity and directionat the surface. They will add to the Earth's main field lines vectorially. For example, a horizontal current system immediately overhead will produce horizontal field lines at ground level. The vector addition of these to the main field will be identical to the effect due to remanence, causing an offset in the whole of the total field. The only way that a full reduction appears practicable is to take all measurements in three orthogonal directions, including the base station readings, and to correct the three main field vector values individually before combining them to form the total field value. Most authors use some form of numerical interpolation scheme, followed by a simple scalar reduction of the field values.

In the course of each day's work, readings were taken at a fixed base station at the beginning and end of each day. It was possible on some of the longer traverses to check the size of the diurnal variation by repeated readings at one station for about an hour (usually mid-day), and for rechecking values obtained at a given point during a walk back to the base station. The usual technique of doubling-back to take a second or third

reading at a given station was frequently not practicable. The time required to do this in mountainous terrain during the short days of Autumn and Winter could extend the working day into darkness.

On several days the temporal variation exceeded 100 nT, but was usually of the order of 25 nT. Erratic readings were checked and were usually found to be due to a malfunctioning magnetometer (two instances), or when moving close to the base of cliff faces, or to discharged batteries.

Although magnetic observatories are able to provide detailed records of changes in all of the geomagnetic elements, these could not be used due to the distance of the survey from the nearest such observatory. Diurnal variations change considerably over distances of 50 to 100 km. Given no accurate knowledge of how the magnetic field varied between readings, a simple linear extrapolation scheme was used to correct the readings. For the base readings a standard straight line equation was used to relate the two readings. For one particular day the readings were 44397 at the start of the day and 44423 at the end of the day, 550 minutes later. The rate of variation is 26/550 or +2.8 nT per hour. Knowing the time at which a reading was taken, the estimated correction could then be subtracted (in this case) from the reading concerned. On those occasions when mid-day readings could be taken errors due to assuming a simple

straight line relationship were estimated to be no greater than ±10 nT.

The same base stations were reoccupied on each trip in order to reduce variations over longer spans of time. To this end the base stations chosen were kept well away from areas of likely development. Readings between years were adjusted to correspond to the base station readings of the first year. A base station at Linn of Dee was used in covering the southern area of the Cairngorms, and at Coylumbridge to cover the northern side. To enable the two stations to be linked, the base station was monitored for two hours at Linn of Dee. A rapid trip was then made to Coylumbridge (one hours drive away), and the process repeated. This allowed the results at Linn of Dee to be extrapolated to cover the time of the reading at Coylumbridge.

2.2 Aeromagnetic maps as a source of data

The aeromagnetic data used in this study were acquired by Hunting Surveys under contract in the period 1963 to 1964. The aircraft collecting the data flew at a clearance of 300 metres along East-West flight lines at 2 kilometre intervals. North-South tie lines were at 10 kilometre intervals. Following collection the data points were interpolated onto a regular grid and contoured. The data points were then reduced by subtracting a plane having a slope of 2.1728 nT per kilometre North, and 0.258 nT per kilometre West. This allows the anomaly to be related to the I.G.R.F. by simple linear interpolation between the corners of each map.

One of the major factors affecting interpretation is the relationship between line spacing and anomaly wavelengths. The shortest spatial wavelength which can be found from a regular line of samples of spacing Δx is the Nyquist wavelength given by

$$W_n = 2\Delta x \qquad 2.2.1$$

Wavelengths shorter than W_n will be aliased into wavelengths longer than W_n. Thus, in the present case, with a maximum of 2 kilometres between the flight lines, the Nyquist wavelength is 4 kilometres. Any wavelength shorter than this in a north-south direction will cause aliasing.

The total power in the signal is given by

$$\text{Power} = \int_0^\infty \langle E(r) \rangle dr \qquad 2.2.2$$

Here $\langle E(r) \rangle$ is the expectation of the power in each wavenumber interval dr, r being the wavenumber. The Nyquist wavenumber (r_n) is related to the Nyquist wavelength (W_n) by

$$r_n = 2\pi / W_n \qquad 2.2.3$$

The fraction of aliased power above the Nyquist wavenumber (r_n) is given by

$$F_{alias} = \frac{\int_{r_n}^\infty \langle E(r) \rangle dr}{\int_0^\infty \langle E(r) \rangle dr} \qquad 2.2.4$$

The expectation value of the power spectrum profile is given by Spector and Grant (1970) as

$$\langle E(r) \rangle = 4\pi^2 \bar{k}^2 e^{-2\bar{h}r} \langle C^2(r) \rangle \langle S^2(r) \rangle \qquad 2.2.5$$

where:

r is the wavenumber

$\bar{k}$ is the mean value of the magnetic moment per unit depth.

$\bar{h}$ is the average distance between the sensor and the

top surface of the magnetised rocks.

$\langle C^2(r) \rangle$ is a term that depends upon the depth extent of the sources.

$\langle S^2(r) \rangle$ is a term that depends upon the dimensions of the upper surfaces of the magnetised rocks.

Following the short note given by Reid (1980), the value of $\langle E(r) \rangle$ can be approximated by

$$\langle E(r) \rangle = 4\pi^2 \bar{k}^2 e^{-2\bar{h}r} \qquad 2.2.6$$

The assumption was made by Reid that an assemblage of small bodies of considerable depth extent were present. Although not strictly true the assumption can be used as an approximation to the true situation to get a feel for the effects of aliasing.

Using this approximation we can calculate the aliased power along the lines suggested by Reid in equation 2.2.6

$$F_{alias} = \frac{((e^{-2\bar{h}r})/-2\bar{h}) \Big|_0^\infty}{((e^{-2\bar{h}r})/-2\bar{h}) \Big|_{r_n}^\infty} \qquad 2.2.7$$

$$= e^{-2\bar{h}r_n} \qquad 2.2.8$$

$$r_n = 2\pi/W_n$$

giving $$F_{alias} = e^{-2\pi\bar{h}/\Delta x} \qquad 2.2.9$$

For the aircraft carrying the sensor Δx is the spacing between flight lines, which is 2 km. The mean value of h will be shown in chapter 3 to be about 3 km below the surface. Thus

$$F_{alias} = e^{-2\pi(3/2)}$$

$$= 8 \times 10^{-5}$$

$$= 0.008\%$$

This reflects the lower limit on the aliased power under the assumptions made. The upper limit for an aircraft at an altitude of 0.3 kilometres is given by

$$F_{alias} = e^{-2\pi(0.3/2)} \times 100\ \%$$

$$= 39\%$$

Thus the aeromagnetic maps must be used with caution for surface interpretation. For less than 5% aliasing we need $\bar{h}/\Delta x \geq 0.5$, ie for $\Delta x = 2$ km $\bar{h} \geq 1$ km. For $\bar{h} = 0.3$ km $\Delta x \leq 0.6$ km. Anomalies at depths greater than 1 kilometre will pose no problem in interpretation on this basis, since the aliasing will always be less than 5%. For field results the aliasing along a profile will be less than 1%. Detailed modelling of an anomaly

depends upon the resolution of the high frequency end of the spectrum for its accuracy. Reliable results will be available only if no aliasing is present. In the case of the Cairngorm pluton, modelling the top surface of the main magnetic anomaly is perfectly feasible, since, as will be shown later, this is at a depth greater than 1 kilometre. However, modelling some of the finer details within the granite at depths less than 1 kilometre is not. The aliasing will distort the results, and the model produced will be of limited accuracy. Hence the need for field data.

2.3 Digitisation of aeromagnetic data

Any aeromagnetic or other potential field data has a continuous variation in space. To represent this data on a contour map, it must first be sampled at intervals, processed in some way (eg interpolated onto a regular grid), and then presented in a contoured form, or treated as a relief map and shaded in some way. The final result may be a relatively poor approximation to the actual field unless:

i) the original data gives a reasonable spatial spread of the area concerned.

ii) the regridding process causes minimal distortion.

iii) the contours used to represent the potential field are at appropriate intervals.

Following on from equation 2.2.1, continuous signals with a bandwidth running from 0 to N cycles per metre can be accurately reconstructed from a sequence of equally spaced samples if the sampling frequency is greater than 2N. This statement of the sampling theorem provides the major criterion for the digitisation of data from aeromagnetic anomaly maps, although it has to be borne in mind that real signals are not necessarily band-limited.

If the sampling frequency is less than 2N, the signal is undersampled. The effect of undersampling is to introduce spurious frequencies with a lower value than

the Nyquist frequency - resulting in a shift in signal power from the high frequency end to the low frequency end. These effects are easier to see and explain in one rather than two dimensions. Figure 2.3.a shows a continuous signal that is undersampled, together with the signal reconstruction. The effect of undersampling is to significantly affect the frequency observed, the undersampled frequencies being observed as lower frequency signals. In a complex signal consisting of a range of frequencies, the signal energy that would have been observed at the higher frequencies appears lower down the frequency range.

This shift in the signal energy will have an effect on the slope of the graph of the power in each wavelength interval against the wavelength, increasing it. Since the slope of this form of the power spectrum has considerable importance to the interpretation of the data, care must be taken in the early stages of digitisation to get the correct sampling interval.

Representing a continuous variable as a set of discrete numbers implicitly involves a mathematical transformation of the data set in several ways. Each discrete value can be thought of as the multiplication of a continuous signal by a Dirac function, a pulse with area 1, width zero and infinite height. The Dirac function, $\delta(x)$, can be moved from the origin to any point x_0 by a simple translation $\delta(x-x_0)$. Thus, we can build up

a set of Dirac pulses, a Dirac comb, as shown in figure 2.3.b, by a set of translations of a pulse at the origin. The multiplication of the Dirac comb with the original continuous data set gives the sampled points, i.e. the product $f(x).\delta(x-x_0)$ gives the value of $f(x)$ at $x=x_0$. Extending the idea to two dimensions, the Dirac comb $\delta(x-x_0,y-y_0)$ can be represented as a set of Dirac pulses on a plane, as shown in figure 2.3.c . Multiplying the map by these pulses gives the data representation as a set of gridded numbers.

The Dirac function is important since it enables us to understand the effects of sampling in the frequency domain, as will be demonstrated below. Its properties in the space domain are twofold.

$$\delta(x,y) = 0 \text{ for } x = 0 \text{ or } y = 0 \qquad 2.3.1$$

$$\int_{-\infty}^{\infty}\int_{-\infty}^{\infty} \delta(x,y)\,dxdy = 1 \qquad 2.3.2$$

The effect of the two dimensional Dirac function on a single point is given by

$$\int_{-\infty}^{\infty}\int_{-\infty}^{\infty} g(x,y).\delta(x-x_0,y-y_0)\,dxdy = g(x_0,y_0) \qquad 2.3.3$$

The result is the sampled point $g(x_0,y_0)$, all other values being zero by equation 2.3.1 . Repeating this for a set of translations along the x and y axes will give the full digitised data set.

During later processing of the digitised data, it is necessary to carry out the operation of Fourier transformation. With the effect of digitization represented as a 2 dimensional Dirac comb multiplied by the continuous data sequence g(x,y), we can write the digitized data as

$$D(a,b) = \sum_{-\infty}^{\infty} \sum_{-\infty}^{\infty} \delta(x-a,y-b).g(x,y) \qquad 2.3.4$$

This now represents the data in the computer. We can use the fact that

$$FT(a.b) = FT(a) * FT(b) \qquad 2.3.5$$

(where * indicates convolution and FT indicates the Fourier Transform) to rewrite the transformed data as shown below:

$$FT(D(a,b)) = FT\left(\sum_{-\infty}^{\infty} \sum_{-\infty}^{\infty} \delta(x-a,y-b) \right) * FT\left(g(x,y) \right) \qquad 2.3.6$$

This equation indicates that the effect of sampling will be to convolve the true Fourier transform of g(x,y) with the Fourier transform of the two dimensional Dirac function. The Fourier transform of a Dirac comb with spacing Δx along both axes is another two dimensional Dirac comb in the frequency domain with a spatial frequency separation between the comb elements of $1/\Delta x$. This is shown in figure 2.3.d

A copy of the spectrum of g(x,y) will occur centred upon each of the Nyquist frequency components f_n, $2f_n$, $3f_n$ etc. as implied by the convolution effect. With a two dimensional situation the copy is an areal one centred upon each tooth of the two dimensional Dirac comb. Figure 2.3.e shows the situation in one dimension, with overlap of the signal frequencies centred upon each tooth. The overlap indicates that undersampling has occurred. To avoid this we can decrease the sampling interval, Δx . This will have the effect of increasing the comb interval in the frequency domain, and, if sufficient, will prevent overlapping of the spectra as shown in figure 2.3.f. Most geophysical signals are not band limited and cover a broad frequency range, making some overlap inevitable. Often there is little power in the high frequency end of the signal (as with gravity data), and we can ignore the aliasing effect. In other cases it may be impractical to decrease the sampling interval. An alternative is to filter the signal in an

attempt to prevent aliasing by cutting down the signal bandwidth.

The power spectrum of a signal reflects the amplitude of different frequency components in the signal and is usually concave downward for aeromagnetic data. This is discussed further in 2.11.

Examination of the aeromagnetic map for the Cairngorm area suggests that a digitising interval of about 0.6 kilometres is enough to prevent major aliasing effects. An interval of 0.5 km was chosen for reasons of convenience (particularly taking values from the aeromagnetic map and reducing the bumpiness of the power spectrum). Since the programs available could run 100 by 100 matrices, this dictated a choice of a 50 kilometre side square and 10,000 data points to cover the area concerned, unless other considerations made this unacceptable. For small anomalies due to near surface sources reliance was placed more upon the field magnetic data than upon the aeromagnetic data, since this was better able to resolve such anomalies.

Having chosen a sampling interval of 0.5 kilometres, the Dirac comb interval in the frequency domain can be calculated as 2 per kilometre. If the signal spectrum is greater than half of this value (1 per kilometre), there will be spectral overlap and it will be

impossible to completely recover the signal from the digitised data.

It is necessary to keep in mind the particular maximum depth of interest when digitising the data. For example, the Curie point of rocks in the Cairngorm area would occur at a depth of approximately 30 kilometres given a 20° C per kilometre thermal gradient. To be able to observe this in the filtered aeromagnetic data would require a data square of $2 \times \pi \times 35$ kilometres side, ie a square of side about 220 kilometres. Combining this with a requirement for a 0.5 kilometre interval between points, then to avoid aliasing would require an array of 440 x 440 data points. To have 193,600 points in a single array is demanding of computer memory and processing time. Previous gravity modelling of the central highland granites, particularly of the Cairngorm pluton (eg Locke 1980) suggested the base of the granites to be at about 12 kilometres. For the main processing work, it was decided to aim at a depth appropriate to a 0.5 kilometre digitisation interval and a 100 by 100 matrix. This would give a square of side 50 kilometres, and allow features at a maximum depth of about 8 kilometres to be resolved. Such a compromise between resolution, distortion, the need to digitize by hand rather than automatically, computer memory availability and the processing time available is inevitable.

To digitise data from the aeromagnetic map, lines were drawn horizontally and vertically. The results were then read from the map verbally for recording onto a cassette tape. The data was then copied into computer memory and contoured. The resulting plot was compared with the original contours on the aeromagnetic map. Large errors were clearly identifiable and easily corrected. The data was then replotted using smaller contour intervals to show up other values giving unacceptable contour variations. It proved impossible to completely remove small variations from the original contours, particularly at the margins of two maps. All hand digitised results contain small errors. The acceptable result was decided on the basis of contour smoothness and agreement with the original map.

2.4 The effects of truncation

In taking results from an aeromagnetic map, for reasons explained in section 2.3, it is necessary to limit the size of the data square. In truncating the spatially varying continuous magnetic field we are multiplying a continuous function by a window function of dimensions Δx, Δy. Denoting the aeromagnetic data by $d(x,y)$ and the window function by $w(x,y)$, the sampled data area can be written as:

$$g(x,y) = d(x,y).w(x,y) \qquad 2.4.1$$

Taking the Fourier transform of this function gives

$$FT(g(x,y)) = FT(d(x,y)) * FT(w(x,y)) \qquad 2.4.2$$

Here * again denotes convolution. The Fourier transform of $g(x,y)$ is therefore not as straightforward as initially discussed in section 2.3 . The original data has been multiplied by a matrix which represents the spectrum of the window function. Since the window function is a square it can be written as

$w(x,y) = 1$ within the window.

$w(x,y) = 0$ outside the window.

The rectangular window function can be pictured (in the space domain) as a box car, shown in figure 2.4.a. The Fourier transform of the boxcar is given by:

$$FT(w(x,y)) = \int_{-\infty}^{\infty}\int_{-\infty}^{\infty} w(x,y).e^{-i2\pi(k_x x+k_y y)}\,dxdy \quad 2.4.3$$

The result of this transformation into the frequency domain is a two dimensional Sinc function which may show rapid changes as in figure 2.4.b or slow changes as in figure 2.4.c, depending upon the size of the boxcar function. For an infinitely wide window, the frequency domain equivalent becomes a Dirac function of area 1, zero width and infinite height. This will have no effect on the frequency amplitudes of the Fourier transform of the signal. With a more normal situation, that of a finite window, the effect of the window is to increase or decrease the frequency amplitudes of the true signal, causing high frequency distortion. This will always be the case when the data are suddenly cut off. To reduce this effect, special window functions are used which give a gradual tapering effect on the data.

Window function properties are usually specified in the frequency domain, whilst the operation of windowing is carried out in the time or space domain. It is normally necessary to specify either the lowest frequency or the highest wavelength of interest, as these will be affected by the window function.

A cosine tapered window, the Tukey window, has been used in this work. The Tukey window gives a suitable means of smoothly reducing the data to zero at the boundaries without having any major effect on the processing gain.

The mathematical definition of the Tukey window function is given by:

$$W(N) = 1.0 \qquad T < \Delta x < N-T$$

or $$W(N) = 0.5(1.0 - \cos(\pi\Delta x/W) \quad \text{for } \Delta x < W \text{ and } \Delta x > N-W \qquad 2.4.4$$

where T is the width of the cosine function which tapers the data to zero and Δx is the number of data points along one edge of the data matrix, at which the cosine function is being evaluated. N is the total number of data points along the profile. The function is shown diagramatically in figure 2.4.d.

For use on aeromagnetic data sets, the Tukey window profile is used as a radius centred upon the centre of the data set and is rotated 360 degrees. This produces a matrix of values ranging from 1 at the centre, tapering to 0 at the outer edges. Multiplying the data set by the Tukey window matrix destroys information at the edge of the data but reduces the processing

distortion that would otherwise occur when a fast Fourier transform is applied to the data.

2.5 The I.G.R.F. and its removal

The total magnetic field measured at or near the surface of the Earth is the vector sum of many separate fields originating from different sources. These fields include transient fields due to ionospheric and other current systems, which may have field line inclinations ranging from 0 to 90 degrees, and declinations across the full 360 degree range. The normal diurnal variation due to ionospheric current systems is about 50 nT. This may rise to 150 nT or more during substorms. Correcting for the transient fields is dealt with in section 2.1

The Earth's main field is divided into two parts, the dipolar and non-dipolar fields. Subtracting the dipolar field from the Earth's main field, a residual or non-dipolar field is left over. This field is thought to be due to vortices within the liquid core. The non-dipolar field has an average drift to the west of about 6 minutes of longitude per year, although this value has varied from 3 to about 9 minutes of longitude per year in the recent past (le Mouel et al 1983).

It is frequently desirable to strip out the Earth's main field from magnetic data acquired during ground based, sea or airborne surveys. However, to do this requires some way of predicting the main field and its temporal and spatial variation across the surface of

the Earth from widely spaced observatory data. This is accomplished by developing an accurate mathematical model to fit the main magnetic field and its variations with time. The mathematical model was aimed at serving all areas of geomagnetism, and as recently as 1983 seven models of the International Geomagnetic Reference Field were available (Regan 1983)

The first widely accepted mathematical model of the Earth's main field was adopted in 1968 and was known as the International Geomagnetic Reference Field (I.G.R.F.). The major part of the field is dipolar in nature and thus satisfies Maxwell's equations

$$\nabla \mathrm{X} \mathbf{B} = \mu_o \mathbf{J} \qquad 2.5.1$$

$$\nabla . \mathbf{B} = 0 \qquad 2.5.2$$

Here $\mathbf{J}$ is the current density.

$\mathbf{B}$ is the magnetic field strength.

μ_o is the magnetic permeability of free space.

The current density $\mathbf{J}$ is normally assumed to be zero giving:

$$\nabla \times \mathbf{B} = 0 \qquad 2.5.3$$

Since $\mathbf{B} = -\nabla V$ and since the divergence of $\mathbf{B}$ is zero then:

$$\nabla^2 V = 0 \qquad 2.5.4$$

Since **B** can be taken as the gradient of a scalar function V that satisfies Laplaces equation, V can be modelled by a spherical harmonic series expansion.

The IGRF was first defined using the terms of spherical harmonic coefficients up to m=n=8 for the main field. This gives 160 coefficients which are used in the Schmidt quasi-normalised form, allowing the geomagnetic potential V to be derived using:

$$V = a \sum_{n=1}^{8} \sum_{m=0}^{n} \left(g_n^m \cos(m\Theta) + h_n^m \sin(m\Theta) \right) (a/r)^{n+1} P_n^m(\sin\phi)$$

2.5.5

g_n^m , h_n^m are IGRF coefficients corrected to the required epoch.

m,n are integers m = order n = degree

Θ is the geocentric longitude positive to the east of Greenwich.

ϕ is the geocentric latitude, positive to the North.

r is the distance from the centre of the Earth.

a is the Earth's radius

$P_n^m(\sin\phi)$ are associated Legendre polynomials of degree m, order n, given by

$$P_n^m(x) = \frac{1}{2^n n!} \frac{\left[\left(\varepsilon_m (n-m)!\ (1-x^2)^m\right)\right]^{1/2}}{\left[(n+m)!\right]^{1/2}} \cdot \frac{d^{m+n}}{dx^{m+n}} (x^2-1)^n$$

2.5.6

ε_m=1 if m=0

ε_m=0 if m=1,2...8

The secular variation is modelled on the basis of data from a number of magnetic observatories across the world. The distribution of the observations is not evenly spread. Hence the models are accurate in the location of the observatories but may not be so elsewhere, where the IGRF main field model could be up to several hundred nanoTesla in error.

The first revision of the IGRF consisted of the original main field model and a new model of the secular variation. The second revision of the IGRF included:
i) A definitive geomagnetic reference field for January 1st 1965, 1970 and 1975. This allowed linear interpolation for intervening dates and was as accurate as possible.
ii) The original geomagnetic reference field (IGRF 1980) model and a secular variation model for 1980-1985.

The most recent revision at the time of writing is a development of the fifth generation IGRF (Peddie 1992).

The IGRF 1980 main field model used in this study is based upon the satellite vector magnetic survey MAGSAT, taken at altitudes of 350 to 560 kilometres.

One of the problems involved in the use of the IGRF is that the data which is to be reduced is the total field. Reduction of the data consists of calculating the main field from the IGRF and subtracting this from the observed total field values. In the case of Britain, the subtracted values form a plane of approximate slope 2.1728nT per kilometre North and 0.259nT per kilometre West, with values reduced by 47,033 nT at the British National Grid false origin. This is related to the IGRF (±4nT) at epoch 1970.5 by applying corrections (for the central highlands of Scotland) as follows:

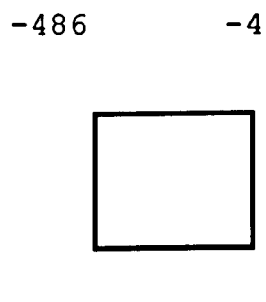

The values at the corners indicate the value to be subtracted at those positions of the map to obtain the IGRF value. Linear interpolation is used for points between the map corners.

The effect of subtracting this plane from the aeromagnetic data is illustrated schematically in profile form in figures 2.5.a and 2.5.b . Removal of the line representing the background involves subtracting the

background field from the data values point by point. The subtraction procedure has an effect upon the slope at any given position, and upon the positions of peaks and troughs, which are displaced to the left in the case shown. This suggests that care must be taken when attempting to understand B.G.S. aeromagnetic anomaly maps.

Using standard vector notation we can describe the main field at any point by

$$\mathbf{xi} + \mathbf{yj} + \mathbf{zk} \qquad 2.5.7$$

A subsidiary vector field ($\mathbf{ai} + \mathbf{bj} + \mathbf{ck}$) due to a magnetised rock will add to the main field to give a total field

$$T_m = ((x+a)^2 + (y+b)^2 + (z+c)^2)^{1/2} \qquad 2.5.8$$

This is the magnetic field measured during a survey.

In stripping the main field we first predict ($\mathbf{xi} + \mathbf{yj} + \mathbf{zk}$) using the IGRF. Then we find T from

$$T = (x^2 + y^2 + z^2)^{1/2} \qquad 2.5.9$$

Finally the main field, T, is subtracted from the measured field T_m to give

$$T_m - T = ((x+a)^2 + (y+b)^2 + (z+c)^2)^{1/2} - (x^2+y^2+z^2)^{1/2} \qquad 2.5.10$$

The anomalous field T_{anom} is $a\underline{i}+b\underline{j}+z\underline{k}$ which has a magnitude given by the expression

$$T_{anom} = (a^2+b^2+c^2)^{1/2} \qquad 2.5.11$$

The expressions 2.5.10 and 2.5.11 will only be equal when x=y=z=0, or when we carry out a full vector subtraction, as shown by

$$(x+a)\mathbf{i} + (y+b)\mathbf{j} + (z+c)\mathbf{k} - (x\mathbf{i} + y\mathbf{j} + z\mathbf{k}) = a\mathbf{i} + b\mathbf{j} + z\mathbf{k}$$

In addition to providing the correct value for the anomalous field, vector subtraction will not affect the position of the peaks or troughs present. However, only the IGRF is available in vector form. In northern latitudes the assumption is usually made that z is very much greater than x and y, with the result that the plane subtracted is near horizontal. This assumption is reasonable for rocks in which remanence has the same direction as the Earth's main field; in which induction is the main source of the field anomalies; for rocks near to the magnetic poles. It will not necessarily be true for rocks with strong horizontal remanence; for rocks away from the magnetic poles. In these cases , the positions of the peaks and troughs will be disturbed to some extent by the removal of the IGRF, and the shape of

the potential fields may be distorted. The distribution of energy within the power spectrum will also be affected.

For the central highland area of Scotland, the anomalies are substantially larger than the plane required to correct the data values to the IGRF. Any distortive effects are therefore ignored for the purpose of this study.

2.6 Topographic corrections

Topographic effects are frequently present in aeromagnetic and ground based data acquired over areas of high topographic relief. Aircraft flying over such areas usually fly a draped survey, following the general trend of the topography but ignoring sudden variations. Even in this situation, if the magnetic region is sub-surface it becomes impossible to eliminate large topographic variations. Draped surveys may reduce or enhance topographic effects depending upon the topography of the magnetically active rocks. It is difficult to deduce such effects from simple inspection of contoured data. Spurious mathematical correlations between topographic variations and magnetic field variations are a risk and resort must be made to all available evidence in deciding whether surface topography is causing an effect.

Topographic effects may be substantial enough to disguise magnetic anomalies. Although it is frequently desirable to try to remove such effects before attempting any interpretation, it is often very difficult to carry out topographic reduction. In the present case, although the low levels of susceptibility found in previous studies involving surface rocks from this area suggest that topographic effects should be negligible, it was felt worthwhile investigating topography as a possible contributor to the observed magnetic anomalies.

A number of authors have used different techniques to reduce topographic effects in magnetic field data, with varying degrees of success. Parker and Klitgord (1972) described a technique for the upward continuation of two-dimensional magnetic data from an uneven path. This technique was applied to the reduction and interpretation of sea floor magnetic profiles.

Plouff (1976) described a means of calculating the gravity and magnetic fields of polygonal prisms for application to magnetic terrain corrections in three dimensions. This particular method has the advantage over previous methods of allowing anomalies anywhere, inside or outside polygonal prisms, to be calculated both as a total field intensity and as a vector at any point.

Bhattacharyya and Chan (1976) derived analytic expressions in the form of a convolution of two functions for gravity and magnetic anomalies. They employed a Fredholm equation of the second kind to continue unevenly spaced potential field data and then applied this technique to the reduction of terrain induced anomalies in the San Juan mountains of Colorado (Bhattacharyya and Chan 1977). They were able to demonstrate the removal of terrain anomalies which could not be duplicated by frequency domain filtering or upward continuation. However, no ground based information was available to confirm there findings.

Blakely and Grauch (1983) described a means of directly calculating magnetic anomalies from digitized topography. Their program calculates the magnetic anomaly on a horizontal plane from 3 sets of gridded data that describe the top and bottom surfaces, and the magnetization, allowing the effect of topography to be estimated and removed.

Grauch and Campbell (1984) considered the effect of draped aeromagnetic surveys on terrain induced anomalies and concluded that such surveys, when corrected, may amplify the effects of terrain rather than reduce them.

Grauch (1985) developed a Fortran program to implement the variable magnetization terrain correction method for aeromagnetic data. This involved calculating synthetic terrain effects from digitised topographic data with an initial magnetization; subtracting this from the original data to get a first residual; using a linear regression method to estimate the magnetization from the residual at each point on the grid, then repeatedly iterating the process to reduce the residuals to a pre-determined level.

Grauch (1987) presented a new variable magnetization terrain correction method for aeromagnetic data from areas of high relief. He assumed that the

sources of interest have no geometric relationship to the terrain and was able to locate magnetization boundaries successfully. A point made in Grauch's work was that terrain correction will not usually be successful where topographic and geologic features coincide, since one will mimic the effect of the other. In the present study the edge of a large granite frequently occurs at the boundary between high and low topographic relief.

Pilkington and Roest (1992) described the use of a Taylor series method to drape aeromagnetic data from a constant altitude survey to a surface with a constant terrain clearance. They were able to use the radially averaged power spectrum of the aeromagnetic data to estimate the degree of filtering that would be required to reach a stable solution using the Taylor series.

A common problem with all of the above approaches lies in the lack of ground truth. Predicting the magnetic field associated with a rugged topography, and subtracting this field from survey data, is known to introduce anomalies where none exist. Rapid variations in magnetic topography may appear to be smooth due to aliasing or to the height at which measurements have been taken. Without ground based observations, particularly bore hole data, to confirm computer based findings, the techniques always carry a degree of subjectivity. Despite this, it was felt worthwhile to attempt to model the

topographic effect to get a feeling for the likely spatial variations that these could cause.

Many of the observed field variations were of low amplitude and could be due to a subsurface magnetised topography within the granites, or to the surface topographic variations. The algorithms developed by Plouff were felt to be a useful approach, permitting terrain reduction and providing a useful tool for work in other contexts. This approach had been used by Plouff following his 1976 paper and no comments on possible problems with it have appeared in the literature.

Plouff (1976) used the work of Talwani (1965) as his starting point. Talwani was able to model the magnetic field arising from a given magnetised body by breaking the body into a set of lamina. By using Simpson's rule, numerical integration to a high level of accuracy could be carried out. Talwani employed this technique to calculate the field values of individual bodies. However, the correct field near to a lamina cannot be found using this method. In addition different arrangements of lamina to form a body frequently give different results for the field. Plouff was able to overcome these defects by integrating the lamina formulae in the vertical plane.

The components of a magnetic anomaly were given by Plouff as:

$$X = J_x V_1 + J_y V_2 + J_z V_3 \qquad 2.6.1$$

$$Y = J_x V_2 + J_y V_4 + J_z V_5 \qquad 2.6.2$$

$$Z = J_x V_3 + J_y V_5 + J_z V_6 \qquad 2.6.3$$

where **X,Y** and **Z** are the components of the magnetic field of an anomalous body in the directions of the x,y, and z axes.The quantities V_1 to V_6 are volume integrals defined for a rectangular prism as

$$V_1 = -\sum_{i=1}^{2}\sum_{j=1}^{2}\sum_{k=1}^{2} s \tan^{-1} \frac{(b_j z_k)}{(a_i R_{ijk})} \qquad 2.6.4$$

$$V_2 = \sum_{i=1}^{1}\sum_{j=1}^{2}\sum_{k=1}^{2} s \ln (R_{ijk} + z_k) \qquad 2.6.5$$

$$V_3 = \sum_{i=1}^{2}\sum_{j=1}^{2}\sum_{k=1}^{2} s \ln(R_{ijk} + b_j) \qquad 2.6.6$$

$$V_4 = -\sum_{i=1}^{2}\sum_{j=1}^{2}\sum_{k=1}^{2} s \tan^{-1} \frac{(a_i z_k)}{(b_j R_{ijk})} \qquad 2.6.7$$

$$V_5 = \sum_{i=1}^{2}\sum_{j=1}^{2}\sum_{k=1}^{2} s \ln(R_{ijk} + a_i) \qquad 2.6.8$$

$$V_6 = -\sum_{i=1}^{2}\sum_{j=1}^{2}\sum_{k=1}^{2} s \tan^{-1} \frac{(a_i b_j)}{(z_k R_{ijk})} \qquad 2.6.9$$

$$R_{ijk} = \sqrt{a_i^2 + b_j^2 + z_k^2} \qquad 2.6.10$$

$$s = s_i s_j s_k \qquad s_1 = -1 \qquad s_2 = +1$$

a_i ,b_j and z_k refers to the location of a corner of the prism relative to a field point.

Having calculated the components **X,Y** and **Z** it is now possible to calculate the total field anomaly using

$$T = \sqrt{(lH + X)^2 + (mH + Y)^2 + (nH + Z)^2} - H \qquad 2.6.11$$

Here **l,m** and **n** are the direction cosines of the Earth's main field vector. H is the magnitude of the Earth's main field.

This equation (2.6.11) is slightly different to that of Plouff (1976) equation 10 page 733. A printing error appears to be present in his paper.

2.7 Reduction to the pole

The presence of a rock polarization vector that differs in direction from that of the main field can have significant effects upon the shape and location of the observed magnetic field. These effects will vary depending upon where on the Earth the magnetised rock is located. The effect is complicated by the distance of the observer from the rock unit and the thickness of the rock unit. For large vertical thicknesses the magentic field has the characteristics of a monopole and the field varies as $1/r^2$. For small thicknesses, the base of the magnetised layer has a larger effect and the magnetic field now varies as $1/r^3$, r being the distance of the observer from the source.

In the present work, it is not clear whether the magnetic anomaly around the Cairngorm granites comes from within the granites or from an area around the edge of the granites. It is possible that remanent magnetisation of the underlying rocks is having an effect upon the observed field. Thus it is important to understand the strengths and limitations of the technique of reduction to the pole, and to have some understanding of the mathematical processes involved.

The distortive effects of remanent magnetization on the magnetic anomaly associated with a rock were recognised as early as 1951 by Vacquier and his

co-workers. Although the effects were recognised as a problem, removing them was not possible until the initial development of the technique for reduction to the pole by Baranov (1957). In Baranov's original paper he developed the mathematics of the numerical techniques for reduction to the pole in the spatial domain. In a later paper (Baranov and Naudy 1964) he further extended the technique and refined the details to allow the practical application of the operation of reduction to the pole of magnetic data in the spatial domain.

The operation of reduction to the pole in the spatial or frequency domain is a means of eliminating the effect of the polarization vector and looking at the magnetic data as if it were at the North pole. This gives the simplest possible symmetry, with the magnetic field anomaly lying directly over the rock units giving rise to it. However, the presence of other rock units with different polarization vectors can give rise to a situation in which some anomalies become more complex when the data is reduced to the pole. If the rock units are close together or overlying, it may be impossible to carry out the reduction operation. In the early stages of reducing data to the pole, although the main field is well known, the polarization field, especially from buried rocks, is normally unknown. Information may be available on magnetisation of surface rocks or their

location on the surface of the Earth at the time of cooling. Hence the probable direction of remanence can be inferred. It is frequently necessary to attempt a trial and error approach using different estimates of the polarization vectors. The success of the reduction operation can then be judged on the basis of improvement in the degree of symmetry of the magnetic field and the geological reasonableness of the transformed data by comparing the reduced anomalies with local geological maps. If the polarisation vector is within 10 degrees of the horizontal, special numerical techniques will be needed to carry out reduction to the pole.

Calculation of the total magnetic field intensity from a variety of geometric shapes has occupied a large number of workers. The work of Vacquier et al (1951) concentrated on the magnetic effects of block shaped bodies and has been used extensively. Bhattacharyya (1964) was able to extend this work to the case of prism shaped bodies with arbitrary polarization, assuming uniform magnetization throughout the body. He also derived expressions for the first and second derivatives of the magnetic field.

Bhattacharyya used, as a starting point, the field element dF produced by a given volume element dV

$$dF = I_p \cdot \frac{\delta^2}{\delta s\, \delta t}\left(\frac{1}{r}\right) dV \qquad 2.7.1$$

where

I_p is the rock polarization intensity

δs is a length element along the polarization vector

δt is a length element along the Earth's main field line

r is the distance from the source

Starting from this Bhattacharyya was able to show that the field element from a prism with an arbitrary polarization vector is given by

$$dF = I_p\left[-\frac{1}{r^3}\cos\phi + \frac{3}{r^5}\left[lL(\alpha - x)^2 + mM(\beta - y)^2 + nN(\gamma - z)^2 + \alpha_{12}(\alpha - x)(\beta - y) + \alpha_{13}(\alpha - x)(\gamma - z) + \alpha_{23}(\beta - y)(\gamma - z)\right]\right] d\alpha\, d\beta\, d\gamma \qquad 2.7.2$$

where

$$\alpha_{12} = Lm + Ml$$

$$\alpha_{13} = Ln + Nl$$

$$\alpha_{23} = Mn + Nm$$

l,m,n are the direction cosines of the Earth's field

L,M,N are the direction cosines of the polarization vector.

$d\alpha$, $d\beta$ and $d\gamma$ are length elements along the x, y and z axes respectively ($d\alpha d\beta d\gamma$ is thus a volume element)

From the expression for dF given in 2.7.2

Bhattacharrya was able to analytically evaluate the total field intensity by integrating over the volume element. This gave the result

$$F(x,y,0) = I_p\left[\frac{\alpha_{23}}{2}\log\left[\frac{r_n - \alpha_1}{r_n + \alpha_1}\right] + \frac{\alpha_{13}}{2}\log\left[\frac{r_n - \beta_1}{r_1 + \beta_1}\right]\right.$$

$$-\alpha_{12}\log\left[r_0 + h\right] - 1L\tan^{-1}\left[\frac{\alpha_1\beta_1}{\alpha_1^2\, r_0 h - \beta_1^2}\right]$$

$$- mM\tan^{-1}\left[\frac{\alpha_1\beta_1}{r_0^2 + r_0 h - \alpha_1^2}\right]$$

$$\left. + nN\tan^{-1}\left[\frac{\alpha_1\beta_1}{r_0 h}\right]\right]_{\alpha_L\ \beta_L}^{\alpha_u\ \beta_u} \qquad 2.7.3$$

where α_u, β_u are the upper limits of the integration

α_L, β_L are the lower limits of the integration

$\alpha_1 = \alpha - x$

$\beta_1 = \beta - y$

x,y,z are position coordinates and the ground surface is at z = 0.

$r_0^2 = (x - \alpha)^2 + (y - \beta)^2 + (z - \gamma)^2$

$\alpha_u = \alpha_0 - x$

$\beta_u = \beta_0 - y$

$\alpha_L = -\alpha_0 - x$

$\beta_L = -\beta_0 - y$

$2\alpha_0$, $2\beta_0$ are the horizontal dimensions of the prism.

A problem with this approach lies with the method employed to find the field from a prism of limited depth extent. This involves calculating the field from a prism that extends from the top surface down to infinity on a plane (at z = 0), and subtracting from this the field calculated from a prism that extends from the bottom surface down to infinity, the calculation being done on the same plane.

The field is treated as a scalar quantity by the integration when, in reality, it is a vector quantity. For prisms of small depth extent the field lines from each infinite depth prism at any given point will be approximately parallel and can be subtracted as if they were scalar quantities (each calculated field intensity at a point is actually the resultant of all field lines arising from the prism and passing through the given point). For prisms of large depth extent the field lines from the lower prism will have different directions to those from the upper prism, but the intensity of the field from the deep prism will be negligible. In both cases the error in treating the field values as scalar will be small. However, for bodies of medium depth extent (vertical thickness) the magnetic field vectors will both be significant and the directions different. A scalar subtraction will not give an accurate result in this case.

Bhattacharyya (1966) derived an algebraic expression for the Fourier transform of the total magnetic field anomaly due to a rectangular prismatic body with arbitrary polarization. By deriving the expression analytically, Bhattacharyya was able to give the exact expression for the Fourier transform as

$$F(k_x,k_y) = 2\pi I_p \left[-lLk_x^2 - mMk_y^2 + nN(k_x^2 + k_y^2) - \alpha_{12}k_xk_y \right.$$
$$\left. +j\alpha_{13}k_x(k_x^2 + k_y^2)^{\frac{1}{2}} + j\alpha_{23}k_y(k_x^2 + k_y^2)^{\frac{1}{2}}\right].I \qquad 2.7.4$$

where

$$I = \frac{4}{k_xk_y}\mathrm{Sin}\left[\frac{k_xb}{2}\right]\mathrm{Sin}\left[\frac{k_yc_0}{2}\right]\frac{e^{-h(k_x^2+k_y^2)^{\frac{1}{2}}}}{(k_x^2 + k_y^2)}$$

k_x = wavenumber along the x-axis

k_y = wavenumber along the y-axis

b_0, c_0 are body dimensions.

The expression 2.7.4 for $F(k_x,k_y)$ can be written more succinctly as:

$$F(k_x,k_y) = 2\pi I_p . D(k_x,k_y).B(k_x,k_y).H(k_x,k_y) \qquad 2.7.5$$

where

$$D(k_x,k_y) = \left[-lLk_x^2-mMk_y^2+nN(k_x^2+k_y^2)-\alpha_{12}k_xk_y \right.$$
$$\left. +j\alpha_{13}k_x(k_x^2+k_y^2)^{\frac{1}{2}} + j\alpha_{23}k_y(k_x^2+k_y^2)^{\frac{1}{2}}\right] \Big/ (k_x^2+k_y^2)$$

$$H(k_x, k_y) = e^{-h(k_x^2+k_y^2)^{\frac{1}{2}}}$$

$$B(k_x, k_y) = \frac{4}{k_x k_y} \operatorname{Sin}\left[\frac{k_x b_0}{2}\right] \operatorname{Sin}\left[\frac{k_y b_0}{2}\right]$$

The effect of converting the expression for the magnetic field of a prism into one for its continuous spectrum, is to separate the field into factors that depend upon depth to the top surface $H(k_x, k_y)$, horizontal dimensions $B(k_x, k_y)$ and a dimensionless factor $D(k_x, k_y)$ that depends only upon the geomagnetic latitude of the prism and the polarization characteristics.This considerably simplifies any attempt to correct for the effects of the geomagnetic latitude and the polarization of the body.In the space domain these factors are convolved together.

Spector and Grant (1970) in describing a statistical approach to the interpretation of aeromagnetic data, gave an expression equivalent to the Fourier transform derived by Bhattacharyya. They used polar wavenumber coordinates to describe the power spectrum as

$$E(r,\theta) = 4\pi^2 k^2 . e^{-2\bar{h}r} . (1-e^{-tr})^2 . S^2(r,\theta) . R_T^2(\theta) . R_k^2(\theta) \qquad 2.7.6$$

$S(r,\theta) = (\sin(arCos\theta)/arCos\theta)(Sin(brCos\theta)/brCos\theta)$

$S(r,\theta)$ represents the effect of the horizontal dimensions of the prism and is equivalent to Bhattacharyya's $B(k_x,k_y)$ term.

$$R_T(\theta) = (n^2+(lCos(\theta)+mSin(\theta))^2)^{\frac{1}{2}} \qquad 2.7.7$$

$$R_K(\theta) = (N^2+(LCos(\theta)+MSin(\theta))^2)^{\frac{1}{2}} \qquad 2.7.8$$

These terms are together equivalent to Bhattacharyya's dimensionless factor $D(k_x,k_y)$.

k is the magnetic moment/unit depth.

$r=(k_x^2+k_y^2)^{\frac{1}{2}}$

$\theta=atan(k_x/k_y)$

$\bar{h}$= average depth to top of prism

t=thickness of prism

a,b are the horizontal dimensions of the prism

Reduction to the pole now involves removing $D(k_x,k_y)$ from Bhattacharyya's expression, or, equally, removing $R_T(\theta)$ and $R_K(\theta)$ from that due to Spector and Grant. These operations are not equivalent. The effect of reduction to the pole upon the induced magnetic field from a prism is shown in figure 2.7.a.

Bhattacharyya's expression shows the Fourier transform as a complex number A+iB. Since the factor $D(k_x,k_y)$ is also a complex number of the form C+iD,

reduction to the pole is carried out by the operation $(A+iB)/(C+iD)$. The equivalent operation for $E(r,\theta)$ is $E(r,\theta)/(R_T(\theta)R_K(\theta))$. However, $E(r,\theta)$ is equal to (A^2+B^2) and does not contain the phase information present in the Fourier transform. In addition Bhattacharyya has used a geophysical coordinate convention with the vertical axis positive downward, where Spector and Grant use the mathematical convention of a z axis positive in the upward direction.

The initial developments of the operation of reduction to the pole have been followed by other developments aimed at reduction under specific circumstances. Aina (1986) described several variations on the theme of reduction to the pole in both the space and frequency domain, with the aim of accurately locating the edges of a causative body. Ervin(1976) described an algorithm for reducing data to the pole in the frequency domain. Ervin's approach was limited by consideration only of inductive effects and could not take account of situations where the rock polarization vector had a different direction to that of the Earth's main field. Fedi(1989) described a more general reduction to the pole technique for situations where the rock magnetization vector was of significant intensity and had a different direction to the Earth's main field vector. Kis et al (1989) described the use of a linearized function to determine the polarization vector direction based upon

the use of Poisson's relation. Lack of information on the polarization vector is a major handicap when attempting reduction to the pole. It is normal practice to guess the direction of the vector, reduce the data to the pole, and then estimate whether the result is correct based upon geological and mathematical criteria. Kis (1990) described the operation of reduction to the pole and reduction to the equator. The latter method is an alternative to the use of numerical techniques aimed at avoiding instabilities caused by finite discontinuities.

Arkani-Hamed and Urquhart (1990) carried out a large scale reduction to the pole of magnetic anomalies over North America. They were able to take into account directions of both the core field and the crustal field and to relate gravity and magnetic data in looking for common sources of the potential fields.

Substantial amounts of computer processing time can be required for reduction to the pole of large matrices of data. In addition, any attempt to reduce to the pole data that has been acquired in equatorial regions, where the Earth's main field vector is near horizontal, will not succeed using the approaches described above due to numerical instabilities. A number of authors have attempted to overcome the problems of numerical instability in low latitude cases. Arkani-Hamed (1988) described the use of inverse theory in the

frequency domain to reduce magnetic anomalies in low latitudes to the pole. Hansen and Pawlowski (1989) described reduction to the pole at low latitudes by the use of filter theory. Their aim was to reduce data to the pole and to reduce artefacts that can arise during the data processing. Their procedure was aimed particularly at noisy low latitude data, and does destroy much of the high frequency information within the data. Kis (1990) described a similar filtering approach in reducing magnetic data to the pole. These approaches, while necessary for low latitude data, can generally be avoided for high latitude data, even when rock polarization vectors are within fifteen degrees of the horizontal. Numerical instability usually starts to cause substantial problems when attempting to reduce data with vector directions within ten degrees from the horizontal.

Spector (1968) described the operation of double reduction to the magnetic pole. Apart from Spector's original work no publicised use of this extension to the basic reduction technique can be found. Reducing the main field and polarization field to the pole usually produces an increase in the symmetry of the observed magnetic anomaly and a closer spatial relationship between the field contours and the rocks giving rise to them. However, as mentioned in the previous section, we may have several magnetically active

rock units present with different polarization vectors. Reduction to the pole will cause an increase in asymmetry for those contours caused by apolarization vector whose direction is significantly different from the one assumed during the reduction process. The increase in asymmetry may be small and hard to detect.

Repeating the operation of reduction to the pole a second time on the same data set will further enhance any asymmetries present. For rocks with induction as the major effect, but with a small remanent vector of different direction to that of the main field, it is possible to detect the presence of the remanence in this way if the magnitude of the vector is large enough. The initial reduction assumes induction only ie from equations 2.7.7 and 2.7.8

$$R_T(\theta) = R_k(\theta)$$

This correction will reduce asymmetry due to the induced field, but will enhance any asymmetry due to a remanent field. Repeating the reduction will again enhance the asymmetries present.

2.8 The frequency spectrum

All data manipulation carried out in the frequency domain could equally well be carried out in the space domain, avoiding the use of a fast Fourier transform. However, it would then be necessary to use filtering techniques in the space domain to carry out the operations such as reduction to the pole and pseudogravimetric transformation. Indeed, reduction to the pole was originally carried out in the space domain by Baranov. The advantages of working in the frequency domain include simplicity of the filtering operations and greater ease of understanding of the processes being carried out.

The filtering operations generally require a specified filter to be multiplied into the Fourier transformed data. Examples of such filters include:

Upward continuation	$e^{-2\pi z(k_x^2 + k_y^2)^{\frac{1}{2}}}$	2.8.1
Downward continuation	$e^{2\pi z(k_x^2 + k_y^2)^{\frac{1}{2}}}$	2.8.2
First vertical derivative	$2\pi(k_x^2 + k_y^2)^{\frac{1}{2}}$	2.8.3
Second vertical derivative	$4\pi^2(k_x^2 + k_y^2)$	2.8.4

In these formulae, z is the depth or height for continuation; k_x and k_y are wavenumbers. These filters have their origins in the fundamental properties of the

Fourier transform. For example, the shift property of a Fourier transform is given by:

$$f(x - a) = e^{-2\pi i a k_x} . F(k_x) \qquad 2.8.5$$

Equation 2.8.1 and 2.8.2 show shifts from $f(x,y,z=0)$ in the vertical direction to $f(x,y,-z)$ and $f(x,y,z)$ respectively, noting that the z axis is positive downward in the northern hemisphere.

2.9 The fast Fourier transform

The Fourier transform is one of a set of related integral transforms used in signal processing to convert data between the time (or space) and frequency domains. Originating from the Fourier series, the formal definition of a signal $f(x,y)$, and its Fourier transform ($F(k_x, k_y)$) is given by:

$$F(k_x, k_y) = \int_{-\infty}^{\infty} f(x,y).e^{-2\pi i(k_x x + k_y y)}\,dxdy \qquad 2.9.1$$

where

$$f(x,y) = (1/2\pi) \int_{-\infty}^{\infty} F(k_x, k_y).e^{2\pi i(k_x x + k_y y)}\,dxdy \qquad 2.9.2$$

$F(k_x, k_y)$ and $f(x,y)$ are a transform pair. Equation 2.9.1 is a description of how the energy in the signal $f(x,y)$ is distributed in the whole frequency range of the resulting Fourier series. Equation 2.9.2 is a description of the signal as an infinite set of weighted exponential functions, or, more usefully, as a set of weighted orthogonal sine and cosine functions. Thus 2.9.1 can be rewritten

$$F(k_x, k_y) = (k_0, k_0) + \sum_{\substack{x=1 \\ y=1}}^{\substack{n \\ m}} (k_x, k_y).e^{-i2\pi(k_x x + k_y y)} \qquad 2.9.3$$

Euler's relationship, $e^{ix} = Cosx + iSinx$ allows 2.9.3 to be rewritten in a more useful form as a sum of Cosine and Sine functions, ie as

$$F(k_x, k_y) = \sum_{\substack{x=1 \\ y=1}}^{\substack{n \\ m}} (k_x, k_y)\,(Cos2\pi(k_x x + k_y y) + iSin2\pi(k_x x + k_y y) \qquad 2.9.4$$

The Fourier transform has limitations which must be kept in mind when applying it to transform data. The Fourier integral can only exist if the right hand side of equation 2.9.1 is finite. Since e^{ix} has magnitude 1 at all times, then the condition for the existence of $F(k_x, k_y)$ becomes the Dirichlet condition

$$|f(x,y)| < \infty \qquad 2.9.5$$

In addition to this the data set $f(x,y)$ must have no more than a finite set of discontinuities. Both conditions are normally met by signals of geophysical interest.

The need for an infinite integration interval is fulfilled by assuming that the data set repeats itself indefinitely in all directions. In copying the data set in the x and y directions, the presence of non-zero means or steep trends in the digitized data can cause distortion in the low frequency end of the spectrum. Such distortion usually shows up as spurious oval shaped

anomalies at the edge of the filtered data. To overcome this, some pre-conditioning of the data is usually necessary.

Removal of the mean and linear trends is one way of overcoming this problem. Surrounding the data map with zeroes or with extra data is another. The most common technique is to use a circular window function.

The basis of the present methods used for calculating the Fourier transform were developed by Cooley and Tukey (1965). Following the Cooley and Tukey paper and its application by Gentleman and Sande (1966) the technique became widely known and applied.

The Fourier transform of N data points can be shown to be equal to the sum of two Fourier transforms of N/2 data points. These could be further subdivided in the same way until we are dealing with the Fourier transforms of 2 values, provided that $N=2^x$, where x is an integer. This then allows the efficient use of binary arithmetic to find the Fourier transform. An algorithm designed to work in this way is known as a fast Fourier transform (FFT).The algorithm employed in the present work is the mixed radix fast Fourier transform (FFT) due to Singleton (1967).

Many FFT algorithms deal with the special case where the number of data points is some integer power of

2. Some algorithms will accept products of other factors in any particular combination. Singleton's algorithm is one of these. It permits a wide range of data sets to be used, greatly increasing the convenience of use of the FFT.

The number of calculations required to calculate a spectrum is proportional to N^2. Thus the time to calculate a spectrum is proportional to N^2. Many of the multiplications are repetitions of one operation. The FFT eliminates these repetitions, and as a result requires a time proportional to $N.\log_2 N$ to carry out the computations. Singleton's algorithm is particularly good at this for large data sets, even when the number of values is not a factor of two. As an example, the computer time improvement in using Singletons' algorithm on 100 points is a factor of 15 times faster than most other FFT algorithms available. For 4096 points this rises to 340 times faster. As the number of data points increases so the gain of the algorithm increases. For the 100 by 100 arrays used in this study, the time saving is substantial.

2.10 The power spectrum

The power spectrum, or power spectral density, describes the distribution of signal power in the frequency domain. In magnetic field interpretation the power spectrumplays an important role since it contains much of the information about the magnetic sources. With the introduction of the Fast Fourier Transform and modern computers, calculation of the power spectrum on a routine basis became feasible. Of the possible methods of computing the power spectrum, the use of the Fast Fourier Transform proved to be the fastest (see for example Bingham et al (1967)).

The power spectral density gives the power in each frequency or wavenumber interval (the power at a given frequency or wavenumber is effectively zero since the number of frequencies or wavenumbers is potentially infinite).

When the spectrum G(w) is known, the power spectrum can be found from

$$P(w) = |G(w)|^2 = G(w).G^*(w) \qquad 2.10.1$$

Here $G^*(w)$ is the complex conjugate of G(w).

For most geophysical situations the power spectral density is red, ie most of the power lies in the low wavenumber end of the spectrum, very little at the high wavenumber end.

The power spectrum is the frequency domain counterpart of the autocorrelation function, which can be written as:

$$r_{xx}(\tau) = \lim_{x \to \infty} \frac{1}{x} \int_{-x/2}^{x/2} f(x).f(x+\tau).dx \qquad 2.10.2$$

The autocorrelation is thus the average of the product of a signal f(x) with a version of itself shifted by an amount τ. In the case of sampled data signals 2.10.2 has to be modified to

$$r_{xx}(k) = \lim_{N \to \infty} \frac{1}{2N+1} \sum_{m=-N}^{N} (x_m.x_{x+m}) \qquad 2.10.3$$

where x_m and x_{x+m} are two signal samples separated by $k\Delta x$ metres. Each component in the signal f(x) gives rise to a term in the autocorrelation function with the same period in the space shift variable as the original component has in the variable x, and an amplitude signal equal to half the squared value of the original. The autocorrelation function and the power spectral density are fourier transform pairs. Both have lost all phase information.

Skilbrei and Kihle (1992) described the use of the autocorrelation function for estimating the depth to magnetic basement. The technique, whilst predicting accurately the required depth, requires an independent estimation of the width to depth ratio or an assumption

that this ratio lies between 1.5 and 4.0. This makes the technique less useful than the one employed in the present study based upon the power spectrum.

Many types of geophysical signals have some power in the high frequency end. Cordell and Grauch (1982), in comparing the discrete and integral fourier transforms of a signal, suggested that the high frequency spectral tail is inevitably present in the discrete Fourier Transform as a result of sampling a limited number of times over a finite range. In addition, by deliberately adding noise to a signal, the high frequency end of the spectrum can be raised upward without affecting the slope of a graph of power against frequency.

The total signal power is also given by the expression:

$$P = \frac{1}{\pi} \int_{-\infty}^{\infty} P(w).dw \qquad 2.10.4$$

where P(w) is the power in a wavenumber or frequency interval dw. In the present case P(w) reflects the statistical distribution of the parameters of the magnetically active bodies giving rise to the aeromagnetic field under consideration.

The first central moment (y_1) and second central moment (y_2) are given by

$$y_1 = \int_{-\infty}^{\infty} x.P(x).dx \qquad 2.10.5$$

$$y_2 = \int_{-\infty}^{\infty} (x-\bar{x})^2.P(x).dx \qquad 2.10.6$$

where $P(x)$ is the probability associated with x.

The power in the signal can also be written as:

$$P = y_2 + y_1^2$$

y_1^2 is the D.C. power
y_2 is the AC power, or the power in all other frequencies apart from the zero or DC frequency.

Third and higher order central moments which pay more attention to the extreme values of a signal are useful in looking at the skew and symmetry of a signal.

A number of workers have made use of these statistics. For example Naidu (1970) used the first order statistics (mean, variance, skewness and probability distribution function) to study an area of southern Ontario. He was able to demonstrate variations in these statistics related to variations in the underlying geology, in particular to the strike of the local rocks. Bhattacharyya and Leu (1975) developed a method of interpreting the first order moments of the spectrum of an anomaly . They used this method to interpret an aeromagnetic anomaly in the Yellowstone National Park.

In plotting the power contained in particular

frequency intervals in this work two stages were used. First, the power was calculated in the normal fashion, using equation 2.10.1 on the data after passing the data through a fourier transform. The data was two dimensional, resulting in a two dimensional power spectrum. This form of the power spectrum contains information on spatial trends within the data. Plots of the power spectrum used in this work follow the generally accepted convention of plotting log P as the values arise from the fourier transform. The wavenumber resolution of 0.02 per kilometre used for the aeromagnetic data requires that to convert the presented values of the power spectrum to the true values of power density per square kilometre all values need to be multiplied by 2500. The second stage used in dealing with the power spectrum is to convert the two dimensional power spectrum into a one dimensional azimuthally averaged power spectrum. This will be dealt with in the next section.

2.11 The azimuthally averaged power spectrum.

The azimuthally averaged power spectrum is an averaged version of the two dimensional power spectrum. Concentric circles are traced out on the two dimensional power spectrum. The power between each pair of concentric lines is calculated, and the results are displayed as the power density per unit area of wavenumber space at constant values of wavenumber. The logarithm of the result is plotted against the wavenumber.

There are several problems with this approach. In particular, if there are dominant trends within the two dimensional data, these trends will show up in the wavenumber/frequency spectrum. This will add to the power density in some areas of the azimuthally averaged power spectrum, causing the plot of the logarithm of the power density against wavenumber to become bumpy. It is possible to carry out the averaging process in a way which takes account of the trends (for example by using an ellipse rather than a circle to carry out the averaging process) but this has not been necessary in the present work.

The importance of the azimuthally averaged power spectrum is related to the information that it contains. Bhattacharyya (1966) showed how the power spectrum related to information on the parameters of the

body causing the magnetic anomaly.

Spector and Grant (1970) related Bhattacharyya's work to the power spectrum and in particular to the statistics of the power spectrum. They used as their starting point the definition of the power spectrum from a prism:

$$\langle E \rangle = \int \ldots\ldots \int E(r,\theta) . \phi(a,b,t,h,I,D,k)\ dV \qquad 2.11.1$$

where

$\langle E \rangle$ is the ensemble average of $E(r,\theta)$

$E(r,\theta)$ is the power spectrum

2a,2b are the horizontal dimensions of the body.

t is the vertical thickness of the body.

h is the depth to the top surface of the body.

I is the inclination of the polarization vector.

D is the declination of the polarization vector.

k is the magnetic moment per unit depth.

ø is the ensemble joint frequency distribution for the parameters defined above.

dV is a volume element in the statistical parameter space.

If it can be assumed that the parameters above vary independently of each other, then, from the fundamental postulate of statistical mechanics (eg Lindsay (1941)), we can write

$$\phi(a,b,t,h,I,D,k) = \phi(a).\phi(b).\phi(t).\phi(h).\phi(I).\phi(D).\phi(k) \qquad 2.11.2$$

By using the simplifying assumption that each parameter has a rectangular distribution and is uniformly distributed within some interval (for example h is in the interval $(h \pm \Delta h)$, Spector and Grant were able to rewrite equation 2.11.1 as

$$\langle E(r,\theta)\rangle = 1/V \int.....\int E(r,\theta).da.db.dt.dh.dI.dD.dk \qquad 2.11.3$$

here V is the statistical volume of the 7 dimensional parallelepiped which has been defined in terms of the rectangular frequency distribution functions a,b,t,h,I,D and k. The upper and lower bounds on the integrations are set by the rectangular distribution. This allows $\langle E(r,\theta)\rangle$ to be written as in equation 2.11.3, which is an equivalent expression for $\langle E(r,\theta)\rangle$ (equation 2.7.6) in terms of the statistical parameters. $S(r,\theta)$ relates the power spectrum to the dimensions of the causative body.

In carrying out the azimuthal averaging of the power spectrum, we are taking the average of $\langle S(r,\theta)\rangle$ with respect to θ ie

$$\langle S^2(r)\rangle = \frac{1}{\pi}\int_0^{\pi}\langle S^2(r,\theta)\rangle d\theta \qquad 2.11.4$$

The azimuthally averaged power spectrum can now be written as

$$\langle E(r)\rangle = 4\pi^2k^2\langle e^{-2hr}\rangle\langle(1-e^{-tr})^2\rangle\langle S^2(r)\rangle\langle R_t(\theta)\rangle\langle R_k^2(\theta)\rangle \qquad 2.11.5$$

Rather than plot $\langle E(r) \rangle$ against wavenumber it is normal practice to plot $\ln\langle E(r) \rangle$ against wavenumber (or frequency). The reason for this becomes obvious when the logarithm of 2.11.5 is taken

$$\ln(\langle E(r) \rangle) = \ln(4\pi^2 k^2) + \ln\langle e^{-2\bar{h}r} \rangle + \ln\langle (1 - e^{-tr})^2 \rangle + \ln\langle S^2(r) \rangle + \ln\langle R_t^2(\theta) \rangle + \ln\langle R_k^2(\theta) \rangle \qquad 2.11.6$$

The effect of taking logarithms is to factorise the expression into simple additions of variables relating to the magnetisation, depth, depth extent, size and polarisation vector directions.

The value of $\bar{h}$, the average depth, is present in only one factor $\langle e^{-\bar{h}r} \rangle$. The slope of the power spectrum was shown by Spector and Grant (1970) to be dominated by the term $\exp(-2\bar{h}r)$, provided that $\Delta h \leq 0.5\bar{h}$. Hence the power spectrum can be used to find the value of $\bar{h}$ if this assumption is met. Other assumptions relate to the type of probability distribution of the average depth $\bar{h}$. Gaussian probability distributions will affect the slope of the power spectrum causing an increased concavity with wavenumber and deviation away from a straight line.

The effect of the expression $(1-e^{-tr})^2$ when combined with $e^{-2\bar{h}r}$, is to produce a peak within the power spectrum, the position of which will shift to the low frequency/wavenumber end of the power spectrum as t

increases. Finally, the effect of the horizontal dimensions in $\langle s^2(r) \rangle$ is to increase the rate of decay of the power spectrum with wavenumber. Uniformly magnetised rock masses of large horizontal dimensions will produce a very convex power spectrum which is difficult to interpret.

The correctness of the initial assumption of independent rectangular distributions of the parameters in 2.11.1 depends upon the geology of the area under consideration. Given the high levels of variation both of geological surfaces and of the magnetic susceptibility of the rocks, the assumption of independence, or at worst of very weak coupling of the parameters, seems to be reasonable. A further, implied, probabilistic assumption is that a relatively large number of bodies are present. Although this is not strictly the case for a single rock unit, each irregularity in susceptibility or topography may be classed as an independent body. If the area from which the original data is drawn is large enough, then the presence of a reasonably large number of independent magnetic field anomalies can be guaranteed. For one ensemble of sources at a constant depth, the logarithm of the power spectrum decays in an approximately linear fashion. For two ensembles of sources at different depths, the decay of the power spectrum usually shows two distinct linear sections.

2.12 Pseudogravimetric and pseudomagnetic transformations

The pseudogravimetric transformation is a technique for converting a magnetic anomaly into an equivalent gravity anomaly using an assumed density contrast which is proportional to the magnetization contrast of the body. The original idea was introduced by Baranov (1957) who showed how to calculate the transformation for the case when the polarization vector lies in the same direction as the Earth's magnetic field vector. Bott et al (1966) used the technique to estimate the direction of magnetization of a body assuming a constant direct of magnetization throughout. They extended the theory produced by Baranov to a more general one involving polarization vectors of arbitrary direction.

In many respects, the technique of pseudogravimetric transformation is similar to that of reduction to the pole. For example, it can be shown that the vertical gradient of the pseudogravimetric anomaly is directly proportional to the anomaly reduced to the pole.

Cordell and Taylor (1971) calculated the pseudogravimetric transformation by deriving the equivalent relationship in the frequency domain. By applying the transformation, and then transforming the

data into the space domain using the fourier transform, they were able to calculate the pseudogravimetric anomaly of a north atlantic seamount.

The basis underlying this technique is Poisson's relationship

$$V = \frac{\Delta J . \nabla U}{4\pi . \Delta\rho . G} \qquad 2.12.1$$

where

U is the gravitational potential at a given point

V is the magnetic potential at the given point

ΔJ is the magnetization contrast

$\Delta\rho$ is the density contrast

G is the gravitational constant

The magnetic anomaly at a given point may be written as

$$T(x,y,z) = \frac{\mu o . \Delta J}{4\pi \Delta\rho G} \frac{d^2 U}{ds\ dy} \qquad 2.12.2$$

μ_o is the magnetic permeability of free space

d/ds is the rate of change along the direction of the Earth's main field.

d/dy is the rate of change along the direction of magnetization of the body

This assumes a density contrast $\Delta\rho = \frac{\mu o \Delta J}{4\pi G}$ 2.12.3

that is constant, and hence that $\Delta J/\Delta\rho$ is constant. This assumption is usually questionable, but once made allows the calculation of a theoretical gravitational potential from which the theoretical gravity anomaly can be calculated. This is the pseudogravity anomaly.

Like all such techniques, there are limitations that must be borne in mind. In determining the boundaries of a magnetically active body, geological considerations are paramount. For example, Grauch and Cordell (1987) pointed out that when the geological boundaries are non-vertical, the horizontal gradient will be offset from the boundary by a factor proportional to the depth to the top surface of that boundary. Nevertheless, as discussed by Blakely and Simpson (1986), the pseudogravimetric transformation can be useful in locating the boundaries between rock units. Blakely and Simpson (1986) devised a sequence of programs to locate the boundaries of a rock unit automatically. They then used these to successfully locate geological boundaries in the Stillwater complex of Montana and on the isostatic residual gravity anomalies of the U.S.A.

Muniruzzaman and Banks (1989) reversed this process to derive a pseudomagnetic map from a gravity map, in order to estimate the magnetization beneath the Lake District. Gravity data for an area of northern England was converted into a pseudomagnetic map by use of the Poisson relationship. The pseudomagnetic map was used

to calculate a response function and a coherence value between this map and the magnetic map reduced to the pole. An estimate of the ratio of magnetization contrast to density contrast was obtained, in addition to an estimate of the direction of the total magnetization vector based upon a zero imaginary response and a maximum magnetic/pseudomagnetic coherence. One of the major problems encountered with this approach is the effect of the shape factor <S(r)> discussed in 2.11. Rock masses can produce magnetic anomalies of considerable horizontal dimensions, distorting the power spectrum and interfering with attempts to interpret it.

The pseudogravimetric transformation of the aeromagnetic data for the Cairngorm and Loch Doon areas has been carried out and is discussed later.

Chapter 3 The Cairngorm granites.

Granites have been classified in numerous different ways. The schemes of classification are generally based upon rock series, source rocks, chemical composition and tectonic environment.

Classifications based upon rock series reflect the effects of partial melting, fractionation and mixing. A number of rock series are in use, categorising granites using major and trace element levels and significant ratios of these elements.

Classification by source rock attempts to recognise the origin of the granites by geochemical means and to use schemes based upon geochemical criteria. Such schemes include estimated original $^{87}Sr/^{86}Sr$ ratios, $^{143}Nd/^{144}Nd$ and rare earth element ratios. Three major granite types based upon geochemical criteria are the M, S and I type granites. M type granites are thought to originate in the mantle and are generally found in volcanic arcs. I type granites are thought to be derived from crustal igneous rocks and are poor in potassium. S type granites are potassium rich granites thought to be derived from crustal rocks rich in potassium. Like all such classification schemes, considerable overlap occurs, usually reflecting a mixed history.

Various tectonic regimes can be associated with particular granite features. For example potassium poor tonalites and granodiorites relate to the continental side of plate margins.

3.1 Geology of the central highlands

The basement structure of the central highlands is thought to be formed by the Lewisian Metamorphic Assemblage, the oldest rocks in the region which outcrop in the north western part of the highlands. Overlying this basement are sediments of the Torridonian system. During the ascent of a magma, interaction with the host rock can affect its chemical composition. Braxland, Aftalion and van Breemen (1979) for example used Pb isotopic from Caledonian granitic feldspars to show the presence of a Lewisian Pb component in the Caledonian granites of northern Scotland, but not in the Southern Uplands granites. In these latter the feldspars were found to be significantly more radiogenic. This relationship was used to infer the presence of an older crustal layer beneath the north of Scotland, but not beneath the Southern Uplands.

These rocks form part of an accumulation of sediments which extend from Scandinavia to Greenland, and are divided into two groups in the present area of interest. The first are the Moinian group of rocks. These comprise thick, uniform, shallow water sediments deposited unconformably upon eroded Lewisian rocks. The other group are the Dalradian, which were deposited conformably upon the lower Moinian group over a 200 Ma period from 700 Ma onward.

Both groups represent rocks characteristic of a subsiding basin in an extensional tectonic regime. This regime is typical of spreading oceans and can be observed today in areas such as the Red Sea. The Moinian group probably represent sedimentary accumulation in a slowly subsiding basin, where the Dalradian group have been deposited in a more rapidly subsiding basin. The geosyncline in which the rocks were deposited was named the Caledonian Geosyncline, marking it out as a major event associated with the Caledonian orogeny which folded and faulted the Caledonide rocks.

The main Caledonian orogeny is associated with a number of events related to the closure of the Iapetus ocean. The principal events are:

1) The formation of recumbent folds and shear zones at about 590 Ma, typical of crustal thickening.
2) The intrusion and extrusion of a large range of igneous rocks.
3) Extensive regional metamorphism from about 520 to 490 Ma.
4) The intrusion of basaltic magma followed by the intrusion of the late Caledonian granites.
5) Probable movement along some of the large north easterly wrench faults.

The closure of the Iapetus ocean is thought to have involved subduction of oceanic crust. Much of the

evidence for subduction is based upon the effect this process has upon surface rocks. There is no direct evidence for the presence of ocean floor material except for the occurrence of an ophiolite type rock at Ballantrae in the Southern Uplands.

Isacks et al (1968) proposed a northward dipping subduction zone, the geological evidence for which is now thought to be at Ballantrae. Dewey (1969) attempted to provide a model to explain the stratigraphic and structural similarities of Newfoundland, Scotland and Norway. He proposed two subduction zones. Other workers have proposed three such zones.

Dewey and Pankhurst (1970) discussed the evolution of the Scottish Caledonides in relation to their isotopic age patterns. They suggested three stages in the evolution of the Scottish Caledonides. A depositional stage, when the Moine and Dalradian sediments were deposited in an ocean separating the Archaean cratons which are now located in Greenland, North America, North Western Scotland and Scandinavia; a metamorphic stage during which subduction occurred, and a final evolutionary stage during which the orogen was uplifted and eroded, in association with the intrusion of granitic magma.

The granites of central Scotland are 300 kilometres away from the proposed suture zone. They range

from migmatites to large volume granites such as those of the Cairngorms, with a surface area of over 400 square kilometres.

Read (1961) classified the granites into older granites, early forceful granites and later, permitted granite intrusions. This classification reflects the relationship of the granites to the Caledonian tectonic events. The early granites were thought to have been intruded into their host rock with considerable force, causing deformation of the host rock and usually lacking any significant metamorphic aureole. The later, permitted intrusions show contact aureoles and less deformation. They have much larger volumes than the earlier intrusions.

The relationship between the forceful and permitted intrusions was discussed by Brown et al (1981) who concluded that a combination of adiabatic melting due to rebound following the closure of Iapetus, a tectonically induced increase of sediments resulting in a high temperature regime, and possible continued subduction, were all possible factors that could be used to explain the regional deformation.

3.2 Geology of the Cairngorm granites

The Cairngorm granitic pluton is one of a number of Siluro-Devonian granites located in the highlands of Scotland, and is the largest of the post-tectonic granites emplaced into the Scottish Caledonian belt between 435 and 390 Ma.

Early research on the Cairngorm granite by Barrow and Cunningham-Craig (1913) suggested that the granite was a single, homogenous concordant sheet, with the base of the sheet visible in places. Harry (1965) re-mapped the area and described the faulting and mineralogy of the Cairngorm pluton. He suggested that the pluton consists of at least two units forming a stock like mass, with steep contacts. He also described the main granite as having cut the Moine country rock without producing any major movement or metamorphism.

Harrison (1986) presented a detailed account of the geology and textural variation within the Cairngorm pluton. The geological map published in his paper is shown in figure 3.2.a.

The granite can be divided into four major units. The main granite is a porphyritic biotite granite containing few xenoliths. Biotite inclusions are found in K-feldspar and quartz, and hence must predate both minerals. The absence of biotite inclusions from

plagioclase is interpreted as indicating the first crystallization of plagioclase.

The textural variations within the main granite led Harrison to conclude that a number of successive intrusions rather than a single intrusion were responsible for producing it. Phenocrysts in the porphyritic texture are mainly potassium feldspar with small amounts of plagioclase feldspar. The contact between the porphyritic and non-porphyritic sections of the main granite show a gradation over several hundred metres. It has been dated isotopically at 408 Ma.

The Glen Avon granite on the northern side of Cairngorm is coarser and predominantly composed of a white biotite. It is porphyritic and, in contrast to the main granite, contains xenoliths of varying diameter up to 30 cm., with evidence of partial digestion. This granite has a lower average silica level than the other granites, and a different suite of accessory minerals. Potassium feldspar phenocrysts are reported to be vertically aligned in this area, with a strike along a NNW-SSE axis. The Glen Avon granite appears to be the oldest of the granitic masses comprising the Cairngorm pluton.

Harrison (1986) reported the likely age sequence of the granites as the Glen Avon granite (oldest); Main granite; Beinn Bhreac granite, porhyritic

aplogranites and Carn Ban Mor granite, with the intrusion of aplite and pegmatite sheets as the final event.

The Beinn-Bhreac granite is a coarse, pink granite associated with aplites. Following the intrusion of the Beinn-Bhreac granite, a series of small porphyritic aplogranites were intruded into the main granite. Some of these alpogranites occur at the contact of the main granite with the host rock. No gradation is observable between the main granite and the aplogranites, which appear to have been the final stages of the intrusion, developing as late stage residual fluids, frequently containing drusy cavities, and with little lateral or vertical movement. They are similar in texture to the Carn Ban Mor granite. The Beinn-Bhreac granite is also thought to have developed as a late stage residual fluid.

Few of the contacts between the host rock and the granites are visible at the surface. Where contacts are visible they are reported as being steep, with no hornfelsing. No chilling or thermal metamorphism of the granite margin has been reported. Neither is there any sign of veining of the host rock or disturbance of foliation. This evidence is taken to indicate high level emplacement under tensional conditions, probably by stoping. The presence of wollastonite, cordierite and andalusite are taken as indicating a depth of emplacement of less than 12 kilometres. Harrison (1990) suggests that

emplacement occurred at a depth of 4 to 6 kilometres but quotes no evidence in support of this. The same author suggests the presence of the intrusion to have been controlled by the formation of a tensional cavity. Rapid stoping of large blocks of the host rock was also described by Harrison, although again no evidence was presented to support this.

Harrison (1988) described the presence of euhedral, Mn rich garnets in the western section of the Cairngorm granites. The garnets were found at the margin of the granite. Their presence was interpreted as being due to crystallization within the magma rather than of interaction with the host sediments. The marginal distribution was ascribed to ponding of Mn and volatile rich magma against the walls of the pluton.

The Cairngorm granites contain radioactive elements in U-Nb-Ti-Ta oxides, uraninite, silicates, monzanite and thorite. Webb et al (1987) attribute the presence of high levels of uranium along with high levels of Nb, Y, Ta and Yb to strong fractionation effects within the granitic magmas. The Cairngorm granites were described by him as slightly peraluminous with SiO_2 > 70 wt.%, K_2O > Na_2O. Relatively high levels of U, Rb, and Li with low levels of Cao, Fe_2O_3, MgO, Ba, Sr and Ti were also described by Webb. The north east granite, with lower SiO2 and higher Ti and Zr than the main granites,

is described as being less geochemically evolved than the main granite.

The Cairngorm granites have a negative Europium anomaly. Micas are enriched in rare earth elements (REEs) compared to feldspar and tend to be depleted in Eu, where feldspars are enriched in Eu. Crystal fractionation involving feldspar, but with little initial involvement of mica was an explanation accepted by, for example, Webb et al (1987). The same authors attributed the enrichment of heavy REEs and some HFS elements to the complexing of highly charged metal ions with fluorine. In addition they described levels of uranium increasing with fractionation of the granites, where levels of thorium decreased.

A problem in dealing with the geochemistry of the Cairngorm granites is the high level of weathering at the surface. Such weathering is known to remove for example uranium from uraninite, giving anomalously low levels at the surface compared to values obtained from borehole samples.

Harrison (1990) described the Cairngorm pluton as having no systematic difference in chemistry between the various units and no discernible differentiation sequence within the pluton. He also quoted field evidence to suggest that pink granite typical of the Cairngorm plutons appears to form a one kilometre thick cap on top of a white granite.

3.3 Previous interpretation and modelling of the Cairngorm area

Previous geophysical work on the granites of the central highlands has concentrated upon relatively large scale interpretation of the gravity and magnetic anomalies.

McGregor and Wilson (1967) attempted a qualitative interpretation of the Aberdeenshire magnetic and gravity anomalies as part of a large scale survey of north-east Aberdeenshire. Their results allowed the prediction of substantial hidden granitic intrusions, although the survey did not cover the Cairngorm area.

Rollin (1980) modelled the Grampian Highlands gravity anomaly using a three dimensional polygonal prism. This was improved by Locke (1980) who modelled the eastern highland granites using gravity data. Cairngorm was modelled with a single density contrast of -80 kg m^{-3} and a depth to base of 10 kilometres. Locke suggested that the Cairngorm and Monadliath granites are connected at a depth of about 7 kilometres. Locke noted, in modelling the eastern highlands, that a lower density contrast of -90 kg m^{-3} was required for westerly granites than for the easterly granites, which needed a density contrast of -100 kg m^{-3}. Monadliath was modelled by Locke using a density contrast of -80 kg m^{-3} and a depth to base of 10 kilometres.

Rollin (1984) modelled the gravity data for the eastern highland granites using variable density prisms as part of an investigation into the geothermal potential of the U.K. The surface contours of the resulting three dimensional model are shown in figure 3.3.a . In Rollin's model, Cairngorm was modelled with a density contrast of -100 kg m^{-3} and Cairngorm was treated as an homogenous mass. A cross section of Cairngorm from Rollin's model is shown in figure 3.3.b. Neither Rollin's model nor Locke's model are able to account for the observed variations in the region of the Cairngorm plutons.

As part of the heat flow study mentioned above, rock samples were collected by Rollin from a borehole in the northern part of the the granite (the position is marked as X on figure 3.3.a) . The physical properties of the core samples were measured and provide, for the first time, an insight into the vertical variation of the physical properties of the Cairngorm granite. Similar boreholes were carried out for the Mount Battock, Ballater and Bennachie granites. The results are summarised in Table 1 and will be referred to again in the next section.

A seismic survey was carried out across the northern part of Britain in 1974 (Bamford et al 1978) and reinterpreted by Barton (1992). The survey line is shown

in figure 3.3.c and Bamford's interpretation is shown in figure 3.3.d.

The original interpretation of Bamford et al showed the presence of a thinned pre-Caledonian basement at a depth of about 14 kilometres beneath the Dalradian sediments. This pre-Caledonian basement was shown not to extend further south than the Southern Uplands. Barton was able to show a change in seismic velocities under the Cairngorm area at about 18 kilometres depth and a modelled density, based upon seismic velocities, of 2750 to 2850 kg m^{-3} for the top 18 kilometres. Bouguer gravity and aeromagnetic anomaly maps for northern England and Scotland have been produced using contour and relief image techniques to enhance the data acquired by the British Geological Survey following long term regional gravity and aeromagnetic surveys (see for example Lee, Pharaoh and Soper (1990)). This type of presentation has some advantages over the use of contours, but provides no extra information.

3.4 Vertical variations in the physical properties of the Cairngorm and surrounding granites

One of the major problems involved in interpreting the aeromagnetic variations of a granite is the lack of knowledge of the way in which the physical properties of the granite vary vertically. Although modelling allows some attempt at predicting possible vertical variations, even a single simple anomaly may be produced by a whole range of realistic models. The use of additional independent data sets from the same area helps to restrict the number of possible models, and provides some control on the interpretation of the magnetic field variations.

An initial investigation of the topographic effect of the Cairngorm granites was carried out. Other workers (eg Locke 1980) have noted the low magnetic susceptibility of the surface rocks. Sampling of the surface rocks during field work allowed the magnetic susceptibility to be measured. Table 2 shows my results obtained for granites. Although the surface rocks cannot be responsible for the whole of the magnetic anomalies seen around the Cairngorm area, they will contribute to some extent.

To assess the extent of their contribution the topography of the Cairngorm area was digitised at 1 kilometre intervals. A plot of the digitised data

following contouring is shown in figure 3.4.a . A Fortran computer program based upon the work of Plouff (given in Appendix 1) was written and used to calculate the magnetic field from the Cairngorm plutons using a single value for magnetic susceptibility. One example of the output for a magnetic susceptibility of 10^{-4} SI is shown in figure 3.4.b . The aeromagnetic map (discussed in section 3.5 and shown in figure 3.5.a) shows no similarity. If anything, there is an inverse relationship between the two. Topographic effects therefore appear to contribute little to the observed magnetic field.

The physical properties of some of the local granites were measured by Rollin (1984) following drilling as part of an investigation into granite heat production and heat flow. The data (see Table 1) show clearly that vertical variations do occur, although for Cairngorm, only three values of the magnetic susceptibility are available at different depths.

There are a number of possible causes of the observed variation in magnetic susceptibility with depth. These include variation in chemistry; variation in size of the magnetic grains with depth; the effect of pressure upon the bulk susceptibility and the effect of pressure upon the rock polarization vector.

A varying degree of haematization with depth was noted by Rollin. Figure 3.4.c shows the variation in

magnetic susceptibility with concentration for common magnetic minerals. To increase the magnetic susceptibility by nearly two orders of magnitude would require an increase in haematite concentration of over 100 times. This is unlikely.

The weathering processes of oxidation and hydration can alter both grain size and chemical composition. This is likely to be a significant effect at the surface, and perhaps at depths where reasonable sized cracks allow circulation of water.

Variation in bulk susceptibility with depth may depend upon the presence of crack growth as the granite is unloaded by weathering processes at the surface. Pressure does not necessarily vary systematically with depth in the near surface environment,in part due to the effects of nearby valleys and hills. Cracks affect seismic velocity. Their presence at depth is detectable by changes in seismic velocity. Figure 3.4.d shows average values for the variation in V_p with depth in both granites and basalts. Velocities stabilise at about 3 kilometres depth, implying that all cracks are fully closed. Variations in the presence of cracks will affect physical properties such as the porosity and saturated grain density of a rock. Rollin (1984) measured both of these factors. Only porosity would be expected to affect magnetic susceptibility, provided that the porosity has developed as a result of crack growth, thus affecting the

distance between magnetically active grains. Porosity development due to weathering would not be expected to affect the distance between magnetic grains and would thus not affect susceptibility, although weathering could affect the chemistry and indirectly the magnetic susceptibility.

A plot of magnetic susceptibility against depth for the three values obtained from the Cairngorm borehole is shown in figure 3.4.e. The general trend of increasing magnetic susceptibility implies that at three kilometres depth, a magnetic susceptibility of approximately 0.04 SI is feasible. This is sufficient to account for the local aeromagnetic anomaly. However, three points are insufficient to allow reliable extrapolation to such depth.

Figure 3.4.f shows a logarithmic plot of porosity against magnetic susceptibility for the Cairngorm, Mount Battock, Ballater and Bennachie granites. There appears to be a systematic negative relationship between the two. It is possible that unloading of the granite during weathering is allowing the propagation of cracks, which affect the intergranular distance and the bulk susceptibility. Much of the work reported in the literature (eg Nagata 1970) describes the reverse effect, that of compression, on the remanent magnetization or magnetic susceptibility of a rock. Nagata (1970) pointed out that the magnetic

susceptibility of a rock under compression increases along the axis perpendicular to the compression, and decreases along the compression axis. Jelenska (1975), investigating the effects of compression on the magnetization of igneous rocks, concluded that compression affects the 90° domain walls and the domain configuration in grains. Under different conditions the magnetic susceptibility could increase or decrease. The main stress axis in the case of a granite being unroofed would eventually be horizontal, assuming that lateral forces remain relatively constant. The presence of an in situ anisotropic susceptibility, with a maximum magnetic susceptibility in the vertical axis, is a possibility.

Making an initial assumption that

$$k = aP^x \qquad 3.4.1$$

where k is the magnetic susceptibility

P is the porosity

a and x are constants

then $$\log k = \log a + x \log P \qquad 3.4.2$$

the slope of the graph in figure 3.4.f thus represents the value of x. The general trend of the data in figure 3.4.f is linear. The values of a and x were found using a least mean square best fit for the line. This gave a value for a of -7.6E-7 and for x of -1.5. Hence equation 3.4.1 may be rewritten as

$$k = -0.000000767P^{-3/2} \qquad 3.4.3$$

As far as can be determined this relationship has not been noted in the literature.

Vertical variations in magnetic susceptibility with depth appear to occur in all of the central highland granites for which data are available. These variations are systematic and significant. They may be due to the effects of decompression. Mineralogical variations occur in addition to the variation in bulk susceptibility. Since the data available cover a limited depth range, major mineralogical variations would not necessarily show up, but may be more significant at deeper levels.

3.5 Raw aeromagnetic data

It is worthwhile describing the relationship between the unprocessed aeromagnetic data and the known geology of Cairngorm and its surroundings. This provides an initial estimate of likely areas of interest and ensures that probable relationships between the two can be noted. Following filtering of the data, significant relationships can be destroyed unless care is taken. For example, reduction to the pole can offset the magnetic anomalies by several kilometres. If reduction is incorrectly carried out, the spatial relationship between the magnetic anomalies and the bodies giving rise to them can be destroyed. For magnetically active rocks at depth, with no geological controls, any interpretation would then be wrong.

An outline map of the raw aeromagnetic data is shown in figure 3.5.a. For comparison the geology of Cairngorm and the major surrounding geological features are shown in figure 3.2.a . This data was digitised from the B.G.S. Moray Buchan 1:250 000 series aeromagnetic anomaly map.

3.5.1 Western Cairngorm

The large positive magnetic anomaly halfway between the Cairngorm and Monadliath granites coincides very closely with the major fault shown on the geological map running north east from east 280, north 800. This magnetic anomaly lies along the south eastern edge of the Monadliath granite and appears to curve around the eastern edge of Monadliath rather than to follow the fault to the north east. Between Cairngorm and Monadliath the contours start to close but do not fully do so due to the presence of a positive magnetic anomaly at 290,800 coinciding with Glen Einich. This second anomaly lies immediately north east of the Carn Bàn Mór granite. The faults truncating this area to the south have no obvious expression on the aeromagnetic map. The aeromagnetic contours cut across the strike of the granite edge to the south east in the area 292,797 and 292,806.

3.5.2 Central Cairngorm

A low amplitude magnetic low occurs at 298,800 (this is not apparent on figure 3.5.a due to the contour intervals). This coincides approximately with the presence of one of two local porphyritic aplogranites and lies between the Ben Macdui and Cairngorm mountains. The presence of these two mountain peaks does not show up in the aeromagnetic data. The central section of Cairngorm is relatively quiet magnetically and is surrounded by a

positive magnetic anomaly which fails to completely surround the central section on the western side. A small positive magnetic anomaly occurs at 303,799 and is coincident with the presence of a small body of diorite in the granite. Another small positive magnetic anomaly occurs at 305,800 coincident with the central section of the Beinn Bhreac granite. On the south side of central Cairngorm a 300 nT circular positive anomaly occurs with its centre located on the edge of the granite, at 303,793.

3.5.3 Eastern Cairngorm

This is by far the noisiest magnetic area of Cairngorm. The aeromagnetic contours follow the general trend of the granite but have a number of sudden changes in direction suggesting the presence of small, near surface, magnetically active bodies. Just off the eastern side of the granite a number of diorites are coincident with sharp variations in the aeromagnetic contours.

3.5.4 The Boat of Garten granite 295,819

This granite has no expression on the aeromagnetic map.

3.5.5 The Tomintoul granite 310,819

This granite is closely associated with diorite on its eastern flank. The granite has a positive magnetic anomaly associated with it of 70 nT.

3.5.6 The Lochnagar granite 325,790

This granite is closely associated with diorite on the south-eastern and the northern side, together with a small surface expression of diorite within the granite. a positive aeromagnetic anomaly is associated with the diorite in the southern half of the granite. Smaller anomalies appear to be associated with the other diorites. The major part of the granite appears to be relatively quiet magnetically.

3.5.7 Unnamed granite at 290,780

This granite is associated with diorite on its south-eastern flank and has a complex positive magnetic anomaly of 150 nT.

3.5.8 The relationship between the aeromagnetic anomalies and textural variations within the Cairngorm granites

There appears to be a relationship between the texture of the Cairngorm granites shown in figure 3.5.b and the aeromagnetic field. The general trend of the

aeromagnetic field lines follow the strike of the main porphyritic granite. The Glen Avon granite and the surrounding main porphyritic granite are particularly associated with a positive aeromagnetic anomaly.

It appears that diorites are closely associated with the presence of positive magnetic anomalies throughout the area of interest. Small granites with no obvious relationship to diorite give no magnetic anomalies. Within the Cairgorm granites, granitic texture appears to be associated closely with variations in the aeromagnetic field.

Magnetic anomalies appear to be located immediately over the main granite, suggesting relatively high magnetic susceptibility rock beneath the surface of the granite. However, magnetic fields may appear several kilometres away from their source if the polarization vectors have a significantly different direction to the main field vector and the source is relatively deep. The overall shape of the anomaly on and around the Cairngorm area may arise from a single rock unit at depth or from a combination of rocks at varying depths and with varying magnetic properties. A rapid way of checking for the former possibility is to compare the major magnetic field structure with the collection of calculated and contoured magnetic fields for a standard prism produced by Andreasen and Zietz (1969). None of the collection of 825 calculated data sets matches the main magnetic field over

the Cairngorm area. In addition to this the magnetic field from a variety of prisms was calculated using a computer program developed from an algorithm due to Plouff (1976). It was not possible to reproduce the main features of the aeromagnetic field over the Cairngorm area from a single prism model. Lateral and vertical variations in magnetic susceptibility appear to be present.

The relationship between granite texture and aeromagnetic field values suggests that grain size may be a factor in the magnetic susceptibility variations. If the original grains within the granite were magnetized in a direction different to that of the present day magnetic field, the direction of magnetization would eventually move to line up with the direction of the Earths' main field lines. The time for this to occur, the relaxation time, was given by equation 1.2.3 in chapter 1.2, and varies exponentially with the volume of the grain. Variations in relaxation time for different grain sizes would give rise to a varying magnetic texture. Magnetic susceptibility is also a function of grain size. Granites with varying texture could thus be expected to have varying magnetic susceptibility.

3.6 Field data

Over a five year period, trips were made to the area for the purpose of carrying out a ground magnetic survey and to collect rock samples for susceptibility measurements. Most of the field work was done in the autumn, with one period of winter work. The corrected field values are shown in Appendix 2.

The lines walked are shown in figure 3.6.a and the contoured field data are shown in figure 3.6.b. The general structure of the contours is similar to those of the aeromagnetic map. There is better resolution (in some areas) of individual structures on the field map. However, considerable aliasing is present in other areas due to the distribution of the points, mainly in the more remote eastern areas of Cairngorm.

Sampling the whole of the area on a uniform grid to give comparability with the aeromagnetic data would be an ideal solution. In practice distance, weather and time provide considerable limitations to what can be done.

3.6.1 Western Cairngorm

The broad 150 nT aeromagnetic anomaly on the western side of Cairngorm is resolved into two

separate magnetic anomaly highs at 293,800 and 293,805. There is also a minor magnetic anomaly at 291,798. The anomaly at 293,800 lies immediately adjacent to a fault. The anomaly at 293,805 appears not to be related to the known geology. The change in direction of the contours just to the south of this anomaly occur immediately over the fault. This area is just on the southern edge of the granite.

3.6.2 Central Cairngorm

Within the central region lies a broad, low amplitude, magnetically quiet zone which shows no obvious correlation with topography. This area coincides closely with a similar quiet magnetic area on the aeromagnetic map. A small magnetic low lies at 302,802 just to the north of the diorite located within the granite. The 49500 contour intrudes into this area from the north, and to the east the area is surrounded by a magnetic high, just as it is on the aeromagnetic map.

On the south side of central Cairngorm the encircling 49600 contour shows three magnetic highs enclosed within the southern arm of the encircling high amplitude magnetic anomaly. The three highs occur in a line.

The Beinn Bhreac granite cuts across the magnetic contours throughout this area. This implies that

this granite has low levels of magnetic minerals and/or is of little vertical thickness. Table 1 from the paper by Harrison (1986), reproduced in Table 3 here, gives the modal abundances of the minerals in the main granite types. Beinn Bhreac contains no opaques and low levels of biotite by comparison with the other main granite types. Hence it could not be expected to produce a relatively strong magnetic field unless it were very thick vertically. The lack of effect upon the magnetic field contours suggests that the granite is relatively shallow and that the cause of the encircling magnetic anomaly lies beneath this granite.

The relationship between the textural variations within the granites and the aeromagnetic field discussed in section 3.5 is also present with the field magnetic data. Comparing textural variations between the granites with the field magnetic data in figure 3.6.b shows a less marked relationship. The main non-porphyritic granite shows as a magnetically quiet area. The area of the main porphyritic granite generally shows up as having higher magnetic field readings.

3.6.3 Eastern Cairngorm

This area is dominated by a broad magnetic high of 49600 nT. On the field map it appears to be magnetically quiet. This is one of the more remote areas of Cairngorm, with sparse data points. The aeromagnetic

map shown in figure 3.5.a tends to hide some of the true variations due to the choice of contour interval. There is variation of the aeromagnetic field within this area. It does not show up on the field map due to the sparseness of the data points. Beyond the point East 305 the density of field data points is not sufficient to allow identification of any small scale features.

In many areas there is no obvious relationship between the surface geology of the Cairngorm granite and the magnetic field data. In some areas the geological features actually cut across the magnetic field contours. In other areas the presence of faults is closely related to the presence of high magnetic field anomalies, particularly in western Cairngorm. The field data show a general correspondence with the aeromagnetic data but give better resolution in some areas, and poorer resolution in others. The lack of a relationship between the main granite types and the magnetic field, and the clear relationship between Cairngorm and the overall aeromagnetic field, suggests that the magnetic field either arises from within the granites, or has suffered a considerable offset due to the presence of remanent magnetisation. The relationship of some magnetic highs to faults suggests that postgranitic intrusions may play some part in the producing the observed anomalies.

Lateral variations in magnetic susceptibility beneath the surface of the granite appear

to be causing some of the features described above. Part of this variation may be due to variations in grain size within the granite.

3.7 Gravity data

3.7.1 Raw gravity data

With little data available for use to control interpretation of the ground based and aeromagnetic data, it was necessary to make use of gravity data for this purpose. The gravity data was digitised from the Moray Buchan 1:250 000 series gravity anomaly map. Data spacing and the area sampled were identical to that for the aeromagnetic map. Having digitised the data, low pass filtering was employed to eliminate near surface effects in order to allow comparison with the low pass filtered aeromagnetic data.

The raw gravity data is shown in figure 3.7.a. Cairngorm has an elliptical gravity anomaly with its centre just to the south of Ben Macdui. The anomaly is elongated to the east, where the contours almost close in following the surface outline of the granite. The contours then open up again into the Lochnagar granite. A notch in the gravity data on the western side of Cairngorm does not show up on this map due to the contour values used.

Several other granites have an expression on this map. The Lochnagar and Glen Gairn granites show up clearly as significant features on the eastern side of

the map at 325,790 and 325,800 respectively. The Tomintoul granite is visible as a -21 mgal anomaly 308,818. The Bienn Dearg granite shows as a -35 mgal anomaly with the contours not completely closed on the south eastern side at 290,780.

The general trend of the gravity contours follows the south west to north east trend of the main geological structures in this area - as do the aeromagnetic contours.

Gravity data is usually collected at much wider intervals than aeromagnetic data. Following processing and contouring the result is usually a much lower degree of spatial resolution than is possible with magnetics. In the frequency domain the consequence of these processes is the loss of power in the high frequency end of the spectrum, together with a rapid fall off of the power spectrum. When attempting to filter such data there is inevitable difficuly due to the overlap of components arising from different sources.

In trying to interpret the origin of the major features of the gravity data, low pass filters were used on the gravity data to suppress what high frequency components were present.

3.7.2 Low pass filtered gravity data

The result of subjecting the gravity data to a low pass filter is shown in figure 3.7.b.

The central low remains as before, but two positive gravity anomalies have appeared on the northern and southern edge of the map. These two positive anomalies are artefacts of the data processing. The gravity low at 302,798 has an elliptic shape with the long axis of the ellipse trending east to west. This matches the position of the major magnetic low seen in the aeromagnetic map (figure 3.5.a) and the field magnetic map (figure 3.6.b).

3.8 Aeromagnetic data reduced to the pole

In reducing the aeromagnetic data to the pole it is necessary to assume a direction for the remanent magnetization vector. Reduction was attempted using a variety of assumed directions, and the resulting output compared with the surface geology for geolgical consistency and symmetry.

The most consistent and geologically reasonable results were obtained with with an inclination of 70 ± 20 degrees and a declination of 0 degrees, ie an assumption of inductive magnetization. The aeromagnetic data reduced to the pole assuming induction is shown in figure 3.8.a. When comparing the maps of filtered data it has to be borne in mind that the absolute values of the field have been affected by the data processing. For example a plane has been removed from most of the filtered data sets to reduce distortion. This does not affect the patterns and textures present within the contoured map.

3.8.1 A comparison of the aeromagnetic map with the reduced to the pole map

The overall pattern of a negative anomaly to the north of Cairngorm with a positive anomaly around the central area of Cairngorm remains. The negative

anomaly to the north at 305,810 now has the contours fully closed and shows a high degree of symmetry. Previously, the aeromagnetic data had the deepest part of the low offset to the east and the contours had not closed.

On the southern side of central Cairngorm the large positive anomaly at 303,793 has broadened out and become slightly more asymmetric. The magnetic anomaly encircling central Cairngorm remains. A central broad anomaly located at 308,805 is now located immediately over the Beinn Bhreac granite. The eastern side of Cairngorm remains relatively noisy magnetically.

On the eastern side of Cairngorm the previously noted and modelled anomaly at 292,802 remains present.

It proved impossible to obtain a single anomaly for the Cairngorm area with a centrally symmetric pattern, although comparison of the reduced maps with the gravity map indicate that the best fit of the two maps occurs for an assumption of induction. A reasonable hypothesis to explain this result is that the Cairngorm magnetic anomalies are due to a number of different sources of varying magnetic susceptibility, position, dimension and depth. The possibility of varying magnetization directions in different parts of Cairngorm is not supported by these results nor by the profile

modelling results, discussed later. The major pattern of the anomaly continues to suggest that the sources of the magnetic field are underneath or within the Cairngorm pluton. Many of the smaller scale variations are located at the edge of the granite, over faults located in or near the granite, or over diorites which are visible at the surface. Some of the low amplitude large scale magnetic variations appear to be related to the variations in geology within the granite itself.

3.8.2 A comparison of the reduced to the pole map with the map of the ground based magnetic data (figure 3.6.b)

The area at 292,800 shows a 600 nT high on the magnetic field map. The same area on the reduced to the pole map shows sudden directional changes of the contours. The anomaly at 302,793 on the reduced map is slightly to the south of the three magnetic anomalies shown in the same area on the field map. The central 500 nT low at 300,800 on the field map matches a similar low on the reduced map, although contour closure has not occurred in this area on the reduced map. The 600 nT contour that encircles central Cairngorm on the field map of figure 3.6.b corresponds approximately with the same feature on the reduced map, except in the area of 310,810 where the field map shows the contour to extend to the north.

3.8.3 A comparison of the reduced to the pole map with the geology of the Cairngorm area

The Car Ban Mor granite at 290,800 is marked by sudden change in contour directions at its northern end. The low at 302,810 is unrelated to the geology and is typical of the effects of inductive magnetization. The Beinn Bhreac granite has a broad magnetic high immediately underlying it. The diorite at 302,799 continues to have a magnetic high associated with it. The magnetic high at 302,792 continues to overly a fault at the edge of the granite. Eastern Cairngorm remains complex. The reduced data is, in part, related to the presence of surface diorites. In other areas of eastern Cairngorm there is no obvious geological cause for the anomalies seen.

In conclusion the reduced magnetic field continues to show a clear relationship to diorites at the surface. The diorites are assumed to be predominantly inductively magnetized since reduction to the pole of the aeromagnetic data provides the most symmetric and geologically reasonable fit. There is some association between the reduced field and the surface granites, mainly the Carn Ban Mor granite. In other areas there is little association between the surface expressions of the granite and the reduced magnetic field, although variations in granite texture show a relationship to the reduced map similar to that noted previously. The Beinn-

Bhreac granite does not show in the reduced map.

3.9 Filtered aeromagnetic data.

Following reduction to the pole, the power spectrum was examined in three dimensions and as an azimuthally averaged power spectrum. The three dimensional power spectrum is shown in figure 3.9.a. Structures causing trends within the power spectrum are aligned at right angles to the trend, exactly as with optical diffraction patterns and their corresponding mask. There are relatively minor trends in the north-east, north-south, and north-west directions. These are probably due to the magnetic high partially encircling central Cairngorm. The majority of the three dimensional power spectrum shows no preferred orientation, in keeping with the circular nature of the magnetic field anomalies.

Azimuthal averaging of the power spectrum gives the result shown in figure 3.9.b . Three linear areas can be observed within the power spectrum. Regression analysis on each of these linear sections gives the results shown in figures 3.9.c . Employing the theory outlined in chapter 2, the slope of each section of the power spectrum can be used to calculate the depth to the top surfaces of the bodies concerned. The values obtained are:

Wavenumber range (nyquists)	Distance beneath flight path (km)	Depth beneath surface (km)
0.04 to 0.2	3.25	3.05
0.2 to 0.7	0.88	0.68
0.7 to 1.0	0.2	0.0

The high wavenumber, high frequency part of the spectrum representing a depth of 200 metres below the flight path is the effect of variation due to topography, near surface sources and variation in altitude of the aircraft carrying the magnetometer. The middle section of the curve (0.88 kilometres) reflects the variation due sources at 0.7 kilometres below the ground surface. The low frequency section of the curve represents sources at a depth of 3 kilometres. When attempting to interpret these maps it is of note that the texture and patterns present are more meaningful than the absolute values of the magnetic field anomalies.

3.9.1 High pass filtered data

A filter was applied to the data to exclude all wavenumbers lower than 0.7 nyquists. The result of applying this filter to the data is seen in figure 3.9.d. This represents the high frequency, near surface magnetic field anomalies. The linear feature running horizontally, at 792 (slightly below the centre of the map) is the result of digitisation errors at the junction of two aeromagnetic maps. The large number of small anomalies

make plotting contour values very difficult for any contouring program.

A comparison of this map with the field geology (figure 3.2.a) shows a number of relationships. Western Cairngorm is relatively quiet, although the schists at 290,810 show some evidence of magnetic activity. Central Cairngorm shows the presence of near surface magnetic anomalies over the diorite at 302,799. A second, similar area, just to the south of this at 302,794 ,has no obvious geological correlate. The porphyritic aplogranites show no magnetic activity.

The north eastern section of Cairngorm around 310,803 is well marked by magnetic field anomalies, particularly the area around and including the Glen Avon granite. Barritt (1983) noted this area as containing extremely coarse granite characterised by large, pink, subhedral feldspars and found the area distinctive enough to name it the north eastern granite. Table 3 shows the Glen Avon granite to have the highest level of biotite and opaque minerals.

The area around 311,803 is associated with a large number of minor magnetic anomalies that mark the area out as having a different magnetic texture to the surrounding areas. The magnetic anomalies in this area suggest that the north eastern granite may extend further to the south than was shown by Barritt. This area is the

main porphyritic granite occurring in the north eastern section of Cairngorm seen in figure 3.5.b .

The area at 318,802 marks the edge of the granite as containing a number of small magnetic anomalies. Immediately next to this area at 318,800 are diorites, with a considerable magnetic texture present just to the north of the diorites. This area is known to be mineralised. Post granitic intrusions causing mineralisation is a reasonable explanation for the difference in appearance of this area on the high pass filtered map. If true, then two other areas are also possible candidates for postgranitic mineralisation. These are the western parts of the Glen Gairn (320,800) and Lochnagar (320,785) granites. They are also distinctive in having large numbers of magnetic anomalies on the high pass filtered map and are also associated with local dioritic intrusions.

The unnamed granite at 290,780 is also magnetically very noisy, and is associated with dioritic rocks. This area has been severely affected by the window function and cannot be interpreted.

There is only one minor high frequency magnetic anomaly near the Tomintoul granite and diorite at 311,818. This area is severely affected by the window function. The anomaly is associated with the diorite rather than with the granite.

3.9.2 Band pass filtered data

The data was band pass filtered to eliminate wavelengths outside the range of 0.2 to 0.7 nyquists. The band pass filtered map is shown in figure 3.9.e.

There are many similarities between the band pass data and the main aeromagnetic field data. Wherever diorites are present on the surface (excepting the Tomintoul area where the window function is having a major effect), the aeromagnetic map contains features also seen in the band pass filtered map.

Several minor anomalies occur over eastern Cairngorm, the main one immediately overlying the northern end of the fault at 293,800. The diorite in central Cairngorm again has a magnetic field anomaly over it. The magnetic field contours in the area of the Beinn Bhreac granite (307,804) cut across the granite. This implies that the cause of the magnetic anomaly has its top surface at a depth of about 0.7 kilometres in this area, and that the Beinn Bhreac granite is less than this thickness in vertical extent.

A number of magnetic anomalies occur along the southern edge of central Cairngorm at 304,792.

The major fault running along the eastern edge of the Cairngorm granites has magnetic anomalies

overlying it. Some are associated with surface diorite, others are not. Most are slightly offset to the eastern side of the fault, suggesting that, if the fault was used by the diorite for upward ascent, then the fault dips to the east. The western side of the Glen Gairn and Lochnagar granites show magnetic anomalies some of which are not associated with surface diorite. These are the same areas seen to be extremely noisy on the high pass filtered map. The band pass map shows a reasonably close fit to the textural variations on the eastern side of the Cairngorm plutons, with the Glen Avon granite and the associated main granite porphyry being a particularly close fit to the band pass data.

The oval shaped contour along the north eastern and north western areas of the map are affected by the window function and cannot be interpreted.

3.9.3 Low pass filtered data

The data was filtered to eliminate all wavenumbers greater than 0.2 nyquists. The low pass filtered map is shown in figure 3.9.f.

The map shows a large circular low around the eastern and northern side of Cairngorm. The area covered by this low includes the negative aeromagnetic anomaly on the northern side of Cairngorm at 308,810 together with the area covered by the diorites on the western side of

Glen Gairn and Lochnagar. This could be explained by a rock mass with its top surface 3 kilometres beneath the aircraft flight line in this area. It is spatially related to the presence of surface diorites, magnetic anomalies seen on the band pass and variations in the gravity data seen in this area. The large, circular, positive magnetic field anomaly at 302,793 marks a high at the 3 kilometre depth, which extends to the western side of Cairngorm.

In conclusion dioritic intrusions appear to be responsible for many of the anomalies seen around the Cairngorm plutons, as well as for one anomaly within the main mass.

A large mass of relatively basic material encircles the eastern and northern aspects of the Cairngorm area, underlying many of the observed surface doleritic intrusions. This mass wil be referred to again in section 3.11.

Mineralisation of the eastern side of the Cairngorm area may be related to this intrusion. If so, both the Glen Gairn and the Lochnagar granites may also be mineralised on their western side. There is evidence for a relationship between granite texture and magnetic field variations (in some areas) down to depths of at least 0.7 kilometres. Variations in the filtered

aeromagnetic field below 0.7 kilometres depth does not show evidence for mineralisation.

3.10 Pseudogravimetric transformation of the Cairngorm aeromagnetic data.

The principles of pseudogravimetric transformation have been described in section 2. When this process is carried out, the resultant map shows the equivalent gravity effect due to a magnetized body. This gravity effect represents a density contrast proportional to the magnetization contrast at each point of the body. The map as such will not resemble a gravity map of the area, since the density contrast in the Cairngorm area is mainly due to low density rocks. Instead it will emphasise the presence of magnetized bodies.

The pseudogravimetric data has been applied to a 32 by 32 grid of data from the map (every third point along each row and column). This was done due to constraints of processing time and memory.

The results of the pseudogravimetric transformation are shown in figure 3.10.a . The pseudogravimetric anomaly map and the unfiltered gravity anomaly map show some similarity. However, the pseudogravity highs are displaced to the east of the gravity lows. This suggests different causative rocks for the magnetic and gravity anomalies.

The pseudogravity high just to the east of Monadliath almost immediately overlies the fault between Monadliath and Cairngorm. The centre of the anomaly actually lies slightly to the west of the fault. The positive magnetic anomaly implies that inductive magnetization of the rock mass is responsible for this anomaly.

The pseudogravity high to the east of the Cairngorm area also appears to be fault bounded. The centre of the high is west of the major fault at 315,800. However, the southern part of the of the anomaly curves away from the fault and tends to follow the edge of the granite at 310,796, along the line of the minor fault at 303,792. The entire area of Cairngorm east of 810 shows up in the pseudogravimetric map. This suggests a higher magnetization contrast for this area.

In conclusion the results for the pseudogravimetric transformation imply that the eastern side of the Cairngorm granites is significantly different from the remainder, having a higher magnetization and pseudodensity contrast. This supports evidence from field work and filtering of the aeromagnetic data.

3.11 Interpretation of selected profiles over the Cairngorm pluton and surrounding area

Profile interpretation is based upon the calculation of the magnetic field of a rock mass with a particular shape and set of physical properties lying along and usually beneath the profile line on which the magnetic or gravitational field is calculated. By comparing the calculated profile with the field data collected along the profile, corrections can be made and the process repeated until the calculated profile matches the actual profile as closely as required. However, the iteration process does not take into account the nearby presence of offline bodies which contribute to the observed field data. Such bodies contribute to the observed field and can be modelled immediately underneath the profile, when in fact they are several kilometres off the line. Other difficulties with profile modelling include spatial aliasing, the non-uniqueness of potential field data and the presence of a variable subsurface magnetized topography.

A wide range of possible models can thus be made to fit the observed data. Some constraints such as minimum rock volume or maximum matching of the spectral frequencies can be used without regard to the geology. Obtaining a realistic model requires the use of all available geological data.

In the present case the models have been kept as simple as possible, consistent with the known geological and geophysical data. In addition the modelling process has been started in relatively simple areas before being extended to more difficult areas.

Numerous algorithms exist to carry out the calculations in profile form, and in full three dimensional form (eg Broome 1992). Since much of the work was done on a personal computer, it was necessary to restrict the level of sophistication used for modelling. Profile calculations were carried out using a program based upon the work of Talwani and Heirtzler (1963) attributable to Begg et al (1987).

The lines that have been modelled are shown in figure 3.11.a. The data used was digitised by the author from the BGS Moray Buchan 1:250 000 series aeromagnetic anomaly and gravity anomaly maps.

3.11.1 Western Cairngorm aeromagnetic and gravity profiles

Before attempting to model some of the main anomalies it was decided to choose a relatively simple profile in an area where some geological information was available. This gives constraints on possible models that could fit profiles in the local vicinity.

The initial line chosen covered the area drilled by the B.G.S. (Rollin 1984) and is shown in Figure 3.11.a as line E-E. The best fitting model is shown in Figure 3.11.b . This gives a rock unit of average magnetic susceptibility 1.2 x 10^{-2} SI with a variable depth to the top surface of 0.8 to 3 kilometres and a depth to the bottom surface of 12 kilometres (below the aircraft flight line). The model has been kept as simple as possible. Modelling the northern end of the profile proved difficult. This was thought to be due to the effects of either the positive Monadliath magnetic anomaly to the west, or the large negative anomaly on the northern edge of the Cairngorm pluton, possibly sourced from rocks at a deeper level. The presence of an offline body apart from Monadliath is also possible and will be referred to again.

Figure 3.4.e showing the variation in magnetic susceptiblity with depth gives an approximate linear increase of 10^{-3} SI per 100 metres increase in depth. This implies that a magnetic susceptiblity of 10^{-2} SI would occur at about 1 kilometre beneath the surface (about 1.2 kilometres beneath the aircraft flight line). The results of the modelling and the extrapolation of the magnetic susceptibility results are in reasonable agreement despite the difficulties with the northern end of the profile. If the extrapolation of the susceptibility continues as shown in Figure 3.4.c, then no major compositional change is required to explain the

magnetic anomaly. However, the aeromagnetic field strength just south of profile E-E is less than that near the borehole. With no major lateral changes in rock type nearby, this suggests that compositional variations are occurring at depth. Telford et al (1978) table 3.2 page 121, gives susceptibility values for a range of rock types. Given the geological setting, diorite or some similar intermediate rock type present at depth seems to be the most reasonable explanation for the magnetic anomaly in the area of the B.G.S. borehole.

The modelling was extended from this area to cover line C-C on Figure 3.11.a. The line runs parallel to contours from a nearby magnetic anomaly associated with the Monadliath granite. Rollin (1984) attempted to model the whole of the Cairngorm area as part of a large scale crustal heat flow investigation. Figure 3.3.b shows his model of this area on a north-south and east-west line. It is worth noting that in the central region of the main Cairngorm mass Rollin had problems with a sudden increase in residuals. In addition Rollin employed a modified iterative technique, modelling a variable surface vertically downward and upward from a depth of 6 kilometres, and employing a single density contrast for the Cairngorm granites.

Modelling this area proved to be difficult. Initial models based upon a variety of assumptions gave a poor fit to the aeromagnetic data. An attempt was made to

obtain an approximate model of the gravity anomaly along this line to get a feel for the range of models that could provide a good fit. It was found that the gravity data could not be reasonably modelled along the profile by a single value for the density contrast.

The modelling process was continued with a series of simple prisms with a density contrast of -110 kg m^{-3}. The density contrast of the prisms was first adjusted to give an approximate fit. Then the shape of the prisms was adjusted to improve the fit. This contrasts with Rollin's method of keeping the density contrast fixed and varying the prism dimensions to obtain the best fit.

During this process the surface geology was used as a constraint upon the position of the surface prisms and their likely densities, although evidence presented previously suggested that the density was likely to vary with depth. Since the granite outcrops at the surface, and variations in the type of granite are known to occur along the profile, lateral density variations highly probable. The final model is shown in Figure 3.11.c. Both vertical and lateral density variations were required to obtain the best fitting profile. The residuals resulting from this model average less than 3% along most of the profile. The subsurface body at the northern edge of the profile with a density contrast of +480 kg m^{-3} is unrealistic. It was required

to reduce the residuals in the area away from the main granite. It probably results from a rock unit in the local vicinity of the profile line. Similar effects were found along the whole of the northern edge of the Cairngorm granites and will be referred to again.

Given this approximate model of the gravity data, a similar process was used to model the aeromagnetic data along the same profile line. The best fitting magnetic model along line C-C is shown in Figure 3.11.d. The lack of any observed structure in the top layer is a reflection of the low magnetic susceptibility near the surface and the effect, noted previously, of having flight lines so far apart that aliasing of near surface features occurs. Aliasing will smooth out the magnetic field from near surface features and can make them appear to come from a deeper level.

Both vertical and horizontal variations in magnetic susceptibility were required to obtain a good fit. The magnetic susceptibilities required were all of the order of 10^{-2} SI, in reasonable agreement with the area around the borehole.

Both gravity and magnetic models show a zoned intrusion. The gravity model differs from the magnetic model in showing structure from the surface down to the 3 kilometre mark. At the 3 kilometre level the model becomes much simpler but remains zoned. The effect

of the off-line body at the northern edge is felt to have affected the gravity model in that area. The density contrasts of -80 and +60 kg m^{-3} are not felt to be reliable due to the need for a density contrast of +480 kg m^{-3} to model the northern end. The difference between the magnetic model and the gravity model is most obvious at this end. The gravity model shows a thin sheet of material at 0.5 kilometres depth where the magnetic model shows a thick prism of material. Despite this difference, the gravity model, borehole data and the profile over the borehole area are felt to support the interpretation of the magnetic field along most of the line E-E in figure 3.11.a .

The similarity between both models for line C-C is clear. Both show a sudden change at 3 kilometres depth. Both models require a central differentiated zone. At deeper levels the gravity model requires a low density contrast and the magnetic model requires a high magnetic susceptibility contrast. The surrounding zones have higher density contrast. This suggests a lower level of SiO_2 and higher level of mafic minerals in the outer layers. Spectral analysis of the aeromagnetic field shows that the main magnetic field originates from rock units whose top surface lies at an average depth of 3 kilometres. The present models of the gravity and magnetic field are consistent with this.

The much larger density contrasts in the top 3 kilometres compares well with the very low susceptibility value in this region. However, the susceptibility and density increase relatively quickly with depth in the top layer and the situation is probably more complex than is shown here. The gravity data suggests that the central zone is still present at depth but this time it has a higher density contrast than its surroundings rather than a lower one. Assuming the broad outlines of the model are correct, then it clearly implies that eastern Cairngorm is underlain by more basic material at a depth to its top surface of 3 kilometres.

It is worth noting the presence of a small body on the model of the aeromagnetic profile at a depth of 3 kilometres, 12 kilometres along the profile. This was found to be necessary to get a good fit to the profile data, but such a body is not present on the gravity model. The small size of the body together with the low resolution of the gravity survey are the probable reason for this.

3.11.2 Western Cairngorm field data profile

The positive anomaly modelled above matches very closely the anomaly at East 292, North 800 on the map of the field data (figure 3.6.b). To obtain a better understanding of what is actually present near the surface, a second profile, this time from the ground based results, was modelled. This is shown as the line F-F on the map in figure 3.11.a. The results are shown in figure 3.11.e. They show three prism shaped bodies, with a depth to top surface of 200 to 300 metres, and a susceptibility of 0.01 to 0.025 SI. The more southerly anomaly is located 1 kilometre north of a known fault. All three bodies appear to be inductively magnetized. These anomalies cover the same area as the aeromagnetic anomaly mentioned in part a) above, which was modelled as a small extension to the top surface of the central section of the granite at three kilometres depth. Aliasing of the aeromagnetic data has occurred in this area.

Only surface diorites are observed to give positive magnetic anomalies in the area under study. The predicted susceptibilities agree with a dioritic composition. Diorite or some similar intermediate composition rock is thus likely to be the cause. The material at depth in the model of figure 3.11.e is probably of intermediate composition. The model of the field data has produced magnetic susceptibilities for

three near surface rocks which fall in the same range as those at depth. It is possible that they have developed from the intermediate material at depth. For this to happen the top 3 kilometres must have formed at about the same time as the bottom 9 kilometres of intermediate material, since some mixing would have to occur. Alternatively, and more likely, the dioritic material was sinking in the main granitic mass when it became frozen into place. In this case the dioritic material must have been present at the time of emplacement of the granitic mass surrounding it. In addition the granitic mass must have been low temperature, mainly crystalline, and close to its freezing point at the time of intrusion.

3.11.3 Tomintoul area profile

To further clarify which type of rock is most likely to be responsible for the anomalies modelled above, the positive magnetic anomaly at Tomintoul (310,819) was investigated. This has the advantage that diorite is clearly present on the surface in close association with the granite at this location. In addition samples were taken from both the Cairngorm pluton and the diorite for measurement of magnetic susceptibility. The line modelled is shown as line H-H on figure 3.11.a. The measured magnetic susceptibility results are shown in Table 3 and the preferred model of the profile line is shown in figure 3.11.f.

The model of the Tomintoul diorite suggests a magnetic susceptibility of 0.01 SI. This compares well with the modelled values of 0.011 to 0.024 SI at 3 to 12 kilometres depth on the western side of Cairngorm.

The measured volume susceptibility of the surface rocks varies between 1.04×10^{-4} and 9.97×10^{-4} SI. The variation of susceptibility with depth could be five or ten fold over the first few hundred metres, based upon the BGS borehole data for the northern edge of the Cairngorm granites. The profile results and measured values are felt to be in reasonable agreement provided that this vertical variation in susceptibility occurs to the same extent in the Tomintoul diorite as in the B.G.S. borehole.

3.11.4 Central Cairngorm diorite.

This diorite is located at 302,798 . It lies on the top of the main granite and is associated with a positive magnetic anomaly. A profile running west to east was modelled along the line marked D-D on figure 3.11.a . The results are shown in figure 3.11.g. The model shows a simple prism, about 300 metres thick, with a magnetic susceptibility of .019 SI . This is similar to, but slightly higher than, the magnetic susceptibility of the Tomintoul diorite, and is similar to the values

obtained in the western section of Cairngorm between 3 and 12 kilometres depth.

3.11.5 South central Cairngorm

On the south side of central Cairngorm, the field magnetic map shows three magnetic anomalies. (see figure 3.6.b at location 300,793). The profile line marked G-G on figure 3.11.a, covering these magnetic anomalies, was modelled. The results are shown in figure 3.11.h. The model suggests that the anomalies are due to variations in the top surface of a deeper body marked out by the 49600 magnetic field contour. The model has a calculated magnetic susceptibility of 3.06×10^{-2} SI, lies within 20 metres of the surface at one point, and extends to a depth of 900 metres below the surface. This area is marked as granite on the geological map. The underlying material has a magnetic susceptibility significantly higher than any yet found on the western side of Cairngorm. Although still within the range for diorite, the results suggest that the rock is more basic than the assumed diorite on the western side.

3.11.6 South eastern Cairngorm.

A line cutting through the previous profile but avoiding most of the effects of the central diorite was modelled to extend the results for the western area of the Cairngorm granites. The line is shown

as B-B on figure 3.11.a and runs along the Beinn Bhreac granite.

Because of the complexity of the magnetic field an initial attempt was again made to model the gravity field along the same line. The gravity model is shown in figure 3.11. The results show a similar structure to that found in western Cairngorm. A top layer of high density contrast material overlies a more substantial layer of lower density contrast. Although the granite below 1 kilometre depth is not shown zoned, there was found to be little to choose between slight density zonation and no density zonation of the main granitic mass at depth. The variance of the residuals was slightly less for the non-zoned model and the figure shown represent this case.

The magnetic field model for the same line is shown in figure 3.11.j. The similarity to the results for western Cairngorm are clear. The granite appears to be zoned with a central core of susceptibility 0.019 SI surrounded by material with a higher magnetic susceptibility averaging 0.029 SI.

The magnetic susceptibility of the material on the southern side of profile B-B is 0.014 SI. This magnetic unit is situated in the area of 300,778. On the gravity model of figure 3.11.i it is shown to be underlain by relatively non-magnetic rock with a density

contrast of -110 kg m^{-3}. This may be an extension of the granite at 290,775, which is associated with diorite on its southerly and south easterly margins.

The zonation of the granites below 1.6 kilometres stands out on the model of the aeromagnetic data, when compared with the gravity data. This is assumed to be due to the greater sensitivity of the magnetic field results to variations at depth. Aliasing can show up in the modelling process as variations in the physical properties of the body, as variations in the dimensions, or as variations in the depth. With wider spacing for the gravity data, there will be more aliasing and less resolution. This effect will be more marked for aeromagnetic data between the aircraft flight lines where it will have its lowest resolution.

The surface of the Cairngorm granites again show up as having very low magnetic susceptibilities. However, the thickness of this layer is much less than was present for the western side of the Cairngorm granites, averaging about one kilometre on the gravity model and 1.6 kilometres on the magnetic model. The magnetic field in the area of the Beinn Bhreac granite appears to come from the northern part of the main underlying mass whose top surface is at about 2 kilometres depth with a magnetic susceptibility of 0.027 SI. The large increase in the residuals at 20 to 23 kilometres along the magnetic and gravity profiles is

probably due to the effects of the nearby dioritic mass at 302797.

Both gravity and magnetic models require a prism on the northern end of the line. The line at this point cuts through the Tomintoul diorite and granite. This is assumed to be the cause. The encircling magnetic anomaly on the eastern side of the Cairngorm mass runs beneath the Beinn Bhreac granite. This magnetic anomaly arises from the outer zone of the main subsurface granitic mass. The central section of the Cairngorm granites appears to be material of low magnetic susceptibility compared to the outer zones north and south. By contrast, the western section of the Cairngorm granite below 3 kilometres depth has material with a high magnetic susceptiblity in the centre. This implies a possible different mode of origin for granites in the two areas. Fractional crystallization of the original granitic material on the western side of Cairngorm would explain the relationships observed there, but not in the central section of the Cairngorm granites.

3.11.7 Eastern Cairngorm

This is the most complex area of Cairngorm. The gravity anomalies were first attempted along line A-A on figure 3.11.a . Modelling the gravity anomalies proved difficult due to the effect of the outcrop of basic rocks

at Morven, north-east of Cairngorm. One of the best fit gravity models obtained is shown in figure 3.11.k.

The results show a lower density contrast than was found for western or central Cairngorm. The model of the gravity data indicates a centrally zoned area. The central zone has a density contrast of -51 kg m^{-3} and is surrounded by zones north and south with a much lower density contrast. The zone on the northern side, with a density contrast of -14 kg m^{-3} breaks the surface in the magnetically noisy area at 310,803 on the high pass filtered map.

On the equivalent magnetic profile model (figure 3.11.l) a prism of susceptibility 0.006 SI lies just beneath the surface on the northern edge of the Glen Avon granite, within the main granite. To the north of it lies a second smaller prism of susceptibility 0.004 SI.

The encircling negative anomaly corresponds very closely to the profile mass with a density contrast of +85 kg m^{-3} on figure 3.11.k. Despite this density contrast, the mass has not appeared in the magnetic model for the area (figure 3.11.l) and is assumed to have a very low magnetic susceptibility contrast. The average density of the Tomintoul diorite samples collected during field work was 2772 kg m^{-3}. Rollin (1984) gives the average Moine density as 2700 kg m^{-3}. It is possible that this mass is similar to the local diorites, but if so the

lack of magnetic activity suggests that it must have a different composition. The upper block with a density contrast of +130 kg m^{-3} has the appearance of a horizontal intrusion. Rollin (1984) gives the density contrast of local basic intrusions at Cabrach as ranging from 2700 to 3200 kg m^{-3}. This upper rock unit could be a basic rock mass associated with the nearby Morven intrusion.

There was less certainty over the presence of a central zone in the granite using a magnetic profile model, a reasonable fit being obtained with one large mass together with several near surface masses. Some lateral variation in the magnetic susceptibility is showing through in the top surface of the main mass at a depth of about 4 kilometres. The area is magnetically noisy, resulting in larger residuals, a higher variance for the residuals, and less certainty in the modelling process in this area. The high frequency of the residuals suggests that a numer of near surface sources are present in this area which have not been included in the model.

The magnetic model implies that near surface material with a magnetic susceptibility of 0.004 to 0.006 is present over the northern edge of the granite outcrop, intruding up to 5 kilometres along the profile line into the host rock. This corresponds to the upper block seen on the gravity map. The southern edge of the granite also appears to have a similar magnetically active mass. The top surface of the granite is modelled as having a

negligible magnetic susceptibility down to three kilometres. The gravity and magnetic models are similar in respect of horizontal size and depth.

3.12 Conclusions and summary

Profile modelling and interpretation of the Cairngorm granites show a mass not dissimilar to that modelled by Locke (1980), but with more internal structure. This contrasts sharply with that of Rollin (1984). Rollin attempted a much broader approach, ignoring the aeromagnetic data, but including many of the major igneous masses in the area. One of the major weaknesses of taking a broad approach to the modelling of potential field data is the loss of resolution. Automated routines also make it difficult to introduce geological controls. Equally however, one of the weaknesses of a small scale approach is the inability to take account of effects due to nearby rock masses. Ideally some mixture of the two approaches would give both local resolution of detail and allow the effect of nearby masses to be accounted for.

The western side of Cairngorm appears to be a zoned pluton in its own right, with differing characteristics to those of the central and eastern side. The zonation occurs at depth and is hidden by a top layer 3 kilometres in depth, with a high density contrast and low magnetic susceptibility contrast.

The central section of Cairngorm shows similar zonation on the magnetic profile model of the area, although this did not show up unequivocally on the

gravity model. The central section is more basic than the western section with the top closer to the surface, at about 2 kilometres depth, as opposed to 3 kilometres depth on the western model.

The eastern side of the Cairngorm granite showed some evidence of zoning, but not to the same extent as was found on the western side. The magnetic susceptibility of the underlying material was found to be close to that for the inner zone of the central profile of the Cairngorm granites. The northern flank of material on the gravity profile, with a density contrast of -14 kg m^{-3} , was found to break the surface in the area of the Glen Avon granite. On the magnetic profile, material of relatively low magnetic susceptibility was found to break the surface in the same area. This probably represents Barrit's (1983) north eastern granite. The gravity model suggests the presence of two distinct masses, one above the other, at the junction of the Moine-Dalradian boundary. It was possible to relate many of the profile models to structures in the filtered aeromagnetic maps, giving some confidence in the interpretation.

Barritt (1983) noted a discrepancy between the high heat production from samples of the Cairngorm granites, and the relatively low heat flow found in this area. This was attributed to a low background heat flow in northern Scotland. However, the present study suggests that only the top 3 kilometres of the Cairngorm granites

are as evolved as the surface rocks would imply. Much of the remainder of the pluton, which forms the bulk of the underlying mass, has a lower density contrast and higher magnetic susceptibility, suggesting a more basic rock, probably of dioritic composition, with lower levels of heat producing elements.

The combined approach of spectral analysis and profile modelling is equivalent in many respects to full three dimensional modelling. Confidence in a number of aspects of the profile modelling was gained by using geological constraints as far as possible, and by comparison of the profiles with the filtered maps. The pseudogravity map relates relatively well to the magnetic profile models, agreeing with the eastward increase in magnetic susceptibility at depth.

The reason for this eastward increase in magnetic susceptiblity together with a reduction in the density contrast, would appear to be due to lateral variations in granite chemistry and mineralogy, the more basic eastern side having lower Si_2 levels. The granites are probably the result of multiple pulses of magma occuring close together in space and time, when the magmas were still able to flow. Subsequent differentiation may have led to the production of the central and top section of highly evolved granite seen in the models. The diorites appear to have been present at the time of intrusion of the major granite masses, and

are present both on, within and around the granites. Stoping thus seems to have been one method utilised by the magma to reach its present position. The size of the prisms modelled within the granite could not be kept floating by simple upward convection currents, unless the density contrast with the granite was extremely small. The granite would need to be close to its freezing point at the time when these dioritic masses started to move downward. Given that the diorites form a small proportion of the surface area of the surrounding host rocks, it is likely that a considerable volume of relatively non-magnetic host rock lies within and/or beneath the main granitic mass, or has been absorbed.

During upward motion of the granite from depth, a sideways force will occur due to the requirement for conservation of angular momentum. The magnitude of this horizontal force will be proportional to the speed of ascent of the granitic magma. In the event of two separate pulses of magma, the later pulse (assumed to be more silicic) will tend to be forced to the western side of the earlier pulse. This is one possible explanation for the increase in magnetic susceptibility to the east.

Mineralization on the eastern side of the main Cairngorm granite mass is known to be present. There is evidence for the presence of a partially encircling basic mass on the eastern side of the Cairngorm granites, although this was within the influence of the window

function. The mineralization may be related to the presence of this nearby mass.

There is no simple correlation between density and magnetic susceptibility across the whole of the Cairngorm plutons. This may reflect the intrusion of a suite of granites differentiating by different amounts, or arising from multiple sources, or absorbing varying proportions of the host rock.

Chapter 4 The Cairnsmore of Fleet and Loch Doon granites

Aeromagnetic data for the area around the Cairnsmore of Fleet and Loch Doon granites has been studied using spectral analysis and frequency filtering techniques. In addition reduction to the pole and pseudogravimetric transformation of the aeromagnetic field was carried out together with a field magnetic survey of the eastern section of the Cairnsmore of Fleet pluton.

4.1 The geology of the Southern Uplands

The Southern Uplands of Scotland has held the interest of geologists for many years. Initial attempts at interpreting the structure of the area were carried out by Lapworth (1889) who proposed a northern anticlinal structure and a southern synclinal structure. Since this time the area has generated considerable controversy and the Southern Uplands has played a major role in understanding the development of the British Caledonides in the context of plate tectonics.

The surface geology of the Southern Uplands is shown in figure 4.1.a. The rocks young to the south east and consist generally of basalt and pyroclastics underlying thin cherts, which in turn are overlain by very thick greywacke turbidites. Deposition of the turbidites appears to occur later in the Silurian at more southerly positions. Strong isoclinal folding and north

westerley dipping thrust faults are common throughout the area. The thin cherts suggesting deep water deposition contrast strongly with the turbidites, suggesting deposition on an unstable slope.

Early plate tectonic models proposed the Southern Uplands to be in a forearc position with a spreading ocean between the north west and south east parts. Dewey (1969) initially proposed a destructive margin near the Southern Uplands in order to explain the sedimentary sequence; the presence of high pressure, low temperature metamorphic rocks at Ballantrae and in Anglesea, and the close proximity of different sets of Cambrian and Ordovician trilobite and graptolite species from apparently very different habitats. These faunal contrasts are thought to occur next to the originally proposed Iapetus suture and can be traced from Ireland through the Isle of Man to the Southern Uplands. The lack of any surface trace for a subduction zone south of the Southern Uplands has remained a source of controversy. Geophysical and geological evidence was intially interpreted as placing such a suture zone just south of the Southern Uplands. Investigation of this area as a possible suture zone (eg Leeder et al 1989) has revealed a system of early Carboniferous extensional basins with an ENE orientation, following a structural trend in the basement rocks of the lower Palaeozoic. Extensional faulting during the Carboniferous is assumed to have reactivated a large basement fault.

The complexity of the area led a number of workers such as McKerrow et al (1977) and Leggett and Casey (1982) to suggest that the structural and sedimentological evidence could be explained by a series of accretionary prisms forming at an active margin, giving rise to a series of fault bounded areas similar to present day accretionary prisms. Subsequent work by for example Soper and Hutton (1984) suggests that the Southern Uplands structures are a series of terranes accreted onto the southern region of the Laurentian plate.

The accretionary prism hypothesis has been questioned by workers such as Morris (1987) who, with others, developed varying interpretations based upon a shortened back-arc basin in the northern belt and a foreland basin in the southern and central belts of the Southern Uplands. Needham (1993), in the light of new evidence from deep seismic surveys such as LISPB, concluded that the structure of the Southern Uplands is explained by the development of an accretionary prism in a forearc situation.

Three major granite masses are present at the surface in the local vicinity. The Criffell pluton, a 397 Ma zoned granite, is one of the new granites which were intruded in the final stages of the Caledonian orogeny. Stephens (1992) pointed out that the granite varies from

an I type at the outer margins, to granite which has some of the features of S-type granites in the central region. The Cairnsmore of Fleet granite, a 392 Ma zoned granite, is located to the north of the Criffell pluton and will be described in more detail in sections 4.3 and 4.4. To the north of Cairnsmore of Fleet lies the Loch Doon pluton, a 408 Ma granite, also zoned but having a more elliptical outcrop than the previous two. The Criffell and Fleet granites are associated with aeromagnetic anomalies. By contrast the Loch Doon granite has little expression on the aeromagnetic map. This granite will be dealt with in more detail later.

4.2 Previous geophysical work in the Southern Uplands

Al-Chalabi (1970) interpreted the broad aeromagnetic high trending WSW to ENE as being due to lower Palaeozoic basement rocks, placing them at 11 kilometres depth.

Hutton and Jones (1978) conducted a magnetovariational and magnetotelluric investigation of the Southern Uplands over the period 1973 to 1975. They were able to identify a conducting layer to the north of the Southern Uplands fault ranging from depths of 10 to 65 kilometres. They were also able to identify a good conductor beneath the Southern Uplands at a depth appropriate to the upper mantle and also within the crust beneath the Northumberland Basin. The crust beneath the Southern Uplands was found to have a relatively high electrical resistivity.

Beamish and Smythe (1986) interpreted a geoelectrical survey to suggest a zone of high conductivity beneath the Northumberland basin, dipping to the north. They were able to produce depth contours for the dipping structure consistent with subsequent seismic images.

Geophysical evidence for the deep structure of Great Britain has been obtained by the British Institutions Reflection Profiling Syndicate (BIRPS). Freeman et al (1988) describe the NERC seismic reflection

profile on the eastern coast of northern England and southern Scotland. They were able to tentatively identify four different terrane types within the crust, and concluded that during the destruction of the Iapetus Ocean the southern continent was partially subducted beneath the northern continent. The presence of reflective bodies cutting through the Moho led them to suggest that sections of the subducting crust and sediments had been preserved at the base of the Moho, which represents, in their interpretation, a ductile shear zone between crust and mantle. They suggested that the subduction zone has its closest approach to the surface near the centre of the Lake District.

In 1974 a 700 kilometre north to south seismic line was shot across the northern part of Britain. An initial interpretation of the the data was made by Bamford et al (1978) and refined by Barton (1992). The line shot is shown in figure 3.3.c and Bamfords interpretation of this is shown in figure 3.3.d . Barton was able to refine the crustal velocity structure. Her interpretation is shown in figure 3.3.e. By converting velocities to densities Barton was able to calculate gravity values based upon her model. The calculated gravity values were shown to be a good match to the actual gravity field over the area covered.

The proposed model shows the Moho beneath the Southern Uplands to be at a depth of about 34 kilometres

with a change in the velocity profile characteristics at about 12 kilometres depth. The original geological model shows the presence of lower Palaeozoic sediments overlying a pre-Caledonian basement. Barton's refined model (figure 3.3.e) shows that in the area of the Southern Uplands between 400 and 500 kilometres along the profile line there is a major density contrast at a depth of about 20 kilometres with a discontinuity at a depth of about 11 kilometres.

El-Batroukh (1975) carried out a gravity survey of an area in the Southern Uplands of Scotland. His data, together with that produced by other workers (Parslow 1968) was used by El Batroukh to produce a bouguer anomaly map of the area, shown in figure 4.2.a.

Hall et al (1983) carried out a seismic profile of the Southern Uplands at right angles to the LISPB line. The near surface seismic velocities were found to be higher than those for the LISPB model. They suggested that igneous or metamorphic rocks were caught up in accretionary wedge prisms to produce an anisotropic structure.

Soper et al (1992) attempted to reconcile problems arising with previous attempts at interpretation of geophysical data, particularly the surface trace of Iapetus compared to its trace at depth. They reinterpreted the broad outlines of previous seismic data

to conclude that a northward inclined reflective boundary is present in the middle and lower crust, separating seismically unreflective crust in the north from reflective crust in the south. The reflective boundary projects back approximately to the present position of the Iapetus suture.

Floyd and Trench (1988) carried out in situ measurements of the magnetic susceptibility of the greywackes of the Southern Uplands finding susceptibilities ranging from 0.16 to 13.81 x 10^{-6} SI. They also established that major differences in petrography were paralleled by variations in magnetic susceptibility.

4.3 Previous geophysical work on the Fleet granite

The Cairnsmore of Fleet granite lies in the western part of the Southern Uplands of Scotland (see figure 4.1.a), just to the south of the Loch Doon granite.

Parslow and Randall (1973) carried out a gravity survey of the Fleet granite and its local area. They measured the densities of several hundred rocks to find saturated bulk densities for the biotite granite (2630 kg m^{-3}) and for the muscovite biotite granite (2610 kg m^{-3}). Their model of the Fleet granite assumes a density for lower Palaeozoic sediments of 2730kg m^{-3}.

On the basis of their model they proposed that the eastern section of the granite is fault controlled. This would explain the 5km vertical edge of the granite, and the absence of a metamorphic aureole in the Loch Ken area. They pointed out that the western lobe of the granite is tentative. The gravity data could also be interpreted as an extension of the Wigtown Bay sedimentary basin.

El Batroukh (1975) carried out a geophysical investigation of the western part of the Southern Uplands. He interpreted his data in terms of the presence of an underlying batholith surface. The contours of the batholith (figure 4.3.a) shows a steep drop to a depth of

2.5 kilometres on the eastern side, followed by a gradual increase in depth to the top surface toward the east. El Batroukh's model also shows a shallower depth to top surface on the western side than that of Parslow and Randall.

4.4 Geology of the Fleet granite

The Cairnsmore of Fleet granite is shown in its regional context in figure 4.1.a and at a larger scale in figure 4.4.a . The granite is oval shaped with the long axis of the oval following the strike of the Lower Palaeozoic host rocks to the north east. The host rocks consist of a series of alternating greywackes, flags and grits with some black shale.

The Fleet granite is composed of two distinct types of granite. The central section consists of a biotite-muscovite granite with quartz, muscovite, biotite, microcline, oligoclase and orthoclase as the main minerals. The grain size of the central section is coarse with porphyritic feldspars ranging up to 3 cm in length. Parslow(1968) described a fine grained biotite-muscovite granite outcropping in the region of Loch Fleet with sharp contacts to the east and north, and more gradational contacts elsewhere. This granite covers 70% of the total exposed area of 210 km^2. Parslow and Randall (1973) mention that the central area of the main granite is cut by a circular, fine grained biotite-muscovite granite.

Surrounding the main granite is a coarse grained biotite granite with quartz, microcline, oligoclase and biotite as the main minerals. This granite has a variable width of up to 1.5 kilometres. Muscovite

does appear within this granite away from the contact with the host rock. The transition from biotite to biotite-muscovite granite is gradational.

The granite has a sharp contact with the local sediments and has a metamorphic aureole up to 1.5 kilometres wide. The bedding planes of the host have been intruded by granitic sheets and veins, which are larger and increase in number to the south west and north east, where the host-granite contact cuts across the strike of the sediments. Veins of quartz are present throughout the granite, trending north to south. In addition, the granite contains small xenoliths up to the contact with the host rock. They show little digestion. Parslow (1968) interpreted this, together with the coarse grain of the granite, to indicate that the granite was at a low temperature and almost completely crystalline during intrusion.

The host sediments immediately next to the granite have dips up to 90^{0} ,except on the northern edge where the dip falls to about 40^{0}. Chlorite is a common mineral in the host sediments. The conversion of chlorite to biotite marks out the extent of the metamorphic aureole. The development of other metamorphic minerals within the aureole is sporadic and less reliable as a marker of the aureole.

4.5 The Fleet aeromagnetic anomaly

Figure 4.5.a shows the aeromagnetic field over the Fleet granite at 255,570. The data was provided by the BGS from their geophysical data base.

The granite does not show up in the magnetic field although a positive anomaly to the east of the Fleet granite appears to encircle one end. The positive anomaly at 265,570 is close to 5 local dykes.

When filtering the aeromagnetic data it has to be noted that the eastern side of Fleet is affected by the circular window function.

The apparent lack of structure in the aeromagnetic field over Fleet is a reflection of the automatic contouring routines used and the low magnetic susceptibility contrast of the granite. The high amplitude anomalies in the north western section of the map are stretching out the contouring intervals and consequently hiding relevant magnetic textures between the contour intervals.

The apparent low magnetic activity parallels the large negative gravity anomaly over the Fleet granite, implying high levels of SiO_2 and low levels of mafic minerals.

4.6 Aeromagnetic data reduced to the pole - Fleet granite

The reduction of the aeromagnetic data to the pole (figure 4.6.a) gives the highest degree of symmetry of most of the magnetic anomalies when an assumption of induction is made. Inclination values 15° either side of 70° gives little change although distortion becomes more pronounced above inclination values of 85° and below values of 55°.

Figure 4.6.a shows magnetic anomalies centered in the Fleet metamorphic aureole. At 248,565 a broad positive low amplitude magnetic anomaly is centred on the westerly edge of the Fleet granite. At 265,578 a high amplitude positive magnetic anomaly occurs on the north eastern edge of the granite with two centres about 4 kilometers apart. At 261,565 a broad, negative, low amplitude anomaly is centred on the edge of the granite. This anomaly may form a dipole pair with the 248,565 anomaly. There is no obvious relationship with local rock units.

The presence of magnetic anomalies within the metamorphic aureole can be identified in several areas. Most of the metamorphic aureole is magnetically quiet. This may reflect the flight line of the aircraft rather than the actual distribution of magnetic anomalies within the aureole.

4.7 Pseudogravimetric data for the Fleet granite

The pseudogravimetric map is shown in figure 4.7.a .

The Fleet granite has no expression on the pseudogravimetric map. This is a reflection of the low magnetic contrast within the granite and between the granite and the host rock.

There is some evidence of a spatial relationship between the pseudogravity low at 255,555 and the presence of dykes on the geological map. This is probably due to the magnetic activity of the dykes in this area.

4.8 The azimuthally averaged power spectrum of the area around the Loch Doon and Fleet granites

The azimuthally averaged power spectrum for the aeromagnetic data from the area around the Loch Doon and Fleet granites is shown in figure 4.8.a .

The spectrum shows three main linear sections from which estimates of the depth to the top of the sources has been calculated. The depths are:-

Wavenumber interval (Nyquists)	Estimated depth (km)
0.04 to 0.26	1.72
0.26 to 0.58	0.84
0.58 to 1.0	0.23

The relevant wavenumbers were used to filter the aeromagnetic data following reduction of the data to the pole. The filtered data will be discussed in sections 4.9 to 4.11.

4.9 High pass filtered map - Fleet granite

The high pass filtered aeromagnetic map is shown in figure 4.9.a. The aeromagnetic data has been filtered to eliminate all wavenumbers below 0.58 nyquists. The high pass map thus reflects sources 0.23 kilometres beneath the flight line of the aircraft. These sources lie at or just beneath the ground surface.

Fleet shows a number of magnetic anomalies within its aureole situated at 250,564, 255,564, 268,573 and 263,575. Some of these anomalies appear to be dipole pairs, such as the anomalies at 268,571 and 263,575. These latter anomalies appear to be due to host rock mineralisation. Within the granite itself a number of minor negative anomalies occur, mainly within the biotite granite, and are due to minerals within the granite itself. One noticeable exception occurs at 253,510 which lies within the muscovite-biotite granite.

To the west of Fleet a number of high amplitude magnetic anomalies at 233,565 are associated with surface dykes.

Hennessy (1978) produced trend surface maps for major elements and mineralogy in the Cairnsmore of Fleet granite. His map of the trend surface for biotite/total mica is shows in figure 4.9.b . There is a general correspondence between the level of biotite/total mica

and the degree of magnetic 'noise' within the granite. The level of biotite/total mica follows the trend of the contact between the 2 granite types.

Previous work on the Cairngorm granites gave no direct evidence that the granites had a sufficient magnetic susceptibility to produce the magnetic fields observed. The high-pass filtered map for the Fleet granite shows some relationship between the magnetic field anomaly and the presence of biotite granite.

4.10 Band pass filtered map - Fleet granite

The aeromagnetic data was filtered to eliminate frequencies outside the range 0.26 to 0.58 nyquists. This represents an average depth to the top surface of 0.84 kilometres beneath the aircraft flight line, or 0.62 kilometres beneath the surface. The band pass filtered map is shown in figure 4.10.a

The anomaly on the eastern edge of the Fleet granite remains pronounced and is in two parts. One part is a major high at 265,576 which appears to extend south along the eastern edge of the granite. The second part is at 263,580, on the northern edge of the granite.

The central area of Fleet remains magnetically quiet, whilst on the western side, a substantial positive magnetic anomaly is present which appears to extend to the west. The surface dykes are concentrated away from the main peaks of the anomalies.

The junction between the Silurian and Ordovician is marked in a number of places by changes in the contour directions. In one place, at 233,567, a minor magnetic anomaly is located at the junction.

There is again a good correspondence between this magnetic anomaly pattern and that of the biotite/total mica given by Hennessy (1978) (figure

4.9.b). Since the magnetic data originates from 0.62 kilometres depth it suggests that this mineralogy is preserved to at least this depth. The high pass data shows the presence of one magnetic anomaly at 262,574 slightly south west of the band pass anomaly mentioned. The two appear to be connected, and to dip to the east.

4.11 Low pass filtered map - Fleet granite

The data was filtered to eliminate all wavenumbers higher than 0.26 nyquists. This represents depths of 1.72 kilometres beneath the flight line, or 1.5 kilometres beneath the surface.

The low pass filtered map, shown in figure 4.11.a, is notable for the absence of the encircling anomaly on the eastern side of Fleet, suggesting that the encircling anomaly is no deeper than 1.5 kilometres beneath the surface.

A positive anomaly occurs at the north eastern end of Fleet (262,580) and at the western end of Fleet (245,566). The north eastern anomaly underlies the northern side of the near surface encircling anomaly at 262,575, implying a possible linked origin.

The absence of major magnetic structures beneath Fleet implies that a fairly homogenous granite is present at this level. The presence of the biotite granite cannot be demonstrated in this data.

4.12 Field data for the Fleet granite

A ground based magnetic survey of the eastern section of the Cairnsmore of Fleet granite was carried out. Values were taken along the lines marked in figure 4.12.a at approximately 0.7 kilometre intervals.

The contoured results are shown in figure 4.12.b and the corrected field values are given in Appendix 3. Several magnetic highs are resolved on the eastern side of the granite at 264.5,571, 263,575 and 261.5,575.5.

Some of the magnetic features are clearly originating from within the granite, for example at 257,574 and 253,573. The granite has a dominant magnetic low at 260,567 with values generally higher on the northern and north-western margin by 40nT.

The observed variations in the magnetic field data and aeromagnetic field data suggest that the magnetic susceptibility within the granite varies consistently from north to south. Possible factors that could cause this have been discussed in the context of the Cairngorm granites. These include variations in bulk susceptibility, grain size or chemical composition. If true, this must reflect the development of the granite.

Hennessy (1978) produced a number of geochemical trend surfaces for the Fleet granite. Uranium data were not available for Fleet but figure 4.12.c shows the distribution of thorium. There is a strong resemblance between the thorium levels and the magnetic field contours in figure 4.12.b for the area on the eastern side of Fleet where sufficient values are available to allow comparison. As the magnetic field increases from south to north, so the level of thorium in the granite increases. Since thorium levels are thought to be controlled by primary fractionation trends, then the corresponding magnetic features are presumably controlled by the same mechanism. However, individual anomalies at the edge of the granite are probably due to hydrothermal mobilisation of minerals from the host rock.

There is also a similarity between the band pass data (figure 4.10.a), and the field data (figure 4.12.b) for the eastern and central area of the Fleet granite. The high pass filtered aeromagnetic map also agrees well with the field data (figure 4.12.b) over this area of the granite. There is less agreement between the data sets on the western side where the field data points are sparse. The high pass filtered map is also similar in this area with figure 4.12.b, particularly with the anomalies at 256,565, 260,568 and 262,575 on the eastern side of the granite. There is less agreement between the two data sets on the western side where the field data points used for contouring are sparse.

4.13 The Loch Doon granite

The Loch Doon granite is a high level plutonic intrusion. It was intruded during the final stages of the Caledonian orogeny, just to the north of the Iapetus suture zone, into Caradocian to Ashgillian greywackes and siltstones.

The surface expression of the granite is shown in figures 4.1.a and 4.4.a. The granite is elongated along a north-south axis. It is zoned, with norite at the outer extremities, followed by zones of tonalite, granite/tonalite and an inner, oval shaped area of granite. The diorites are seen only in two areas, at the opposite ends of the pluton. Grain size generally increases along a line from the granite margin to the granite centre. The diorites contain biotite and orthopyroxene as the main mafic minerals. Halliday et al (1979) concluded that the original magmas were derived from a partial fusion of the lower crust or crustal underplate, and were subsequently modified by fractional crystallization.

Brown et al (1979) summarised the formation of the Loch Doon granite as evolving from a monzodiorite parental magma, passing through a two-stage crystal fractionation process. The major reasons for favouring a fractionation process were based upon geochemical grounds, particularly the observed increases

in U and Th, with corresponding decreases in Ba and Sr, on a line from the periphery to the centre of the granite. The medium to coarse grained lithology shows little variation across the granite and lacks the sharp internal contacts that would have been expected of multiple intrusions. By contrast, there is a substantial petrographic change,as noted previously. The presence of large numbers of xenoliths of two distinct types was noted in the granite.The first, derived from the host rock, consisted mainly of hornfelsed greywackes. Near the margin contacts these can reach 15% by volume of the intrusion. The second type of xenolith was of igneous derivation and more basic in character. It was homogenously distributed within the granite.

El-Batroukh (1975) carried out a gravity survey of the Loch Doon granite. One of the notable features of his model is the presence of a subsurface batholith to the east of Loch Doon which forms a plateau at a depth of about 250 metres, continuing for nearly 10 kilometres to the east before descending at about 20 degrees to a depth of 6.5 kilometres. It is this hidden batholith which El-Batroukh suggested was responsible for a gravity low on the eastern margin of the granite.

Kafafy and Tarling (1985) investigated the magnetic fabric of the Loch Doon granite. They described the granite as having magnetite as the dominant magnetic

mineral, although bulk susceptibilites were found to be low. The susceptibility values showed a large increase in the host rock thermal aureole, followed by a fall further away from the granite.

Heat production of the Loch Doon granite lies in the range 1.5 to 4.5 $\mu W\ m^{-3}$. This is below the levels found in the Cairngorm granites. Webb et al (1987) state that both U and Th are enriched in the more evolved rocks, with little evidence of hydrothermal activity. The U bearing minerals in the Loch Doon granite (apatite, zircon, sphene and allanite) are resistant to weathering, and hence surface samples are expected to be more representative of the pluton as a whole than is the case with the Cairngorm granites. The enrichment of residual liquids in U and Th is assumed by Webb et al (1987) to have varied from dioritic to granitic composition, causing associated variations in radioelement distribution.

4.14 The Loch Doon aeromagnetic anomaly

A 50 kilometre square of data on a 100 by 100 grid for the area 220,550;270,600 covering both the Cairnsmore of Fleet and Loch Doon granites was provided by the B.G.S. A contour map of the data is shown in figure 4.5.a . A problem with interpretion of the aeromagnetic data in this area again lies with the dominating effect that the large amplitude north-eastern anomalies have on the automatic contouring routines employed. In the area of this granite the aeromagnetic map faithfully reflects the major magnetic structures in and close to the Loch Doon granite.

The area of the Southern Uplands in which the Loch Doon granite is emplaced is characterised by a broad, low amplitude positive aeromagnetic anomaly on the southern side, together with a broad low amplitude negative anomaly on the northern side, covering the area of Loch Doon itself. The trough of the negative anomaly covers the middle section of the Loch Doon granite, narrowing from the east to the west. On the eastern side, where El-Batroukh's model indicates a sudden steep descent of the granite, there is contour closure at 230,585 , approximately where the top surface of the batholith surface reaches its deepest point and its most westerly extension. The contours widen on the eastern side of the granite, extending to the north-east, off the

map of Figure 4.5.a. The contours close at the eastern extremity of El-Batroukh's modelled batholith.

The aeromagnetic anomaly over the Loch Doon granite is closely associated with El-Batroukh's modelled batholith. It may originate from within the granite or from the host rocks.

4.15 Aeromagnetic data reduced to the pole - Loch Doon granite

The aeromagnetic data was reduced to the pole using a variety of inclination and declination values for the magnetic polarization vector. No single reduction proved to be totally satisfactory for the whole of the map. As with Fleet, the assumption of induction with an inclination of 70 degrees and a declination of 0 degrees gave the highest degree of symmetry.

The data reduced to the pole is shown in Figure 4.6.a. It shows a magnetic low on the eastern margin of the Loch Doon granite at 250,583. The margins of Loch Doon are associated with sudden changes in the contour directions in several areas. The north eastern and north western margins show this well but the window function is affecting the data in this area. Outside the influence of the window function on the south western margin of the Loch Doon granite at 242,580, a major change in direction of the contours occurs. Elsewhere there is little association between the granite margins and the contour directions. This suggests that the high bulk magnetic susceptibilities found in the magnetic aureole on two traverses by Kafafy and Tarling (1985) may be sporadic in occurrence. The gravity anomaly map produced by El Batroukh is shown in figure 4.2.d. A gravity low occurs on the eastern margin of the granite in the same position as the magnetic low suggesting a possible common origin

in terms of the presence of high silica and low mafic minerals.

The major north western high shows up in both the aeromagnetic and reduced to the pole maps, although the centre of the individual highs have shifted to the south east by several kilometres.

4.16 Pseudogravimetric data for the Loch Doon granite

The pseudogravimetrically transformed map is shown in Figure 4.7.a. The aeromagnetic data for the area has been sampled at 1.5 kilometre intervals in both northerly and easterly directions. The data was then transformed in the manner discussed in section 2.2.

The Loch Doon granite is cut across by the pseudogravimetric contours. To the west of the Loch Doon granite, the pseudogravity contours widen substantially, showing a low rate of change. This is a magnetically quiet area off the western side of the batholith. Over the batholith itself, at 260,590, the pseudogravity contours show a rapid rate of change, culminating in a pseudogravity high at 265,580. The area of high gradient corresponds to a magnetic low on the low pass filtered map in Figure 4.11.a , and the corresponding gravity low on Figure 4.2.d . This same area shows the presence of large numbers of surface dykes on Figure 4.4.a, to the east of Loch Doon.

The pseudogravity data in the area of Loch Doon appears to relate to the presence of surface dykes to the east, and their absence to the west. This in turn suggests that

a) The dykes may be related to the presence of the underlying batholith on the eastern side of Loch Doon.

b) Few subsurface dykes are present to the west of the Loch Doon granite.

The pseudogravity data bears no obvious relationship to the granite.

4.17 High pass filtered map - Loch Doon granite

The aeromagnetic data was filtered to remove all wavenumbers less than 0.58 nyquists. The resulting map is shown in Figure 4.9.a. This data arises from an average depth of 0.23 kilometres beneath the flight line of the aircraft and represents a mixture of magnetic noise and surface sources. Magnetic anomalies mark out about 50% of the surface boundary of the Loch Doon granite. In a number of areas, particularly 252,593 and 242,587 magnetic anomalies are coincident with the presence of surface dykes. In other areas, such as 247,577 there is a large magetic anomaly without the obvious presence of surface dykes.

The eastern side of the Loch Doon granite is very quiet magnetically, where the western side is relatively noisy. Many of the anomalies present on the high pass filtered data appear to be related to the presence of surface dykes, although there are areas where the presence of dykes shows no correlation with the filtered aeromagnetic field.

One anomaly of interest occurs within the granite at 244,592 on the north-western side. No obvious geological feature appears in this area. Despite this, most of the Loch Doon granite is magnetically quiet, and the metamorphic aureole around the granite is not obviously visible. Kafafy and Tarling (1985), surveyed

two lines at 242,580 and 249,594 (marked as A and B respectively on Figure 5.3.a). Their results showed substantial increases in the magnetic susceptibility of the rocks in the metamorphic aureole. Their line at 242,580 has one dyke in the area. The high pass filtered data shows a small notch in the contours near the edge of the granite in this position. The north easterly edge of the granite shows no obvious aeromagnetic anomaly along the traverse carried out by Kafafy and Tarling. While it is possible that a dyke has affected the aureole on the south western margin of the granite, this appears not to be the case for the north easterly margin.

For the south westerly margin Kafafy and Tarling describe the bulk susceptibility as low in the country rocks, the granite and the inner part of the aureole, increasing a few hundred metres from the granite, and then falling again within the outer part of the aureole. This matches the high pass filtered data. It is probable that good resolution of detail exists in this area because of its proximity to the flight line of the aircraft.

4.18 Band pass filtered map - Loch Doon granite

The aeromagnetic data was filtered to exclude all wavenumbers outside the range 0.26 to 0.58 nyquists. The map (see Figure 4.10.a) represents the top surface of magnetic source rocks at depths of 0.84 kilometres beneath the flight line of the aircraft, or 0.62 kilometres beneath the surface.

The high amplitude anomalies at 235,594 lie slightly to the south of the Southern Uplands fault. This is in contrast to the high pass filtered data where similarly positioned anomalies lie on, or just to the north of the Southern Uplands fault. Assuming that both high pass and band pass data in this area come from the same source, it seems likely that this source lies within or parallel to the Southern Uplands fault. The data also suggests that the fault dips to the south east. The window function does have an effect upon this area and these conclusions can only be classed as tentative.

The northern, eastern and parts of the southern margin of the Loch Doon granite at 245,594 , 240,590 and 243,577 are associated with refraction of the magnetic field contours. This suggests that, in these areas, the aureole of the Loch Doon granite is magnetically active or that there is a sharp contrast in magnetic properties between the host rock and the granite. Given that observations on the high pass data show the presence of

some anomalies within the aureole, it is likely that both effects contribute to some extent to the observed variations.

A magnetic low occupies the central section of the Loch Doon granite. This will be referred to again in section 5.6.

4.19 Low pass filtered map - Loch Doon granite

The aeromagnetic data was filtered to exclude all wavenumbers above 0.26 nyquists. The low pass filtered data is shown in Figure 4.11.a. The azimuthally averaged power spectrum indicates that this field arises from an average depth of 1.5 kilometres, beneath the surface.

An anomaly low remains present over 248,582 in the south central section of Loch Doon. The low is oval in shape following the same general direction as the surface dykes.

A single magnetic high is now present just to the north west of the Loch Doon granite, on the northern side of the Southern Uplands fault. This may be due to the presence of basic material within or parallel to the Southern Uplands fault. BGS gravity anomaly maps and the gravity map of El-Batroukh (1975) show no evidence of a substantial positive gravity anomaly. Basic rocks at the surface are associated with a small scale local gravity high of -5 mgals. The effects of the window function are becoming sufficiently severe in this area to make it difficult to provide any reliable conclusions. Around the Loch Doon granite the presence of surface dykes coincides with areas of maximum rate of change of the magnetic field contours.

The central magnetic low at 247,587, persisting down to depth, is of particular interest. It remains in the same location as the negative gravity anomaly on the eastern side of the Loch Doon granite. Hennessy (1978) investigated the levels of uranium and thorium in Caledonian granites. In looking at the level of uranium in the Loch Doon granite he employed trend surface analysis of raw INAA data. One of his maps, showing the second order trend surface can be seen in Figure 4.19.a. Trend surface filtering has similar effects to filtering in the frequency domain. There is a clear correlation between Hennessy's map, the negative gravity anomaly and the low amplitude magnetic anomaly over this area of the Loch Doon granite.

All three sets of data could be related to the presence of a high SiO_2 core of material in this area, lying at and below a depth of 1.5 kilometres. High levels of silica are associated with low levels of mafic minerals and high levels of uranium. Uranium concentrates preferentially in the late phase high silica melt due to its large ionic radius. Magnetite and other mafic minerals tend to concentrate in early formed minerals. Thus the magnetite level would be inversely related to the SiO2 level, and the uranium level would be directly related to the SiO_2 level, giving the observed relationship between the magnetic and gravitational fields and the uranium levels.

4.20 Summary and conclusions

The aeromagnetic anomaly overlying the Cairnsmore of Fleet granite shows little in the way of structure, with the exception of the eastern margin. Reduction of the aeromagnetic data to the pole indicates that inductive magnetization is the most likely explanation of the low amplitude anomalies overlying this granite. The metamorphic aureole surrounding the Fleet granite is magnetically active, although this does not show through on the pseudogravimetrically transformed map. The pseudogravimetric anomalies appear to be related more to the presence of dykes in the area of the Fleet granite.

Use of the azmithally averaged power spectrum to filter the aeromagnetic map allowed the resolution of detail not visible in the main aeromagnetic anomaly map. In the high pass filtered map the Fleet granite, its metamorphic aureole and local dykes could all be related to the presence of near surface magnetic anomalies. Of particular interest was the relationship between the biotite/total mica content of the granite and the increasing magnetic 'noise' noticeable in moving from the centre to the eastern periphery of the granite. The biotite/total mica level of the granite is strongly related to the magnetic activity of the granite. This relationship is also seen in the band pass filtered map, implying that the surface structure of mafic minerals

continues to at least 0.62 kilometres depth. This relationship has disappeared at the 1.5 kilometre depth. This may be due to a change in mineralogy at this depth. A similar relationship exists for the granite thorium levels, implying that primary fractionation trends within the granite determine both the observed mineralogy and the magnetic field structure.

The Loch Doon granite also appears to be inductively magnetized. Contour refraction in some parts of the granite margins indicates that the granite or its aureole is sufficiently magnetically active to produce observable effects. Despite this the pseudogravimetric map shows a strong relationship to the presence of surface dykes rather than to the granite itself. The high pass filtered map confirms this relationship, although some magnetic anomalies are present unrelated to the presence of surface dykes. Subsurface dykes are a possible explanation for these.

The eastern side of the surface expresssion of the Loch Doon granite is magnetically quiet in all of the filtered maps and relates closely to a major gravity anomaly in this area. This relationship, together with a close similarity to the second order trend surface for uranium, has been explained by hypothesizing a high silica core at a depth of 1.5 kilometres.

The work of Tindle and Pearce (1981) indicates a clear trend in biotite and opaque minerals, with high levels of both toward the periphery of the Loch Doon granite. In their paper, they suggest that the surface microgranite at the core of the pluton is due to a late stage build up and removal of volatiles. This is consistent with the presence at depth of a core of high silica granitic material. Tindle and Pearce suggest that two distinct magmas are required to explain the observed trace element abundances. No geophysical evidence is directly available for the presence of a second granitic magma. However, comparing Loch Doon with the presented models of the Cairngorm granites, the most likely location for a second distinct magma source would be in the more eastern section of the subsurface batholith.

Chapter 5 Large scale relationships

The variations in chemical and mineralogical makeup of a granite, particularly of major constituents such as SiO_2, will be reflected in variations of physical properties such as density, magnetic susceptibility and resistance to weathering. Mention has already been made of some of the relationships between the geophysics and geochemistry observed during the course of this study. Other interesting relationships exist. The purpose of this section is to attempt to show the presence of some of these relationships and their possible explanations, together with possible future directions for further research.

5.1 Gravity and magnetization relationships

Differentiation can give rise to related rocks of different physical properties and chemical composition. Such differentiation may occur at depth, during ascent or following high level intrusion. The magma will rise to a level determined by its density and viscosity (and hence its temperature and water content), the density of the host rock, the presence of channels allowing upward motion and local pressure effects.

Following empacement, the unloading of a granite during erosion will eventually bring it to a level at which microscopic cracks form within it,

affecting its density and porosity. Circulation of water through the larger cracks and faults can affect the distribution of soluble elements, given favourable geochemical conditions. The events occurring following differentiation can thus affect the geochemistry, making the interpretation of complex geochemical processes difficult. Processes that affect the geochemistry in this way also have an effect upon the geophysical signature of the rocks, which are mainly controlled by the concentration of mafic minerals and the rock density. However, the nature of the potential fields arising from rocks allows extrapolation of the physical properties to depth. Combining geochemical and geophysical models is a potentially powerful means of constraining possible interpretations of the data sets available.

Attempts have been made to look for and interpret systematic variations in gravity and aeromagnetic fields by some authors. Kanasewich and Agarwal (1970) calculated magnetisation/density ratios in the wavenumber domain for rocks giving anomalous magnetic fields. More recently Brown and Locke (1979), and Locke (1980) attempted to interpret variations in gravity, aeromagnetic and filtered aeromagnetic anomalies for some Caledonian granites. Whilst some relationships have been noted by these authors, there was no obvious geophysical framework in which to fit the observations in order to assess their significance.

One way of describing the evolution of the physical properties of a prism of granitic material is by calculating the effect of unroofing upon the observed gravity and magnetic anomalies at the surface. This appears not to have been done in this way before and was carried out in an attempt to understand how the Cairngorm granites have evolved their present level physical characteristics.

The evolutionary curve of a granite in gravmag (gravity and magnetic) space has several interesting properties which depend upon the history of the granite, its density and magnetisation contrasts, and its volume. Figure 5.1.a shows the evolutionary characteristics of one prism of differentiated granitic material, 12 kilometres thick, of susceptibility/density contrasts respectively of 10^{-4} SI, -100 kg m^{-3} for the top 3 kilometres, and 10^{-3} SI,-10 kg m^{-3} for the bottom 9 kilometres. These values represent a simplified model of a differentiated granite similar in many respects to the Cairngorm granites. The volume of the granite is constant up to the point of its being unroofed. Figure 5.1.b shows a similar diagram for the movement of an undifferentiated granite.

The initial intrusion level was set at 5 kilometres from the top of the prism to the surface. The values in figure 5.1.a and figure 5.1.b show the maximum calculated gravity and magnetic anomaly amplitudes at

different depths to the top surface as the granite is unroofed.

As erosion proceeds, the granite gets closer to the surface. Initially there is a sharp increase in the gravity anomaly until the granite is unroofed, when the gravity anomaly reaches its greatest negative value. By contrast, the magnetic anomaly continues to increase in the differentiated granite until the bottom layer, with a higher magnetic susceptibility, reaches the surface. At this point the curve changes direction sharply and heads toward the origin, as the magnetic anomaly slowly decreases. The undifferentiated granite moves back toward the origin. In gravmag space the differentiated granite spends most of its time in the top one third of the space, and about one quarter of its time in the bottom one third of gravmag space, assuming that erosion proceeds at a constant rate. If the erosion rate depends upon buoyancy effects arising from the presence of the granite, this assumption of a constant erosion rate would not be true. Proportionately, very little time is spent in the middle one third of gravmag space. By contrast the undifferentiated granite spends most of its time in the lower one third of its trajectory in gravmag space.

Figure 5.1.c shows a plot of the results of Brown and Locke (1979), table 1, for the same space. 60% (9) of the granites lie in the top one third, 27% (4) lie in the bottom one third and 13% (2) lie in the middle one

third. The evolutionary curve of a differentiated granite in gravmag space approximately represents the statistics of the present day distribution of the Scottish Caledonian granites in gravmag space, although no account has been taken here of the volume of the granites nor of density and magnetisation variations within the host rocks. If the depth to the top surface of the granites were initially randomly distributed around the 5 kilometre level, progressive erosion would eventually give rise to the result found in Brown's 1979 paper. The true situation is probably more complex than this, but is likely to be amenable to a more systematic analysis.

A sample of the highland granites was chosen for a more detailed investigation. Those chosen were dictated by the availability of relevant BGS 1:250 000 gravity and magnetic anomaly maps. The gravity and magnetic anomaly associated with each granite was estimated by eye, estimating and removing effects that appeared to be due to sources other than the granites. The results are shown in figure 5.1.d.

The granites fall into two distinct groups due to variations in their gravity anomalies. The Helmsdale and Strontian granites are known to contain inherited zircons. By contrast none of the bottom group contain substantial amounts of inherited zircons although Hill of Fare and Etive are known to contain trace amounts. In addition Strontian and Rogart, in the upper

part of gravmag space, are thought to be deeply eroded. A number of interacting factors may explain the distribution of these granites in gravmag space. Differentiation of the granites would give rise to vertical variations in physical properties. Subsequent erosion by varying amounts would give the observed distribution if a fairly sudden change in granite properties occurred. The granites would thus be statistically likely to fall into an upper or lower group, with very few in between. Interaction with host rocks would leave behind the more resistant inherited zircons. These would be more likely to be found in the deeper levels of the granite, especially where stoping has occurred, and would thus be seen more often in granites exposed at depth by erosion.
Such granites would be found in the upper parts of gravmag space.

Figure 5.1.e shows the present situation in gravmag space for most of of the granites of the Southern Uplands. Local backgrounds have been estimated by eye from the relevant B.G.S. 1:250 000 aeromagnetic and gravity anomaly maps. The background value has been removed to leave the anomaly assumed to be associated with the granite.

By contrast with the central highland granites, the Southern Upland granites show much wider scatter in

gravmag space. They appear to be distributed around a line running centrally between the two sets of central highland granites (figure 5.1.d). In addition the variability along the gravity anomaly axis reduces as the residual aeromagnetic anomaly increases. The maximum and minimum variations on the gravity anomaly axis in figure 5.1.e are similar to those for the central highland granites in figure 5.1.d.

Whilst differentiation of the granites is almost certainly a contributing factor to their location in gravmag space, the high degree of scatter of the data suggests that other factors are involved. Threlkeld appears to be a granite of little gravity contrast, implying that it is probably moving horizontally toward the origin. Weardale and Wensleydale have yet to be unroofed and are moving toward the bottom right of gravmag space. The Loch Doon granite has been unroofed. However, its gravity anomaly together with the filtered aeromagnetic anomalies that have been presented earlier, suggest that highly silicic material has yet to be unroofed on the eastern side of the granite. The Loch Doon pluton may be continuing in a direction toward Fleet (in gravmag space) or may have now changed direction in gravmag space. Cheviot, Weardale and Shap have associated metamorphic effects (eg Locke and Brown(1978)) giving substantial positive magnetic anomalies. The position of Criffel, near Shap in gravmag space, suggests that it

also has associated metamorphic effects, although no evidence for this has been found in the literature.

The magnetic anomaly associated with Fleet appears to be due partly to the effects of zonation of composition within the pluton. This may also be true for Criffel which is described as a zoned granite by Stephens (1992).

Variations in gravmag space of the granites in the central highlands of Scotland, the Southern Uplands and northern England show some similarities along the gravity anomaly axis. The maximum extent in both cases is about the same. However, the Southern Uplands granites show more scatter along this axis, possibly reflecting a smaller size and less differentiation. The granites in figures 5.1.d and 5.1.e differ along the magnetic anomaly axis, the central highland granites having much larger aeromagnetic anomalies. This may be also be due to more substantial differentiation processes in the central highland granites, due in part to their greater volumes. The models presented for the Cairngorm granites support such an explanation.

The effects of differentiation in gravmag space appear to be limited to gravity anomalies no greater than -30 milligals and aeromagnetic anomalies no greater than 750 nT for granites in the Southern Uplands, Northern England and the central highlands of Scotland. The upper

limit for the aeromagnetic anomalies probably represents the presence of some complicating factor such as mineralisation effects. These values may also represent geophysical limits to the degree of geochemical differentiation that has occurred although detailed interpretation of them is impossible without further work.

Large scale filtering of an anomaly map will let through local effects such as mineralisation which can substantially affect the position of the granite in gravmag space. Careful use of filtering techniques covering the local area of each granite, allowing an estimate of the gravity and magnetic anomalies associated with each granite, is required to put the interpretations given here on a sounder footing. In addition some attempt has to be made to correct the position in gravmag space for the relative size of the intrusion.

5.2 Relationships between the geophysics and geochemistry of the Caledonian granites

During the course of this work a number of relationships between geophysical, geochemical and geological data have been noted by the author. These include similarities between spatial variations in the magnetic field strength over the Cairngorm granites and the textures of these granites; similarities in the spatial variations of gravity anomaly, filtered aeromagnetic anomaly and the second order trend surface of uranium over the Loch Doon granite, and similarities in the spatial variations of magnetic field strength, thorium concentration and total biotite/mica in the Cairnsmore of Fleet granite.

These relationships could be explained by one major controlling variable, the SiO_2 concentration of the granites, although other variables related to or independent of the SiO_2 concentration may also be involved to a lesser extent.

Other such relationships exist. Figure 5.2.a shows a plot of the residual gravity anomaly against the mean uranium level for some of the Caledonian granites. The granites separate into two groups, with some overlap, indicated on the graphs by the regression lines. It should be noted that an exponential curve could equally well be fitted, but would not affect the interpretation.

The junction of the two regression lines occurs close to the mean uranium levels for all granites given by Hack (1983), which is also close to the average value for the upper crust. Ignoring the effects of granite volume and host rock density upon the gravity anomaly, a possible interpretation would be that the granites have been eroded to different levels. This would imply that differentiation has occurred in most of the granites. This data could also be interpreted to imply that the granites arose from two different sources, producing granites with very different uranium levels. Subsequent interaction with the local rocks during ascent and final emplacement could then have driven the granite uranium levels toward the average level for the upper crust. Work by researchers such as Harmon and Halliday (1980) led these authors to conclude that the British late Caledonian granites were derived from partial fusion of mantle like material together with a crustal component. The relationship between the uranium and gravity anomalies, together with the results obtained from modelling the Cairngorm granites are compatible with this interpretation, despite the limitations mentioned previously.

5.3 The Iapetus suture zone and the Caledonian granites of the Southern Uplands and Northern England

The proposed subduction plate beneath the Iapetus suture zone was briefly investigated employing the hypothesis that a fossilised slab of subducted basalt should show up as a negative magnetic anomaly in the main aeromagnetic field, at least in part of the area concerned. Reversal of the magnetic field during production of the slab could also give rise to a positive magnetic field. It is also possible that both positive and negative anomalies would be present in the area of interest, depending upon how much of the subducting plate is left, the speed of motion of the plate, and the interval between reversals of the earth's magnetic field.

Figure 5.3.a shows a plot of the variation in the aeromagnetic field strength along a line at right angles to the originally proposed Iapetus suture zone (see line X-X on figure 4.2.a) from 308630 to 412472. Values of the aeromagnetic field strength at 10 kilometre intervals were taken from the aeromagnetic map of Great Britain. To simplify the interpretation, the magnetic field values were averaged on a 5 kilometre line at right angles to each point on the line X-X, with the aim of eliminating many of the near surface magnetic anomalies. The reason for showing the position of the granites at right angles to the profile will become apparent later.

A major aeromagnetic low occurs at the 60 kilometre position, south of the Ennerdale granite. However, this low is associated with the Wensleydale granite and has been interpreted as being due to a thick layer of metasediments uplifted by the Wensleydale granite during its ascent and emplacement by Bott et al (1985). Eliminating the effect of this anomaly is difficult without carrying out spectral filtering of the data, but south of this anomaly the upward trend in the magnitude of the main aeromagnetic field appears to continue.

Figure 5.3.b shows that a surprisingly simple slab type model can account for much of the observed magnetic field variations along the profile. The magnetic susceptibility of the slab, shown as 0.06 SI, lies within the range for basalt given by Telford et al (1976). The angle of inclination makes this a reversely magnetised basaltic slab of 5 kilometres thickness. The major difference between the modelled results and the actual magnetic field lies over the area of the Wensleydale granite. Figure 5.3.c shows the inclusion of a simple prismatic model in this area to reduce the residuals. The prism is not geologically realistic and introduces edge effects. Nevertheless, a simple model of a subducting slab does appear to be able to satisfy the requirements of the main magnetic field along this profile.

Figure 5.3.d shows electrical resistivity model of Beamish and Smythe (1986) together with a seismic profile of the WINCH-2E line, (marked on the figure). The depth contours and the seismic reflection model show a good correspondence to the magnetic model given in figure 5.3.b, particularly the depth to top surface of the slab.

If the magnetic profile in figure 5.3.a does relate to a fossilised subducting slab rather than to some secondary source, the ascending granites would interact with a volume of sediment which would depend (at least in part) upon the distance between the original subducting slab and the final position of the granite. Spectral estimates of the distance to the source of the background aeromagnetic field could be done for each area, but would be extremely time consuming. However, interaction of the granites with local sediments would also affect their concentrations of common heat producing elements such as potassium. Projection of the normal from each granite to the line X-X in figure 4.2.a, on which the aeromagnetic field strength has been estimated, gives the position of the granite with respect to the measured aeromagnetic field strength. This assumes that if a subducting slab is present, it can be represented by a wide slab of material at constant depth along the normal mentioned. Figure 5.3.e shows a plot of the average potassium levels in the granites, after Brown et al (1982), as a function of their position along this line. The Ennerdale granite, having the lowest level of

potassium, could be interpreted as having risen the least distance through the host rock, assuming that all of the granites started with similar potassium levels and volumes. The position of the Ennerdale granite occurs where a dip in the surface aeromagnetic field value is present at a position 100 kilometres along the profile line. It is exactly this position at which the proposed fossil subducting zone in figure 5.3.b reaches its closest point to the surface.

Variation in the potash content with depth has been reported for volcanic rocks from continental margins and intra-oceanic magmatic arcs (for example see Nielson and Stoiber 1973), but no report can be found of such variations for granites across a subduction zone. Comparison with the potassium levels of the granites assume that no other processes have affected the chemistry of the rocks and that the values are representative of the granites as a whole.

Given the limitations of this interpretation, the three sets of data support the position of closest approach of a subducting zone to the surface being in an area level with the centre of the Lake District rather than further north. The Loch Doon granite stands out as anomalous on figure 5.3.e. This may be because the fossilised slab is closer to the surface in this area, or that the values are unrepresentative, or that some other process has affected the potassium levels within the

granite. Such a model can only be tentative and subject to many restrictions, but it does provide the basis for further work in modelling the potential fields of the granite, slab and host rock.

5.4 Suggestions for further work

A number of areas are felt to be worthy of further investigation.

The northern and north eastern side of the Cairngorm granites, particularly at the Moine-Dalradian boundary, caused considerable problems in modelling profiles nearby. The reasons for this are unknown but it is possible that the presence of previously unknown high density rock units, mineralisation or some other factor are responsible. It is worthwhile investigating the cause of the observed magnetic and gravitational variations in this area in more detail. This could be done by the collection of high resolution gravity and magnetic data and by modelling on both a small and large scale.

The junction between the Glen Gairn and Cairngorm plutons shows some evidence for the presence of a relatively basic mass. This may be related to local mineralization and is worth further ground work and computer based modelling.

The similarity in texture of the high pass filtered aeromagnetic data covering the areas of western Glen Gairn, western Lochnagar and eastern Cairngorm suggests a similar cause. This may be due to post intrusion mineralisation, primary effects present within the granite or other effect such as the presence of

dolerite dykes. A high resolution geophysical survey of the areas mentioned could help to clarify the reason for the similarities.

The links between the geophysical (particularly magnetic), geological and geochemical data found in some of the Southern Upland granites are worthy of further investigation. Geophysical techniques could allow extrapolation of some major and minor element geochemistry to depth, as well as acting as a constraint on lateral predictions of geochemical variations both within granites and across a range of granites. Uniting two independent techniques in this way would enhance both geochemical and geophysical interpretations.

The relationship between porosity and magnetic susceptibility found in data collected by the B.G.S. for the central highland granites is worth investigating in several ways. Does magnetic susceptibility vary in the same way when a rock unit is progressively unloaded (having cooled from a liquid under load) as when it is progressively loaded? If so then experimental results found in the literature and referred to in this thesis can be applied with confidence. Is it possible to model the variation in magnetic susceptibility with separation distance of the magnetically active grains? This is a substantial problem requiring considerable computer power, but if tackled would allow an explanation for the observed results, and would allow the variation of

magnetic susceptibility with grain size and other factors as a function of intergranular distance to be investigated.

Gravmag space represents a way of observing the effects of the process of differentiation in time and space, in geophysical terms, representing variations in mafic minerals and in S_iO_2 concentrations. The evolution of rock masses in gravmag space is worth following through in more detail, possibly utilising a more complex three dimensional space to introduce the geochemistry. Such an approach is intrinsically interesting; enables some idea to be gained of what stage of its evolution a granite is at; the type of formation processes that have occurred, and how this relates to the observed surface geophysical and geochemical measurements.

The aeromagnetic data around the proposed Iapetus suture zone should be investigated in more detail utilising frequency filtering and modelling techniques. This is a relatively cheap approach compared to the cost of seismic investigations and, if the results shown in this thesis are confirmed, would allow a more thorough investigation of the properties of the suture zone to be carried out.

Appendix 1

Program to calculate orthogonal components of the magnetic field of a prism

```
      DIMENSION VV1(2,2,2),VV2(222)VV3(22,2),VV4(2,2,2)
      DIMENSION VV5(2,2,2),VV6(2,2,2)
      DIMENSION Z(2), S(2)
      DIMENSION YMAG(100,100),XMAG(100,100),XW(100,100),ZMAG(100,100)
      REAL K,L,M,N,JX,JY,JZ,KS(2),TS(2)
      FIM=(69/180)*3.1415927
      FDM=0.0
      H-49000.
      K=0.05
      PR=0.
      PM=0.
      PN=0.
      JR=0.
      L=COS(FIM))*COS(FDM)
      M=(COS(FIM))*SIN(FDM)
      N=SIN(FIM)
      JX=K*H*L+JR*PR
      JY=K*H*M+JR*PM
      JZ=K*H*N+JR*PN
      KS(1)=44.5
      KS(2)=56.5
      TS(1)=44.5
      TS(2)=56.5
      Z(1)=3.1
      Z(2)=12.0
      S(1)=-1.
      S(2)=1.
      DO 10 I=1,100
      X=FLOAT(I)
      DO 10 J=1,100
      Y=FLOAT(J)
      V1=0.
      V2=0.
      V3=0.
      V4=0.
      V5=0.
      V6=0.
5     CONTINUE
      DO 9 KD=1,2
      DO 9 KE=1,2
      DO 9 KF=1,2
      ZZ=S(KD)*S(KE)*S(KF)
      PS=X-KS(KD)
      JS=Y-TS(KE)
      RIJK=SQRT(PS*PS+JS*JS+Z(KF)*Z(KF))
      BZ=JS*Z(KF)
      AR=PS*RIJK
      VV1(KD,KE,KF)=-ZZ*ATAN2(BZ,AR)
      VV2(KD,KE,KF)=ZZ*ALOG(RIJK+Z(KF))
      VV3(KD,KE,KF)=ZZ*ALOG(RIJK+JS)
      AZ=PS*Z(KF)
      BR=JS*RIJK
```

```
      VV4(KD,KE,KF)=-ZZ*ATAN2(AZ,BR)
      VV5(KD,KE,KF)=ZZ*ALOG(RIJK+PS)
      AB=PS*JS
      ZR=Z(KF)*RIJK
      VV6(KD,KE,KF)=-ZZ*ATAN2(AB,ZR)
      V1=V1+VV1(KD,KE,KF)
      V2=V2+VV2(KD,KE,KF)
      V3=V3+VV3(KD,KE,KF)
      V4=V4+VV4(KD,KE,KF)
      V5=V5+VV5(KD,KE,KF)
      V6=V6+VV6(KD,KE,KF)
9     CONTINUE
      XMAG(I,J)=JX*V1+JY*V2+JZ*V3
      YMAG(I,J)=JX*V2+JY*V4+JZ*V5
      ZMAG(I,J)=JX*V3+JY*V5+JZ*V6
      T1=(L*H+XMAG(I,J))*(L*H+XMAG(I,J))
      T2=(M*H+YMAG(I,J))*(M*H+YMAG(I,J))
      T3=(N*H+ZMAG(I,J))*(N*H+ZMAG(I,J))
      XW(I,J)=SQRT(T1+T2+Y3)-H
10    CONTINUE
      DO 30 J=1,100
      WRITE(6,28) (XW(I,J),I=1,100)
28    FORMAT(1X,10F7.1)
30    CONTINUE
      DO 35 J=1,100
      WRITE(6,33) (XMAG(I,J),I=1,100)
33    FORMAT(1X,10F7.1)
35    CONTINUE
      DO 40 J=1,100
      WRITE(6,38) (YMAG(I,J),I=1,100)
38    FORMAT(1X,10F7.1)
40    CONTINUE
      DO 50 J=1,100
      WRITE(6,48) (ZMAG(I,J),I=1,100)
48    FORMAT(1X,10F7.1)
50    CONTINUE
      STOP
      END
```

This program is based upon Plouff(1976)

Appendix 2

Corrected ground based magnetic data from the area of the Cairngorm granites

Distance East (km)	Distance North (km)	Magnetic Field (nT)
304	793.24	49787
304.14	793.22	49776
304.22	793.12	49778
304.33	793	49756
304.44	792.93	49755
304.57	792.88	49733
304.65	792.81	49712
304.82	792.76	49702
304.96	792.7	49681
305.08	792.62	49683
305.2	792.58	49672
305.32	792.48	49669
305.44	792.41	49656
305.56	792.34	49652
305.66	792.26	49632
305.8	792.18	49630
305.9	792.1	49610
306	792.1	49596
306.1	791.92	49592
306.18	791.82	49586
306.22	791.7	49574
306.26	791.6	49577
306.13	791.38	49560
306.06	791.22	49446
306.02	791.06	49543
306.06	790.9	49534
306.16	790.76	49507
306.26	790.62	49509
306.3	790.3	49496
306.34	790.16	49473
306.42	790	49464
306.54	789.88	49454
306.64	788.78	49445
304.0	789.5	49477
304.16	789.5	49472
304.3	789.48	49467
304.41	789.44	49448

304.6	789.46	49463
304.74	789.48	49452
304.9	789.52	49457
305.04	789.56	49462
305.18	789.56	49465
305.34	789.57	49462
305.48	789.6	49462
305.62	789.62	49462
305.78	789.78	49464
305.92	789.66	49455
306.06	789.67	49451
306.23	789.66	49448
306.38	789.67	49448
306.38	789.67	49449
306.26	789.53	49445
306.36	789.4	49449
306.58	789.38	49429
306.68	789.38	49433
306.8	789.38	49425
308.98	789.4	49416
307.18	789.42	49419
307.38	789.48	49418
307.56	789.46	49389
307.79	789.4	49420
308.98	789.32	49410
308.18	789.22	49398
308.36	789.14	49395
308.56	789.08	49892
308.74	789.06	49394
308.92	789.1	49398
309.12	789.12	49391
309.32	789.16	49384
309.54	789.19	49359
309.74	789.22	49433
309.98	789.26	49501
292.7	799.5	49557
292.8	799.5	49557
293	799.5	49564
293.14	799.51	49564
293.28	799.52	49562
293.42	799.56	49549
293.54	799.58	49548
293.68	799.6	49552
293.82	799.62	49550
293.96	799.66	49552
294.08	799.7	49547
294.22	799.72	49549
294.36	799.76	49581
294.5	799.8	49542

294.62	799.84	49537
294.76	799.86	49532
294.84	799.9	49528
294.96	799.94	49531
295.04	799.96	49530
295.22	800	49531
295.36	800.04	49533
295.5	800.06	49535
295.64	800.06	49533
295.74	800.06	49508
295.84	800.06	49508
296.04	800.06	49536
296.12	800.08	49541
296.18	800.14	49543
296.26	800.24	49532
296.3	800.34	49531
296.34	800.46	49533
296.36	800.6	49539
296.38	800.74	49539
296.38	800.88	49536
296.36	801.04	49540
296.35	801.16	49548
296.33	801.3	49548
296.31	801.42	49535
296.3	801.56	49557
296.28	801.7	49538
296.24	801.84	49546
296.22	801.98	49528
296.17	802.12	49525
296.13	802.26	49523
296.05	802.36	49526
295.92	802.34	49522
295.8	802.38	49525
295.7	802.46	49529
295.6	802.56	49530
295.48	802.64	49543
295.36	802.68	49524
295.3	802.78	49524
295.3	802.92	49521
295.34	803.02	49520
295.42	803.14	49517
295.52	803.24	49525
295.59	803.36	49522
295.63	803.48	49517
295.65	803.62	49541
292.7	799.5	49557
292.8	799.5	49557
293	799.5	49564
293.14	799.51	49564

293.28	799.52	49562
293.41	799.56	49549
293.54	799.58	49548
293.68	799.6	49552
293.82	799.62	49550
293.96	799.66	49552
294.08	799.7	49547
294.22	799.72	49549
294.36	799.76	49581
294.5	799.8	49542
294.62	799.84	49537
294.76	799.86	49532
294.84	799.9	49528
294.96	799.94	49531
295.04	799.96	49530
295.22	800	49531
295.36	800.04	49533
295.5	800.06	49535
295.64	800.06	49533
295.74	800.06	49508
295.84	800.06	49508
296.04	800.06	49536
296.12	800.08	49541
296.18	800.14	49543
296.26	800.24	49532
296.3	800.34	49531
296.34	800.46	49533
296.36	800.6	49539
296.38	800.74	49539
296.38	800.88	49536
296.36	801.04	49540
296.35	801.16	49548
296.33	801.3	49548
296.31	801.42	49535
296.3	801.56	49557
296.28	801.7	49538
296.24	801.84	49526
296.24	801.84	49526
296.22	801.98	49528
296.17	802.12	49525
296.13	802.26	49523
296.05	802.36	49526
295.92	802.34	49522
295.8	802.38	49525
295.7	802.46	49529
295.6	802.56	49430
295.48	802.64	49543
295.36	802.68	49524
295.3	802.78	49524

295.3	802.92	49521
295.34	803.02	49520
295.42	803.14	49517
295.52	803.24	49525
295.52	803.24	49525
295.59	803.36	49522
295.63	803.48	49517
295.65	803.62	49541
296.02	803.62	49537
296.12	803.44	49538
296.2	803.34	49541
296.28	803.2	49547
296.36	803.08	49557
296.44	802.94	49558
296.52	802.8	49546
296.6	802.64	49532
296.68	802.52	49518
296.78	802.38	49535
296.82	802.24	49537
296.92	802.1	49528
297.02	801.98	49557
297.08	801.82	49516
297.12	801.66	49512
297.2	801.5	49487
297.26	801.36	49531
297.28	801.2	49497
297.18	801.04	49504
297.26	800.88	49498
297.2	800.74	49519
297.16	800.54	49520
297.16	800.4	49537
297.16	800.28	49519
297.18	800.16	49509
297.2	800.04	49528
297.22	799.9	49522
297.24	799.78	49508
297.25	799.66	49501
297.27	799.52	49525
297.28	799.4	49525
297.31	799.26	49525
297.36	799.24	49527
297.39	799.02	49525
297.43	798.9	49507
297.46	798.78	49509
297.53	798.66	49513
297.58	798.54	49510
297.64	798.42	49506
297.7	798.3	49502
297.75	798.19	49513

297.8	798.08	49512
297.84	797.96	49499
297.86	797.84	49513
297.92	797.72	49513
297.96	797.6	49525
298.0	797.44	49541
298.4	797.34	49544
298.8	797.22	49519
298.14	797.1	49511
298.2	797.18	49530
298.18	796.98	49489
298.19	796.84	49493
298.21	796.72	49511
298.23	796.59	49579
298.26	796.46	49584
298.28	796.34	49562
298.31	796.2	49559
298.32	796.08	49574
298.37	795.94	49576
298.29	795.9	49665
298.96	799.6	49530
299.0	799.72	49521
299.04	799.82	49533
299.12	799.92	49523
299.2	800.02	49515
299.32	800.06	49513
299.44	800.06	49503
299.56	800.04	49524
299.67	800.01	49521
299.78	899.98	49523
299.9	899.96	49515
300.02	899.98	49523
300.12	800.02	49515
300.24	800.02	49503
300.38	799.98	49519
300.48	799.96	49517
300.6	799.96	49547
300.72	799.98	49523
300.8	800.00	49517
300.92	800.08	49514
298.34	797.32	49522
298.4	797.4	49521
298.48	797.48	49515
298.52	797.56	49512
298.6	797.64	49521
298.66	797.2	49533
298.74	797.8	49521
298.81	797.85	49525
298.88	797.93	49527

298.96	798.0	49533
299.04	798.26	49544
299.07	798.13	49531
299.17	798.19	49536
299.25	798.26	49541
299.34	798.31	49521
299.41	798.36	49539
299.39	798.42	49541
299.57	798.48	49531
299.66	798.54	49522
299.52	798.58	49531
299.62	798.62	49525
299.52	798.66	49509
299.44	798.7	49526
299.34	798.73	49531
299.26	798.78	49521
299.16	798.82	49511
299.08	798.86	49511
299.0	798.9	49511
298.92	799.0	49511
298.9	799.12	49487
298.88	799.26	49529
298.88	799.36	49508
298.92	799.48	49514
301.02	800.22	49502
301.12	800.32	49478
301.2	800.4	49496
301.28	800.5	49512
301.36	800.58	49465
301.46	800.66	49473
301.54	800.74	49498
301.64	800.82	49479
301.72	800.92	49491
301.78	801.02	49517
301.88	801.1	49519
301.96	801.18	49518
302.06	801.24	49508
302.14	801.34	49539
302.24	801.4	49527
302.32	801.5	49522
302.42	801.62	49520
302.5	801.74	49514
302.56	801.86	49514
302.62	802.0	49521
302.68	802.12	49537
302.72	802.26	49512
302.76	802.4	49510
302.76	802.54	49494
302.78	802.68	49557

302.76	802.82	49557
302.74	802.92	49557
302.66	803.04	49557
302.7	803.16	49557
302.84	803.21	49574
302.96	803.23	49560
303.12	803.22	49532
303.24	803.24	49478
303.37	803.2	49427
303.5	803.16	49565
303.62	803.1	49597
303.72	803.4	49614
303.78	803.	49515
303.8	802.83	49665
303.78	802.67	49636
303.76	802.5	49528
303.76	802.32	49525
303.76	802.13	49585
303.78	801.96	49568
303.76	801.79	49544
303.75	801.62	49535
303.7	801.44	49546
303.62	801.3	49513
303.53	801.15	49547
303.46	801.02	49531
303.4	800.84	49524
303.32	800.68	49509
303.2	800.46	49521
303.14	800.34	49492
303.06	800.24	49523
302.98	800.16	49496
302.86	800.12	49535
302.74	800.08	49528
302.64	800.06	49508
302.5	800.04	49531
302.37	800.02	49535
302.24	800.6	49539
302.1	799.96	49528
301.96	799.92	49552
301.86	799.94	49552
301.74	799.98	49557
301.62	800.02	49552
301.5	800.04	49531
301.4	800.08	49536
301.28	800.12	49495
301.18	800.18	49489
301.04	800.4	49500
300.94	800.54	49522
300.84	800.68	49502

300.74	800.8	49499
300.66	801.94	49533
300.58	801.08	49531
300.46	801.18	49512
300.36	801.31	49527
300.26	801.45	49509
300.18	801.6	49517
300.2	801.76	49523
300.26	801.9	49507
300.36	802	49488
300.48	802.06	49510
300.6	802.08	49524
300.72	802.13	49505
300.84	802.18	49510
300.96	802.24	49497
301.06	802.3	49495
301.16	802.38	49500
301.28	802.46	49509
301.38	802.34	49547
301.48	802.63	49550
301.58	802.7	49594
301.68	802.78	49590
301.78	802.86	49619
301.88	802.96	49620
301.98	803.04	49601
302.1	803.08	49509
302.12	803.14	49565
302.34	803.2	49562
302.58	803.28	49555
302.7	803.32	49570
302.82	803.36	49594
302.96	803.38	49606
303.1	803.4	49575
303.22	803.39	49510
303.36	803.38	49497
303.48	803.37	49589
303.6	803.36	49605
303.72	803.34	49617
303.88	803.32	49666
303.94	803.3	49594
296.26	797.24	49616
296.22	797.04	49610
296.21	796.86	49615
296.20	796.69	49623
296.26	796.51	49636
296.21	796.48	49615
296.6	796.44	49662
296.72	796.36	49650
296.74	796.16	49631

296.74	795.98	49613
296.73	795.8	49612
296.73	795.62	49622
296.74	795.44	49619
296.88	795.46	49626
297.06	795.52	49640
297.18	795.62	49658
297.36	795.6	49715
297.54	795.66	49697
297.7	795.74	49697
297.86	795.8	49684
298.04	795.86	49814
298.2	795.84	49731
298.38	795.76	49688
298.4	795.58	49674
298.42	795.42	49681
298.43	795.26	49746
298.38	795.11	49721
298.38	794.98	49711
298.37	794.82	49690
298.38	794.47	49671
298.39	794.52	49673
298.39	794.38	49664
298.41	794.24	49651
298.42	794.1	49637
298.44	793.94	49632
298.45	793.8	49683
298.45	793.64	49657
298.46	793.5	49643
298.48	793.32	49619
298.54	793.22	49619
298.7	793.16	49679
298.83	793.04	49627
298.86	793.84	49694
298.86	792.72	49736
298.88	792.56	49705
298.91	792.4	49659
298.92	792.24	49636
298.97	792.1	49622
299.02	791.94	49623
299.06	791.8	49601
299.12	791.66	49597
299.2	791.51	49597
299.28	791.36	49618
299.36	791.22	49509
299.42	791.08	49619
299.54	790.96	49630
299.66	790.86	49601
299.78	790.74	49588

299.82	790.56	49579
299.83	790.42	49552
299.86	790.26	49545
299.92	790.12	49540
300.13	789.86	49530
300.23	789.74	49524
300.34	789.62	49518
300.44	789.5	49508
300.54	789.47	49504
300.66	789.26	49504
300.76	789.14	49493
300.86	789.02	49489
301	788.9	49488
301.16	788.84	49484
301.34	788.76	49477
301.5	787.72	49467
301.64	788.7	49471
301.76	788.68	49472
301.76	788.68	49472
301.92	788.66	49487
302.12	788.64	49455
302.28	788.65	49466
302.45	788.68	49476
302.58	788.74	49485
302.7	788.82	49495
302.82	788.92	49504
302.95	789.04	49471
303.02	789.15	49510
303.12	789.27	49520
303.19	789.38	49516
303.29	789.48	49528
303.45	789.53	49535
303.62	789.52	49526
303.76	789.51	49521
303.92	789.49	49416
299.12	790.91	49621
298.96	790.84	49621
298.8	790.78	49623
298.66	790.71	49621
298.52	790.62	49603
298.42	790.52	49606
298.33	790.42	49594
298.2	790.32	49451
298.08	790.24	49584
297.96	790.14	49580
297.9	789.98	49573
297.95	789.86	49566
298.08	789.78	49566
298.2	789.7	49566

298.3	789.63	49564
298.42	789.54	49562
298.56	789.46	49551
298.68	789.38	49546
298.82	789.32	49542
298.94	789.26	49538
299.08	789.18	49530
299.2	789.1	49517
299.34	789.02	49514
299.44	788.9	49511
299.57	788.82	49507
299.68	788.73	49501
299.78	788.62	49499
299.9	788.51	49495
300.02	788.43	49492
300.16	788.38	49488
300.32	788.34	49486
300.46	788.32	49485
300.6	788.28	49484
300.74	788.26	49483
300.89	788.24	49479
301.04	788.23	49481
301.2	788.23	49478
301.34	788.23	49482
301.5	788.24	49473
299.76	793.96	49701
299.86	793.94	49686
300.02	793.92	49701
300.16	793.92	49699
300.3	793.91	49701
300.44	793.9	49713
300.56	793.92	49768
300.72	793.93	49747
300.86	793.94	49438
301	793.95	49432
301.14	793.95	49719
301.28	793.95	49707
301.42	793.95	49697
301.52	793.95	49693
301.66	793.94	49680
301.81	793.88	49676
301.94	793.82	49709
302.08	793.78	49699
302.22	793.78	49702
302.36	793.8	49742
302.48	793.83	49742
302.64	793.84	49706
302.78	793.84	49721
302.92	793.82	49779

303.04	793.74	49806
303.14	793.65	49815
303.26	793.56	49817
303.37	793.48	49801
303.5	793.44	49782
303.6	793.4	49801
303.78	793.32	49803
303.88	793.3	49810
303.98	793.26	49782
298.77	794.56	49752
299.2	794.18	49741
300.64	793.72	49735
300.6	793.36	49700
300.8	794.5	49700
299.05	795.11	49720
299.04	794.02	49718
302.38	793.16	49703
303.56	794.38	49722
302.81	793.48	49768
302.46	793.44	49726
284.92	796.16	49706
284.9	796.01	49510
284.96	795.86	49515
284.92	795.64	49505
284.97	795.49	49518
284.96	795.34	49515
284.93	795.16	49514
284.86	794.98	49516
284.8	794.86	49517
284.84	794.7	49512
284.91	794.56	49509
284.88	794.41	49504
284.86	794.25	49509
284.94	794.12	49506
284.96	793.94	49506
284.88	793.82	49508
284.84	793.66	49507
285.09	793.5	49504
285.17	793.49	49500
285.29	793.5	49498
285.39	793.5	49498
285.5	793.51	49496
285.1	793.54	49498
285.9	793.61	49499
286.1	793.67	49498
286.28	793.72	49506
286.46	793.8	49509
286.62	793.9	49510
286.78	794.01	49509

286.96	794.12	49514
287.08	794.26	49509
289.88	796.14	49561
290.18	795.9	49561
290.32	795.68	49559
290.61	795.6	49556
290.92	795.64	49547
291.21	795.71	49550
291.52	795.74	49543
291.82	795.78	49541
292.02	795.91	49540
304.08	803.18	49644
304.22	803.16	49631
304.34	803.15	49646
304.48	803.15	49637
304.61	803.15	49644
304.76	803.16	49611
304.89	803.17	49609
305.04	803.2	49595
305.16	803.24	49594
305.28	803.28	49606
305.42	803.32	49590
305.56	803.36	49589
305.7	803.35	49604
305.84	803.3	49612
305.96	803.26	49602
306.1	803.27	49594
306.22	803.3	49572
306.35	803.38	49612
306.46	803.46	49605
306.56	803.57	49633
306.64	803.66	49615
306.74	803.77	49619
306.84	803.82	49639
306.92	803.98	49633
307.0	804.08	49573
307.05	804.19	49555
307.1	804.32	49648
307.14	804.46	49638
307.18	804.58	49649
307.23	804.74	49652
307.28	804.86	49651
307.33	804.97	49662
307.44	805.08	49644
304.22	803.16	49631
304.34	803.15	49646
304.48	803.15	49644
304.76	803.16	49611
304.89	803.17	49609

305.04	803.2	49595
305.16	803.24	49594
305.28	803.28	49606
305.42	803.32	49590
305.56	803.36	49589
305.7	803.35	49604
305.84	803.3	49612
305.96	803.26	49602
306.1	803.27	49594
306.22	803.3	49572
306.35	803.38	49612
306.46	803.46	49605
306.56	803.57	49633
306.64	803.66	49615
306.74	803.77	49619
306.8	799.1	49582
306.84	803.82	49639
306.92	803.98	49633
307.	804.08	49573
307.05	804.19	49555
307.1	802	49597
307.1	804.32	49648
307.14	804.46	49638
307.18	804.58	49649
307.23	804.74	49652
307.28	804.86	49651
307.33	804.97	49662
307.44	805.08	49710
307.51	805.16	49682
307.6	805.28	49674
307.67	805.39	49696
307.74	805.49	49751
307.8	805.61	49673
307.86	805.74	49601
307.92	805.86	49540
307.98	806.	49683
308.06	806.24	49583
308.2	806.4	49741
308.32	806.52	49657
308.42	806.62	49612
308.55	806.7	49629
308.68	806.74	49710
308.84	806.76	49820
308.96	806.66	49719
309.06	806.56	49786
309.21	806.52	49710
309.3	803.9	49605
309.32	806.58	49562
309.4	799.6	49595

309.4	802.1	49602
309.46	806.68	49758
309.64	806.63	49584
309.76	806.54	49750
309.87	806.46	49985
310.02	805.98	49585
310.16	805.96	49772
310.32	805.94	49822
310.45	805.96	49772
310.6	805.99	49531
310.74	806.02	49430
310.88	806.06	49577
311.04	806.49	49630
311.18	806.52	49601
311.48	806.49	49550
311.6	799.9	49620
311.62	806.44	49501
311.7	804.1	49610
311.76	806.37	49524
311.9	806.32	49589
312.03	806.25	49638
312.1	802.1	49615
312.16	806.21	49705
312.21	806.16	49644
312.44	806.16	49546
312.73	806.19	49540
312.87	806.23	49527
313.	806.28	49616
313.14	806.34	49622
313.28	806.38	49575
313.42	806.41	49621
313.56	806.45	49586
313.71	806.5	49579
313.84	806.54	49556
313.99	806.58	49561
314	804.7	49608
314.12	806.64	49570
314.25	806.69	49580
314.38	806.76	49563
314.52	806.72	49562
315.3	800.2	49596
304.04	809.7	49487
304.18	809.63	49486
304.32	809.54	49505
304.4	809.44	49463
304.56	809.4	49458
304.7	809.34	49465
304.86	809.28	49461
305.02	809.27	49455

305.18	809.31	49452
305.32	809.36	49464
305.46	809.41	49461
305.62	809.46	49465
305.74	809.5	49470
305.91	809.56	49455
306.	809.56	49455
306.11	809.58	49465
306.2	809.58	49452
306.3	809.56	49454
306.39	809.51	49445
306.48	809.47	49451
306.57	809.44	49450
306.68	809.4	49447
306.78	809.36	49446
306.76	809.32	49461
306.98	809.28	49449
307.05	809.22	49449
307.12	809.13	49448
307.16	809.05	49458
307.22	808.97	49467
307.26	808.88	49464
307.32	808.8	49464
307.43	808.65	49463
307.52	808.5	49458
307.64	808.35	49456
307.72	808.22	49478
307.81	808.03	49607
307.92	807.91	49569
307.96	807.76	49508
307.97	807.6	49712
307.96	807.48	49596
307.96	807.4	49780
307.95	807.28	49780
307.94	807.2	49682
307.94	807.1	49686
307.94	807.	49620
307.94	806.91	49709
307.94	806.8	49635
307.94	806.69	49570
307.94	805.99	49495
307.95	805.49	49509
307.96	805.31	49641
283	805.5	49798
283.08	805.62	49459
283.14	805.76	49694
283.2	805.84	49724
283.26	806.01	49713
283.34	806.12	49711

283.43	806.23	49710
283.52	806.34	49710
283.62	806.44	49724
283.72	806.56	49699
283.81	806.67	49764
283.91	806.76	49764
284.03	806.86	49752
284.13	806.96	49768
284.22	807.06	49805
284.32	807.17	49775
284.42	807.26	49760
284.5	807.38	49756
284.59	807.48	49773
284.67	807.6	49783
284.76	807.72	49799
284.84	807.82	79756
284.92	807.92	49751
285.02	808.02	49780
285.12	808.1	49801
285.23	808.18	49810
285.34	808.26	49817
285.46	808.34	49799
285.58	808.41	49827
285.68	808.5	49836
285.8	808.57	49892
285.92	808.66	49878
286.04	808.72	49958
286.14	808.78	49942
286.26	808.86	49912
286.39	808.93	49925
286.5	809.02	49937
286.56	809.14	49902
286.6	809.28	49870
286.7	809.2	49858
286.84	809.22	49891
286.95	809.31	49837
287.06	809.39	49885
287.18	809.47	49889
287.28	809.57	49882
287.39	809.64	49924
287.5	809.72	49927
287.6	809.8	49918
287.71	809.88	49864
287.82	809.97	49819
287.93	810.06	49805
288.02	810.16	49835
288.06	810.3	49815
288.09	810.44	49828
288.12	810.58	49805

288.28	810.76	49825
288.42	810.78	49783
288.56	810.8	49756
283.54	805.31	49753
283.58	805.2	49699
283.62	805.08	49734
283.68	804.98	49713
283.72	804.86	49737
283.71	804.63	49712
283.68	804.52	49697
283.66	804.4	49718
283.82	804.42	49674
283.92	804.38	49699
283.99	804.43	49680
284.1	804.48	49706
284.22	804.52	49679
284.36	804.57	49695
284.48	804.62	49692
284.76	804.68	49697
284.82	804.56	49674
284.96	804.54	49647
285.03	804.46	49552
285.1	804.36	49683
285.16	804.44	49657
285.2	804.58	49698
285.23	804.72	49706
285.28	804.84	49706
285.34	804.97	49711
285.4	805.1	49715
285.48	805.21	49728
285.56	805.32	49741
285.64	805.44	49725
285.72	805.56	49540
285.8	805.67	49759
285.87	805.8	49772
285.94	805.91	49756
286.04	805.99	49781
286.12	806.13	49751
286.22	806.23	49779
286.32	806.33	49781
286.42	806.43	49799
286.52	806.53	49809
286.62	806.62	49795
286.72	806.72	49795
286.82	806.82	49787
286.92	806.92	49796
287	807.06	49785
287.08	807.14	49773
287.22	807.2	49788

287.36	807.24	49750
287.5	807.26	49748
287.64	807.28	49748
287.72	807.39	49792
287.81	807.5	49762
287.9	807.6	49761
287.92	807.76	49761
287.98	807.9	49770
288.04	808.02	49753
288.12	808.14	49760
288.19	808.26	49761
288.26	808.38	49727
288.36	808.49	49738
288.43	808.6	49761
288.51	808.72	49642
288.6	808.83	49667
288.56	808.96	49638
288.64	809.08	49621
288.72	809.2	49612
288.8	809.32	49831
288.87	809.42	49608
89.04	809.48	49689
89.1	809.62	49738
89.17	809.72	49731
89.26	809.86	49731
89.32	809.97	49722
89.42	810.08	49703
89.5	810.16	49696
89.58	810.28	49706
89.66	810.4	49700
89.73	810.53	49708
89.8	810.66	49640
89.86	810.78	49698
291.52	810.6	49627
291.54	810.46	49554
291.55	810.3	49584
291.56	810.16	49575
291.58	810.02	49557
291.58	809.88	49554
291.59	809.74	49545
291.6	809.58	49557
291.61	809.44	49562
291.62	809.3	49556
291.62	809.16	49537
291.62	809.0	49524
291.62	808.85	49554
291.6	808.72	49547
291.59	808.57	49576
291.58	808.42	49476

291.58	808.28	49472
291.57	808.13	49493
291.56	807.98	49525
291.56	807.84	49510
291.55	807.71	49495
291.54	807.54	49502
291.6	807.4	49482
291.7	807.28	49505
291.81	807.18	49504
291.92	807.09	49512
292.04	807	49517
292.16	806.92	49526
292.29	806.86	49524
292.42	806.8	49475
292.56	806.73	49482
292.66	806.64	49513
292.74	806.51	49494
292.82	806.38	49506
292.89	806.25	49498
292.92	806.12	49493
292.93	805.97	49513
292.94	805.83	49512
292.94	805.68	49502
292.89	805.53	49518
292.82	805.41	49494
292.78	805.26	49520
292.73	805.12	49483
292.69	804.98	49554
292.64	804.84	49557
292.61	804.71	49554
292.57	804.56	49514
292.54	804.42	49590
292.54	804.28	4.593
292.54	804.16	49572
292.56	804.02	49588
292.58	803.9	49573
292.6	803.77	49601
292.62	803.64	49584
292.64	803.52	49587
292.66	803.47	49547
292.68	803.27	49554
292.7	803.14	49550
292.7	803.0	49531
292.66	802.89	49517
292.61	802.79	49494
292.59	802.65	49580
292.56	802.53	49575
292.52	802.5	49545
292.5	802.28	49557

292.48	802.16	49538
292.42	802.04	49570
292.4	801.92	49590
292.34	801.79	49584
292.32	801.67	49589
292.28	801.54	49581
292.25	801.52	49581
292.21	801.3	49608
292.16	801.17	49592
292.12	801.04	49626
292.09	800.92	49616
292.04	800.89	49628
292.01	800.64	49596
291.96	800.55	49595
291.93	800.42	49574
291.9	800.3	49558
291.87	800.18	49566
291.78	800.08	49558
291.68	799.99	49571
291.62	799.94	49474
291.54	799.8	49572
291.46	799.65	49605
291.38	799.45	49568
291.84	799.41	49512
292.14	799.43	49563
293.08	799.48	49531
291.34	799.29	49562
291.28	799.12	49542
291.24	798.96	49518
291.22	798.76	49533
291.22	798.6	49530
291.22	798.42	49606
291.22	798.24	49657
291.2	798.08	49557
291.12	797.92	49577
290.96	797.72	49657
292	796.22	49539
292.02	796.55	49540
92.02	796.87	49544
292	797.17	49534
291.7	797.08	49536
291.41	797.01	49535
291.09	797	49548
290.79	797.06	49622
290.48	797.16	49546
290.2	797.26	49552
289.62	797.4	49548
289.31	797.5	49550
289.57	797.33	49554

291.92	799.98	49648
291.92	799.91	49668
291.92	799.76	49632
291.9	799.62	49640
292.02	799.59	49650
292.08	799.58	49630
292.17	799.56	49623
292.31	799.55	49617
292.44	799.55	49608
292.62	799.52	49595
292.72	799.51	49587
292.84	799.5	49580
293.0	799.48	49577
293.14	799.48	49573
293.27	799.48	49560
293.39	799.49	49538
285.02	796.22	49505
285.05	796.38	49502
285.06	796.56	49503
285.06	796.7	49515
285.04	796.86	49511
284.98	797.01	49514
284.98	797.16	49514
285	797.32	49515
285.12	797.46	49523
285.34	797.52	49451
285.44	797.48	49457
285.53	797.48	49456
285.63	797.48	49455
285.72	797.44	49458
285.77	797.36	49456
285.82	797.28	49462
285.88	797.19	49455
285.96	797.13	49460
286.06	797.14	49455
286.14	797.21	49456
286.2	797.27	49458
286.29	797.34	49466
286.39	797.39	49462
286.48	797.42	49462
286.6	797.42	49472
286.71	797.43	49483
286.79	797.44	49496
286.9	797.44	49501
287	797.44	49508
287.1	797.44	49509
287.2	797.44	49514
287.3	797.43	49517
287.4	797.43	49515

287.5	797.42	49522
287.6	797.39	49520
287.7	797.36	49519
287.78	797.33	49519
287.88	797.31	49516
287.98	797.28	49516
288.08	797.25	49512
288.17	797.23	49512
287.26	797.2	49523
287.36	797.18	49529
287.46	797.17	49528
287.54	797.14	49531
287.65	797.12	49531
287.74	797.1	49539
287.83	797.07	49538
285.64	803.83	49600
285.32	803.02	49598
285.44	802.26	49544
285.29	801.44	49525
285.02	800.66	49515
284.86	799.86	49487
284.82	799.01	49472
285.08	798.26	49452
293.44	810.11	49545
293.56	810.16	49549
293.6	810.22	49572
293.78	810.28	49568
293.9	810.34	49551
294.02	810.38	49542
294.16	810.37	49533
294.28	810.36	49557
294.41	810.35	49526
294.54	810.34	49542
294.68	810.33	49545
294.78	810.3	49533
294.92	810.29	49498
295.04	810.28	49517
295.17	810.24	49514
295.28	810.18	49496
295.34	810.08	49524
295.4	809.96	49526
295.5	809.88	49508
295.58	809.7	49501
295.57	809.6	49503
295.56	809.48	49526
295.55	809.32	49508
295.52	809.28	49508
295.5	809.24	49512
295.46	808.92	49522

295.38	808.8	49500
295.28	808.7	49511
295.18	808.58	49502
295.08	808.46	49465
295.02	808.32	49522
291.96	808.19	49516
294.92	808.06	49545
294.84	807.92	49507
294.78	807.78	49532
294.74	807.64	49526
294.7	807.5	49548
294.7	807.34	49525
294.71	807.18	49539
294.74	807.02	49483
294.88	806.96	49514
294.98	806.96	49526
295.1	806.96	49539
295.22	806.97	49529
295.34	806.98	49515
295.43	807.02	49535
295.52	807.1	49510
295.62	807.19	49519
295.68	807.28	49500
295.74	807.41	49539
295.82	807.5	49522
295.9	807.58	49522
295.94	807.71	49510
296	807.82	49494
296.06	807.86	49543
296.12	807.9	49525
296.24	807.96	49532
296.34	808.06	49501
296.46	808.16	49501
296.58	808.24	49534
296.72	808.23	49427
296.84	808.21	49468
296.96	808.2	49519
297.12	808.24	49508
297.802	808.36	49515
297.34	808.32	49511
297.43	808.29	49521
297.54	808.34	49485
297.66	808.38	49484
297.78	808.39	49512
297.91	808.38	49536
298.04	808.38	49499
298.18	808.38	49484
298.33	808.38	49458
298.34	808.52	49534

298.3	808.66	49462
298.27	808.78	49436
298.23	808.91	49456
298.2	809.04	49442
298.18	809.14	49439
298.16	809.28	49471
298.13	809.4	49430
298.09	809.54	49454
298	809.63	49466
297.88	809.72	49412
297.76	809.78	49457
297.66	809.84	49441
297.42	809.92	49404
297.28	809.96	49461
297.16	810	49356
297.04	810.01	49445
296.76	810	49476
296.62	809.98	49465
296.49	809.94	49382
296.35	809.92	49496
296.12	809.86	49579
295.97	809.84	49499
295.86	809.82	49491
295.76	809.8	49510
294.36	806.38	49522
294.42	806.26	49528
294.46	806.14	49535
294.53	806	49540
294.6	805.9	49546
294.68	805.79	49564
294.78	805.68	49562
294.86	805.61	49568
294.96	805.51	49566
295.03	805.42	49560
295.14	805.33	49558
295.2	805.22	49558
295.27	805.11	49548
295.34	805.0	49538
295.4	804.86	49544
295.46	804.73	49548
295.52	804.62	49536
295.55	804.5	49533
295.59	804.36	49524
295.61	804.23	49530
295.63	804.12	49517
295.65	803.98	49502
295.66	803.84	49502
295.67	803.71	49510
295.69	803.57	49541

298.44	808.38	49459
298.51	808.32	49456
298.54	808.22	49456
298.57	808.13	49453
298.59	808.03	49472
298.59	807.92	49483
298.58	807.82	49477
298.55	807.72	49544
298.52	807.63	49470
298.49	807.54	49462
298.51	807.44	49522
298.57	807.36	49500
298.63	807.28	49498
298.68	807.2	49510
298.74	807.12	49407
298.79	807.02	49539
298.8	806.92	49512
298.8	806.83	49504
298.8	806.72	49510
298.89	806.76	49524
298.98	806.79	49523
299.08	806.82	49476
299.18	806.86	49456
299.22	806.78	49500
299.18	806.68	49498
299.15	806.58	49560
299.12	806.5	49553
299.08	806.4	49560
299.06	806.3	49555
299.06	806.2	49552
299.05	806.1	49546
299.09	806.02	49544
299.14	805.93	49490
299.19	805.84	49423
299.23	805.76	49542
299.27	805.67	49541
299.34	805.6	49547
299.41	805.52	49555
299.46	805.44	49559
299.47	805.36	49591
299.51	805.3	49586
299.6	805.27	49596
299.62	805.18	49589
299.64	805.1	49591
299.66	805.06	49597
299.73	805.03	49582
299.82	804.98	49508
299.82	804.91	49421
299.86	804.84	49598

299.9	804.8	49596
299.98	804.82	49595
300.06	804.83	49610
300.14	804.84	49599
300.21	804.88	49600
300.28	804.9	49605
300.34	804.94	49608
300.480	805	49597
300.46	804.98	49600
300.5	804.92	49604
300.52	804.84	49606
300.53	804.77	49596
300.54	804.68	49602
300.54	804.6	49602
300.53	804.52	49602
293.84	809.62	49454
298.47	809.61	49457
298.6	809.6	49481
298.72	809.6	49482
298.84	809.61	49464
298.96	809.66	49501
299.08	809.72	49454
299.18	809.78	49447
299.29	809.82	49461
299.4	809.86	49445
299.52	809.92	49443
299.61	10.02	49437
299.69	810.1	49448
299.79	810.18	49436
299.92	810.2	49450
300	810.26	49457
300.06	810.36	49446
300.13	810.48	49443
300.19	810.58	49455
300.27	810.71	49458
300.36	810.78	49494
300.5	810.82	49475
300.61	810.84	49460
300.74	810.85	49455
300.88	810.84	49461
301.01	810.83	49455
301.14	810.8	49454
301.26	810.76	49454
301.38	810.71	49464
301.5	810.66	49462
301.62	810.62	49456
301.72	810.59	49485
301.88	810.56	49459
302.16	810.48	49511

302.3	810.36	49505
302.44	810.25	49472
302.56	810.19	49491
302.7	810.12	49501
302.84	810.06	49505
303	810	49498
303.14	809.94	49508
303.29	809.91	49486
303.44	809.84	49481
303.6	809.81	49492
303.74	809.78	49487
303.89	809.72	49495

Appendix 3

Corrected ground based magnetic data from the area of the Cairnsmore of Fleet granite

Distance East (km)	Distance North (km)	Magnetic field (nT)
254.6	575.1	49067
255.4	575	49035
256.3	574.6	49036
257.1	574.5	49037
257.5	574.2	49996
258.1	573.6	49047
259	573.7	49044
259.8	573.5	49046
260.6	573.4	49045
261.3	573	49041
261.7	572.3	49039
262.3	571.6	49036
263.1	571.2	49034
263.9	570.8	49033
264.6	570.5	49146
263.3	571.4	49017
263.5	571.6	48992
264	571	49117
264.2	571.3	49098
263.8	569.9	49074
264.5	570	49077
265.3	570.1	49037
265	570.2	49075
266	570.4	49024
265.2	571.1	49060
265.4	572	49056
264.3	571.8	49086
264.3	572.6	49100
263.8	572.9	49096
263.3	573.2	49056
264.3	573.3	49052
264.2	574	49021
263.7	574.4	49060
263.8	574.6	49051
262.8	574.7	49055
263.4	574.9	49087
263.4	575.3	49051
263	575.5	49077
262.5	575.5	49014
261.8	575.7	49037
260.9	576.1	49059

261.1	575.4	49124
261.2	574.9	49050
259.5	574.7	49053
260.2	574.5	49048
260	574.1	49046
260.7	574.4	49055
261.2	574.1	49048
261.5	573.7	49046
262.1	573.7	49033
262.2	573	49031
262.3	572.3	49027
262.9	572	49022
261.9	571.4	49015
261.4	571.2	49013
261.1	570.5	49010
261.7	569.7	49010
262.4	570.1	49007
263.1	570	48994
260.9	568.2	48992
260.6	567.6	48988
260	567	48977
260.2	572.9	49015
259.8	572.4	49011
259.8	571.7	49011
259.9	571.1	49005
259.5	570.4	49001
259.9	570.1	49003
259.4	569.6	49007
260.6	570	49007
259.1	569	49008
258.9	567.2	49011
258.8	567.7	49011
258.6	568.3	49007
258.3	568.7	49008
257.9	569.3	49002
257.9	570.1	49009
258.1	570.8	49004
258.2	571.6	49008
258.2	568.8	49017
259.5	573.2	49014
258.8	573.2	49021
258.1	573.2	49023
257.4	573.5	49024
257.8	574	49024
256.2	574.3	49033
255.3	574.5	49035
254.7	575	49029
255	574.5	49029
255.3	573.8	49029
255	573.1	49029
254.9	572.4	49028
255.2	571.7	49028
255.2	571	49028
251.9	570.3	49028

254.7	569.5	49031
254.7	569	49022
254.9	568.3	49023
255.2	567.7	49020
255.4	567.1	49014
255.5	566.3	49026
254.8	565.6	49000
255.4	565.2	49005
255.6	564.8	49007
256	565.2	49009
256	565.6	49023
256.3	566.3	49024
256.6	567	49021
256.9	567.7	49021
257.3	568.3	49015
257.3	569.1	49020
257.1	569.1	49014
256.2	569.4	49015
257.5	566.1	49009
256.8	565.6	49009
254.1	566.8	49019
254.3	567.4	49018
254.4	567.1	49014
254.7	566.6	49019
254.3	567.4	49018
254	568	49013
253.9	568.4	49013
254.3	574.5	49009
254.3	573.7	49055
253.6	573.3	49053
253.8	572.6	49053
254.2	574.4	49033
253.6	574.1	49031
252.9	573.7	49030
252.3	573.2	49031
251.7	572.9	49032
251	572.5	49032
250.3	572.3	49031
249.7	571.9	49022
249	571.8	48973
247.9	569.8	49082
248.3	569.7	49079
248.6	569.3	49044
248.7	568.9	49038
249.1	569.3	49065
252.2	570.5	49034
252	571.3	49031
251.9	571.9	49032
252.2	572.5	49034

Table 1

Physical properties of core samples from boreholes in the Cairngorm, Mount Battock, Ballater and Bennachie granites.

Depth (m)	Saturated Density (Mg/m^3)	Grain Density (Mg/m^3)	Porosity %	Sonic V_p	Magnetic Suscept. S.I. ($x10^{-3}$)
Cairngorm					
095-098	2.585	2.618	2.05	5.52	0.05
215-220	2.610	2.623	0.80	5.71	2.49
294-295	2.617	2.623	0.30	5.81	2.66
Mt. Battock					
090-095	2.614	2.628	0.72	5.77	2.06
186-190	2.616	2.624	0.40	5.76	7.62
256-260	2.602	2.608	1.68	-	0.63
Ballater					
095-100	2.605	2.618	0.68	5.48	2.63
193-197	2.613	2.620	0.58	5.59	5.59
294-298	2.598	2.618	1.08	5.68	0.93
Bennachie					
095-098	2.608	2.618	0.53	5.74	6.04
193-197	2.598	2.610	0.63	5.60	0.38
293-294	2.590	2.620	1.83	5.17	0.15

After Rollin (1984)

Table 2

Magnetic susceptibilities of rock samples from the Cairngorm area

Location		Susceptibility (10^{-4} SI)
Granites		
2988 8072		11.5
2001 8069		1.32
2981 8069		6.04
2982 8029		6.65
2963 8041		0.76
2964 8051		0.38
2965 8053		3.07
2966 8055		0.57
2003 8105		0.99
2998 8042		0.76
2999 8032		0.85
	Average	2.76
Host rock		
2883 8104		2.41
2886 8112		0.33
2997 8192		0.28
2889 8114		2.41
2895 8146		1.98
2895 8146		1.37
2015 8105		0.38
2914 8088		0.8
2914 8089		0.61
2914 8089		0.52
2995 8230		1.3
2078 8220		0.61
2895 8069		1.65
2851 8041		0.99
2851 8041		0.14
2996 8192		2.1
	Average	1.12

Table 3

Modal abundances of the main granite types in the Cairngorm area

	A	B	C	D
Quartz	22.1	30.2	28.5	30.3
K-feldspar	33.3	30.2	30.8	35.2
Plagioclase	36.2	35.8	35.8	31.4
Biotite	6.8	2.9	2.1	2.8
Opaques	0.5	0.2	-	0.4
Sphene	0.9	-	-	-
Allanite	0.2	-	-	-
Muscovite	-	0.8	2.7	-
Fluorite	-	-	0.2	-

A Glen Avon granite
B Main granite
C Beinn Bhreac granite
D Carn Ban Mor granite

After Harrison (1986)

Table 4

Magnetic susceptibilities of rock samples from the Tomintoul area

Location	Susceptibility (10^{-4} SI)
3099 8183	1.04
3099 8183	3.74
3099 8183	1.71
3099 8183	2.31
3099 8183	9.97
3099 8183	7.83
3099 8183	1.45
Average	4.01

All samples are from the diorite at 310,818.

References

Aina A., 1986
Reduction to the equator, reduction to the pole and orthogonal reduction of magnetic profiles.
Exploration geophysics, 17, 141-145.

Al-Chalabi M., 1970
Interpretation of two-dimensional magnetic profiles by non-linear optimisation.
Bull. Geof. Teor. Appl., 12, 3-20.

Andreasen G.E., Zietz I., 1969
Magnetic fields for a 4 x 6 prismatic model.
U.S. Geological Survey professional paper 666.

Arkani-Hamed J., 1988
Differential reduction to the pole of magnetic anomalies.
Geophysics, 53, 1592-1600.

Arkani-Hamed J., Urquhart W.E.S., 1990
Reduction to the pole of north american magnetic anomalies.
Geophysics, 55, 218-225.

Bamford D., Nunn K., Prodehl C., Jacob B., 1978
LISPIV: Crustal structure of Northern Britain.
Geophys. Jnl. Royl. Astr. Soc., 54, 43-60.

Baranov V., 1957
A new method for interpretation of aeromagnetic maps.
Geophysics, 22, 359-383.

Baranov V., Naudy H., 1964
Numeric calculation of the formula of reduction to the magnetic pole.
Geophysics, 29, 67-69.

Barritt S.D., 1983
The controls of radioelement distribution in the Etive and Cairngorm granites: implications for heat production.
Ph.D. thesis.
The Open University.

Barton P.J., 1992
LISPB revisited; a new look under the Caledonides of northern Britain.
Geophys. Jnl. Int., 110, 371-392.

Barraclough D.R., 1987
I.G.R.F. revision 1987 special report of the international association of geomagnetism and aeronomy, division 1, working group 1.

Barrow G., Cunningham-Craig E.H., 1913
The geology of the upper Strathspey, Gaick and Forest of Atholl.
Mem. Geol. Survey of Scotland.

Beamish D., Smythe D.K., 1986
Geophysical images of the deep crust: the Iapetus suture.
Jnl. of Geol. Soc., London, 143, 489-497.

Begg H., McCann C., Mehmeet H., 1987
Programs for the reduction and interpretation of geophysical profiles.
University of Reading.

Bhattacharyya B.K., 1964
Magnetic anomalies due to prism-shaped bodies with arbitrary polarisation.
Geophysics, 29, 517-531.

Bhattacharyya B.K., 1966
Continuous spectrum of the total magnetic field anomaly due to a rectangular prismatic body.
Geophysics, 31, 97-121.

Bhattacharyya B.K., Leu L.K., 1975
Spectral analysis of gravity and magnetic anomalies due to two-dimensional structures.
Geophysics, 40, 993-1013.

Bhattacharyya B.K., Chan K.C., 1977
Computation of gravity and magnetic anomalies due to inhomogenous distribution of magnetization and density in a localized region.
Geophysics, 42, 602-609.

Bhattacharyya B.K., Chan C.K., 1977
Reduction of magnetic and gravity data on an arbitrary surface acquired in a region of high topographic relief.
Geophysics, 42, 1411-1430.

Bingham C., Godfrey M.D., Tukey J.W., 1967
Modern techniques of power estimation.
IEEE Trans on audio and electro acoustics.
v AU-15, 56-66.

Blakely R.J., Grauch V.J.S., 1983

Magnetic models of crystalline terrain; accounting for the effects of topography.
Geophysics, 48, 1551-1557.

Blakely R.J., Simpson R.W., 1986
Approximating edges of source bodies from magnetic or gravity anomalies.
Geophysics, 51, 1494-1498.

Blaxland A.B., Aftalion M., Van Breemen O., 1979
Pb isotopic composition of feldspars from Scottish Caledonian granites, and the nature of the underlying crust.
Scott. J. Geol., 15, 139-151.

Bott M.H.P., Smith R.A., Stacey R.A., 1966
Estimation of the direction of magnetization of a body causing a magnetic anomaly using a pseudo-gravity transform.
Geophysics, 31, 803-811.

Bott M.H.P., Long R.E., Green A.S.P., Lewis A.H.J., Sinha M.C., Stevenson D.L., 1985
Crustal structure south of the Iapetus suture beneath northern England.
Nature 314, 724-727.

Broome 1992
An IBM compatible program for interactive three-dimensional gravity modelling.
Computers and Geosciences, 18, 337-348.

Brown G.C., 1979
Geochemical and geophysical constraints on the origin and evolution of the Caledonian granites.
The Caledonides of the British Isles reviewed, 6445-652.
Scottish Academic Press Ltd.

Brown G.C., Locke C.A., 1979
Space-time variations in British Caledonian granites: some geophysical correlations.
Earth and Planetary Science Letters, 45, 69-79.

Brown G.C., Cassidy J., Tindle A.G., Hughes D.J., 1979
The Loch Doon granite: an example of granite petrogenesis in the British Caledonides.
J. Geol. Soc., London, 136, 745-753.

Brown G.C., Cassidy J., Locke C.A., 1981
Caledonian plutonism in Britain: a summary.
J. Geophys. Res., 86, 10502-10514.

Brown G.C., Webb P.C., Lee M.K., Wheildon J., Cassidy J., 1982

Development of HDR reconnaisance in the United Kingdom.
Int. conf. on geothermal energy, Italy, paper J5.

Busse F.H., Carrigan R.C., 1974
Convection induced by centrifugal buoyancy.
J. Fluid Mech., 62, 579-592.

Cooley J.W., Tukey J.W., 1965
An algorithm for computing the mixed radix fast Fourier transform.
IEEE Trans Audio and electroacoustics, v AU-17, 93-103.

Cordell L., Taylor P., 1971
Investigation of magnetization and density of a North Atlantic seamount using Poisson's theorem.
Geophysics 36, 919-937.

Cordell L., Grauch V.S.J., 1982
Reconciliation of the discrete and integral Fourier transforms.
Geophysics, 47, 237-243.

Denham C.R., 1974
Counterclockwise motion of palaeomagnetic directions 24000 years ago at Mono Lake, California.
J. Geomag. Geoelec., 26, 487-498.

Dewey J., 1969
Evolution of the Appalachian-Caledonian orogen.
Nature, 222, 124-128.

Dewey J.F., Pankhurst R.J., 1970
The evolution of the Scottish Caledonides in relation to their isotopic age pattern.
Trans. Roy. Soc. Edinburgh, 68, 361-389.

Dickinson W.R., 1975
Potash-Depth (K-h) relations in continental margin and intra-oceanic magmatic arcs.
Geology, 78, 53-56.

El-Batroukh S.I., 1975
Geophysical investigation of the Loch Doon granite, S.W. Scotland.
Ph.D. Thesis, University of Glasgow.

Ervin C.P., 1976
Reduction to the magnetic pole using a fast Fourier series algorithm.
Computers and geosciences, 2, 211-217.

Fedi M., 1989
On the interpretation of magnetic anomalies for strong remanent magnetizations.

Pageoph, 130, 4, 721-733.

Floyd J.D., Trench A., 1988
Magnetic susceptibility contrasts in Ordovician greywackes of the Southern Uplands of Scotland.
Jnl. of the Geol. Soc., London, 146, 77-83.

Freeman B., Klemperer S.L., Hobbs R.W., 1988
The deep structure of northern England and the Iapetus suture zone from BIRPS deep seismic reflection profiles.
Jnl. Geol. Soc., London, 145, 727-740.

Gentleman W.M., Sande G., 1966
Fast Fourier transforms - for fun and profit.
Proc. Fall Joint Comp. Cont AFIPS Conf. Proc., 563-568.

Grauch V.J.S., Campbell D.L., 1984
Does draping aeromagnetic data reduce terrain-induced effects.
Geophysics, 49, 75-80.

Grauch V.J.S., 1985
Aeromagnetic and gravity models of the pluton below Lake City caldera, Colorado.
U.S. Geol. Survey, circular 949, 15-16.

Grauch V.J.S., 1987
A new variable-magnetization terrain correction method for aeromagnetic data.
Geophysics, 52, 94-107

Grauch V.J.S., Cordell L., 1987
Short note - limitations of determining density or magnetic boundaries from the horizontal gradient of gravity or pseudogravity data.

Green A.G., 1976
Interpretation of Project MAGNET aeromagnetic profiles across Africa.
Geophys. J. R. Astr. Soc., 44, 201-228.

Greig D.C., 1971
British Regional Geology - The South of Scotland
H.M.S.O.

Hack U., 1983
On the content and vertical distribution of K,Th and U in the continental crust.
Earth and Plan. Sci. Letters, 62, 360-366

Hall J., Powell D.W., Warner M.R., El-Isa Z.M.H., Adesanya O., Bluck B.J., 1983

Seismological evidence of shallow crystalline basement in the Southern Uplands of Scotland.
Nature, 305, 418-420.

Halliday A.N., Aftalion M., van Breemen O., Jocelyn J., 1979
Petrogenetic significance of Rb-Sr and U-Pb isotopic systems in the 400 Ma old British Isles granitoids and their hosts.
In: The Caledonides of the British Isles-Reviewed.
Geol. Soc. London, Spec. Publ. No. 8: 653-661.

Halliday A.N., Graham C.M., Aftalion M., Dymoke P., 1989
Short paper: The depositional age of the Dalradian supergroup: U-Pb and Sm-Nd isotopic studies of the Tayvallich volcanics, Scotland.
J. Geol. Soc., 146, 3-6.

Hansen R.O., Pawlowski R.S., 1989
Reduction to the pole at low latitudes by wiener filtering.
Geophysics, 54, 12, 1607-1613.

Harmon R.S., Halliday A.N., 1980
Oxygen and strontium isotope relationships in the British late Caledonian granites.
Nature, 283: 21-25.

Harrison T.N., 1986
The mode of emplacement of the Cairngorm granite.
Scottish J. Geol., 22, 303-314.

Harrison T.N., 1988
Magmatic garnets in the Cairngorm granite, Scotland.
Min. Mag., 52, 659-667.

Harrison T.N., 1990
Chemical variation in micas from the Cairngorm pluton, Scotland.
Min. Mag., 54, 355-366.

Harry W.T., 1965
The form of the Cairngorm pluton.
Scottish J. Geol., 1, 1-8.

Hennessy J., 1978
Uranium, thorium and Caledonian granite magmatism.
Ph.D. thesis.
University of Liverpool.

Hide R., 1966
Free hydromagnetic oscillations of the Earth's core and the theory of the geomagnetic secular variation.
Phil. Trans. Roy. Soc. London, A259, 615-647.

Hutton V.R.S., Jones A.G., 1978
Magnetovariational and magnetotelluric investigations in southern Scotland.
J. Geomag. Geoelectr., 29, 141-149.

Isacks B., Oliver J., Syker L.R., 1968
Seismology and the new global tectonics.
J. Geophys. Res., 73, 5855-5899.

IAGA Division 1 Working group 1, 1988
I.G.R.F. revision 1987.
Geophysics, 53, 576-578.

Jelenska M., 1975
Stress dependence of magnetization and magnetic properties of igneous rocks.
Pageoph., 113, 635-649.

Kafafy A.M., Tarling D.H., 1985
Magnetic fabric in some granitic aureoles, Southern Uplands, Scotland.
Jnl. Geol. Soc. of London, 142, 1007-1014.

Kanasewich E.R., Agarwal R.G., 1970
Analysis of combined gravity and magentic fields in the wavenumber domain.
Jnl. Geophys. res., 75, 5702-5712.

Kis K., Kloska K., Kovacs F., Toth S., 1989
Reduction to the magnetic pole of total field magnetic anomalies and determination of its parameters based on Poisson's relation.
Acta Geod. Geoph. Mont. Hung., 24, 329-341.

Kis K., 1990
Transfer properties of the reduction of magnetic anomalies to the pole and to the equator.
Geophysics, 55, 1141-1147.

Lapworth C., 1889
On the Ballantrae rocks of South Scotland.
Geol. Mag., 26, 20-4;59-69.

Le Mouël J.L., Ducruix J., Ha Duyen C., 1983
On the recent variation of the apparent westward drift rate.
Geophys. Res. L., 10, 369-372.

Lee M.K., Pharaoh T.C., Soper N.J., 1990
Structural trends in central Britain from images of gravity and aeromagnetic fields.
Jnl. Geol. Soc. of London, 147, 241-258.

Leeder M.R., Fairhead D., Lee A., Stuart G., Clemmey H., Green B., Al Haddeh B., 1989
Sedimentary and tectonic evolution of the Northumberland basin.
Occasional publications of the Yorkshire Geological Society, 6, 207-223.

Leggett J.K., Casey D.M., 1982
On the Ballantrae rocks of south Scotland.
Geol. Mag., 26, 20-24; 59-69.

Lindsay R.B., 1941
Introduction to physical statistics.
Dover publications.

Locke C.A., 1980
Geophysical investigations of Caledonian granites within a regional classification.
Ph.D. thesis.
University of Liverpool.

Locke C.A., Brown G.C., 1978
Geophysical constraints on the structure and emplacement of the Shap granite.
Nature, 272, 526-528.

McGregor D.M., Wilson C.D.V., 1967
Gravity and magnetic surveys of the younger gabbros of Aberdeenshire.
Qtly. Jnl. Geol. Soc. London, 123, 99-123.

McKerrow W.S., Leggett J.K., Eales M.H., 1977
Imbricate thrust model of the Southern Uplands of Scotland.
Nature, 267, 237-239.

McLeod M.G., 1983a
Optimal processing of satellite derived magnetic anomaly data.
Phys. Earth and Plan. Int., 31, 10-26.

McLeod M.G., 1983b
Crustal geomagnetic field: two dimensional intermediate wavelength spatial power spectrum.
Phys. Earth and Plan. Int., 31, 132-144.

Morris J.H., 1987
The Northern Belt of the Longford-Down, Ireland and Southern Uplands, Scotland: an Ordovician back-arc basin.
Jnl. of Geol. Soc., London, 144, 773-786.

Muniruzzaman M., Banks R.J., 1989
Basement magnetization estimates by wavenumber domain analysis of magnetic and gravity maps.

Geophys. Jnl., 97, 103-117.

Nagata T., 1970
Anisotropic magnetic susceptibility of rocks under mechanical stresses.
Pageoph., 78, 110-122.

Naidu P., 1970
Statistical structure of aeromagnetic fields.
Geophysics, 35, 279-292.

Needham D.T., 1993
The structure of the western part of the Southern Uplands of Scotland.
Jnl Geol. Soc., London, 150, 341-354.

Néel L., 1955
Some theoretical aspects of rock magnetism.
Adv. in Phys., 4, 191.

Nielson D.R., Stoiber R.E., 1973
Relationship of potassium content in andesitic lavas and depth to the seismic zone.
J. Geophys. Res., 78, 6887-6892.

Parker R.L., Klitgord K.D., 1972
Magnetic upward continuation from an uneven track.
Geophysics, 37, 662-668.

Parslow G.R., 1968
The physical and structural featurs of the Cairnsmore of Fleet granite and its aureole.
Scott. J. Geol., 4, 91-108.

Parslow G.R., Randall B.A.O., 1973
A gravity survey of the Cairnsmore of Fleet granite and its environs.
Scott. J. Geol., 9, 219-231.

Peddie N.W., 1992
Analysis of geomagnetic secular variations during 1980-1985 and 1985-1990, and geomagnetic models proposed for the 1991 revision of the International Geomagnetic Reference Field.
J. Geomag. Geoelec., 44, 735-743.

Pilkington M., Roest W., 1992
Draping aeromagnetic data in areas of rugged topography.
Jnl. Appl. Geophysics, 29, 135-142.

Plouff D., 1976

Gravity and magnetic fields of polygonal prisms and application to magnetic terrain corrections.
Geophysics, 42, 727-741.

Press F., 1966
Handbook of physical constants.
The Geological Society of America memoir 97.

Read H.H., 1961
Aspects of Caledonian magmatism in Britain.
Liverpool and Manchester Geol. J., 2, 653-683.

Regan R.D., 1983
The current status of the IGRF and its relation to magnetic surveys.
Geophysics, 48, 997-998.

Reid A.B., 1980
Short note on aeromagnetic survey design.
Geophysics, 45, 973-976.

Rollin K.E., 1980
Caledonian magmatism in the Grampian area: preliminary interpretation of the bouguer anomaly map.
Applied geophysics unit report.
British Geological Survey.

Rollin K.E., 1984
Gravity modelling of the eastern highlands granites in relation to heat flow studies.
Applied geophysics unit report.
British Geological Survey.

Singleton R.C., 1967
A method for computing the fast Fourier transform with auxiliary memory and limited high speed storage.
IEEE Trans Audio Electroacoust., AU-15, 91-98.

Skilbrei J.R., Kihle O., 1992
On the use of the autocorrelation method for estimating the depth to the magnetic basement.
Pageoph., 138, 501-506.

Soper N.J., England R.W., Snyder D.B., Ryan P.D., 1992
The Iapetus suture zone in England, Scotland and eastern Ireland: a reconciliation of geological and deep seismic data.
Jnl. Geol. Soc., London, 149, 697-700.

Soper N.J., Hutton D.M.W., 1984
Late Sinistral displacements in Britain. Implications for a three plate collisional model.
Tectonics, 3, 781-794.

Spector A., 1968
Ph.D. thesis.
University of Toronto.

Spector A., Grant F.S., 1970
Statistical models for interpreting aeromagnetic data.
Geophysics, 35, 293-302.

Stephens W.E., 1992
Spatial, compositional and rheological constraints on the origin of zoning in the Criffell pluton, Scotland.
Trans. Roy. Soc. Ed., Earth Sci, 83, 191-199.

Talwani M., 1965
Computation with the help of a digital computer of magnetic anomalies caused by bodies of arbitrary shape.
Geophysics 30, 797-817.

Tarling D.H., Hrouda F., 1993
The magnetic anisotropy of rocks.
Chapman and Hall.

Telford W.M., Geldart L.P., Sheriff R.E., Keys D.A., 1978
Applied Geophysics.
Cambridge University Press.

Tindle A.G., Pearce J.A., 1981
Petrogenetic modelling of in situ fractional crystallization in the zoned Loch Doon pluton, Scotland.
Contrib. Mineral. Petrol., 78, 196-207

Vacquier V., Steenland N.C., Henderson R.G., Zietz I., 1951
Interpretation of aeromagnetic maps.
Geol. Soc. Am. Mem. 47.

Vestine E.H., 1953
On variations of the geomagnetic field, fluid motions, and the rate of the Earth's rotation.
J. Geophys. Res., 58, 127-145.

Webb P.C., Tindle A.G., Barritt S.D., 1987
Factors controlling the distribution of heat production in selected UK granites.
Geophys. Res. Lett., 14, 299-302.

Yukutake T., Tachinaka H., 1969
Separation of the Earth's magnetic field into drifting and standing parts.
Bull. Earthquake Res. Inst. Japan, 47, 65-97.

Figure 1.3.a

Iron-Titanium oxides in magmatic rocks

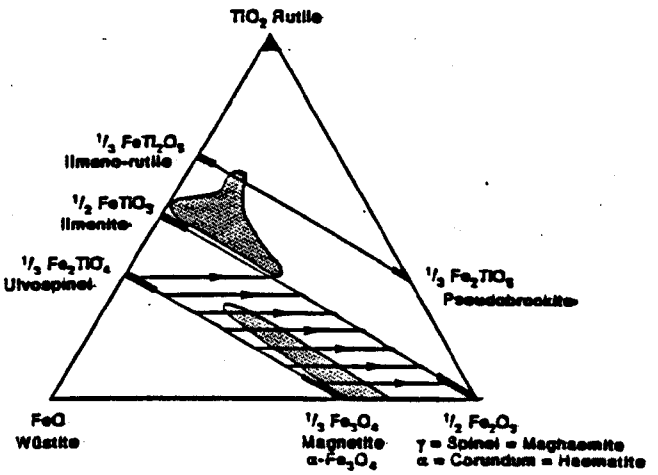

After Tarling D.H. and Hrouda F. (1993)
The magnetic anisotropy of rocks

Figure 2.3.a

A continuously varying signal reconstructed

from undersampled data

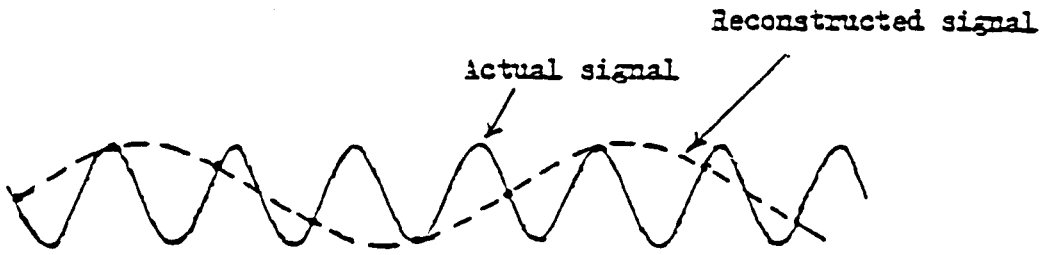

. = sampling points

Figure 2.3.b

A Dirac comb in the space domain

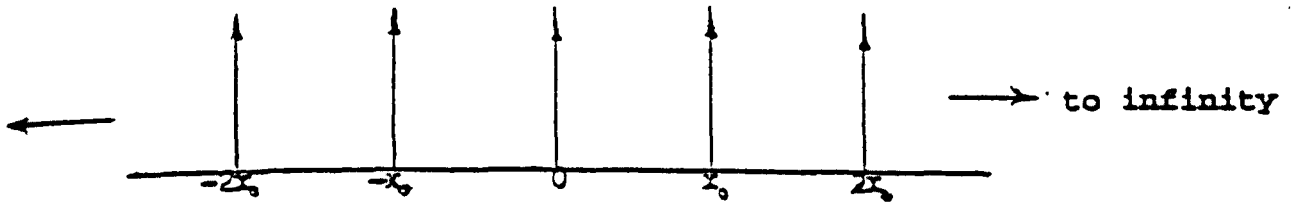

Figure 2.3.c

A two dimensional Dirac comb

in the space domain

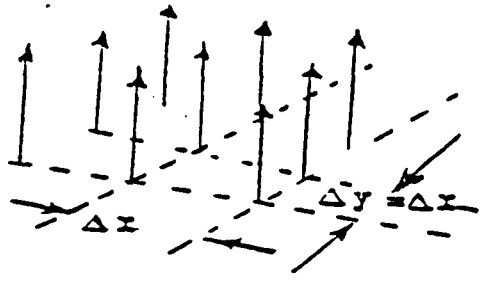

Figure 2.3.d

A two dimensional Dirac comb

in the frequency domain

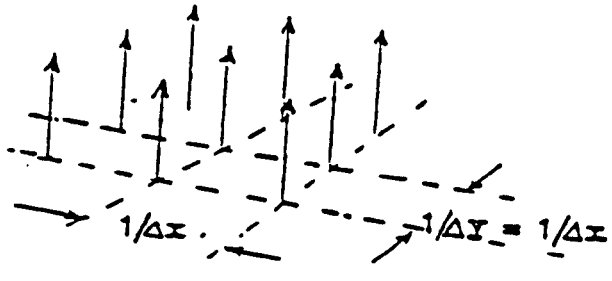

Figure 2.3.e

The frequency domain representation of a signal with overlap

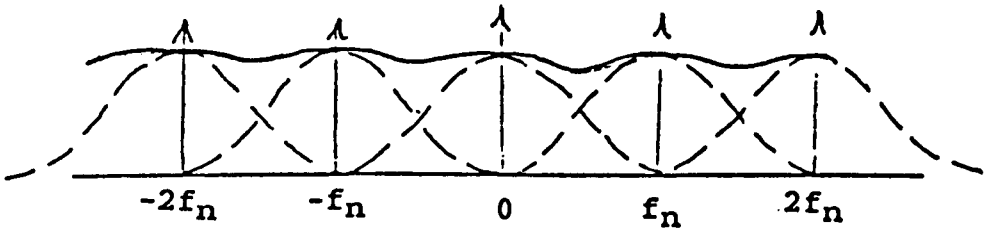

Figure 2.3.f

The frequency domain representation of a signal without overlap

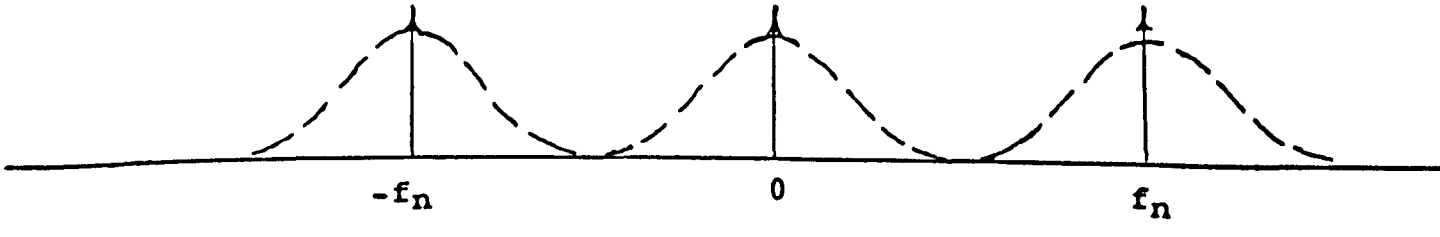

Figure 2.4.a

A rectangular window function

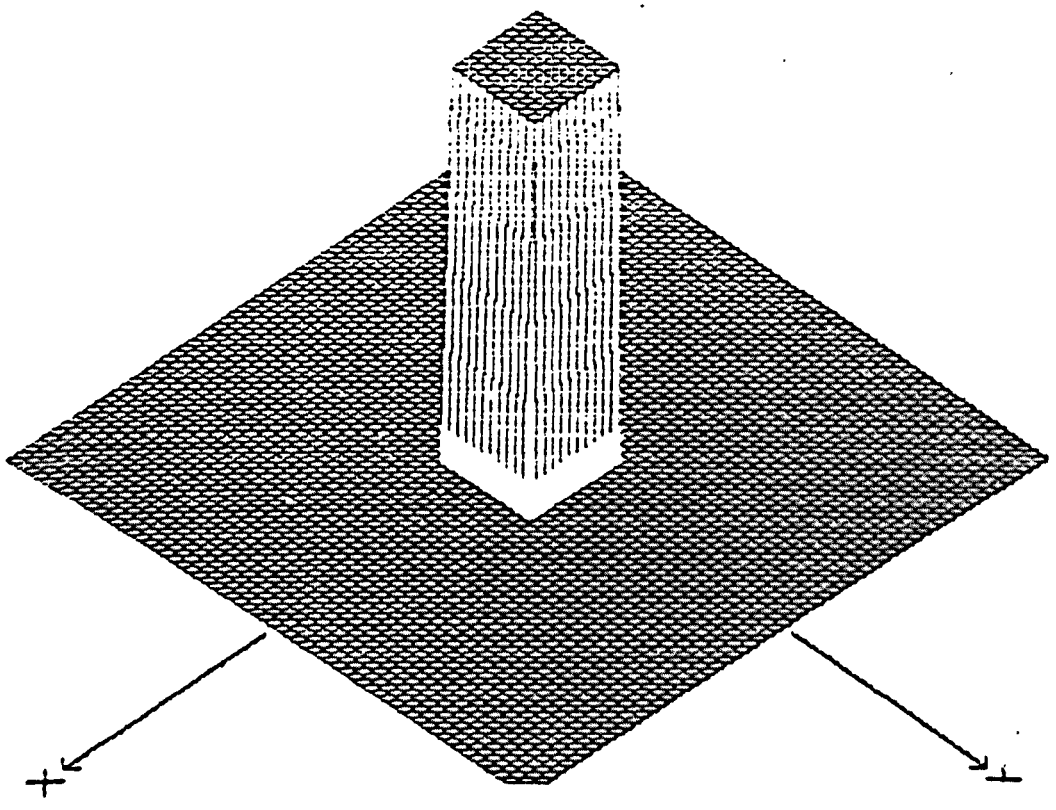

Figure 2.4.b

The two dimensional Fourier transform

of a rectangular window

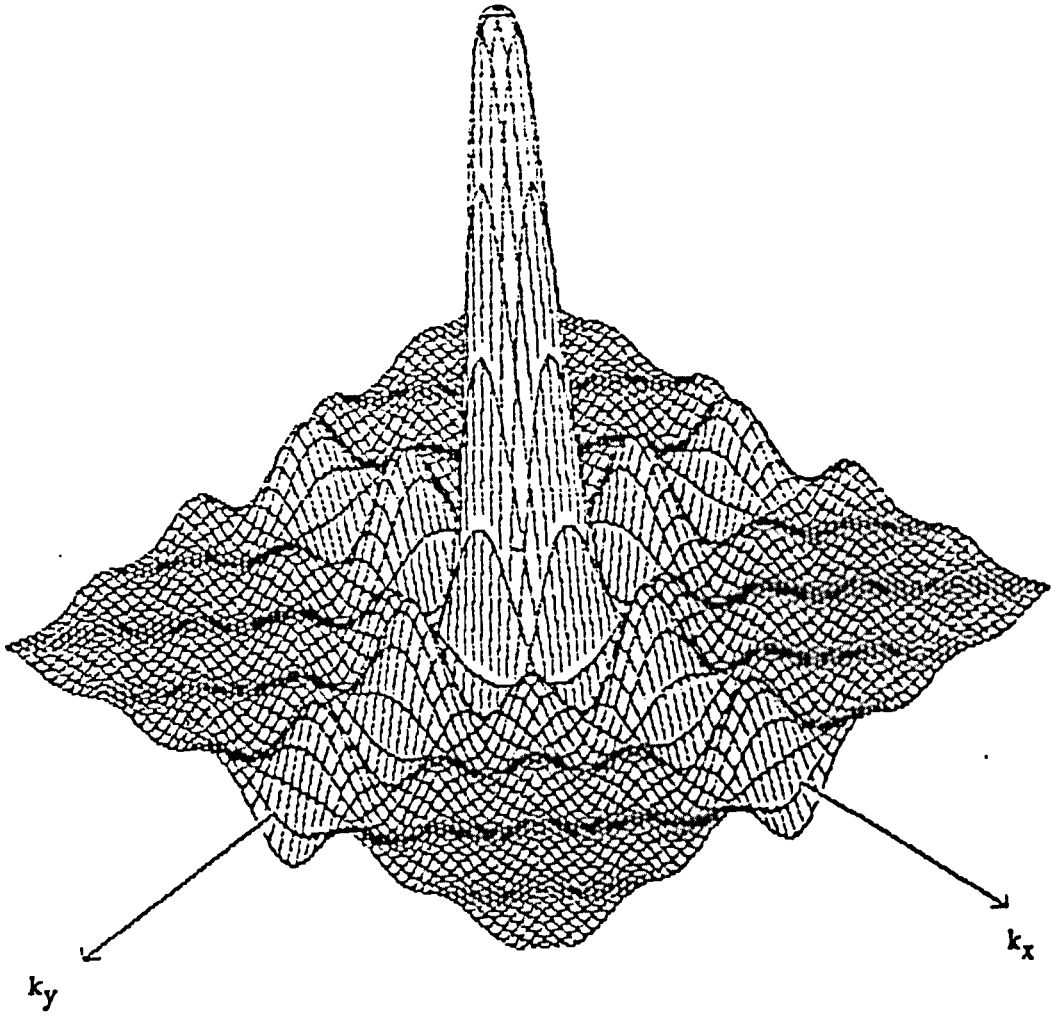

k_x, k_y are wavenumbers

Figure 2.4.c

The two dimensional Fourier transform

of a rectangular window

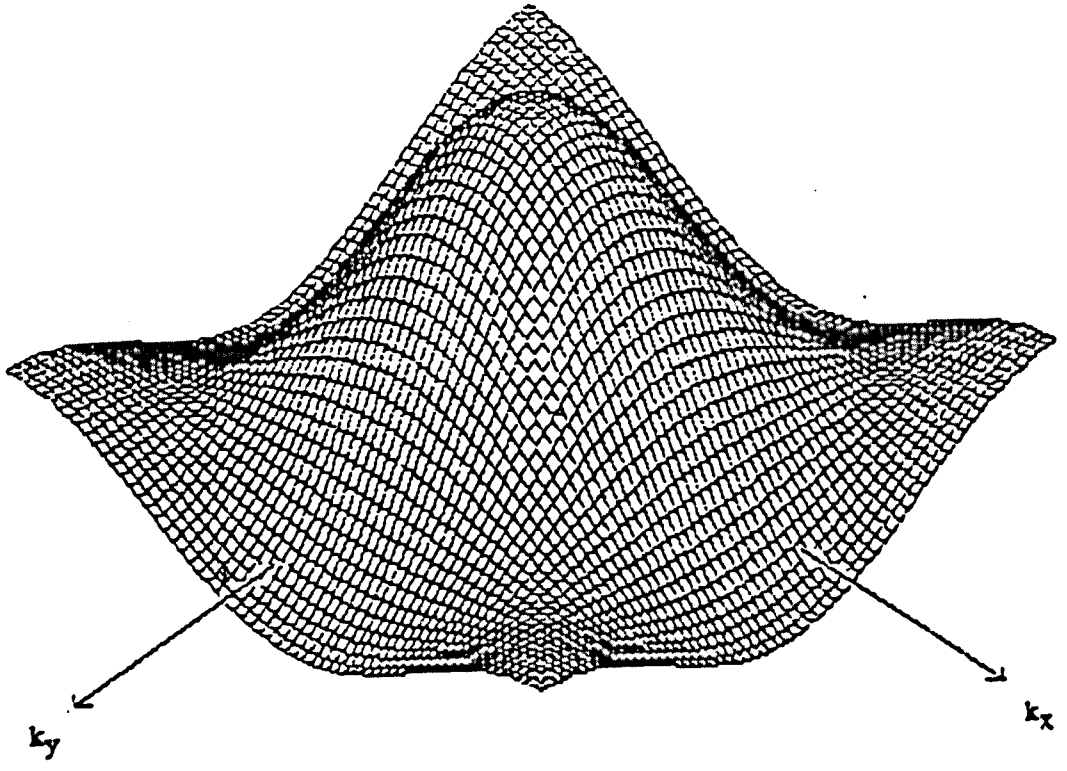

k_x k_y are wavenumbers

Figure 2.4.d

A two-dimensional window function

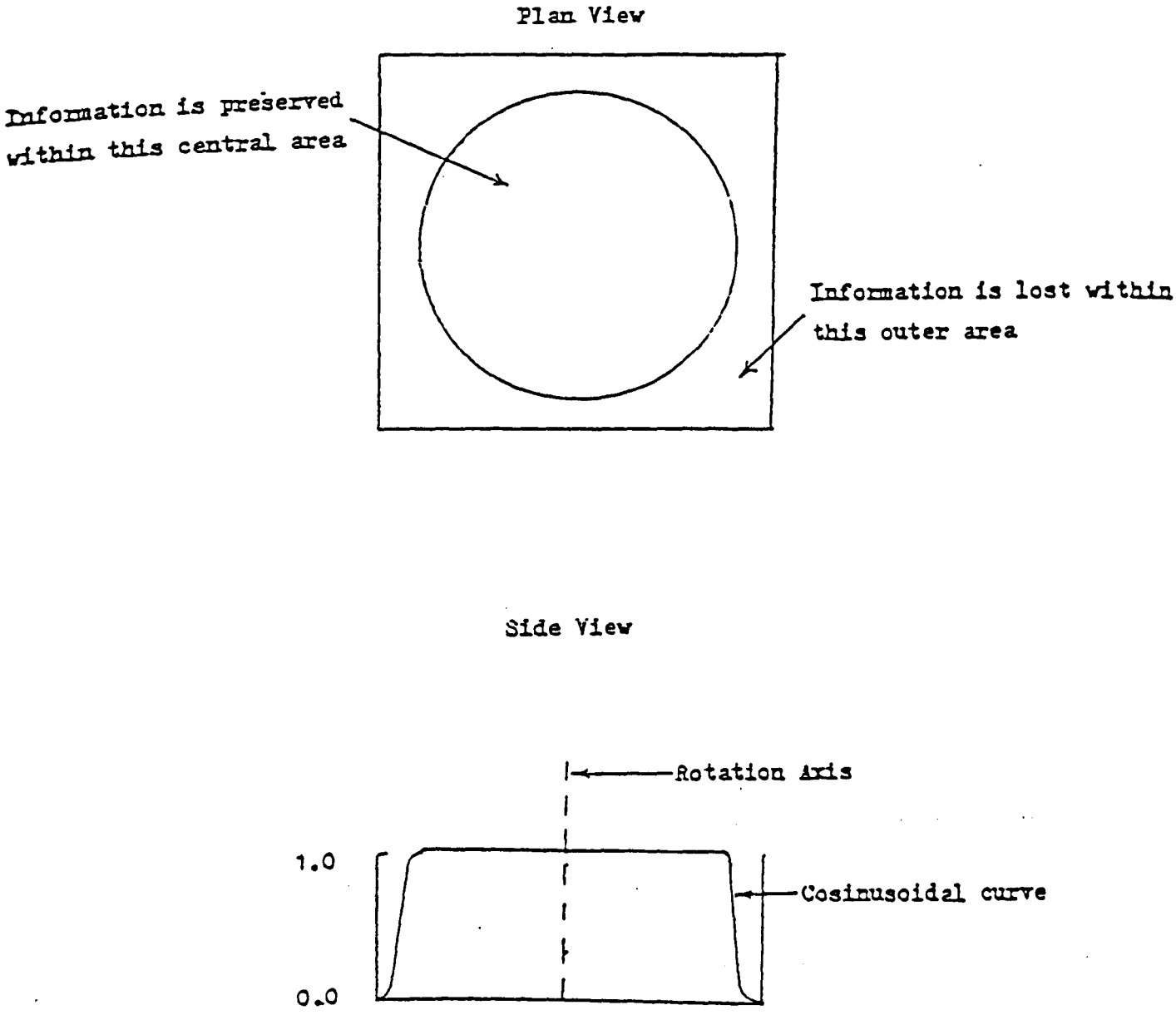

See section 2.4 for discussion

Figure 2.5.a

Field data with linear trend to be removed

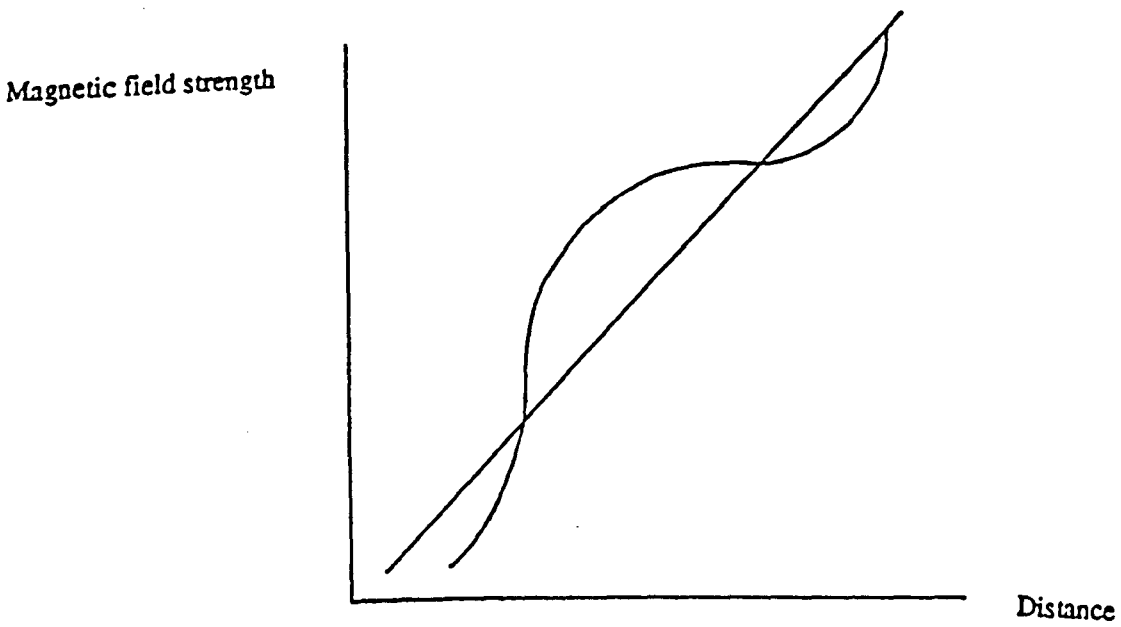

Figure 2.5.b

Field data following removal of linear trend

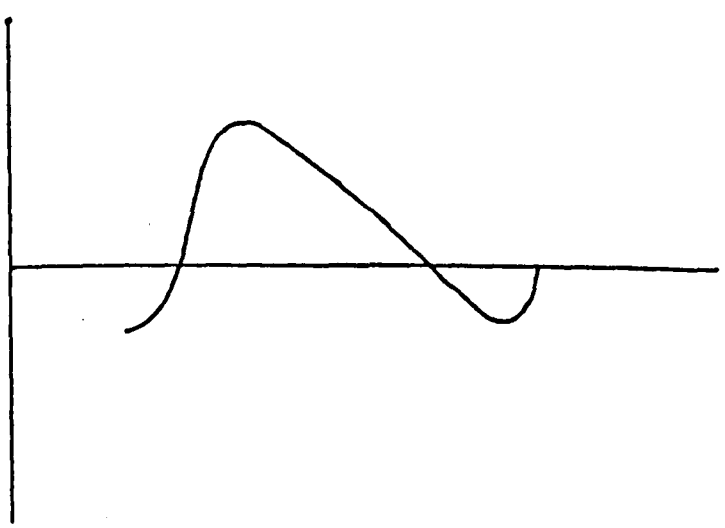

Figure 3.2.a

Major features of the geology of the Cairngorm granites and surrounding area

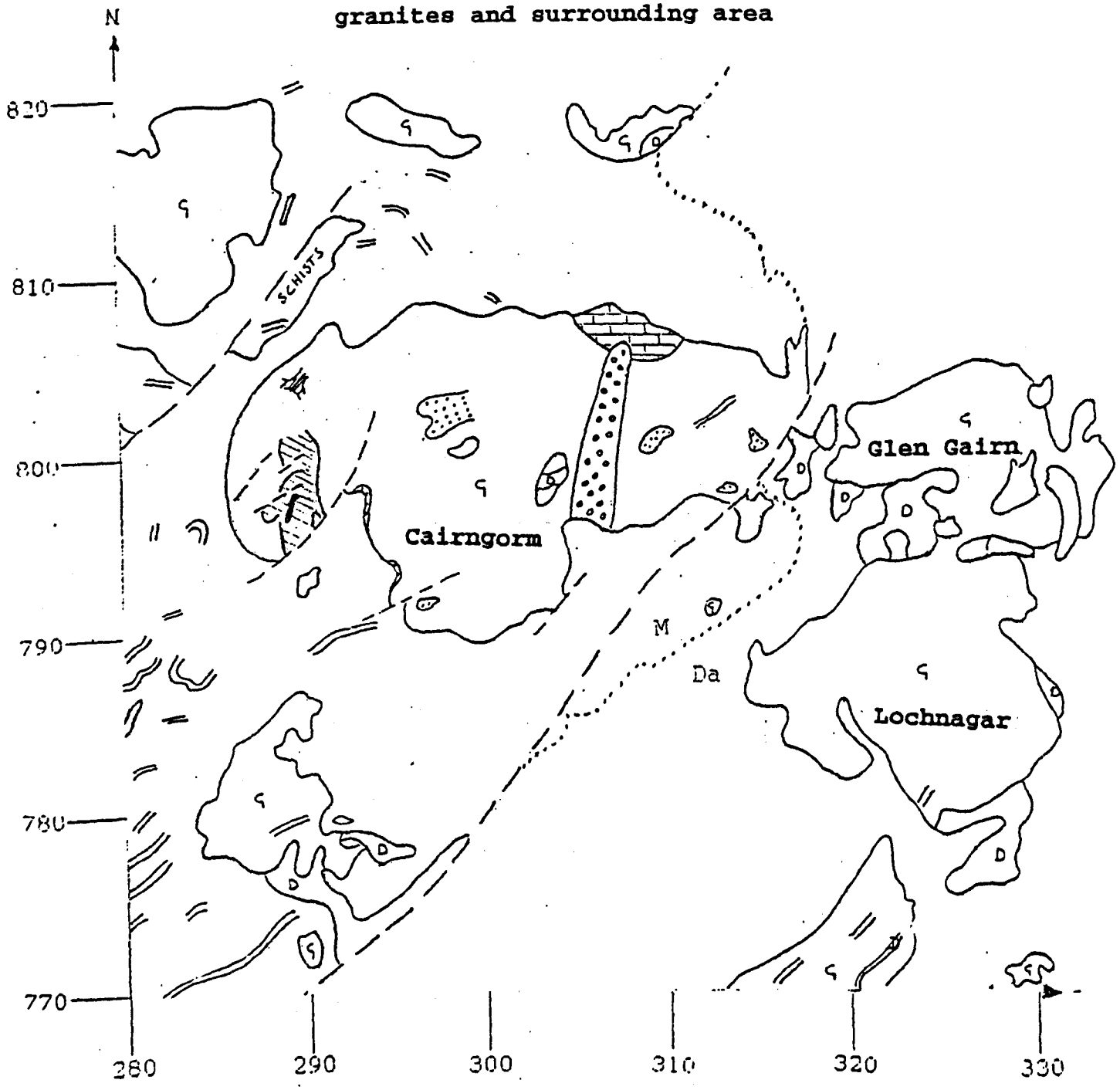

Values indicate National Grid references East and North

Key

G = Granite
D = Diorite
M = Moinian sediments
Da = Dalradian sediments
— — — — = major fault
. . . . . = Moine-Dalradian boundary
\\\\\ = Carn Bán Mór granite
= Glen Avon granite
ooo = Beinn Bhreac granite
::: = Porphyritic aplogranite
/ / / / = Granite porphyry
= Dykes

Figure 3.3.a

Three dimensional model of the eastern highland granites

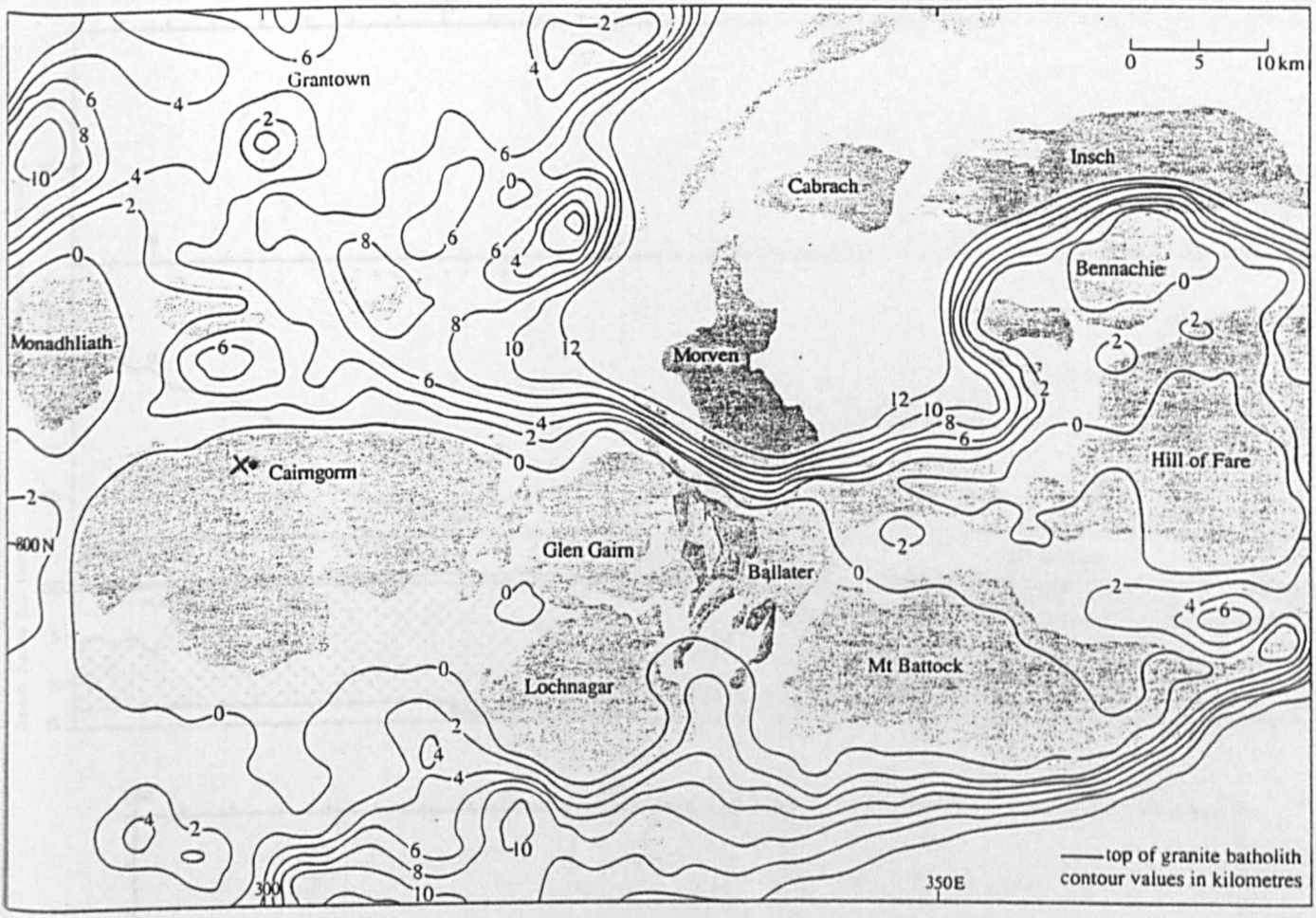

Contour values are in kilometres below O.D. on the upper surface of the granite batholith and basic bodies.

After Rollin (1984)

Figure 3.3.b

Profile model across the Cairngorm area

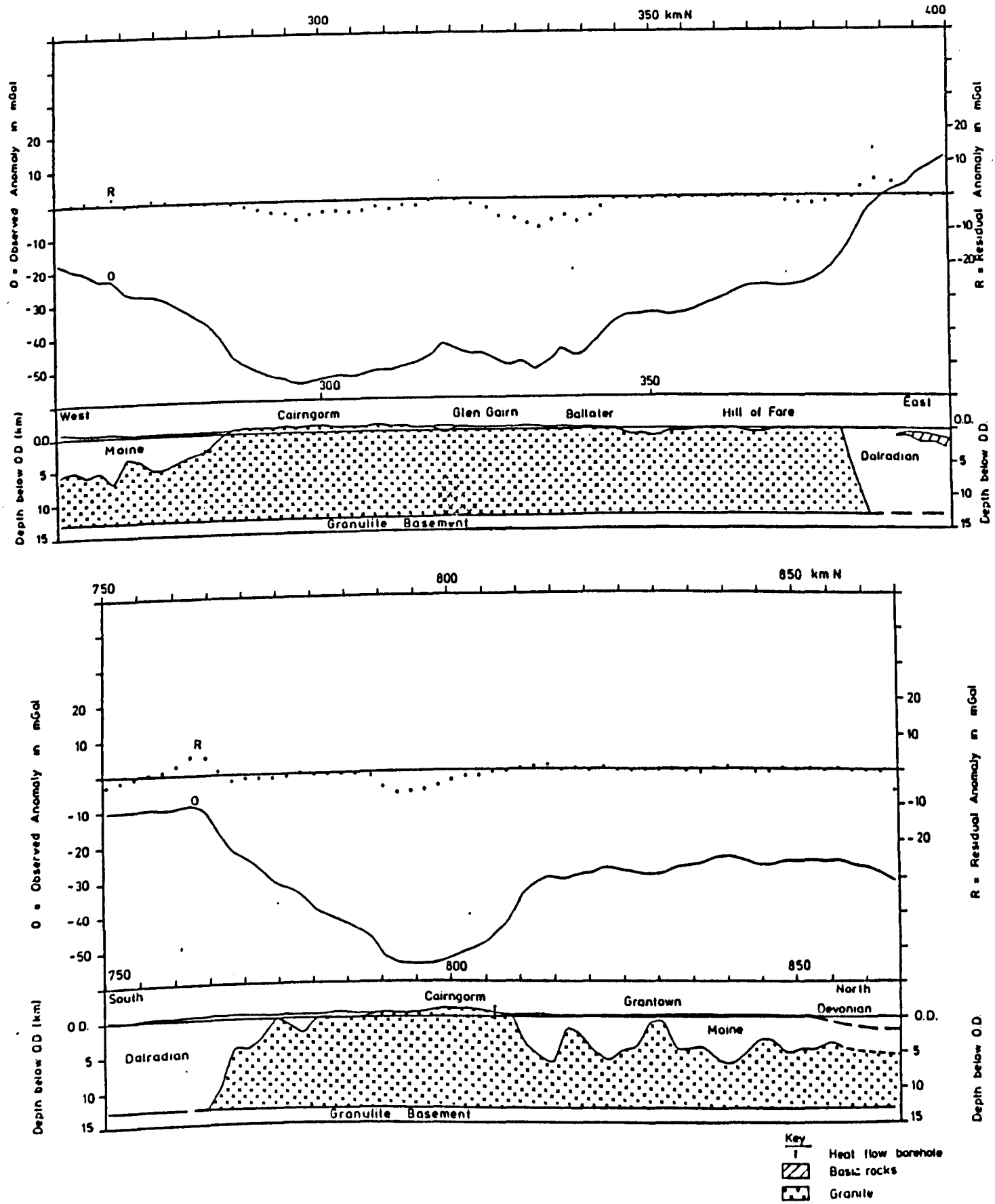

After Rollin (1984)

Figure 3.3.c

Location of the Lisp B seismic line

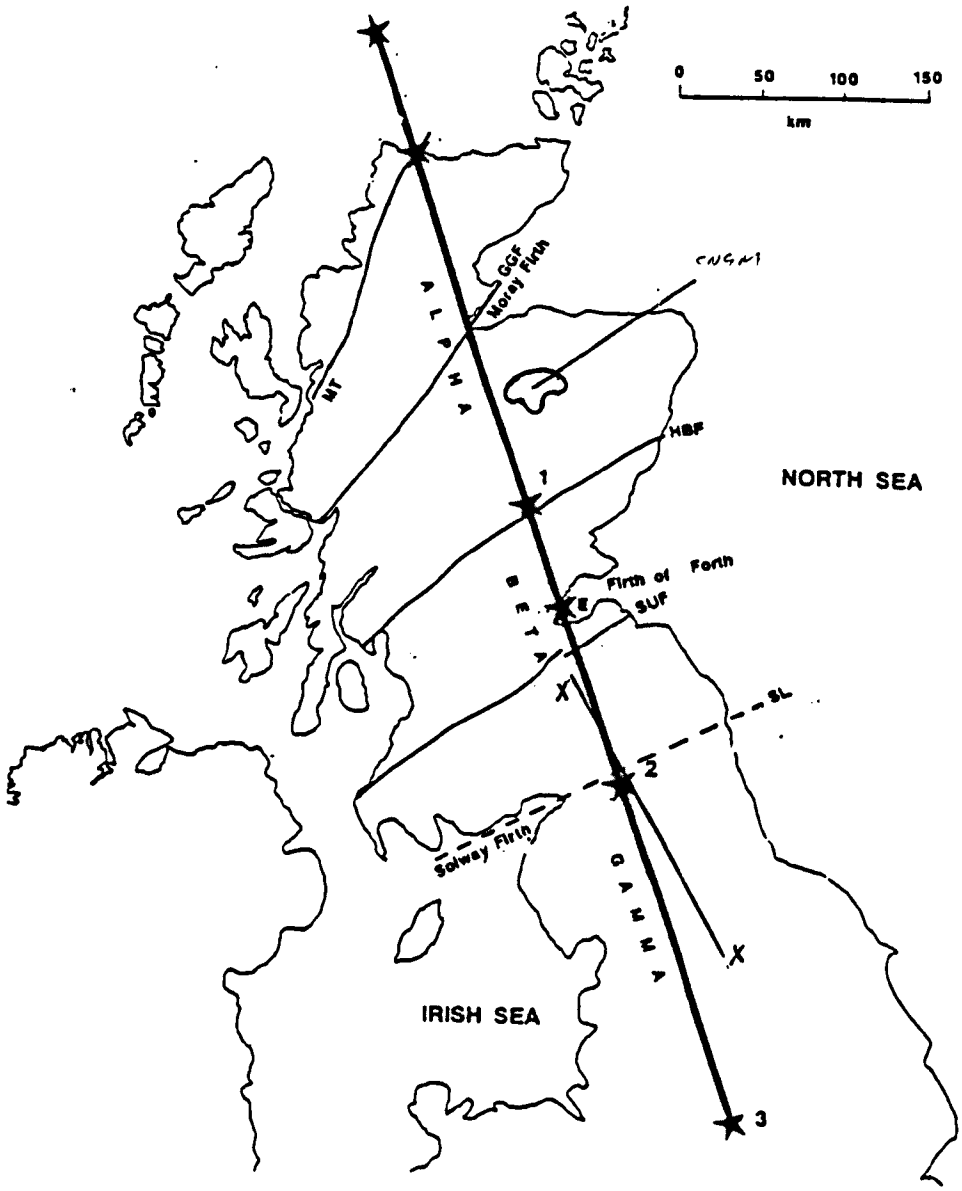

Figure 3.3.d

A model for the crustal structure beneath Northern Britain

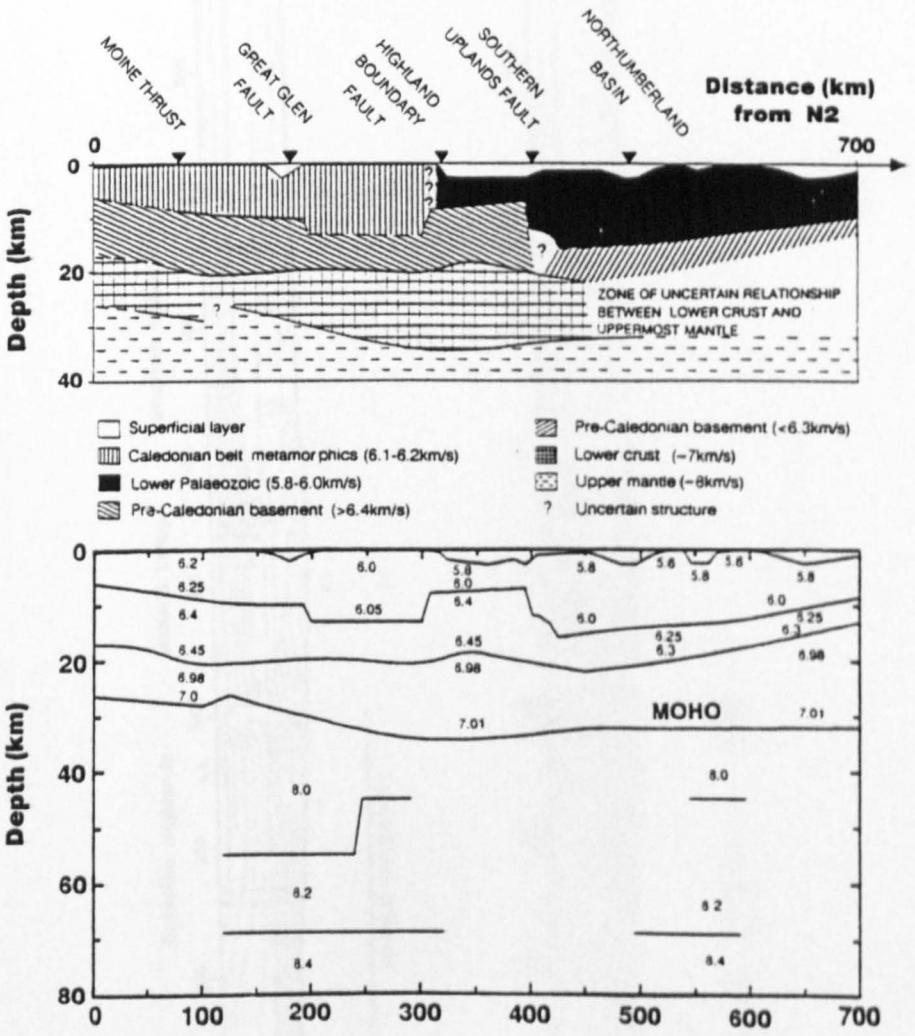

After Bamford et al (1978)

Figure 3.3.e

Barton's refined model for the crustal structure of northern Britain

a) Thin lines are contours of equal velocity. Broken lines are first order discontinuities.

b) Crustal density model for the best fit gravity field (converted from the velocity structure of the new LISPB model)

Figure 3.4.a

Topography of the Cairngorm area

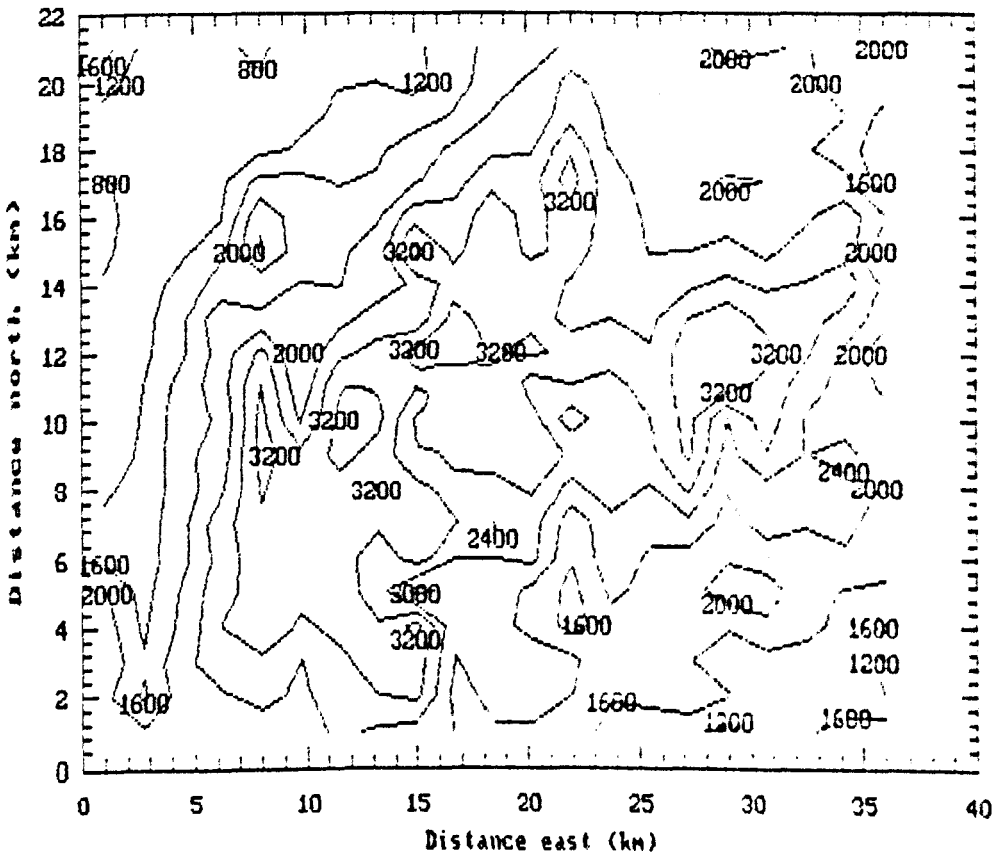

Contour values are in metres above O.D.

Figure 3.4.b

Predicted magnetic field arising from

the Cairngorm granites

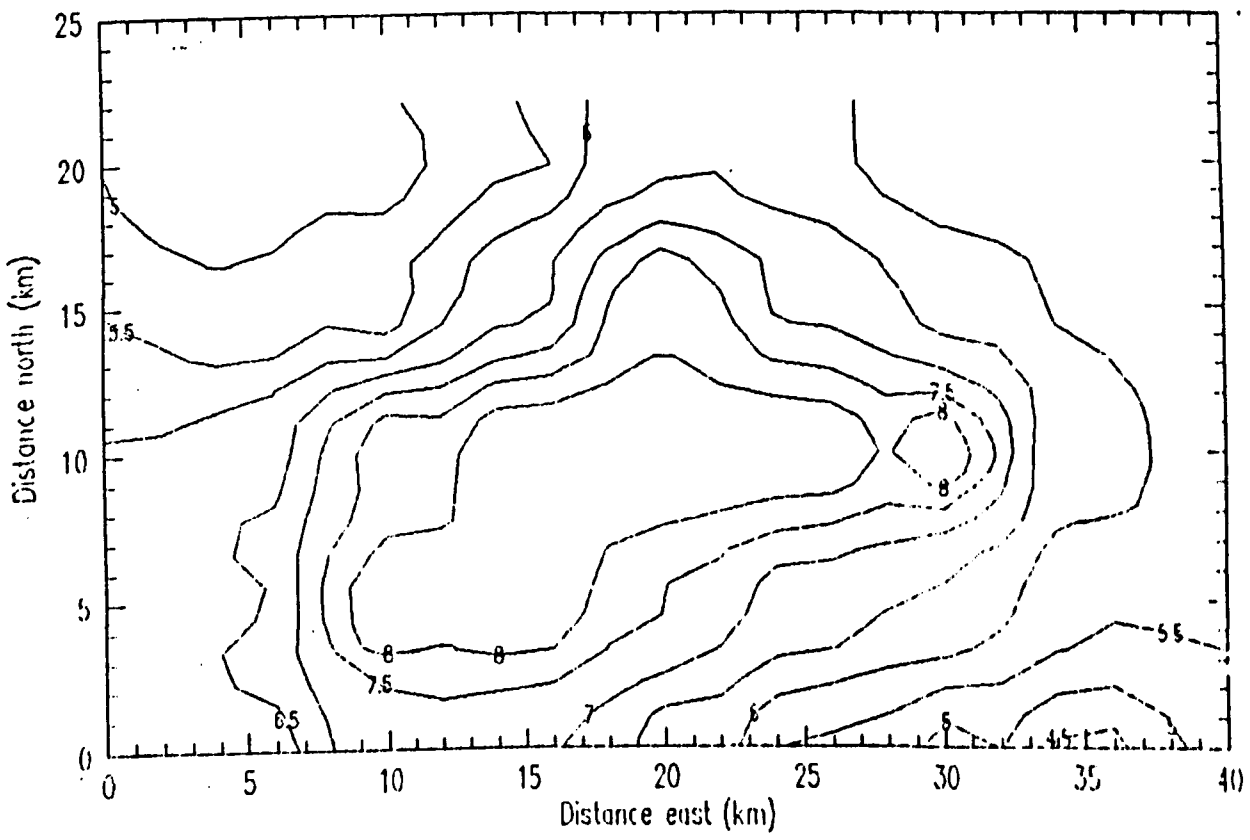

Values are in nT

(0,0) is the position 283,789 on the aeromagnetic map of figure 3.5.a

Figure 3.4.c

The variation in magnetic susceptibilities of some common rock forming minerals

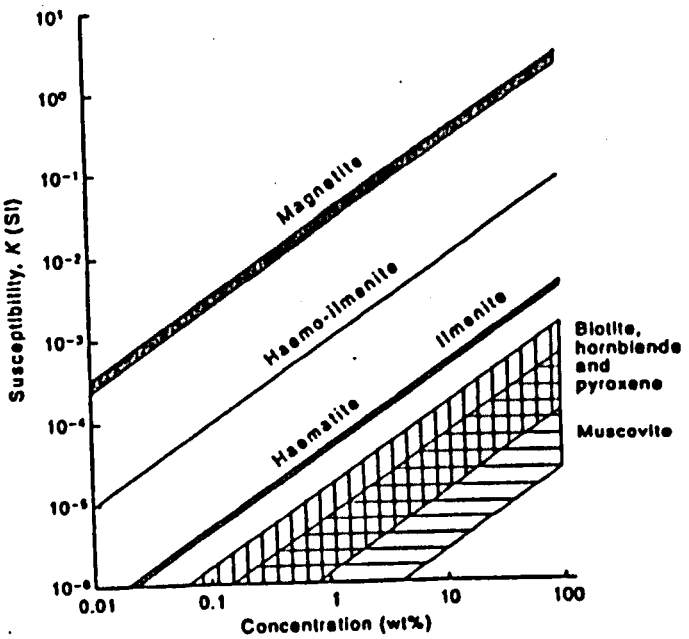

After Tarling and Hrouda (1993)

Figure 3.4.d

Average variation in V_p with depth

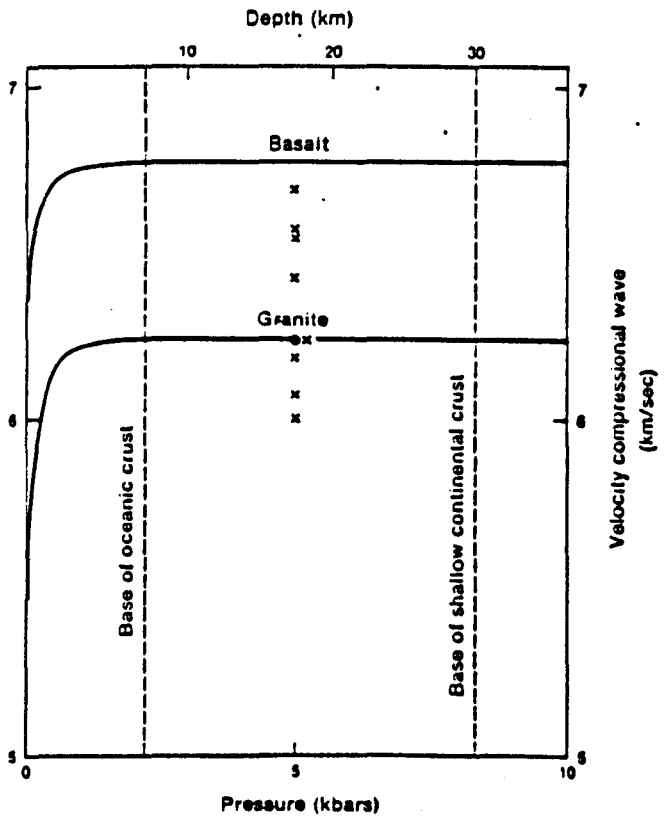

Curves were derived by calculation.

x = values chosen to show the range of continental crustal velocities.

. = average of a large number of measurements

After Press (1966)

Figure 3.4.e

A plot of the variation in magnetic susceptibility with depth in the Cairngorm borehole

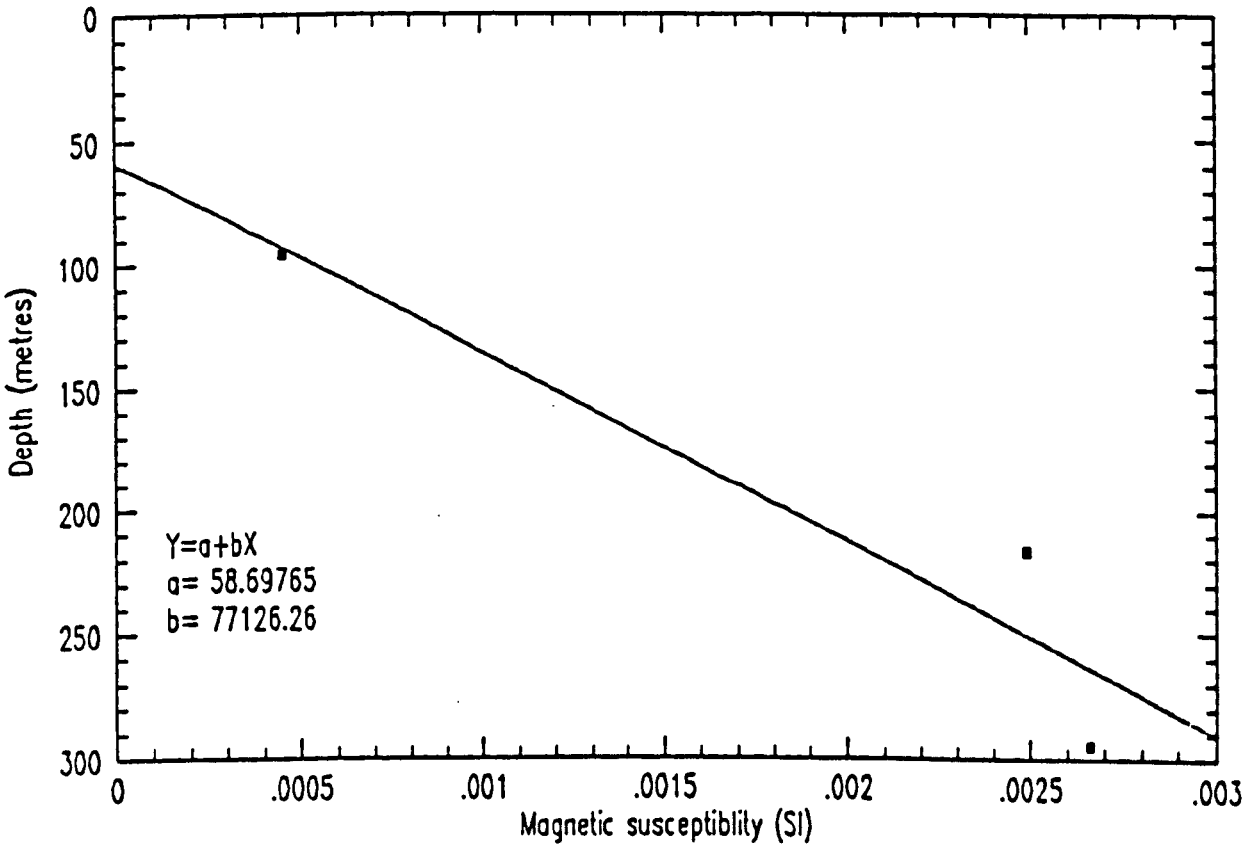

Borehole data after Rollin (1984)

Figure 3.4.f

A logarithmic plot of magnetic susceptibility against porosity for the eastern highland granites

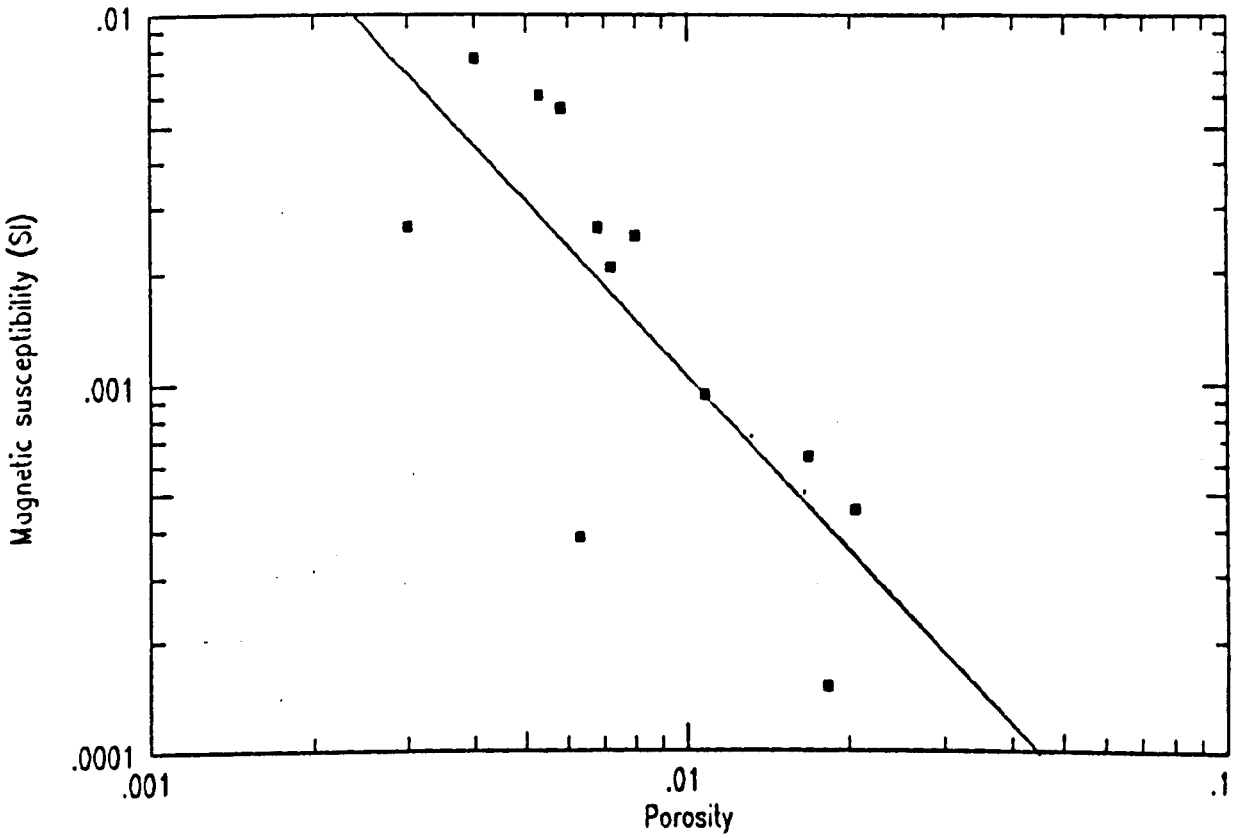

Borehole data after Rollin (1984)

A least mean square line of the form

$y = ax^b$

has been fitted to the data

$a = -7.4 \times 10^{-7}$ $b = -1.5$

Figure 3.5.a

Aeromagnetic field of the

eastern highlands of Scotland

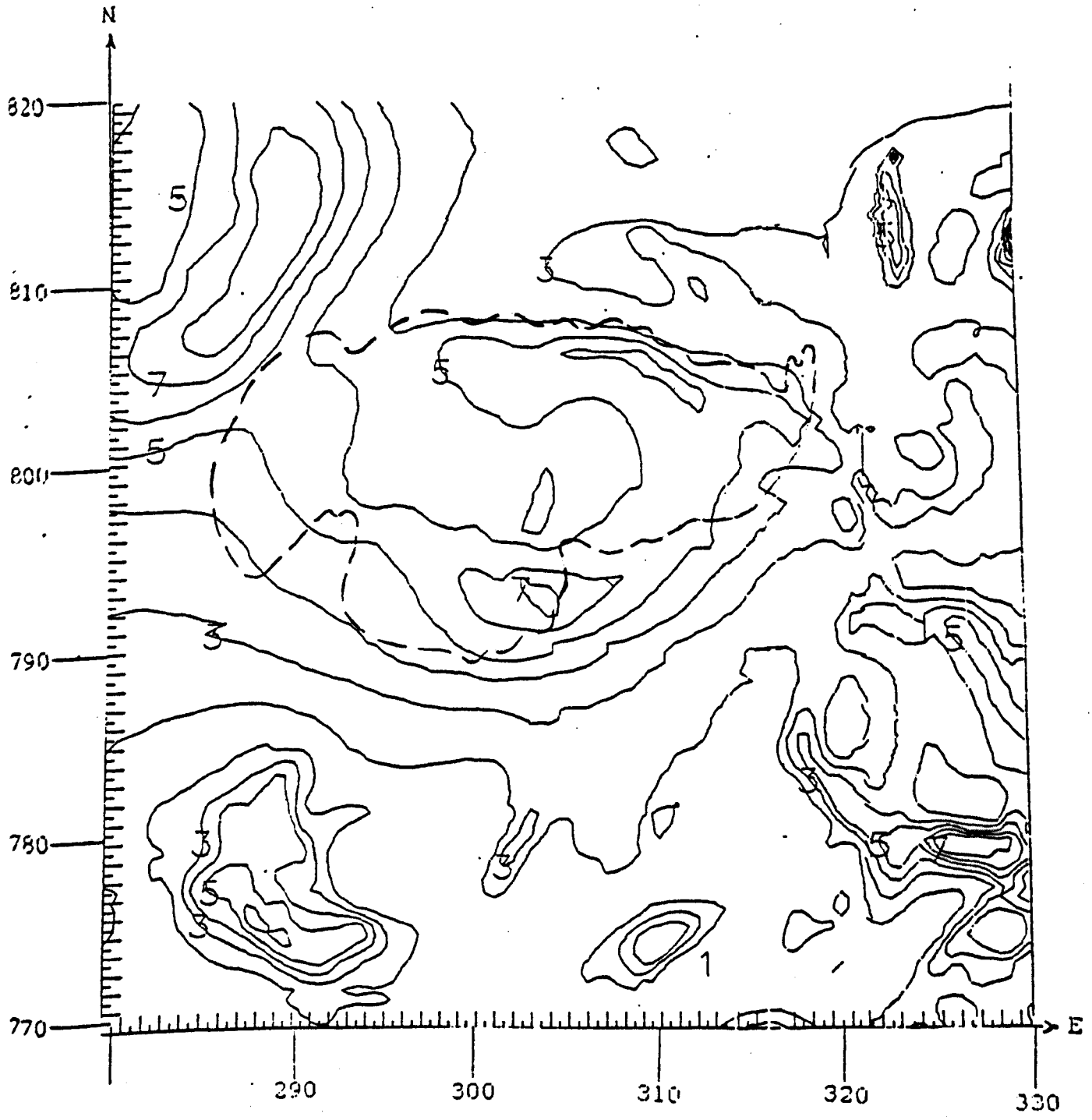

Key for contour values

1 = -100 nT
3 = 0 nT
5 = 100 nT
7 = 200 nT

For the conversion of magnetic anomaly values to total field values see the text for discussion.

Data source B.G.S. (see text) - - - granite outline

Figure 3.5.b

Textural variation in the Cairngorm granites

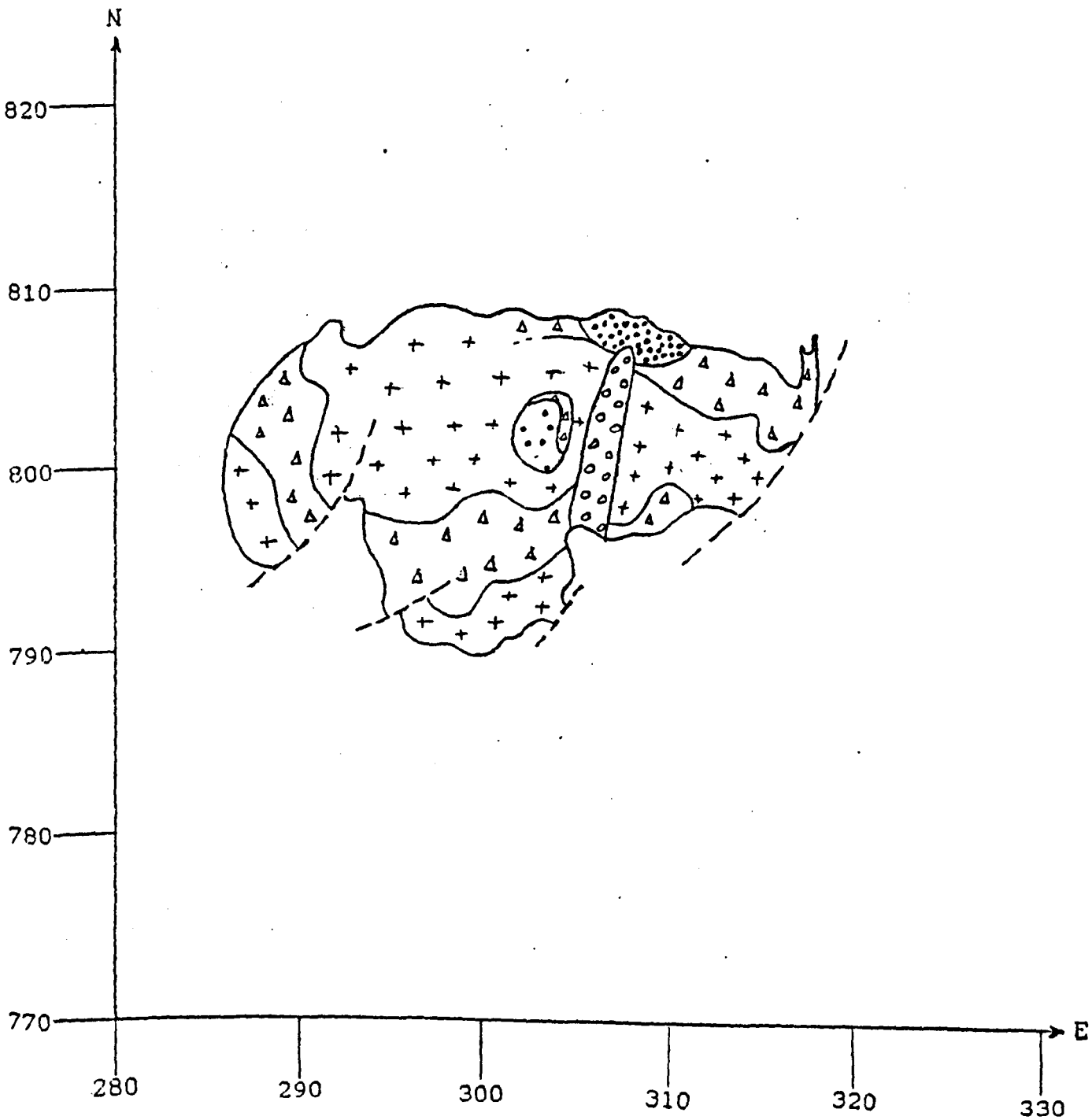

Key

++ Main granite - non-porphyritic
Δ Δ Main granite - porphyritic
• • • Main granite - coarse, non porphyritic
Glen Avon granite
o o o Beinn Bhreac granite

After Harrison (1986)

Figure 3.6.a

Survey lines across the Cairngorm area

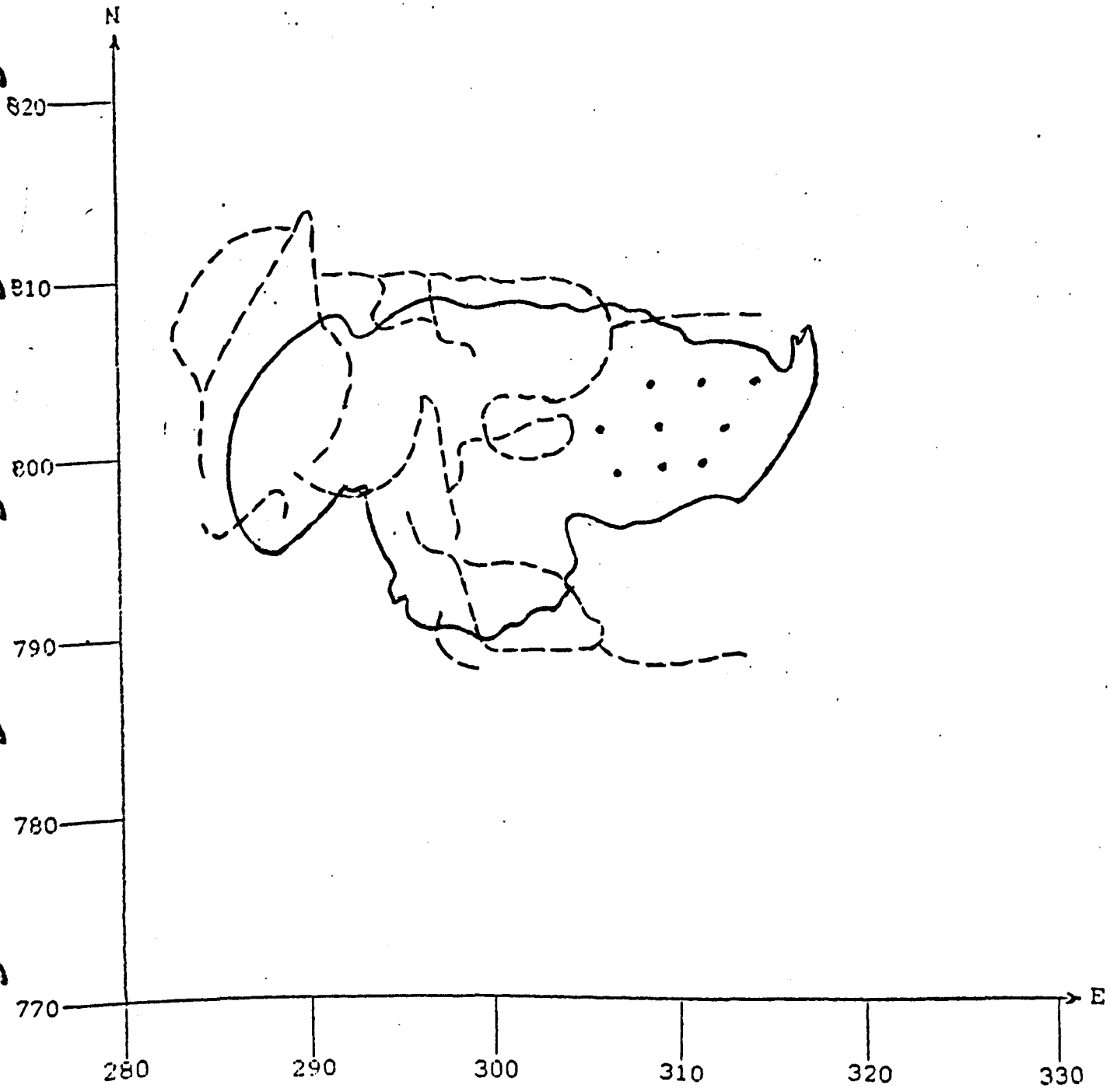

Key

granite outcrop

readings taken at 100 metre intervals

position of single reading

Figure 3.6.b

Contoured ground based magnetic field data from the Cairngorm area

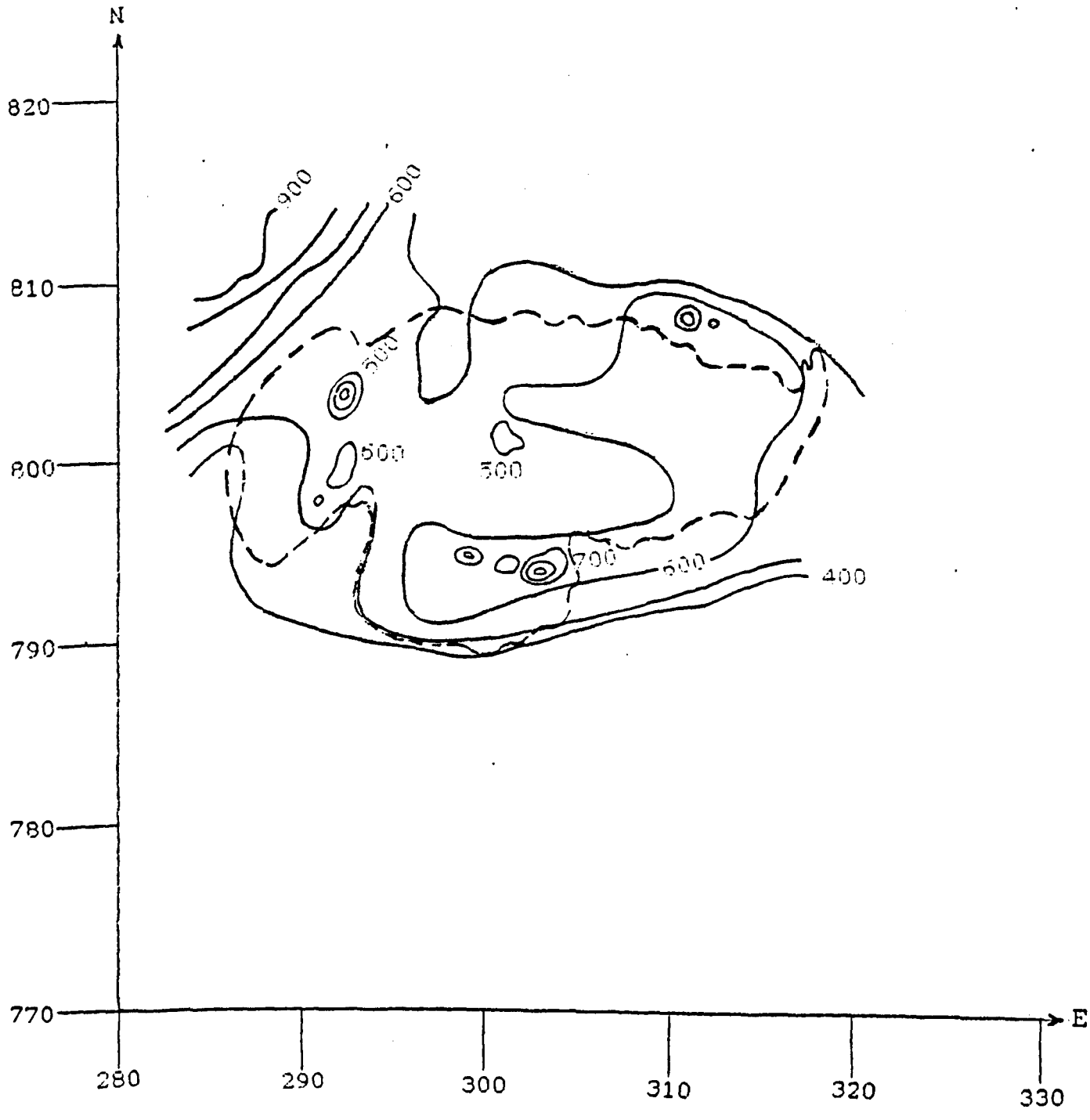

- - - granite outline

Figure 3.7.a

Gravity map of the Cairngorm area

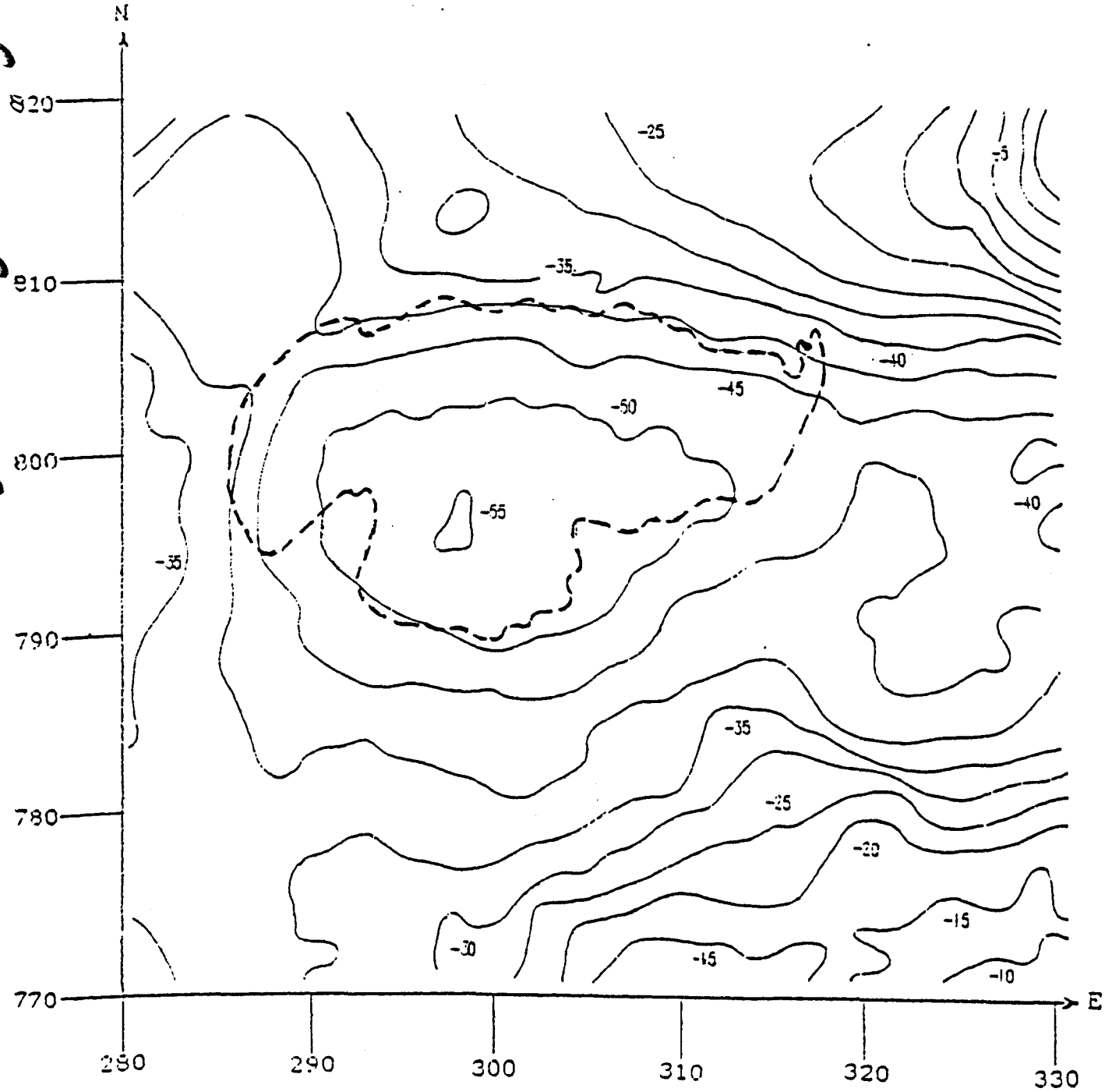

Contour values are in mgals

- - - granite outline

Figure 3.7.b

Low-pass filtered gravity map of

the Cairngorm area

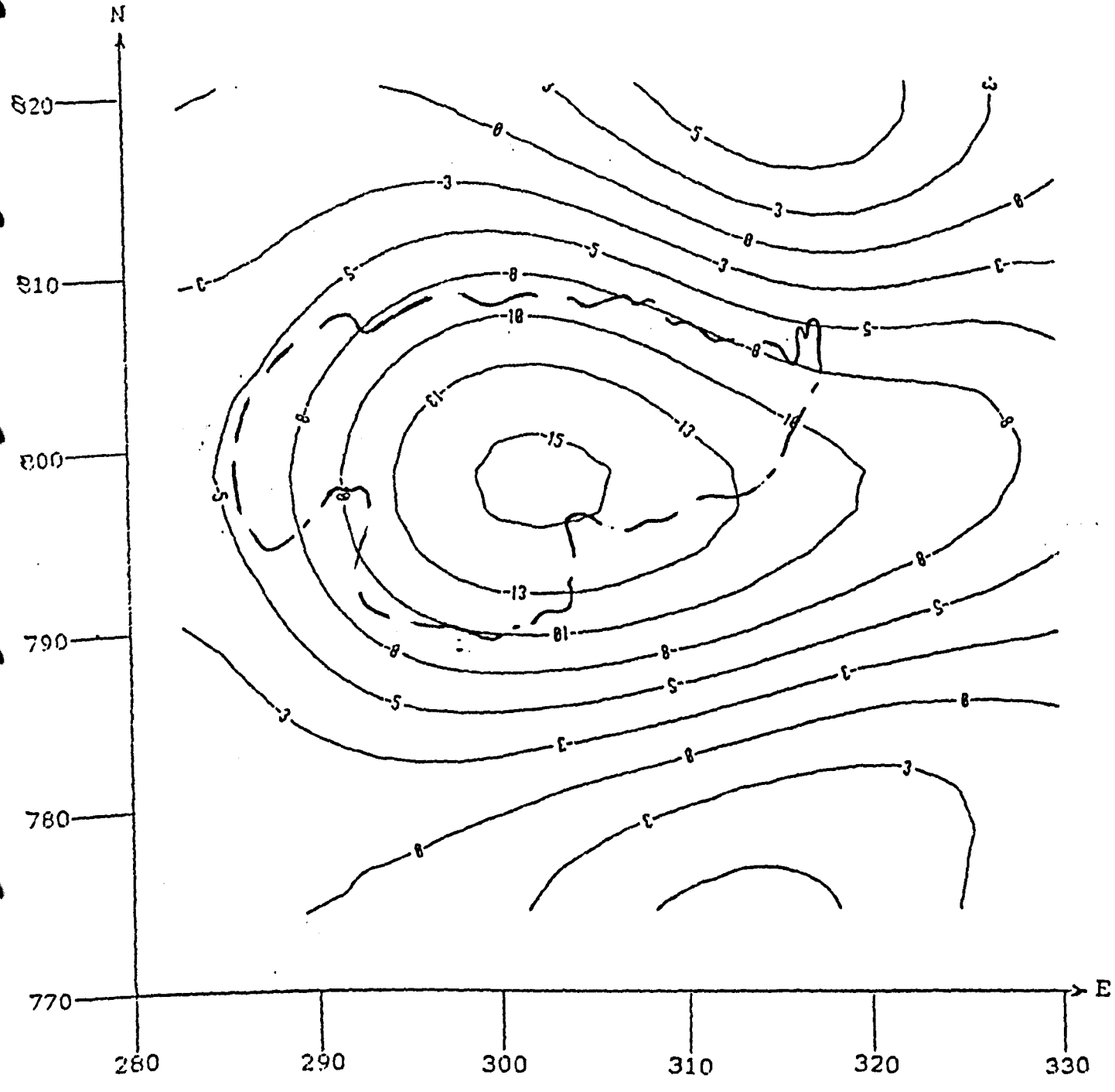

Contour values are in mgals

- - - - granite outline

Figure 3.8.a

Aeromagnetic map of the eastern highlands of Scotland reduced to the pole

The reduction assumes an angle of inclination of 70° and a declination of 0°.

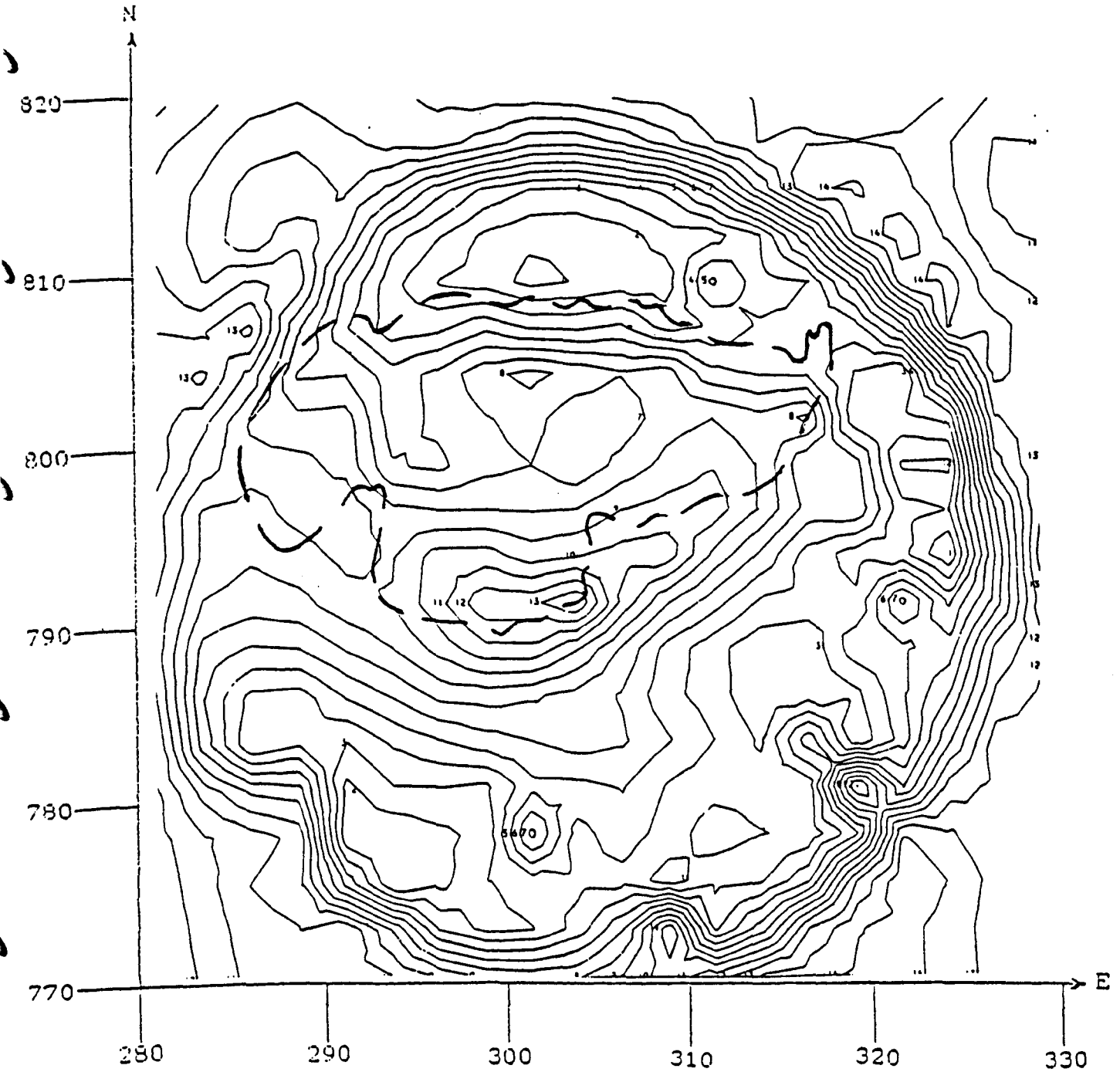

- - - granite outline

Key for contour values

1 =-40 nT
3 = 0 nT
5 = 40 nT
7 = 80 nT
9 = 120 nT

A plane of 170 nT has been removed from the data during processing.

Figure 3.9.a

Three dimensional power spectrum

for the Cairngorm aeromagnetic data

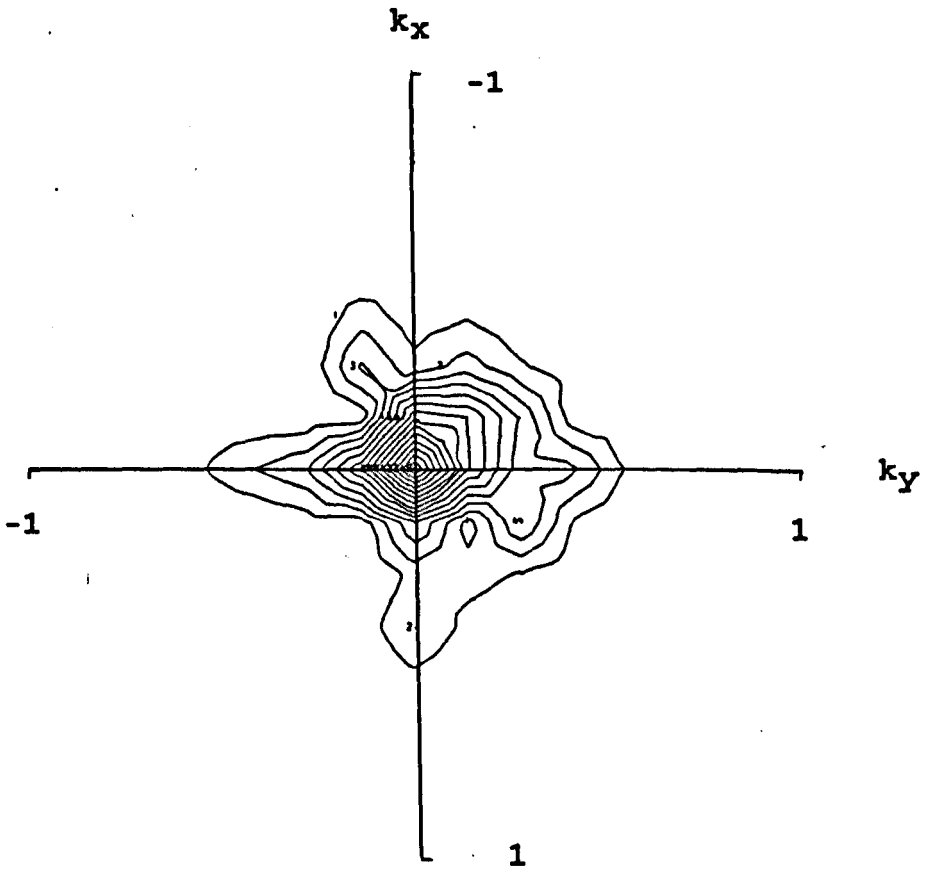

Dimensions of the power spectrum are km^{-2}

Wavenumber values are given in Nyquist wavenumbers where the Nyquist wavenumber is given by $k_n = 1/2a$ (a is the spacing between data points in kilometres)

Figure 3.9.b

Azimuthally averaged power spectrum of the Cairngorm aeromagnetic data

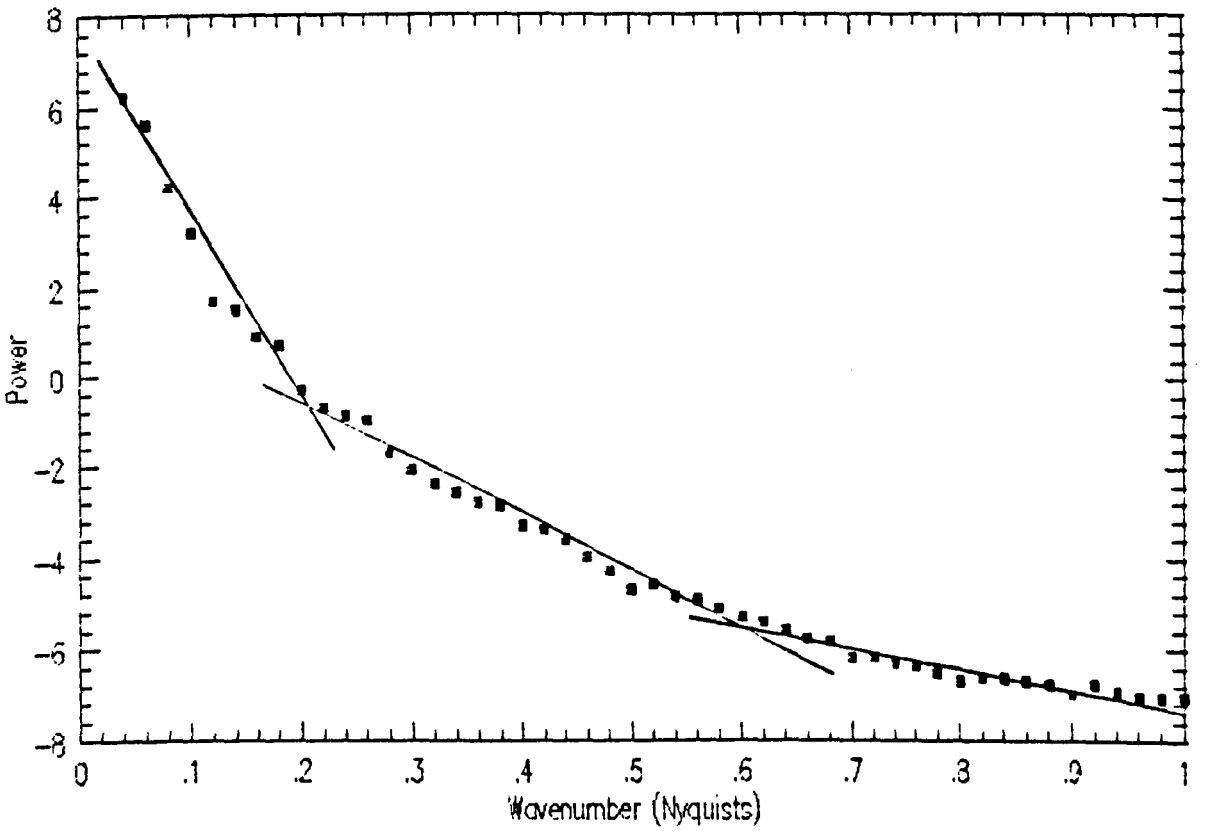

The power is plotted as the logarithm to base e of the power in one wavenumber band of the wavenumber space. To convert the power values to power density per unit area of wavenumber space it is necessary to divide the power by 0.0004.

Figure 3.9.c

Linear regression on sections of the azimuthally averaged power spectrum

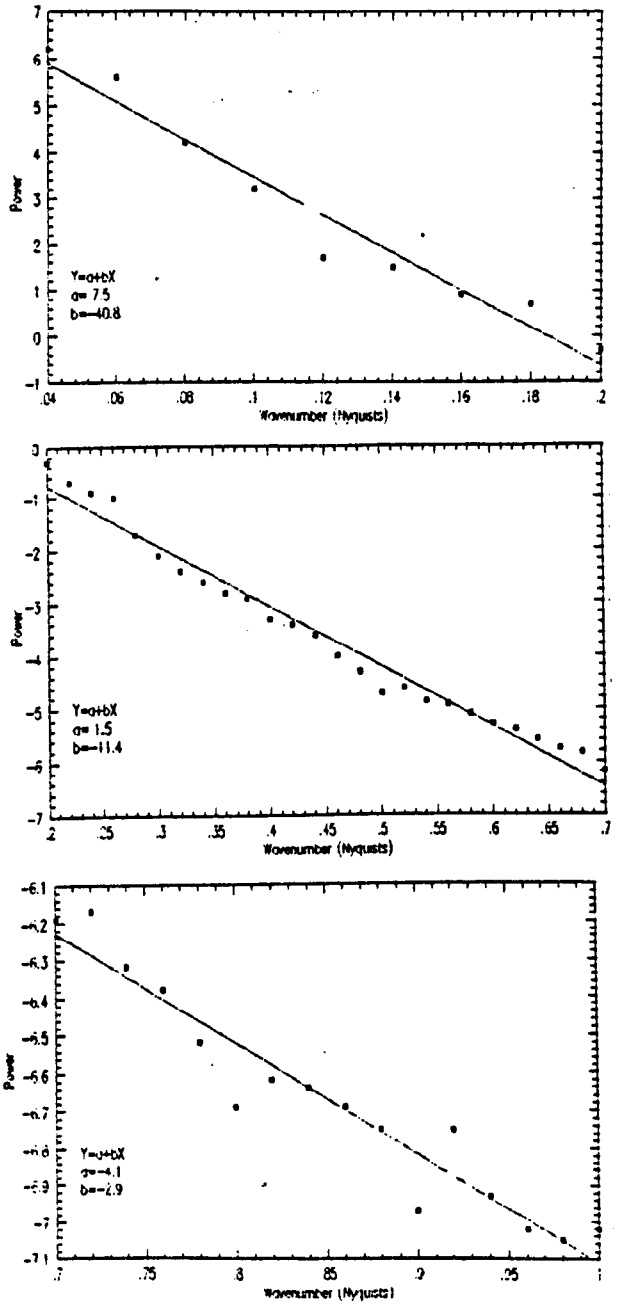

Figure 3.9.d

High-pass filtered aeromagnetic map

of the Cairngorm area

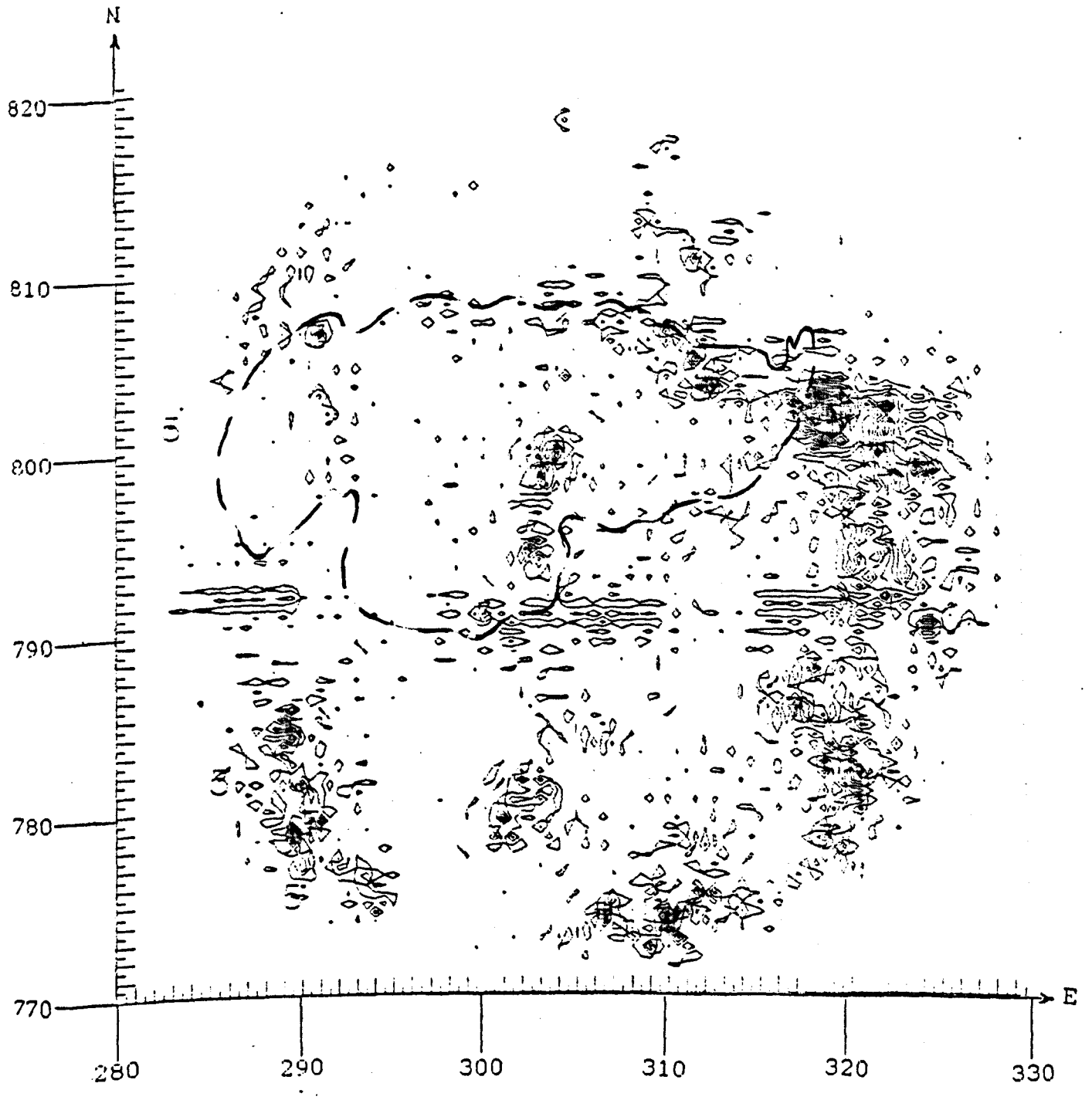

\- - - granite outline

Key for contour values

1 = -19 nT
3 = -9 nT
5 = 1.5 nT
7 = 11.4 nT
9 = 21.5 nT

A plane of 170 nT has been removed from the data during processing.

Figure 3.9.e

Band pass filtered map of the

Cairngorm aeromagnetic data

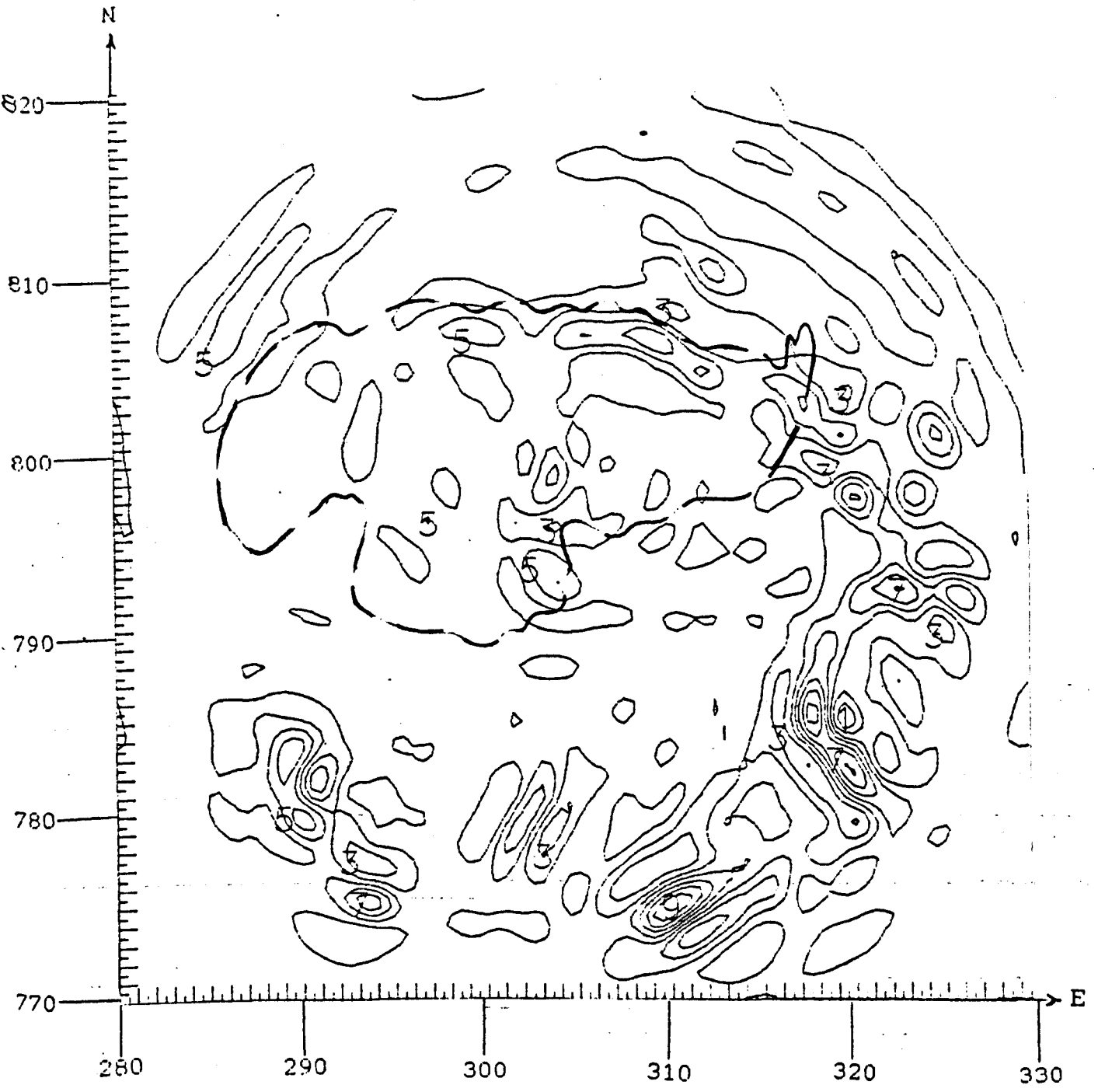

- - - granite outline

Key for contour values

1 = -80 nT
3 = -30 nT
5 = 20 nT
7 = 70 nT
9 = 120 nT

A plane of 170 nT has been removed from the data during processing.

Figure 3.9.f

Low-pass filtered map of the

Cairngorm aeromagnetic data

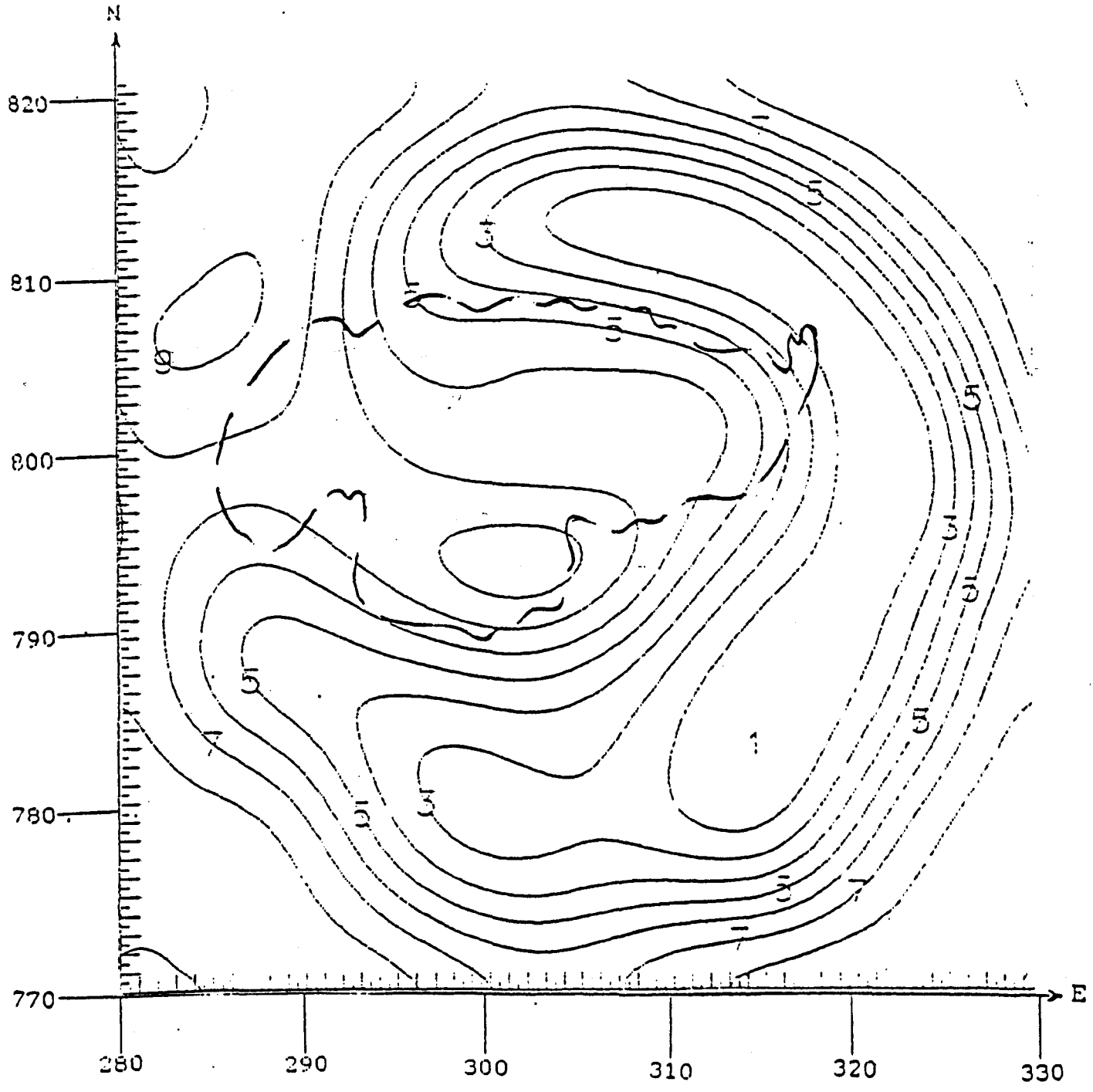

- - - granite outline

Key for contour values

1 = -290	nT	A plane of 170 nT has been removed from the data during processing.
3 = -210	nT	
5 = -130	nT	
7 = 50	nT	
9 = 130	nT	

Figure 3.10.a

Pseudogravimetrically transformed map of the Cairngorm area

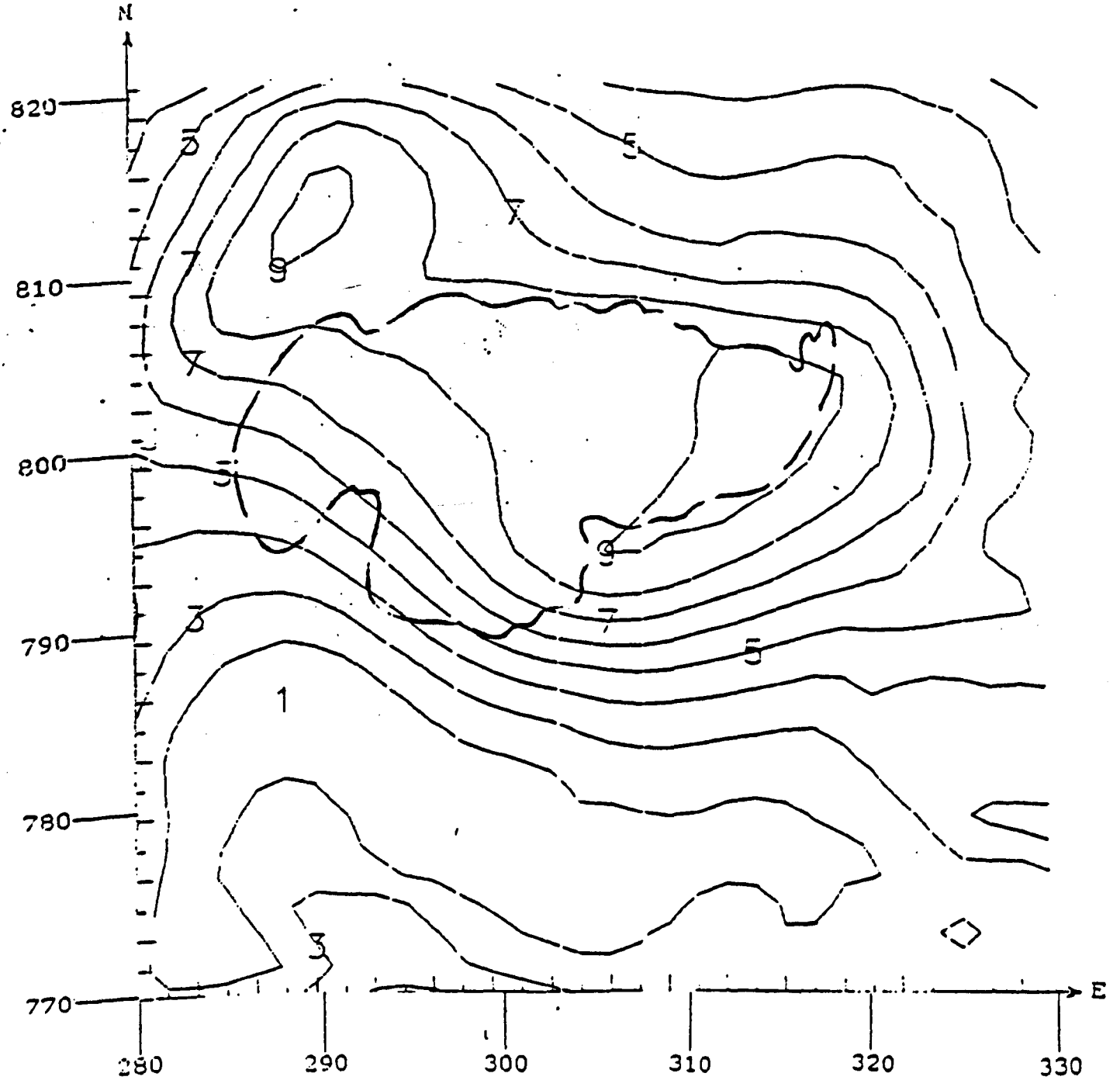

Key for contour values

1 = -67 mgals
3 = -33 mgals
5 = 1 mgal
7 = 35 mgals
9 = 69 mgals

- - - granite outline

Figure 3.11.a

Modelled profile lines in the Cairngorm area

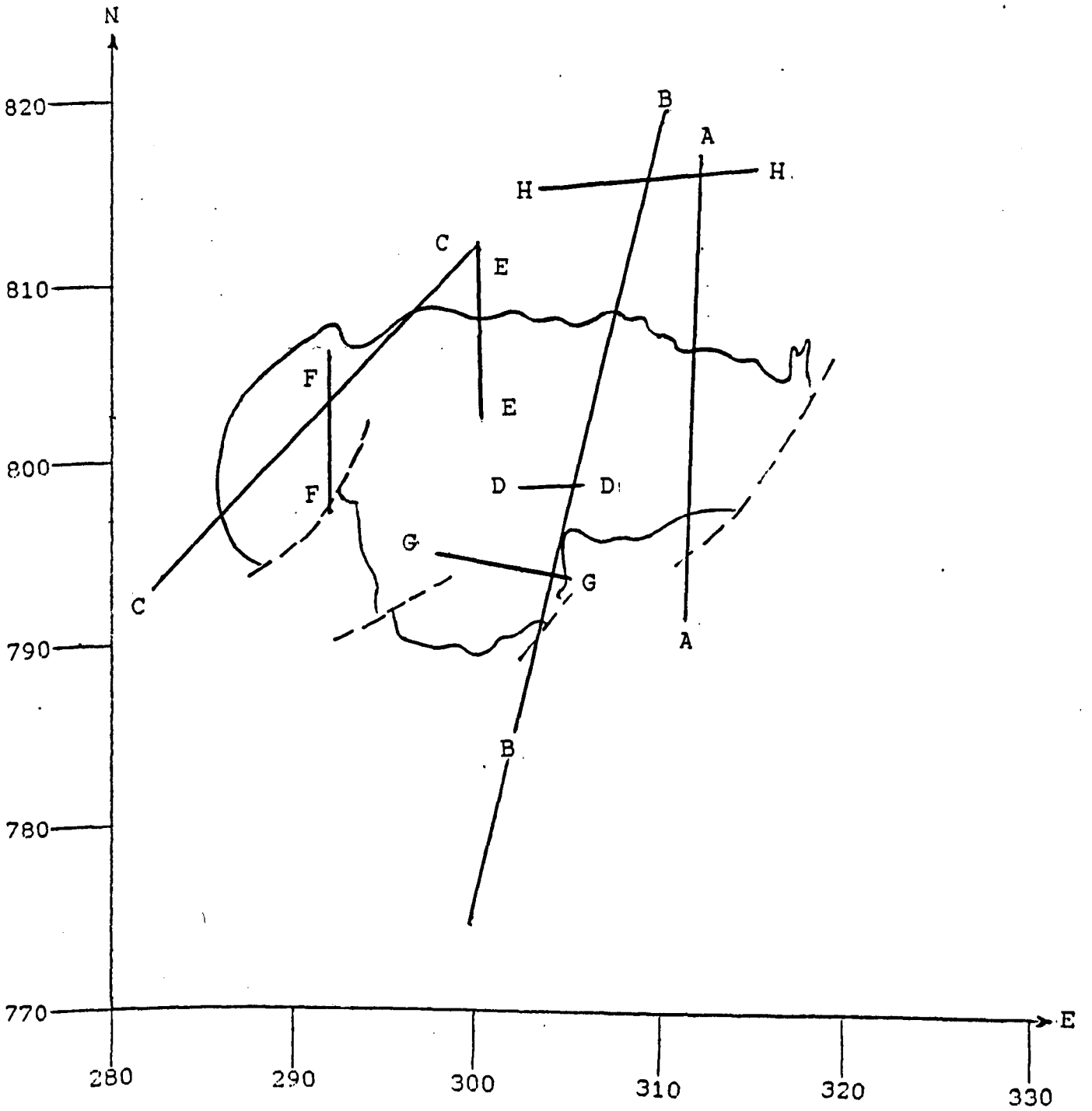

Figure 3.11.b

A model of the magnetic anomaly overlying the north-western boundary of the Cairngorm granites (line E-E on Figure 3.11.a).

North ⇒

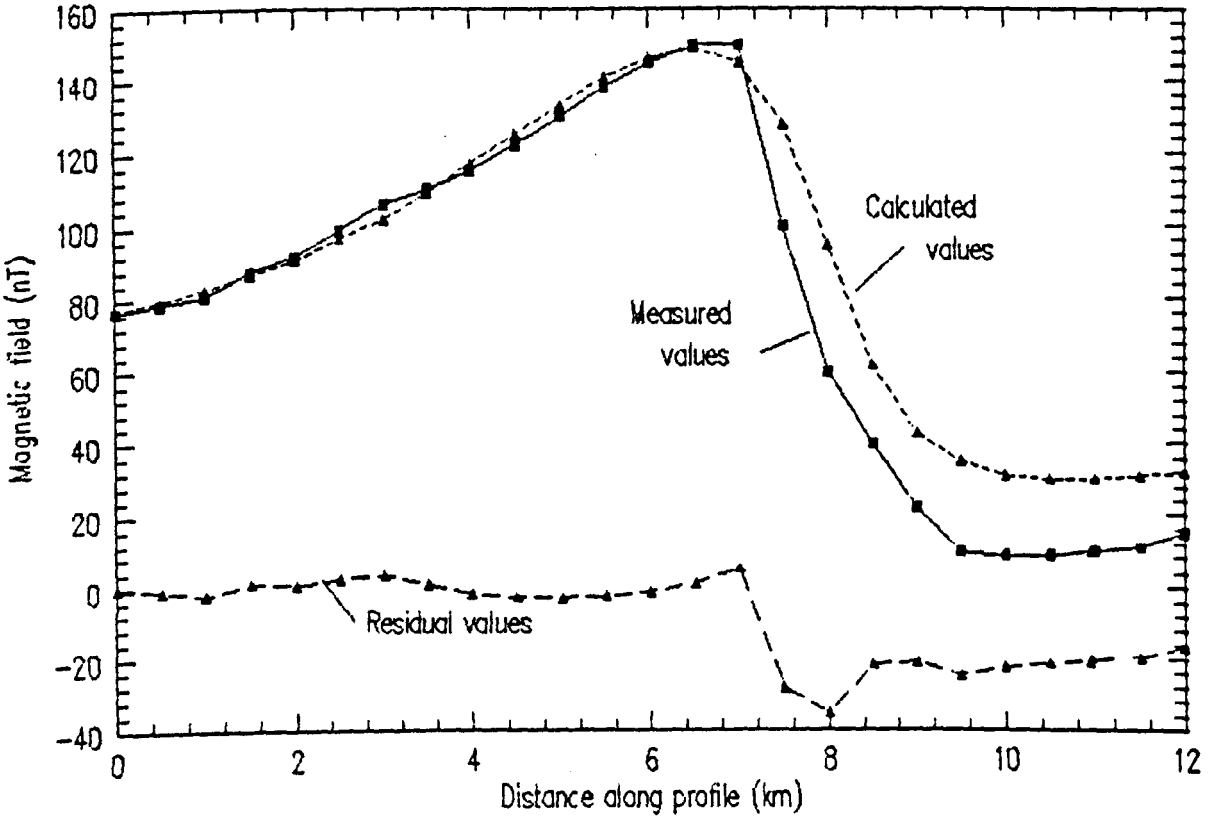

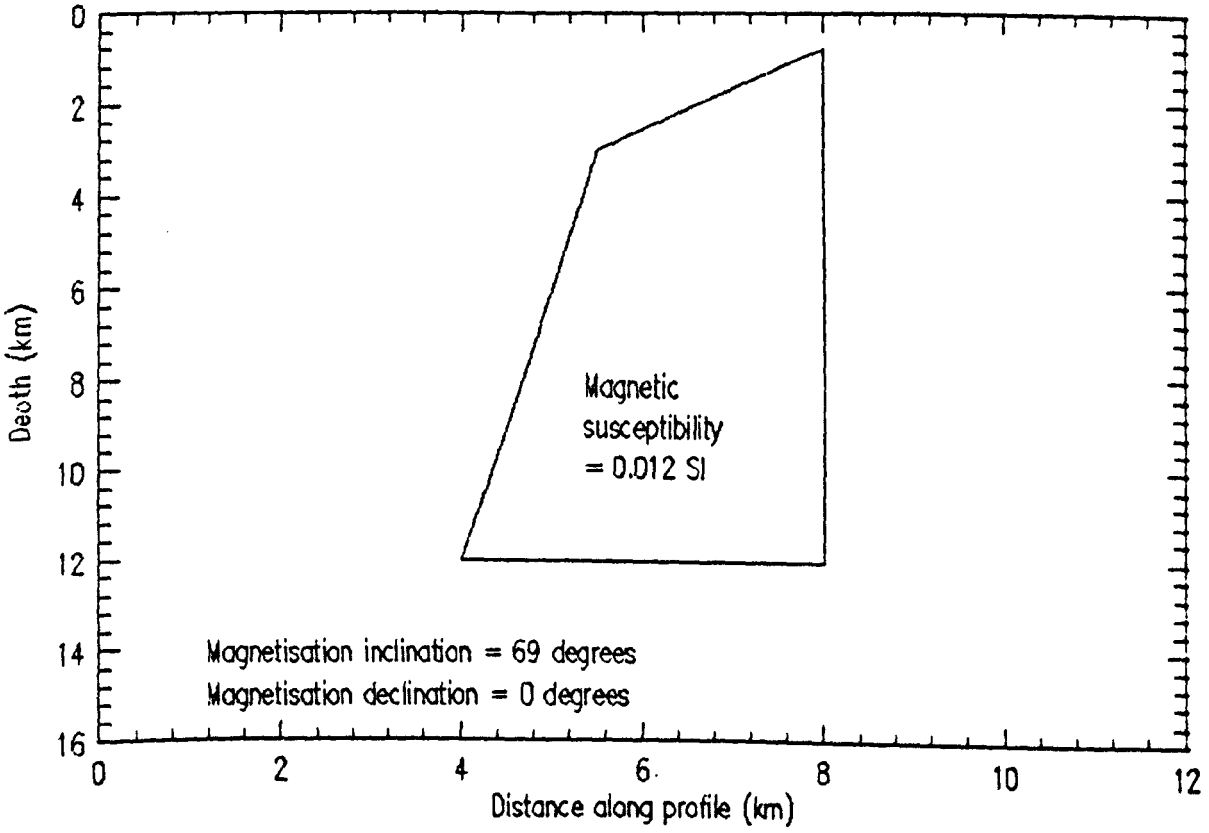

Figure 3.11.c

A model of the gravity anomaly overlying the western side of the Cairngorm granites (line C-C on Figure 3.11.a).

North ⇒

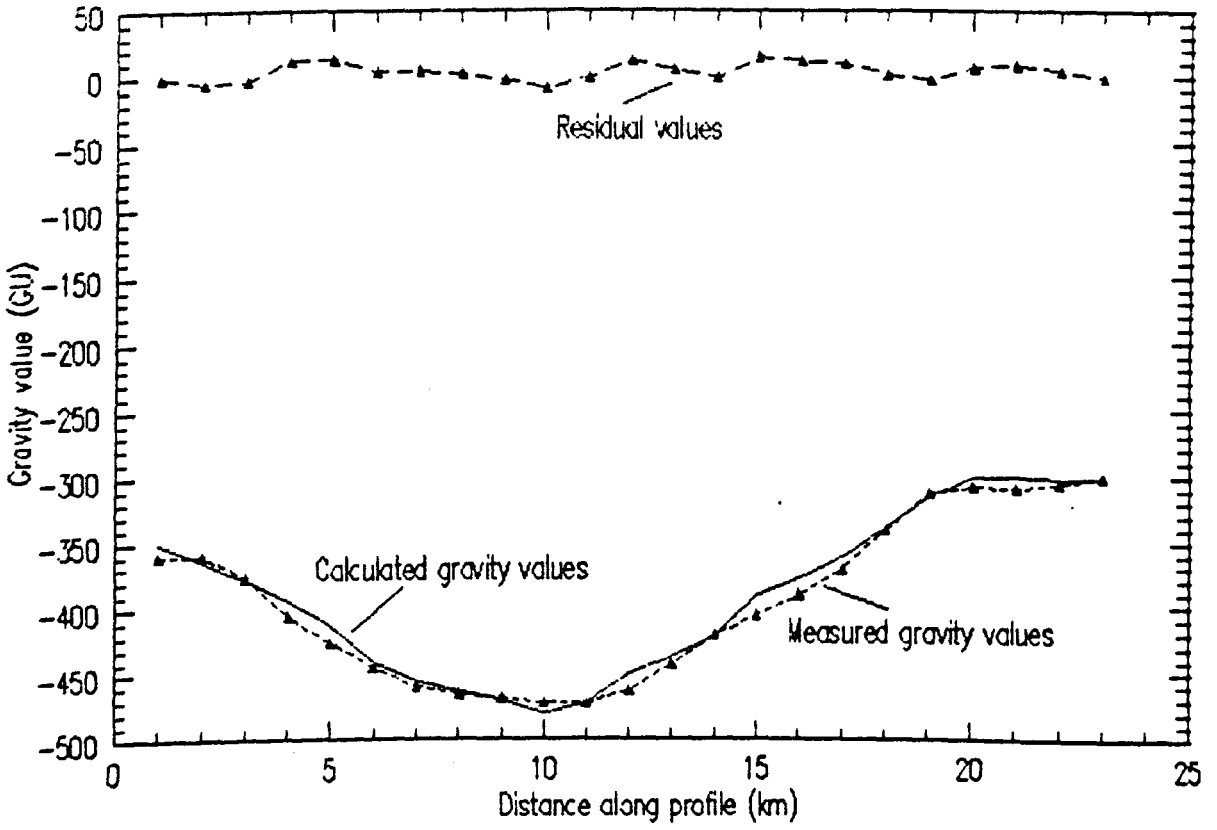

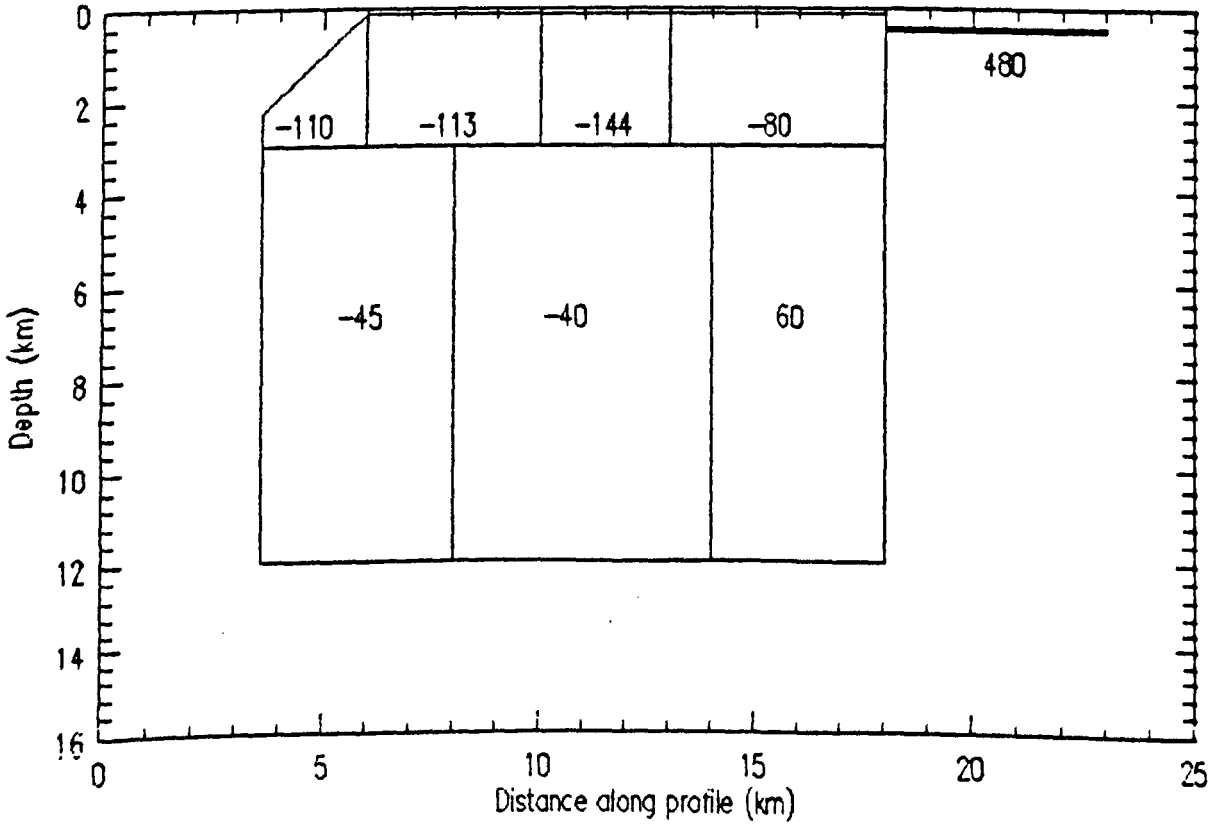

Values are density contrasts in kg m^{-3}

Figure 3.11.d

A model of the aeromagnetic anomaly overlying the western side of the Cairngorm granites (line C-C on Figure 3.11.a).

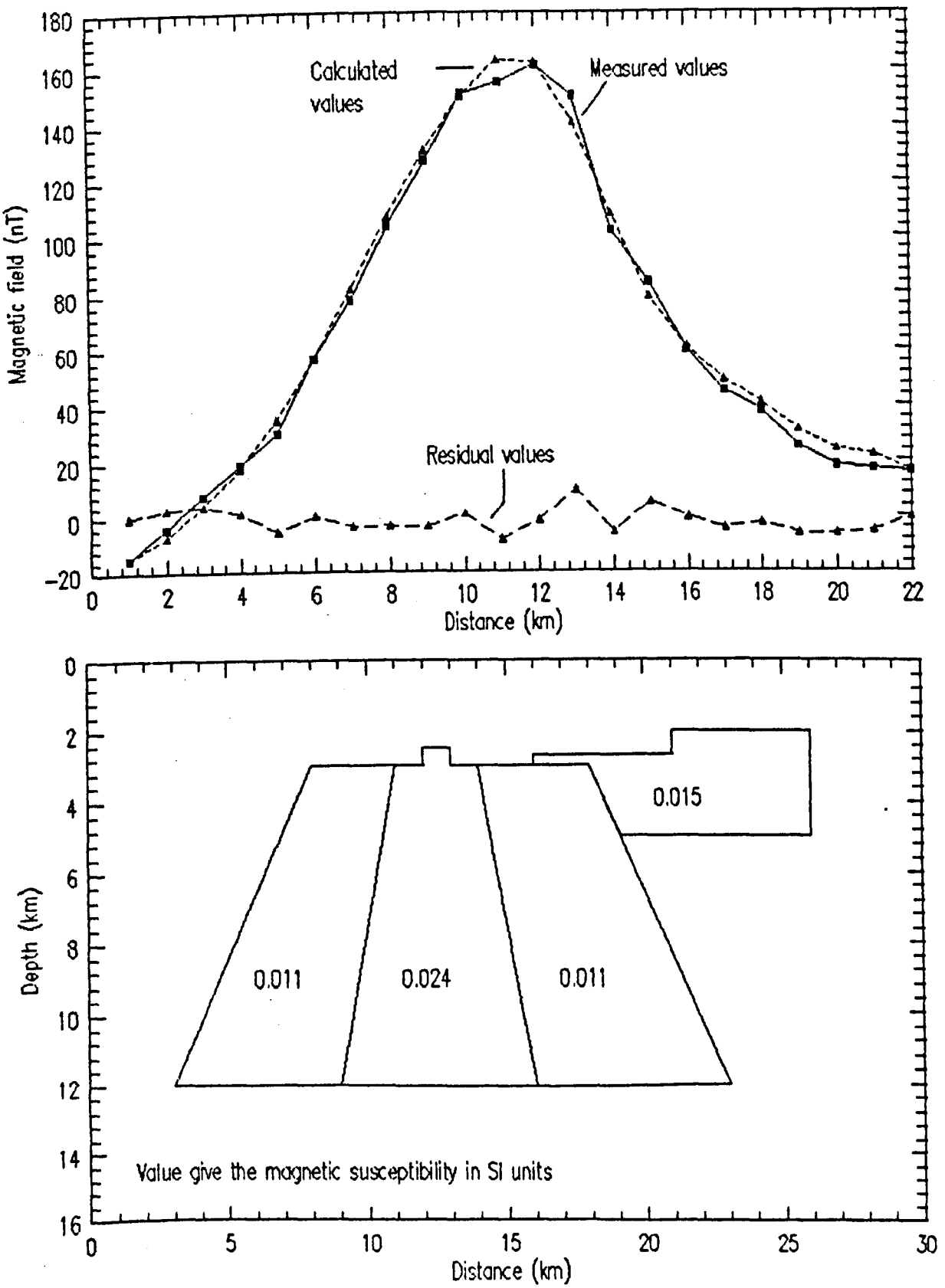

Values are magnetisation contrasts in SI units

Figure 3.11.e

A model of the aeromagnetic anomaly overlying the Loch Einich area (line F-F on Figure 3.11.a).

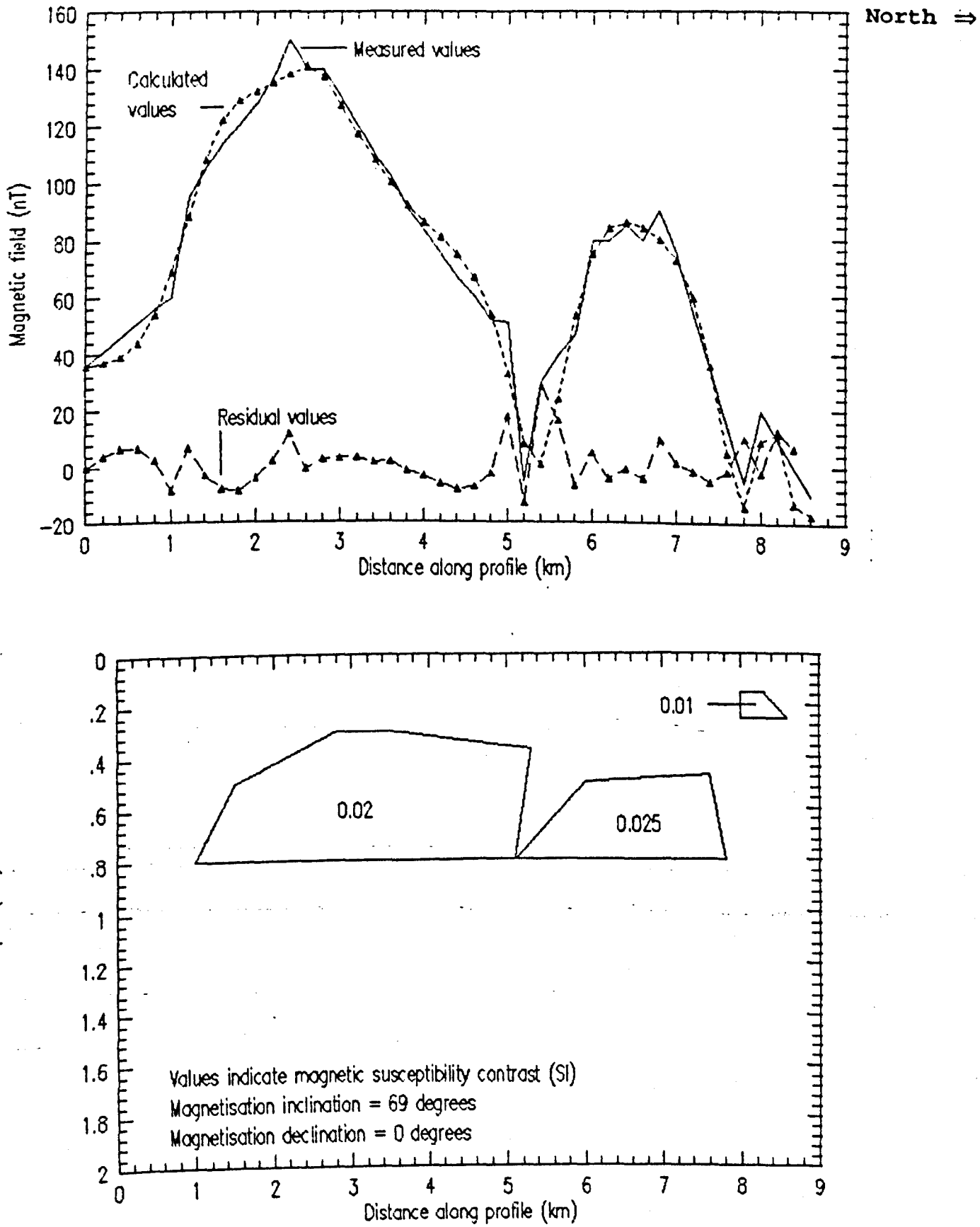

Figure 3.11.f

A model of the aeromagnetic anomaly overlying the Tomintoul diorite (line H-H on Figure 3.11.a).

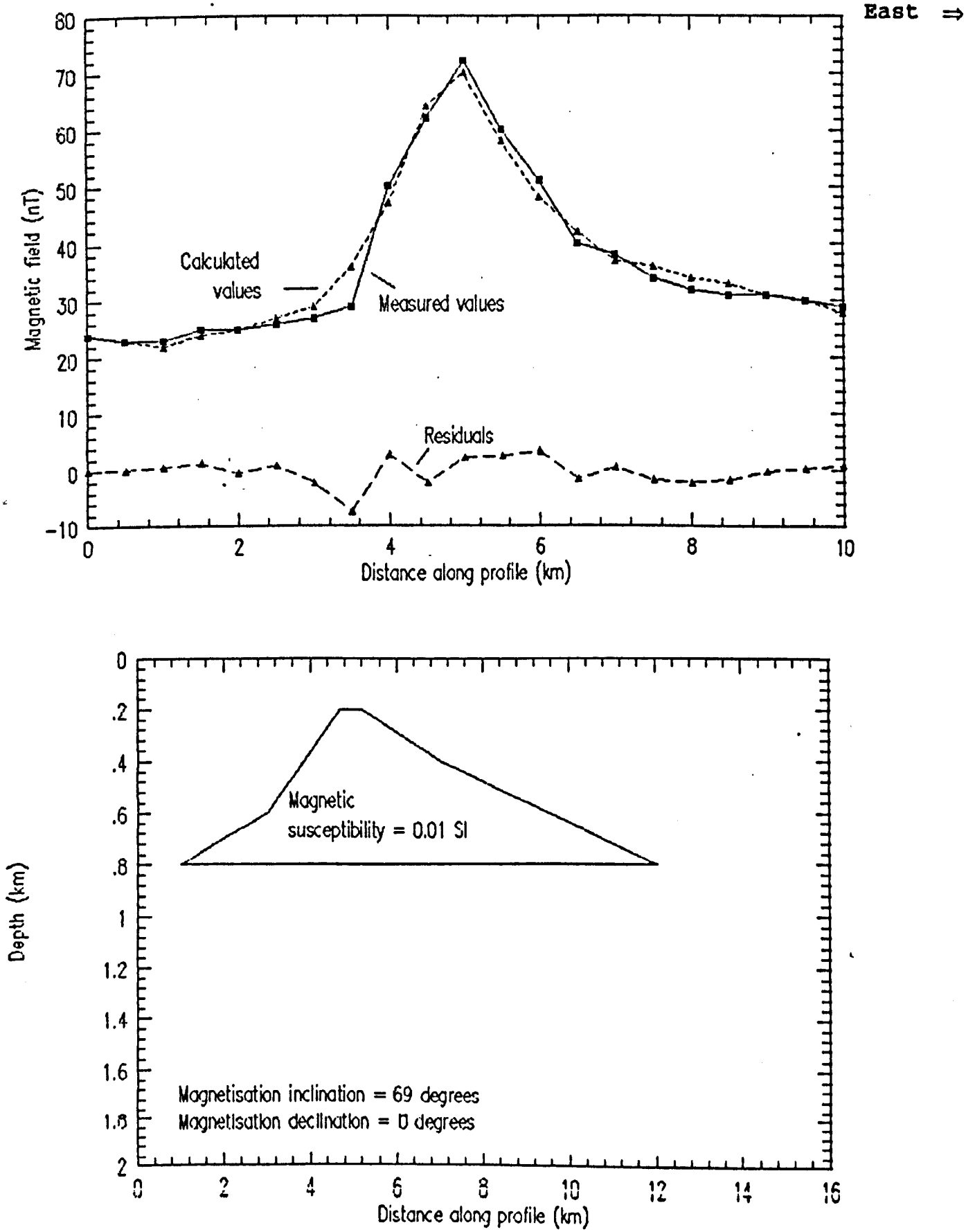

Figure 3.11.g

A model of the aeromagnetic anomaly overlying the central Cairngorm diorite

(line D-D on Figure 3.11.a)

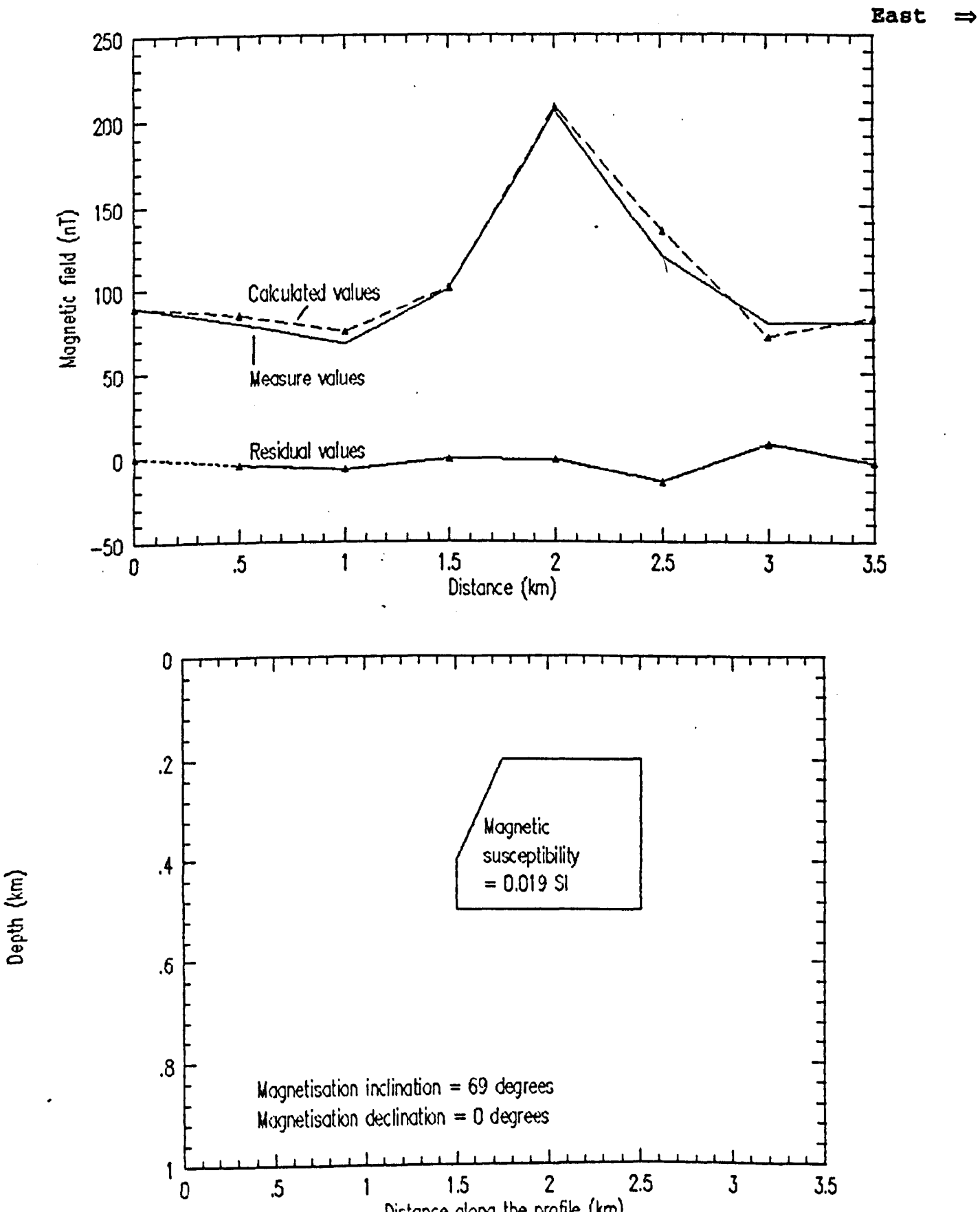

Figure 3.11.h

A model of the aeromagnetic anomaly overlying the Derry Lodge area of south central Cairngorm (line G-G on Figure 3.11.a).

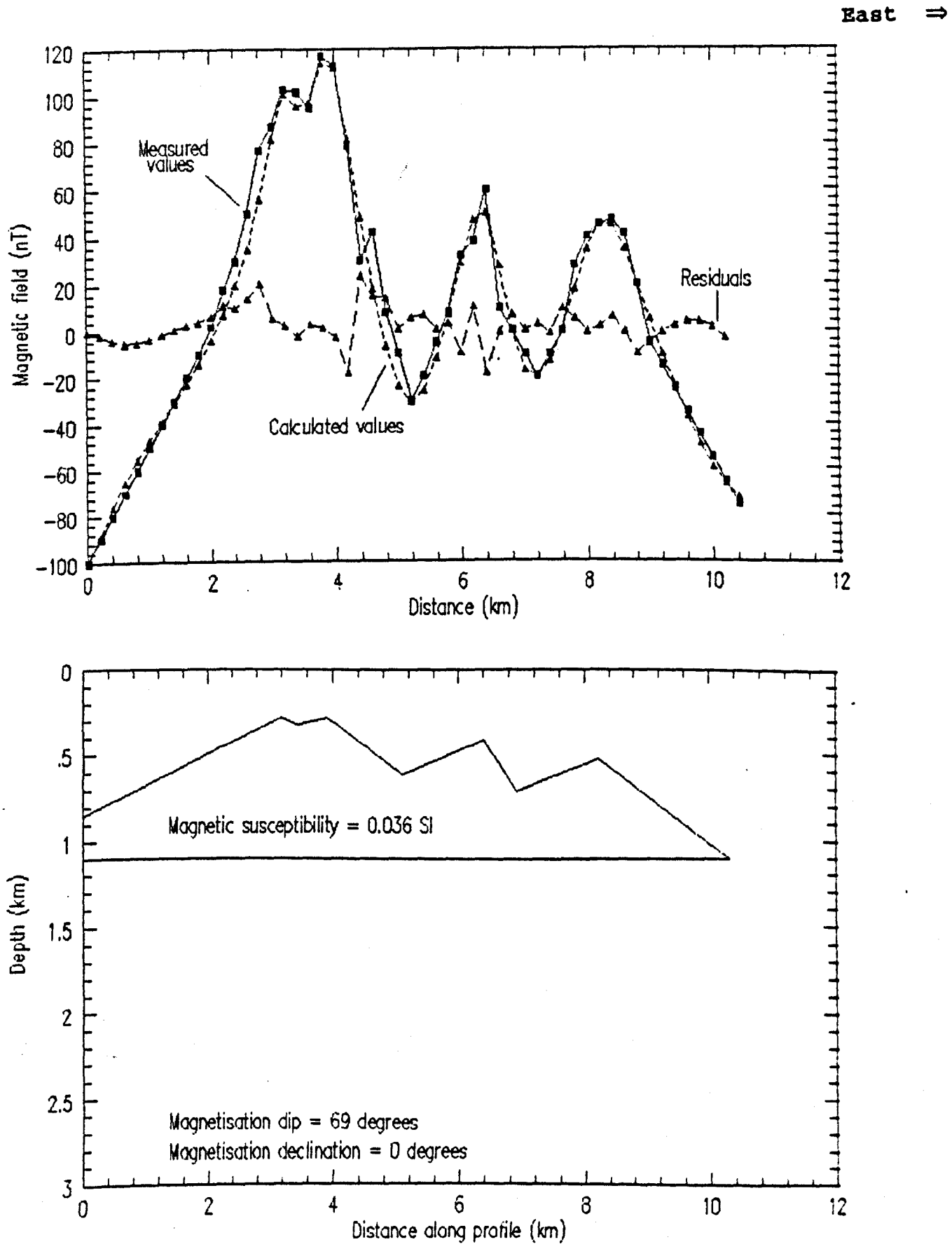

Figure 3.11.i

A model of the gravity anomaly overlying the central section of the Cairngorm granites (line B-B on Figure 3.11.a).

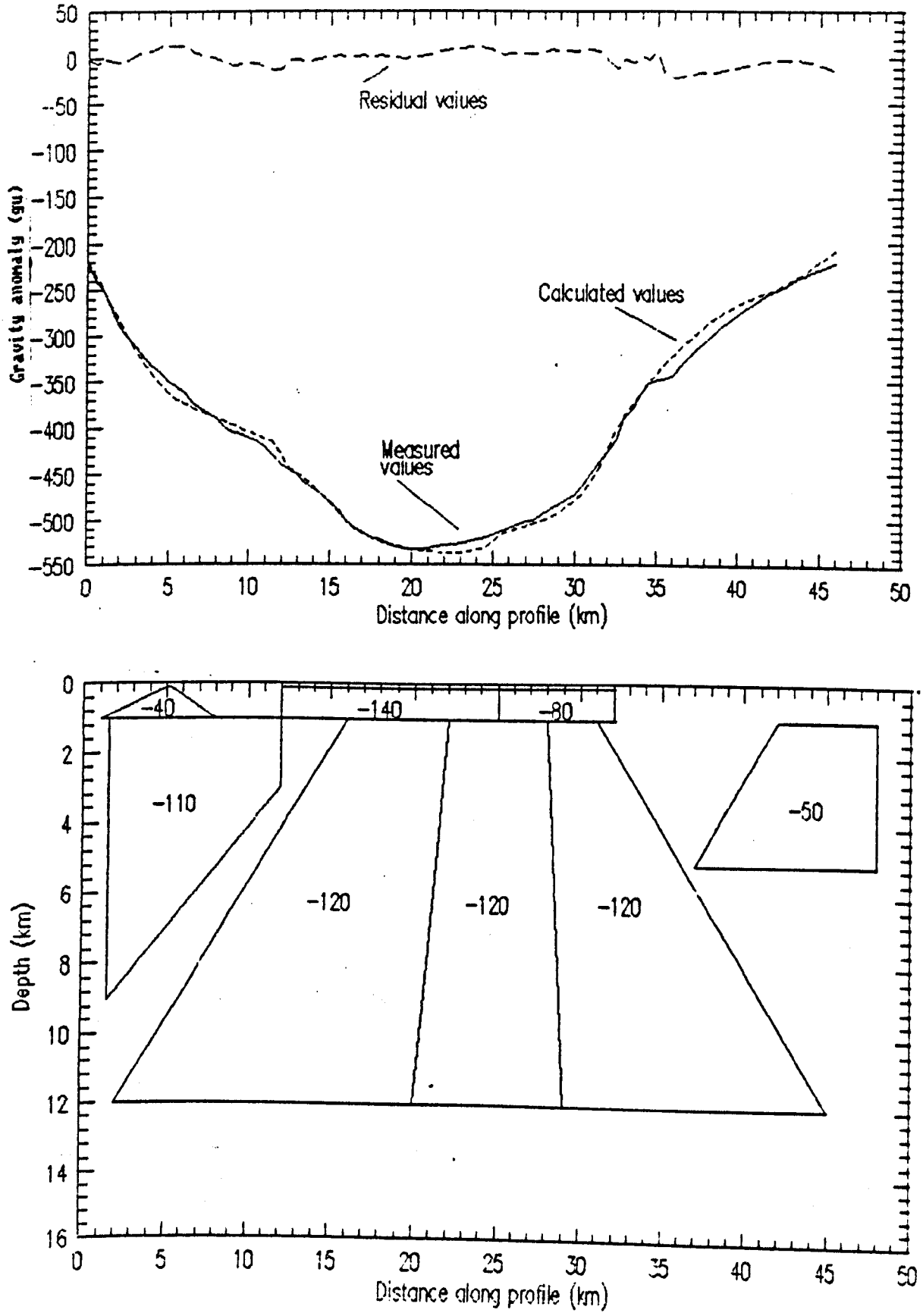

Figure 3.11.j

A model of the aeromagnetic anomaly overlying the central section of the Cairngorm granites (line B-B on Figure 3.11.a).

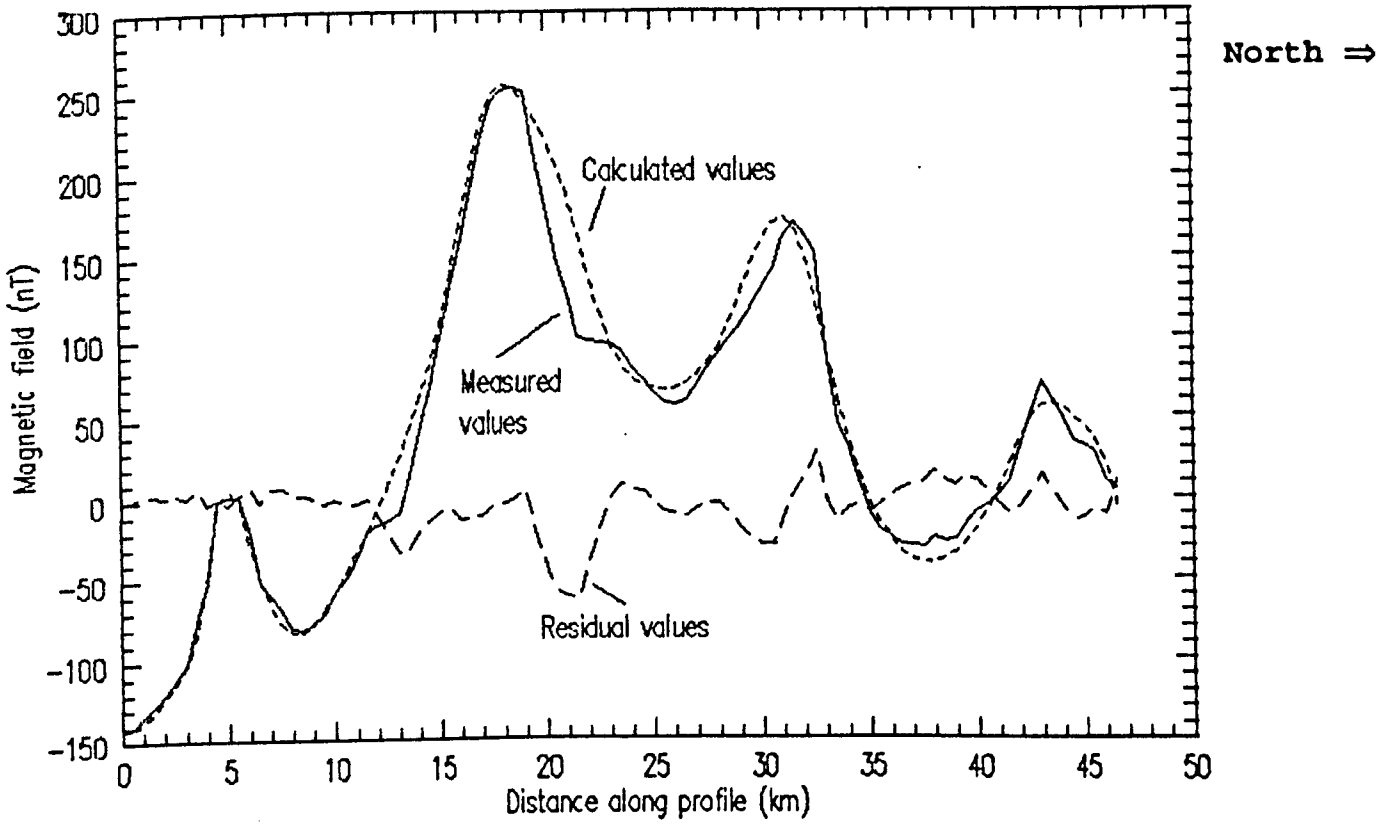

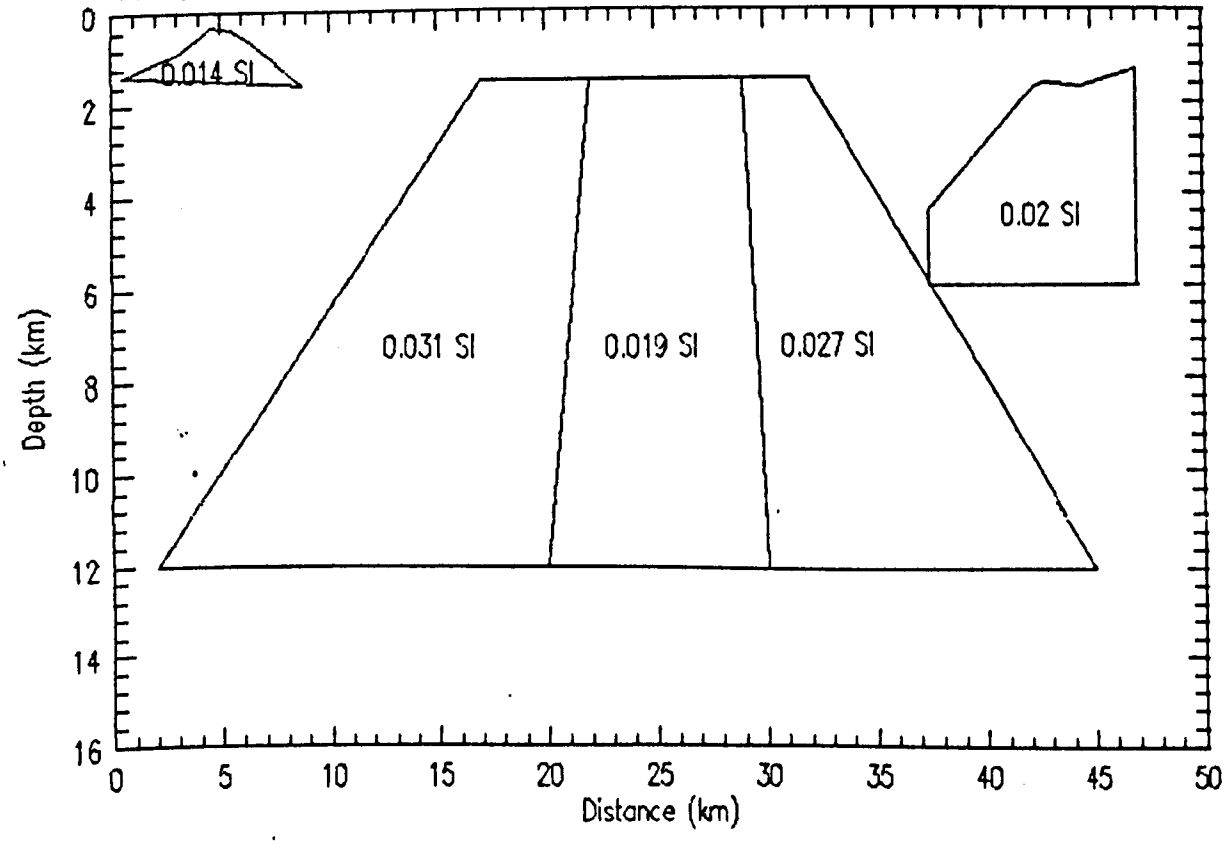

Figure 3.11.k

A model of the gravity anomaly overlying the eastern section of the Cairngorm granites (line A-A on Figure 3.11.a).

North ⇒

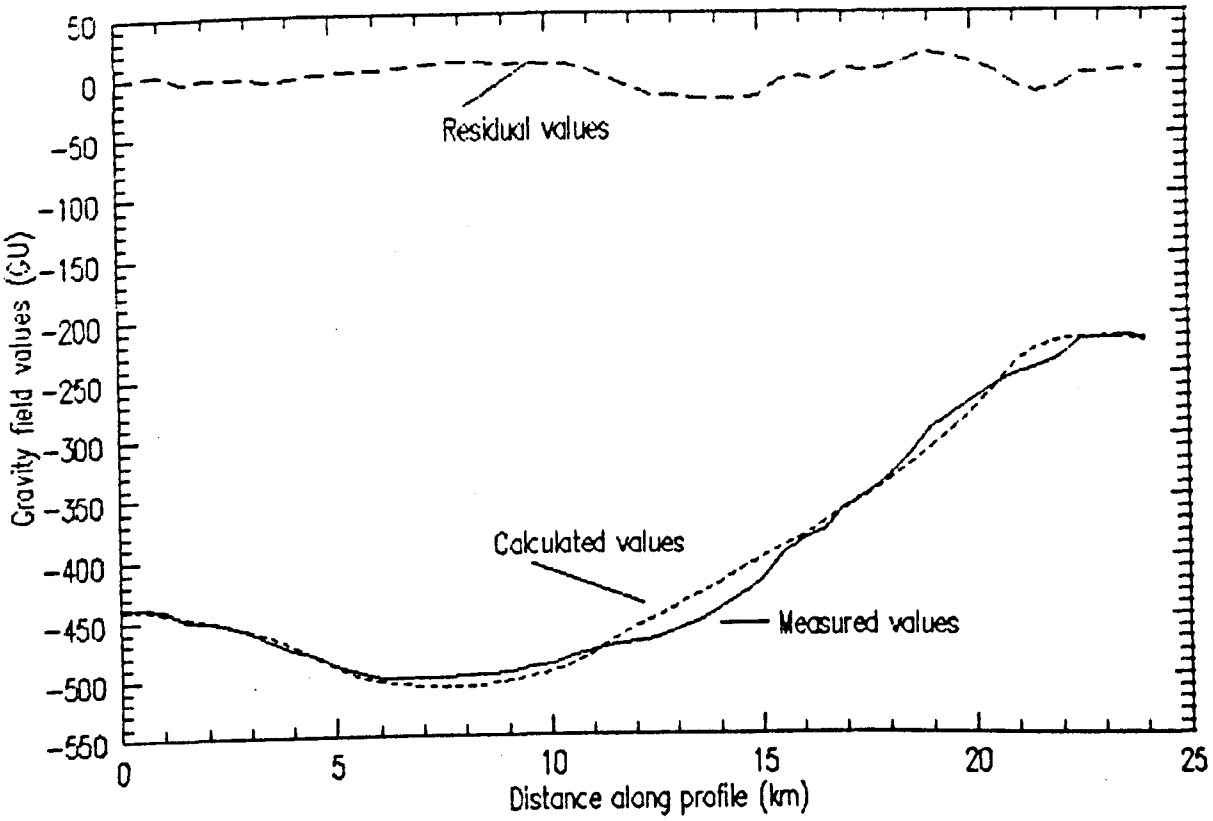

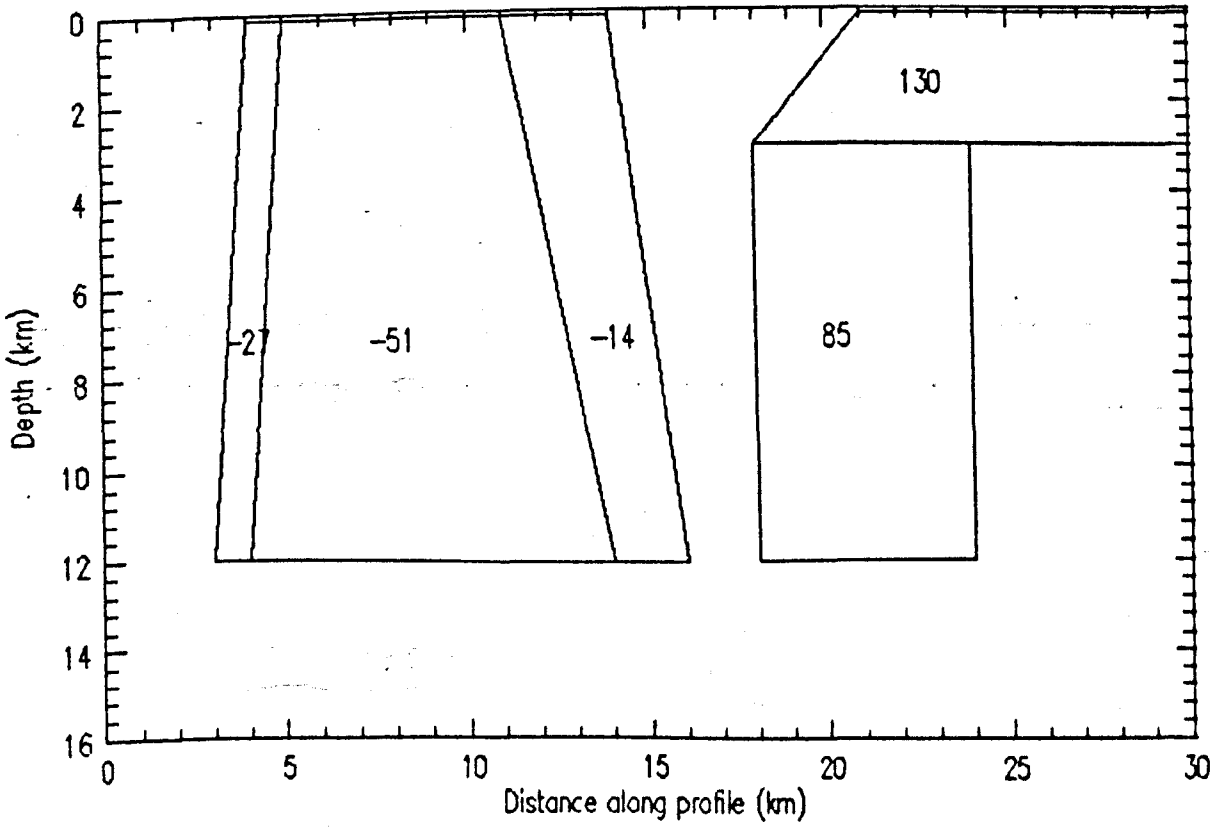

Figure 3.11.1

A model of the aeromagnetic anomaly overlying the eastern section of the Cairngorm granites (line A-A on Figure 3.11.a).

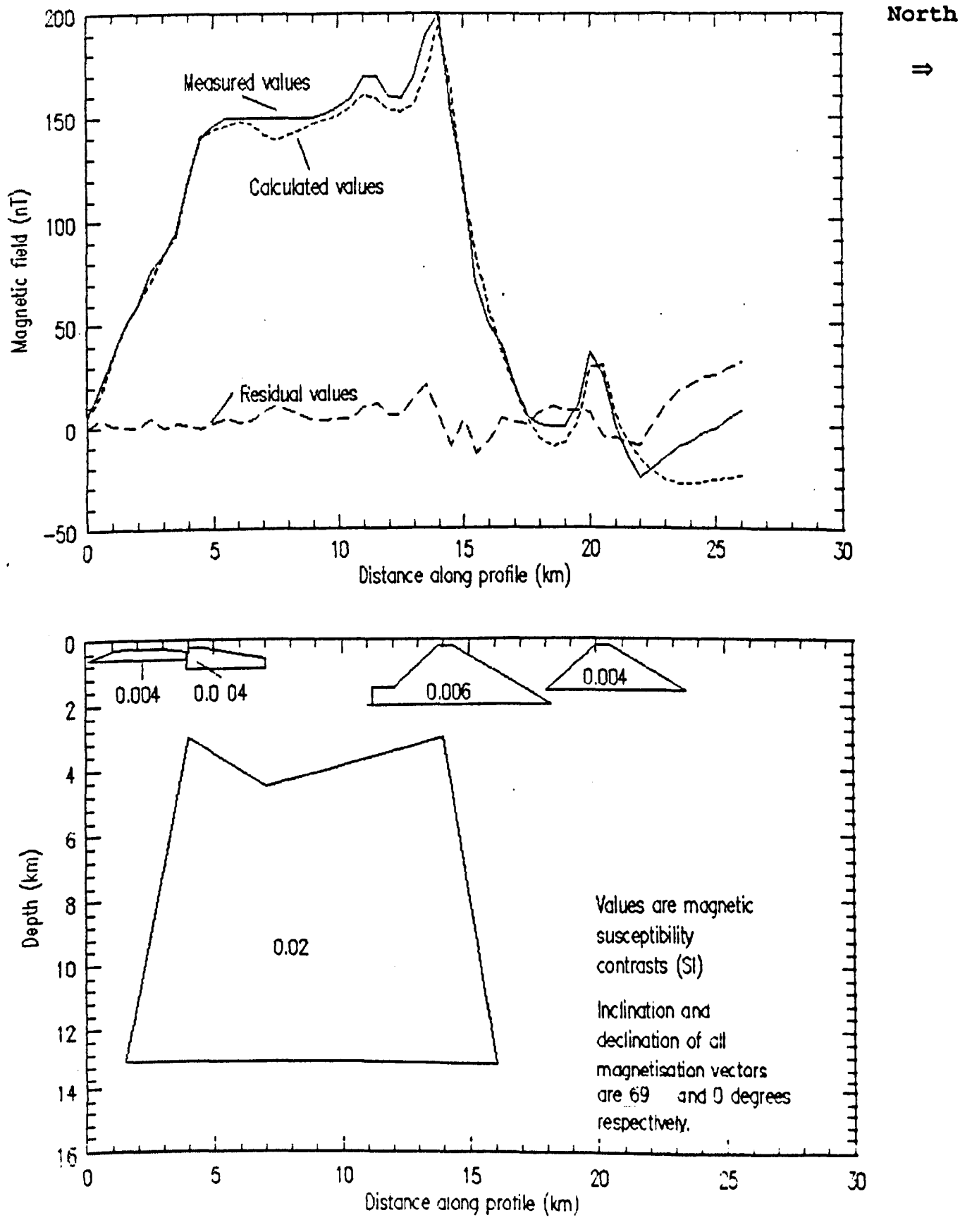

Figure 4.1.a

A geological sketch map of the

Southern Uplands of Scotland

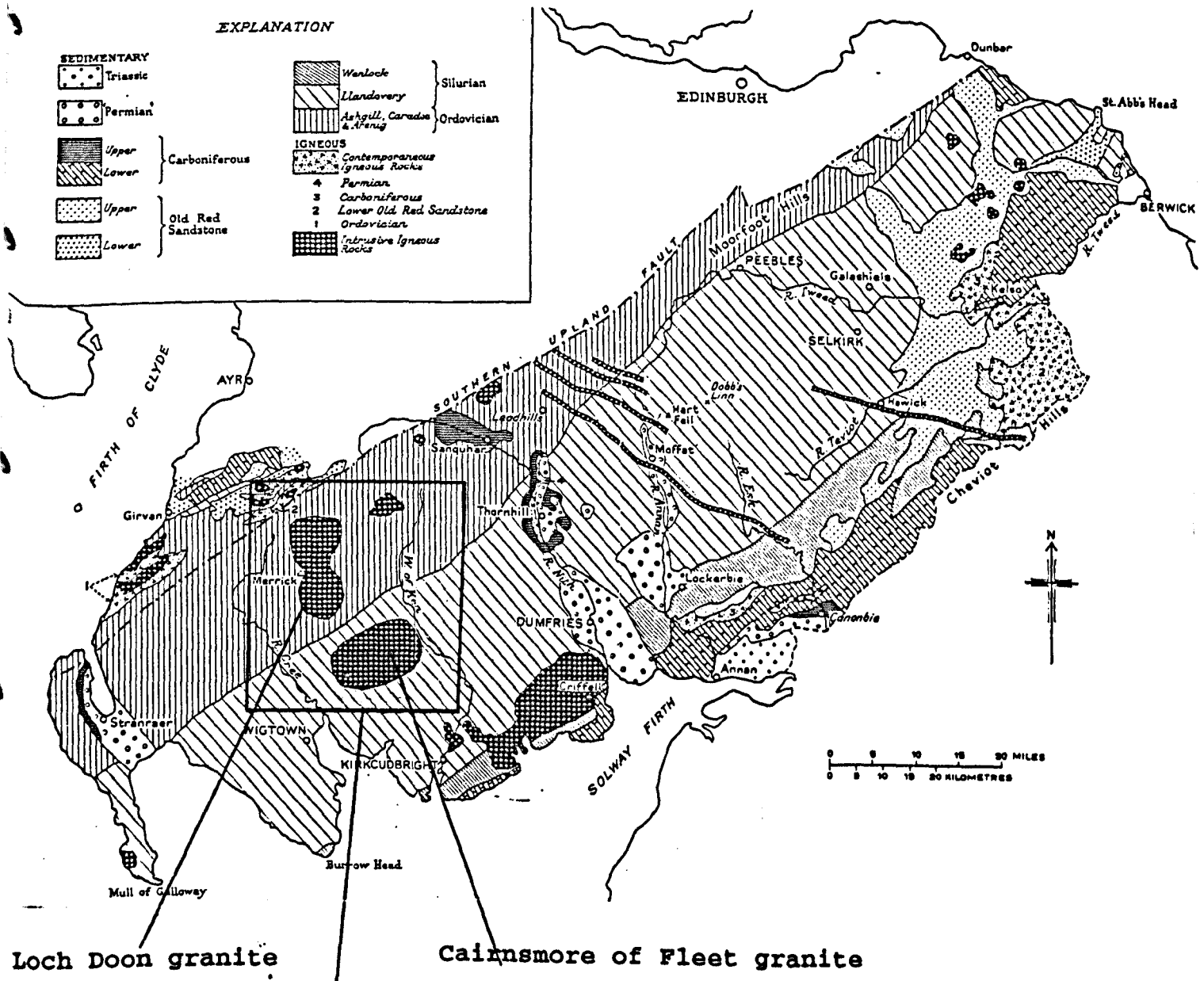

Loch Doon granite

Cairnsmore of Fleet granite

Area covered by aeromagnetic data

After Grieg (1971)

Figure 4.2.a

Residual gravity anomaly map of the

Southern Uplands of Scotland

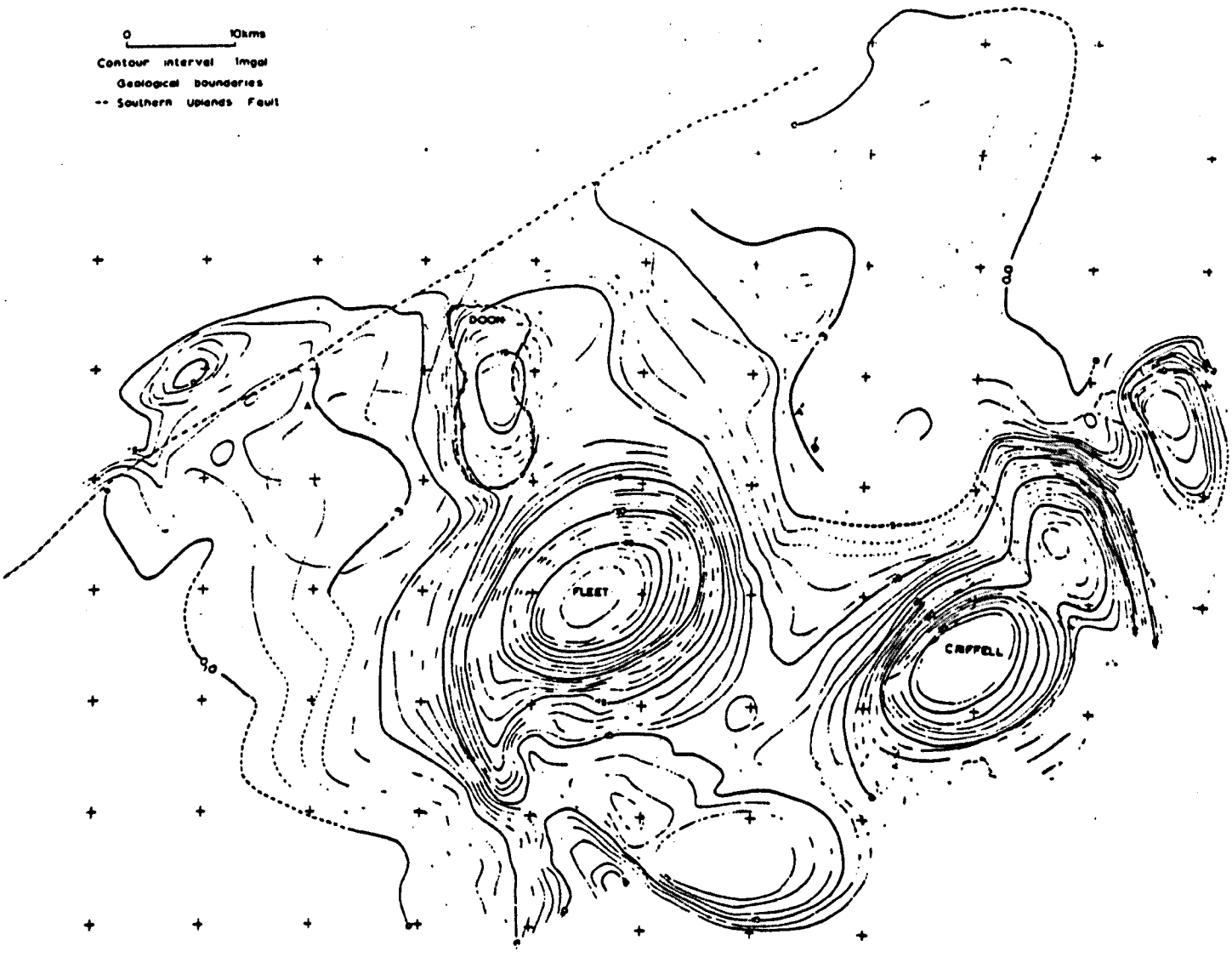

After El-Batroukh (1975)

Figure 4.3.a

Depth to the top surface of the Southern Uplands batholith

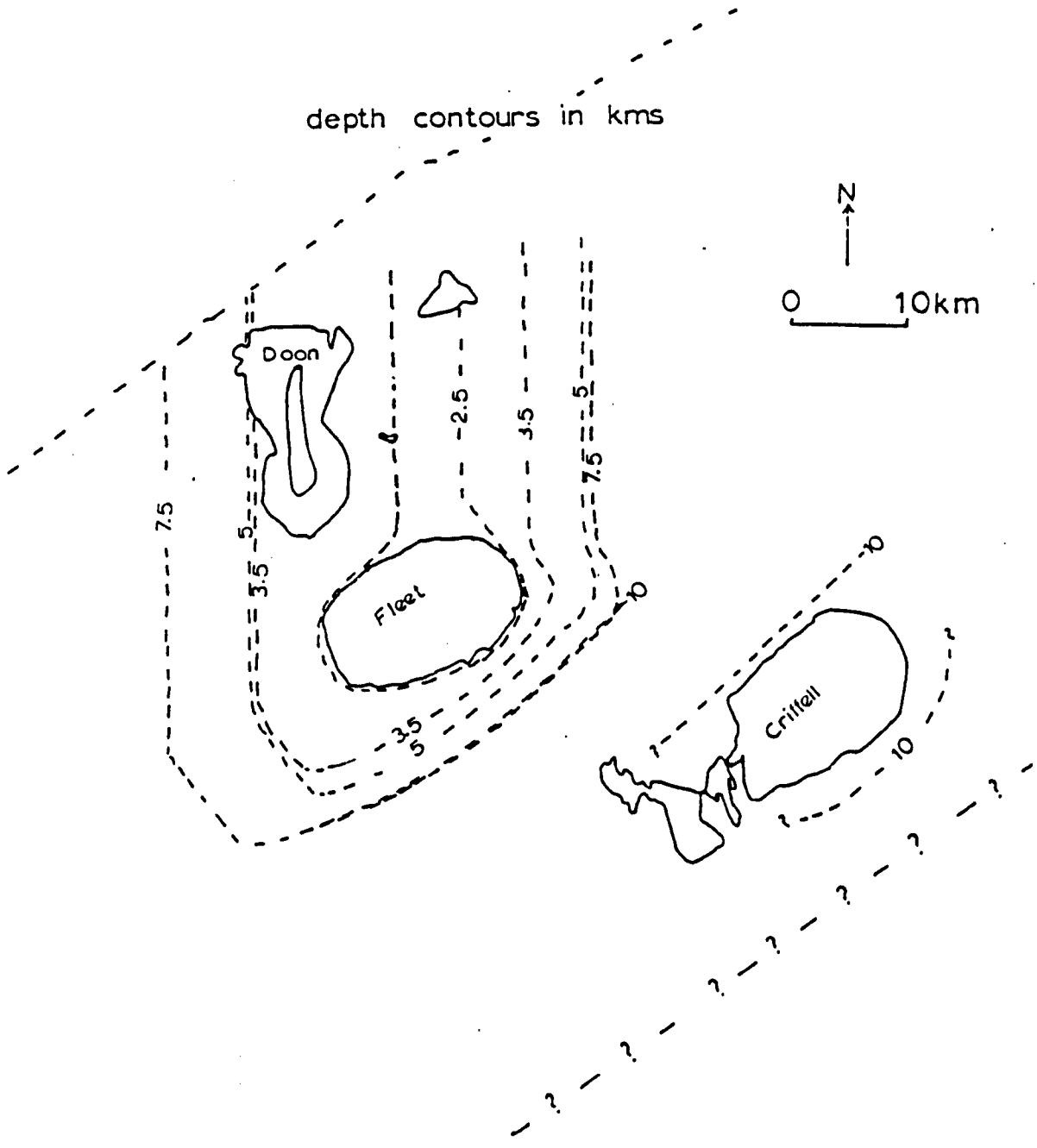

After El-Batroukh (1975)

Figure 4.3.b

Density model of the Cairnsmore of Fleet granite

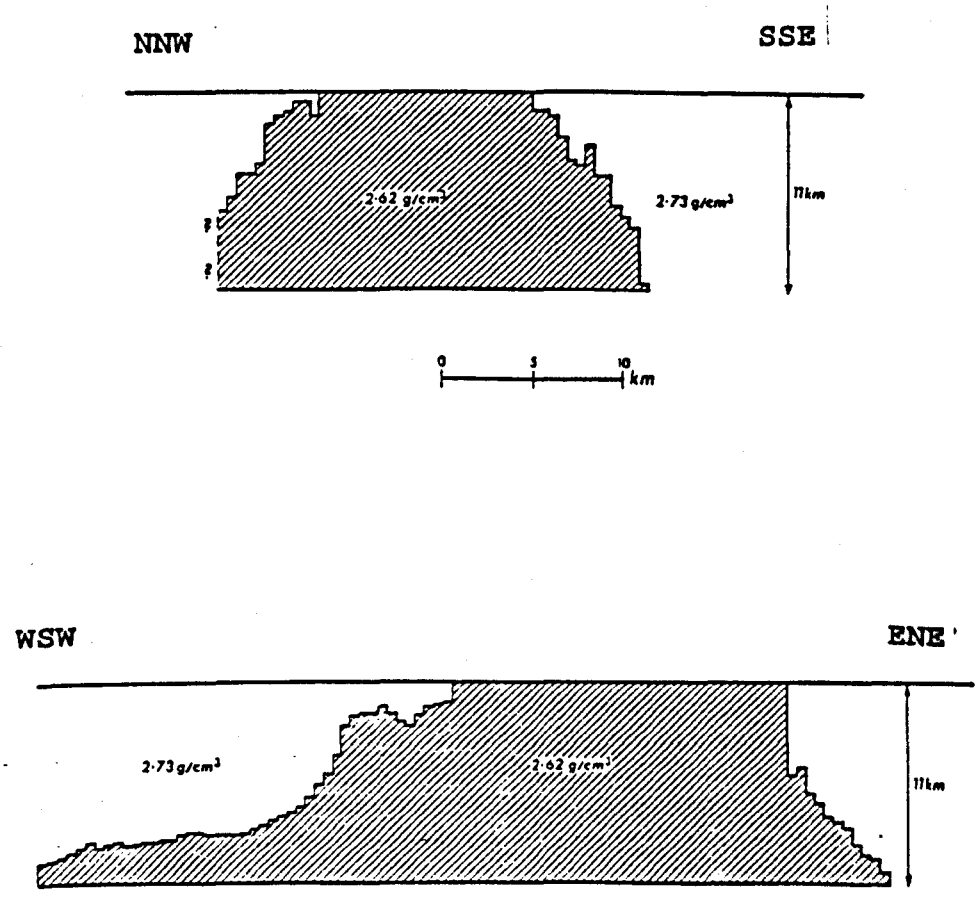

After Parslow and Randall (1973)

Figure 4.4.a

The Loch Doon and Cairnsmore of Fleet granites

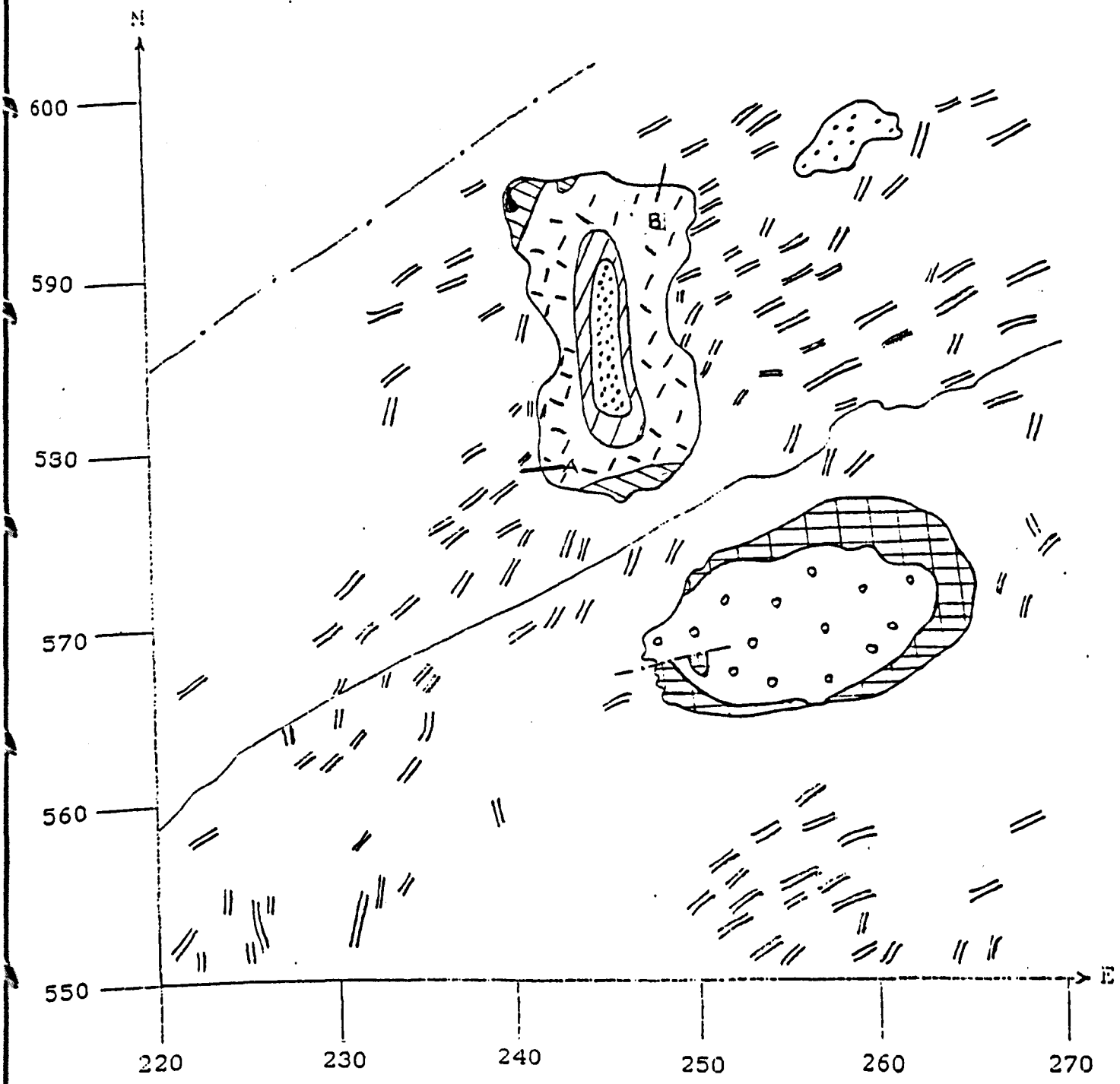

Rocks transitional between Tonalite and Norite

Rocks transitional between Granite and Tonalite

Granite

Tonalite

Norite

Dykes

Muscovite-Biotite Granite

Biotite Granite

Fault

Figure 4.5.a

The aeromagnetic field over the Loch Doon and Cairnsmore of Fleet granites

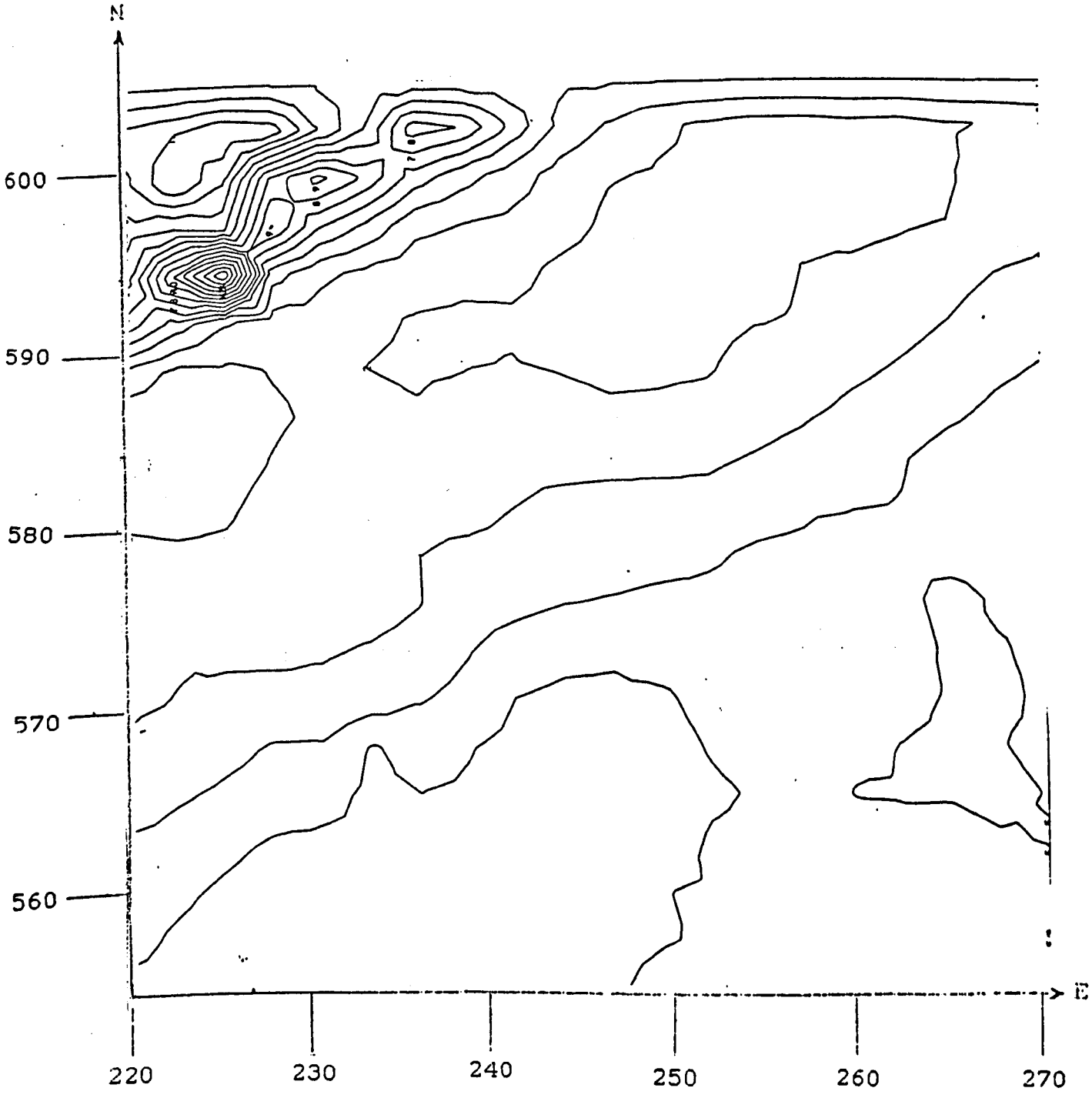

Contour interval = 40 nT

Contour 4 = 40 nT

Figure 4.6.a

The aeromagnetic field over the Loch Doon and Cairnsmore of Fleet granites reduced to the pole

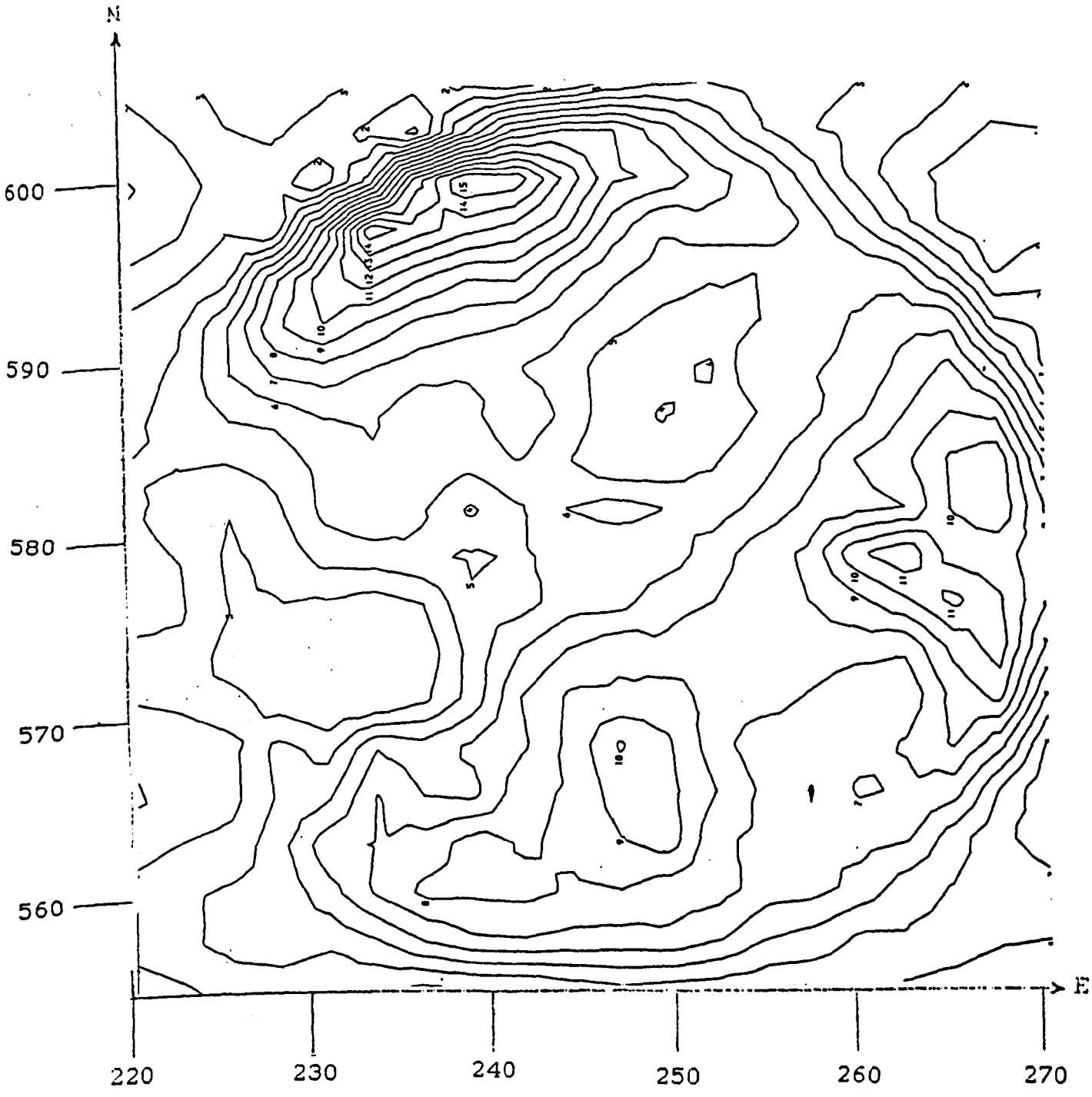

Contour interval = 10 nT

Contour 4 = 8 nT

Assumed inclination = 70^0

Assumed declination = 0^0

Figure 4.7.a

Pseudogravimetric transformation of the aeromagnetic data over the Loch Doon and Cairnsmore of Fleet granites

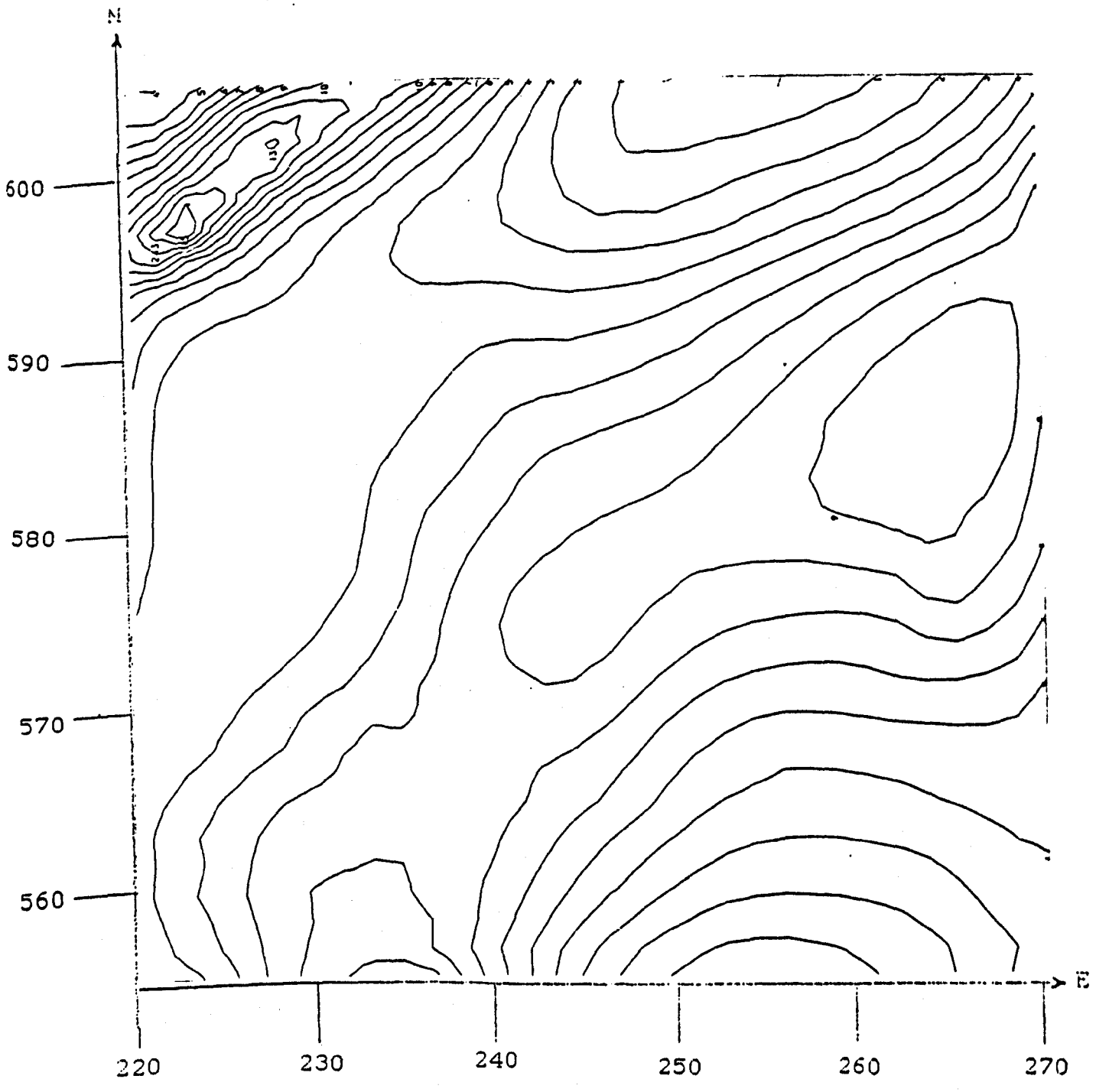

Contour interval = 3 mgals

Contour 9 = 32 mgals

All values are above an arbitrary base line

Figure 4.8.a

Azimuthally averaged power spectrum of the aeromagnetic field over the area of the Loch Doon and Cairnsmore of Fleet granites

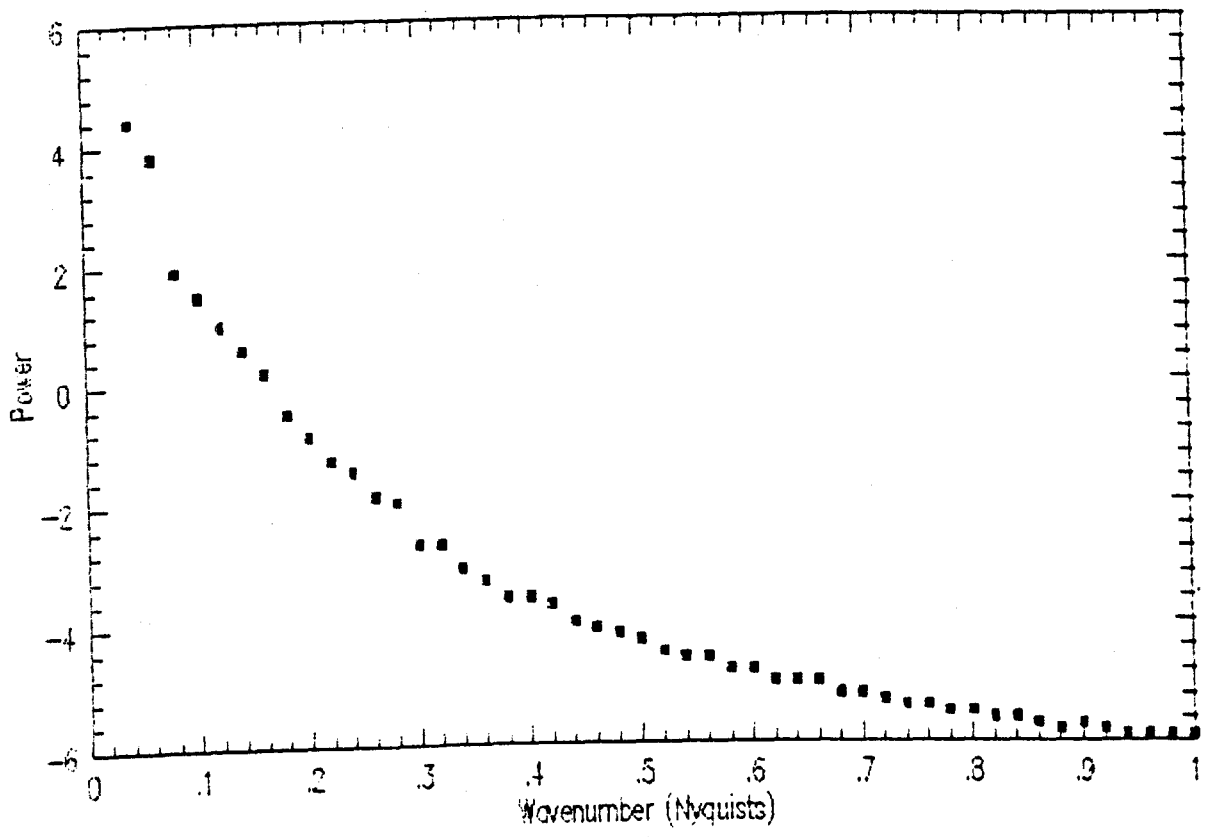

See discussion in text for dimensions of power

Figure 4.9.a

High-pass filtered map of the aeromagnetic field over the area of the Loch Doon and Cairnsmore of Fleet granites

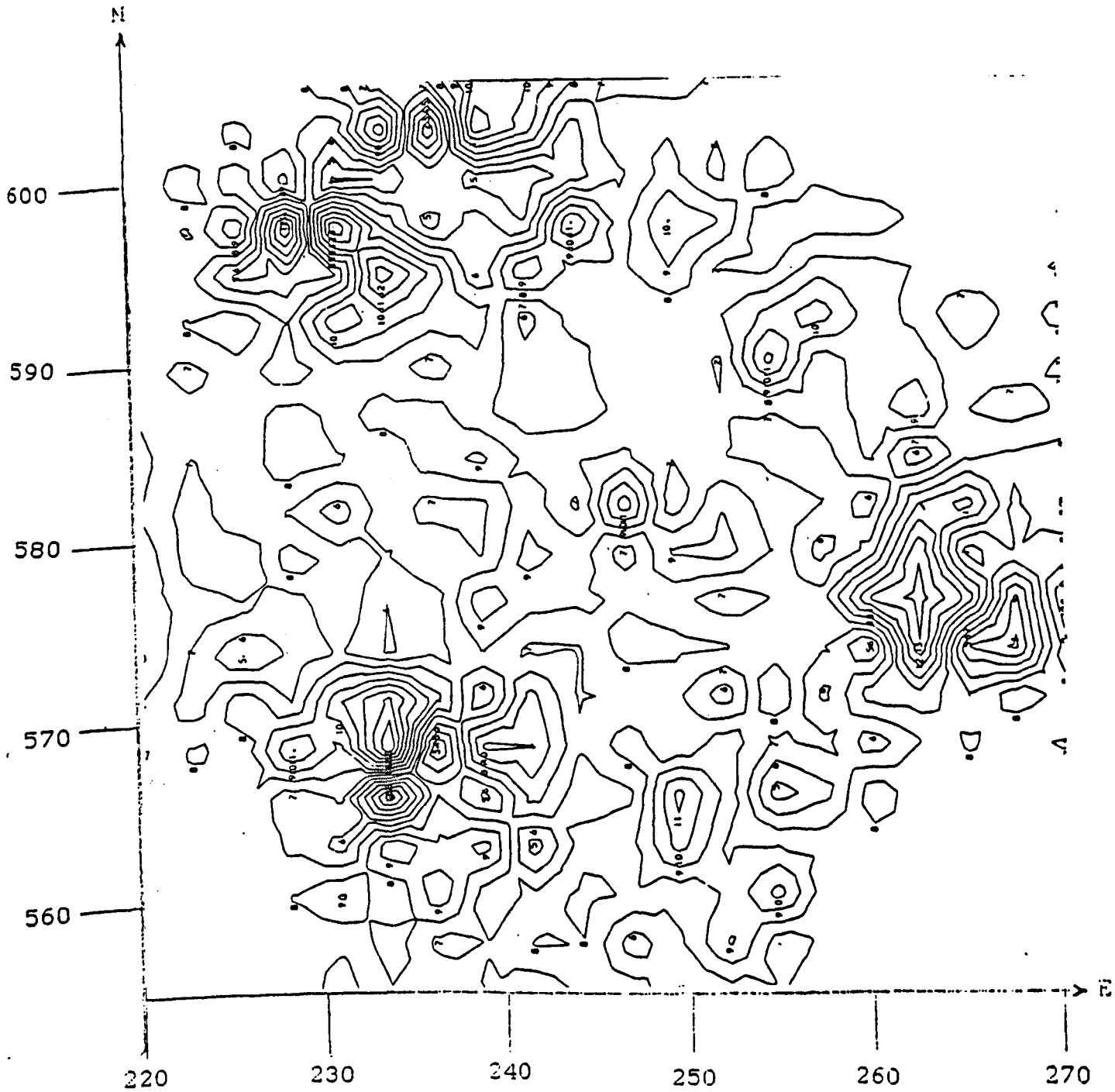

Contour interval = 0.8 nT

Contour 7 = 0.0 nT

Figure 4.9.b

Biotite/total mica in the

Cairnsmore of Fleet granite

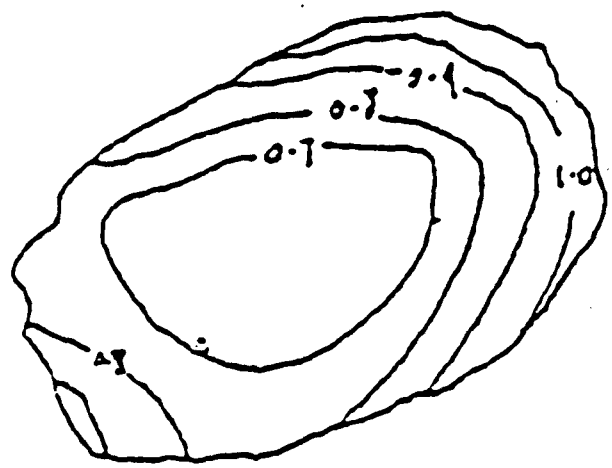

After Hennessy (1978)

Figure 4.10.a

Band pass filtered map of the aeromagnetic field over the area of the Loch Doon and Cairnsmore of Fleet granites

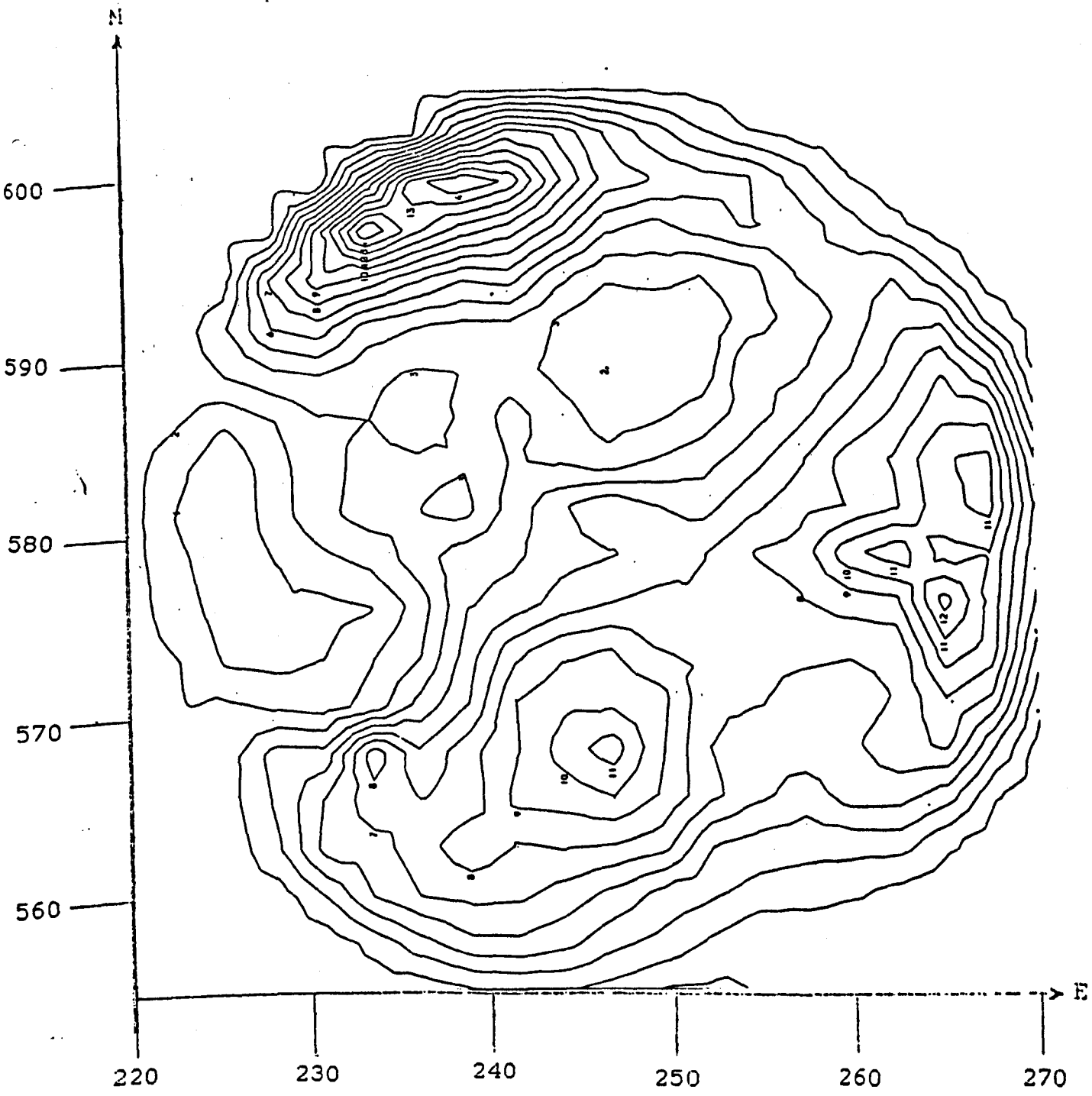

Contour interval = 1.0 nT

Contour 1 = -6 nT

Figure 4.11.a

Low-pass filtered map of the aeromagnetic field over the area of the Loch Doon and Cairnsmore of Fleet granites

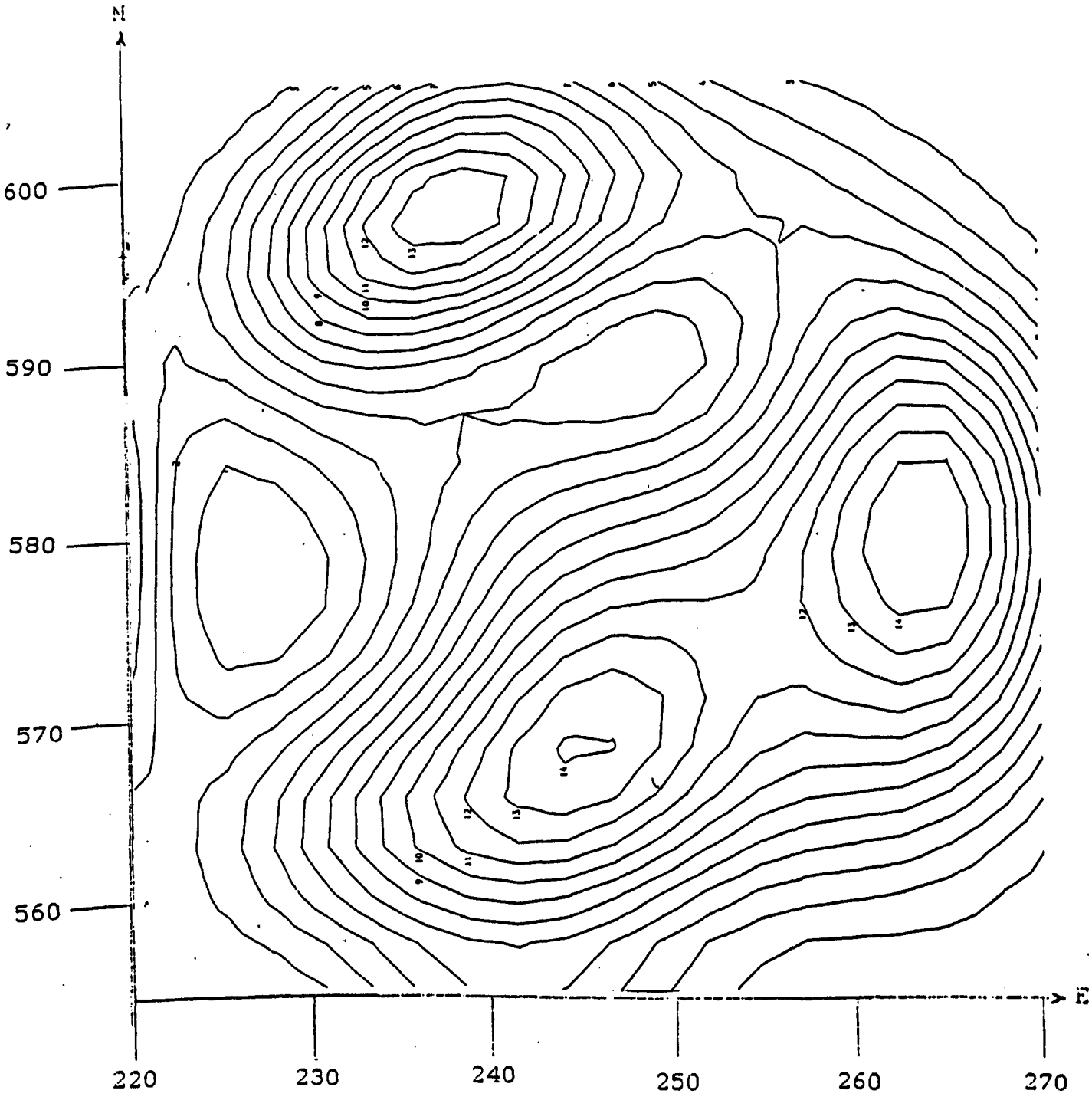

Contour interval = 5 nT

Contour 1 = -25 nT

Figure 4.12.a

Field lines walked in the collection of ground based magnetic readings from the Cairnsmore of Fleet granite

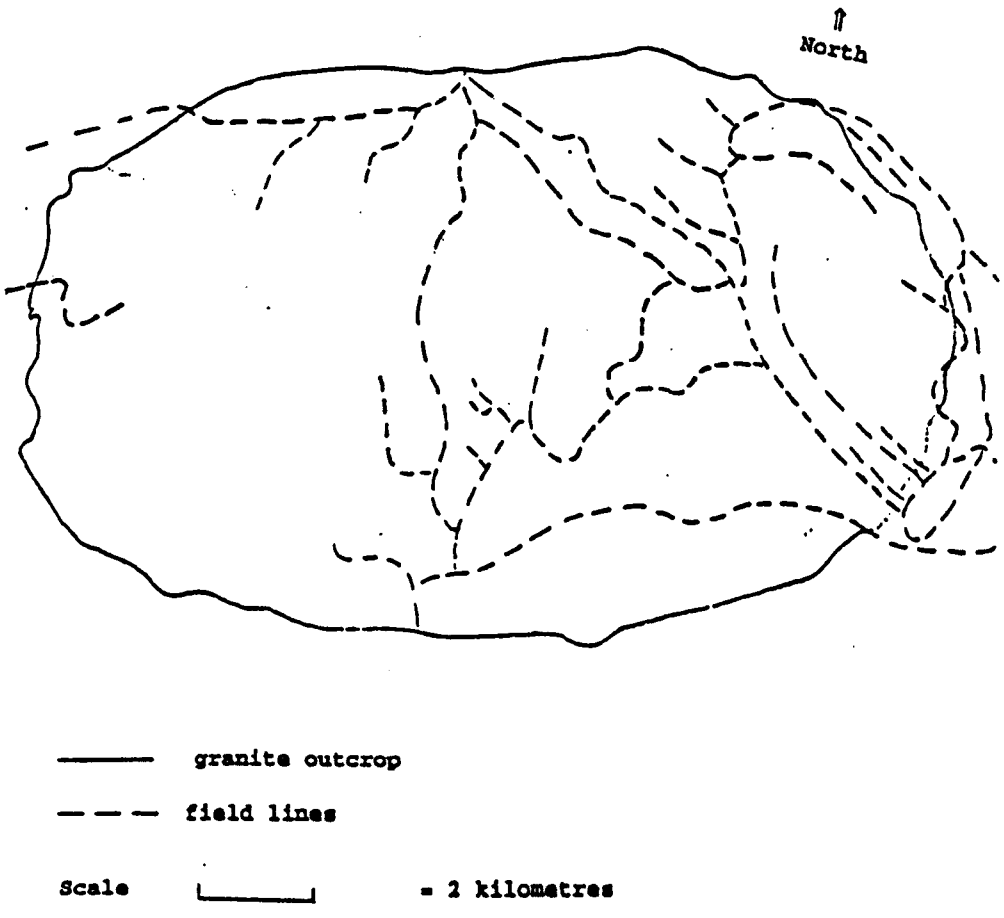

Figure 4.12.b

Contoured magnetic field values for the Cairnsmore of Fleet granite

⇑
North

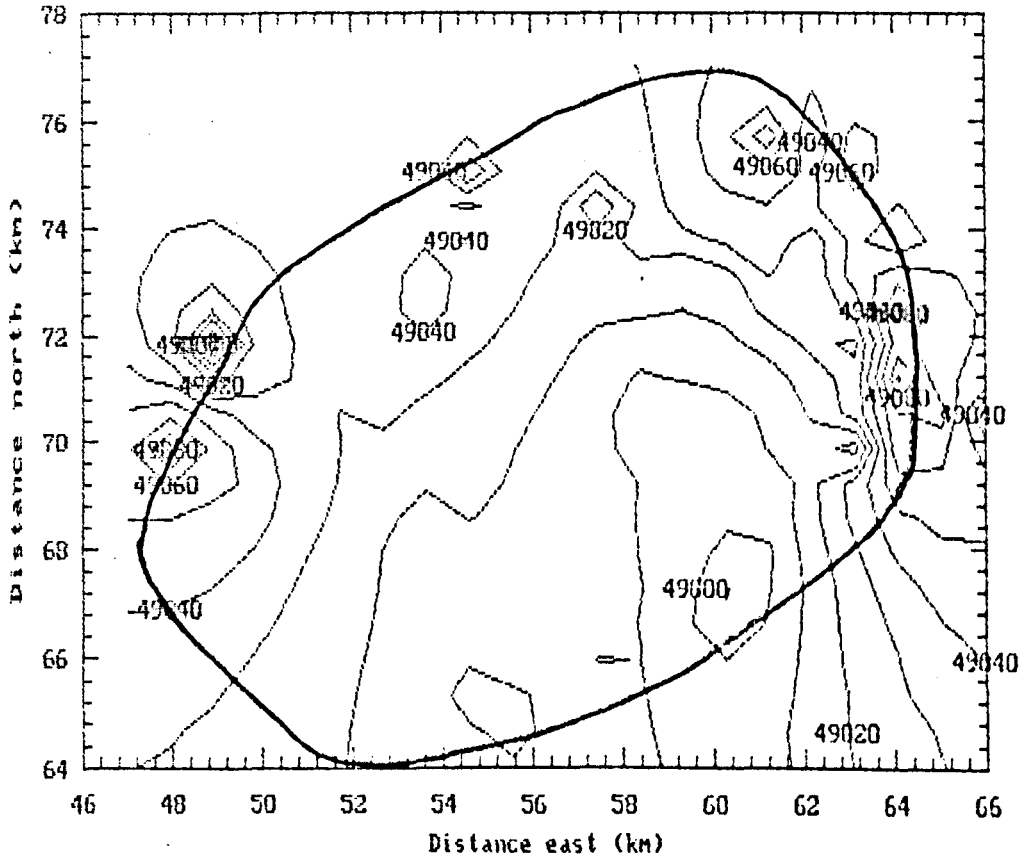

——— **granite outline**

Figure 4.12.c

Thorium concentrations in the Cairnsmore of Fleet granite

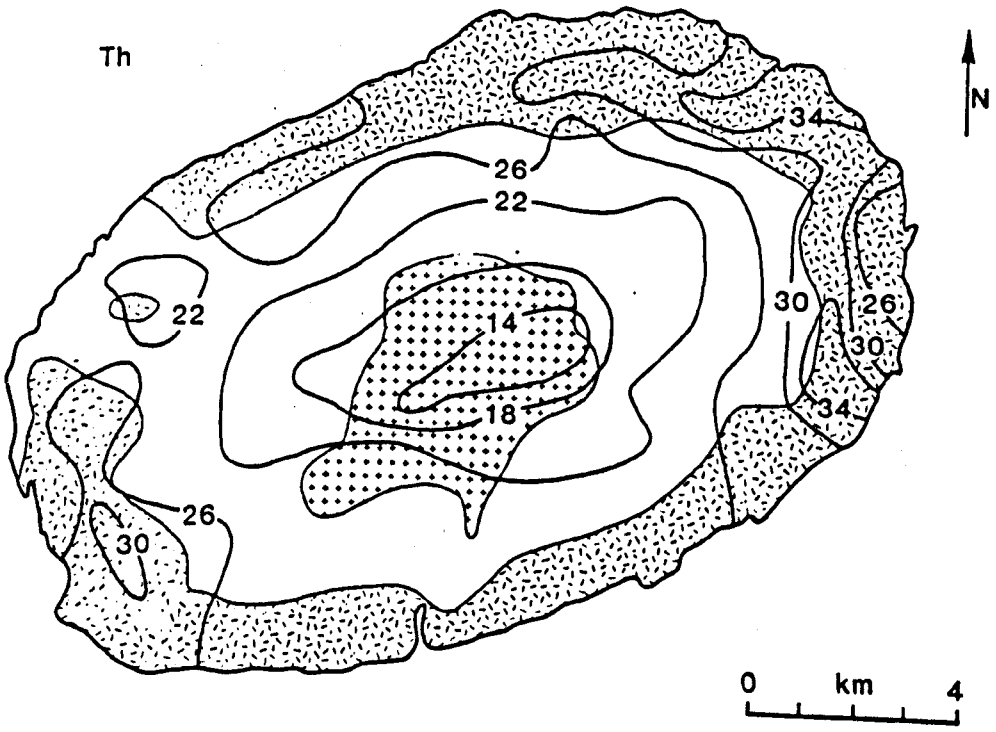

After Hennessy (1978)

Figure 4.19.a

Second order trend surface for Uranium

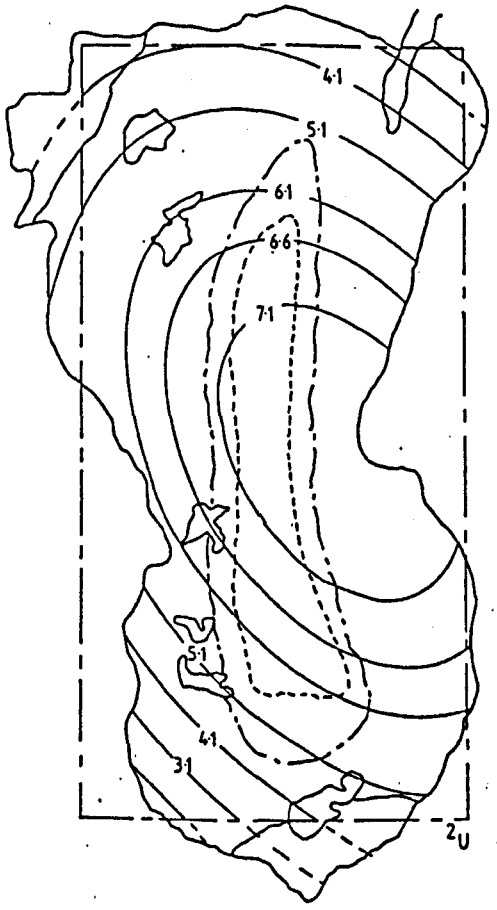

After Hennessy (1978)

Figure 5.1.a

The movement of a differentiated granite through gravmag space

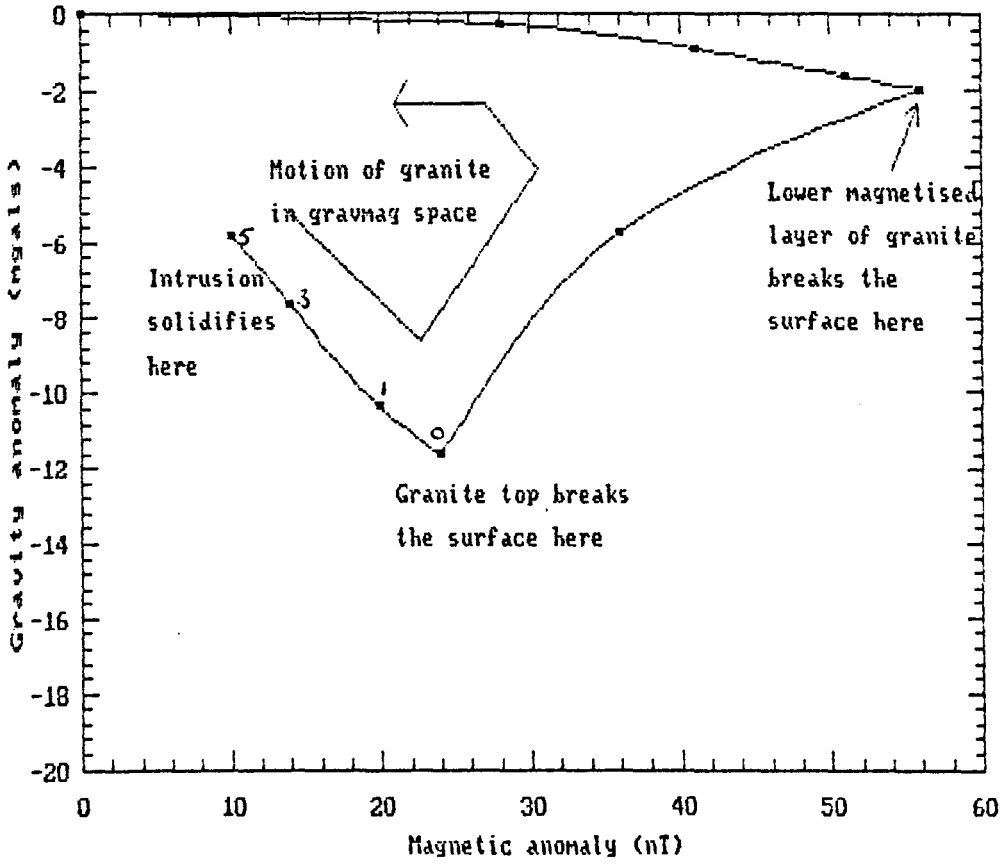

Parameters of granitic prism at the point of solidification

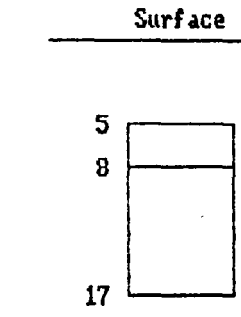

Top layer

Density contrast = -100 kg/cubic metre

Susceptibility contrast = 0.0001 SI

Bottom layer

Density contrast = -10 kg/cubic metre

Susceptibility contrast = 0.001 SI

Values indicate depth beneath the surface in kilometres

Figure 5.1.b

The movement of an undifferentiated granite through gravmag space

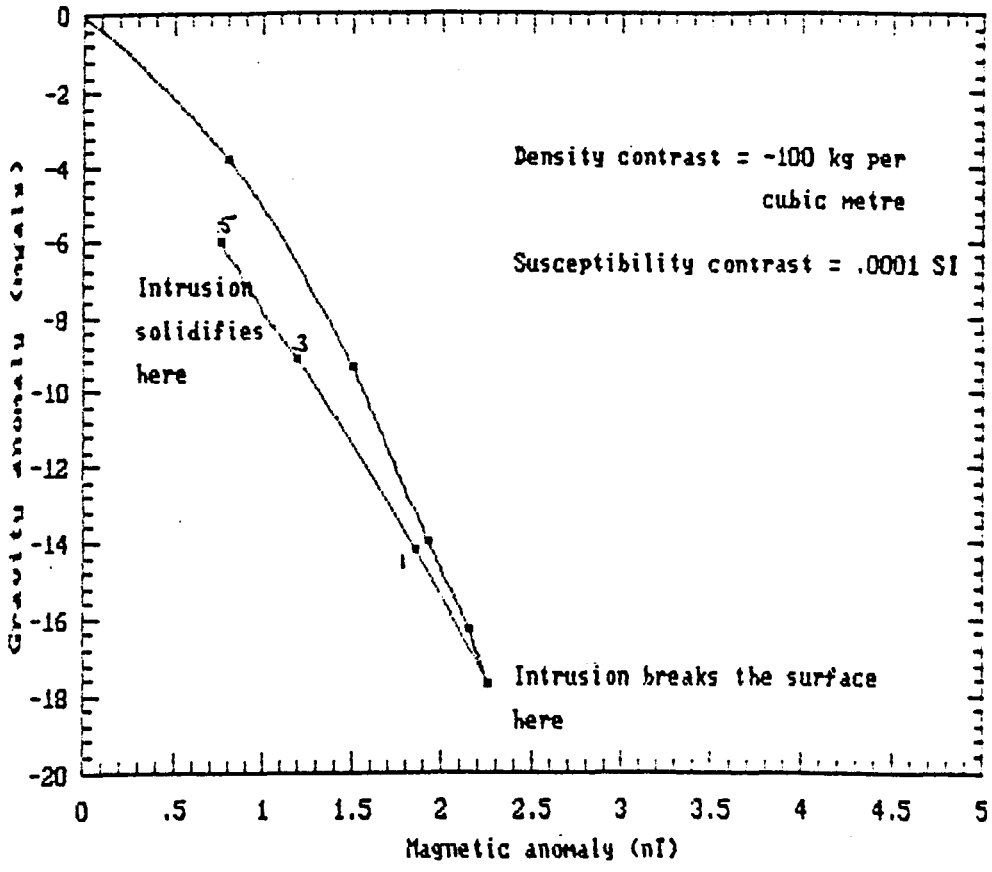

Parameters of granitic prism at the point of solidification

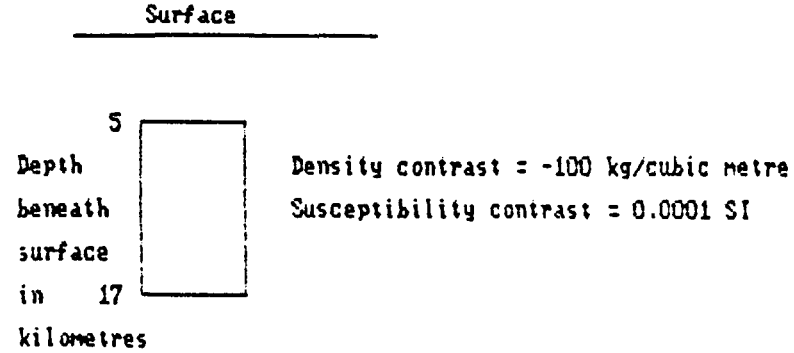

Figure 5.1.c

A plot of the gravity anomaly against the aeromagnetic anomaly for some British Caledonian granites

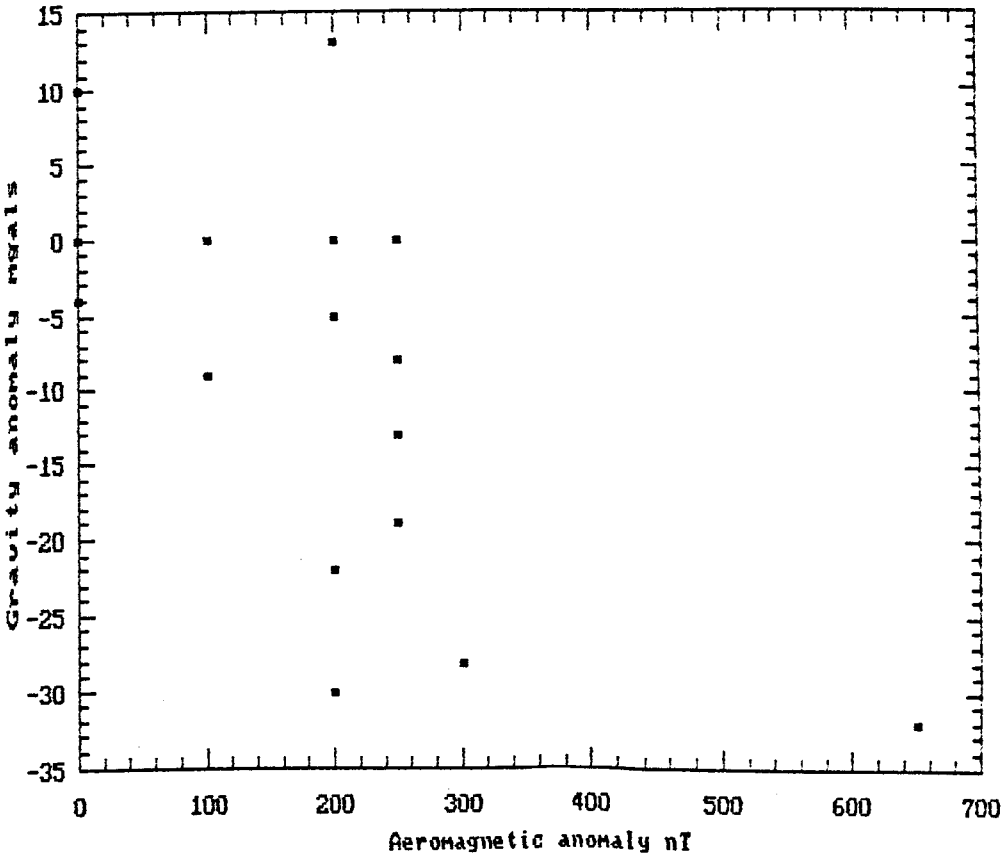

Data after Brown G.C. and Locke C.A. (1979)

Figure 5.1.d

The gravity and magnetic anomalies of some Scottish Caledonian granites

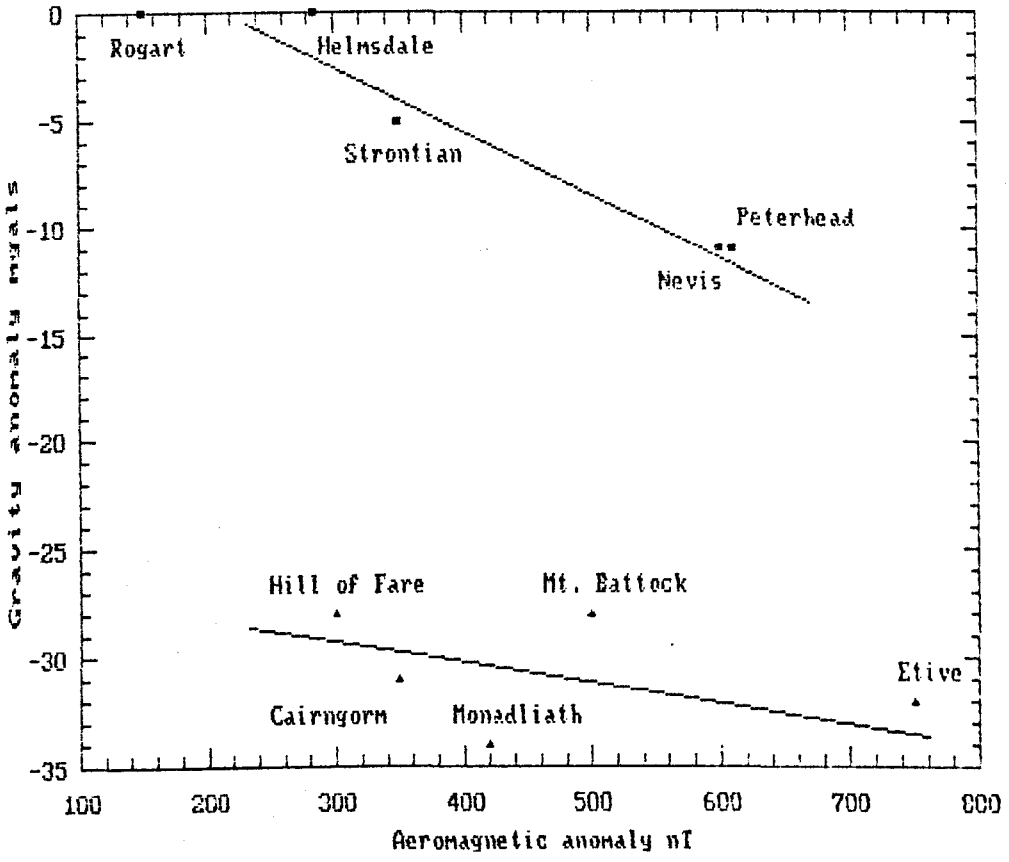

Figure 5.1.e

The gravity and magnetic anomalies of some granites from the Southern Uplands of Scotland and Northern England

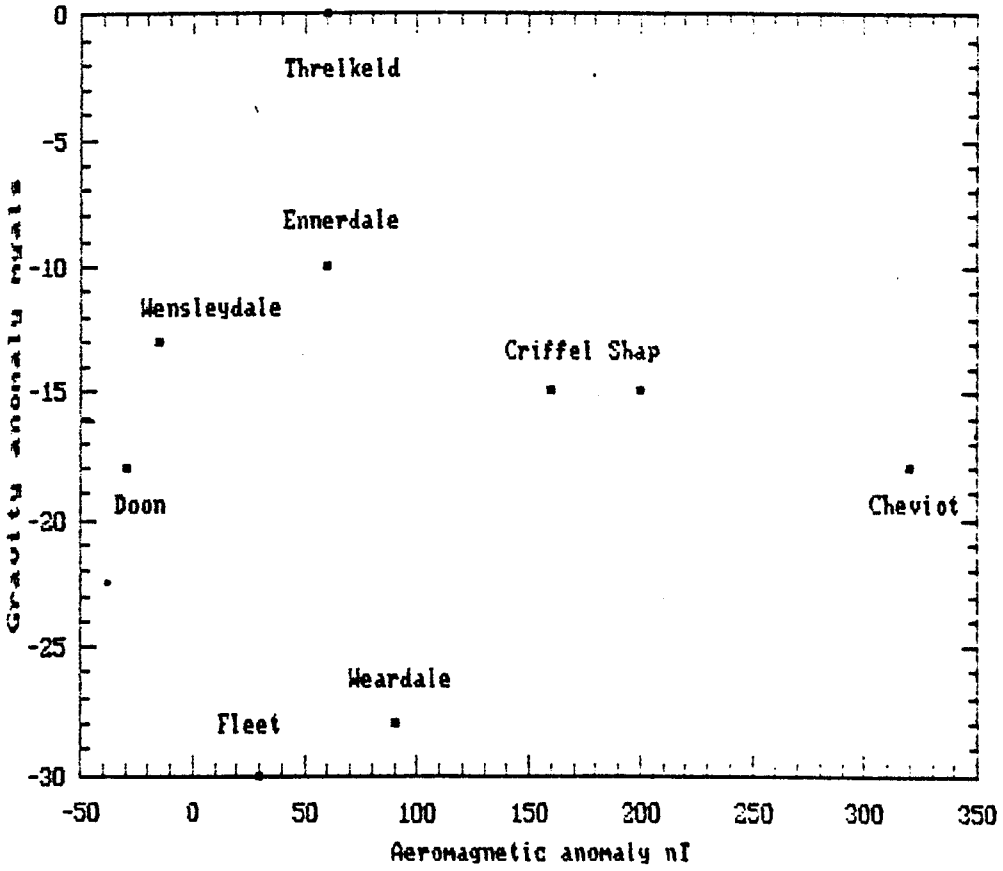

Figure 5.2.a

Uranium concentrations plotted against residual gravity anomalies for some British Caledonian granites

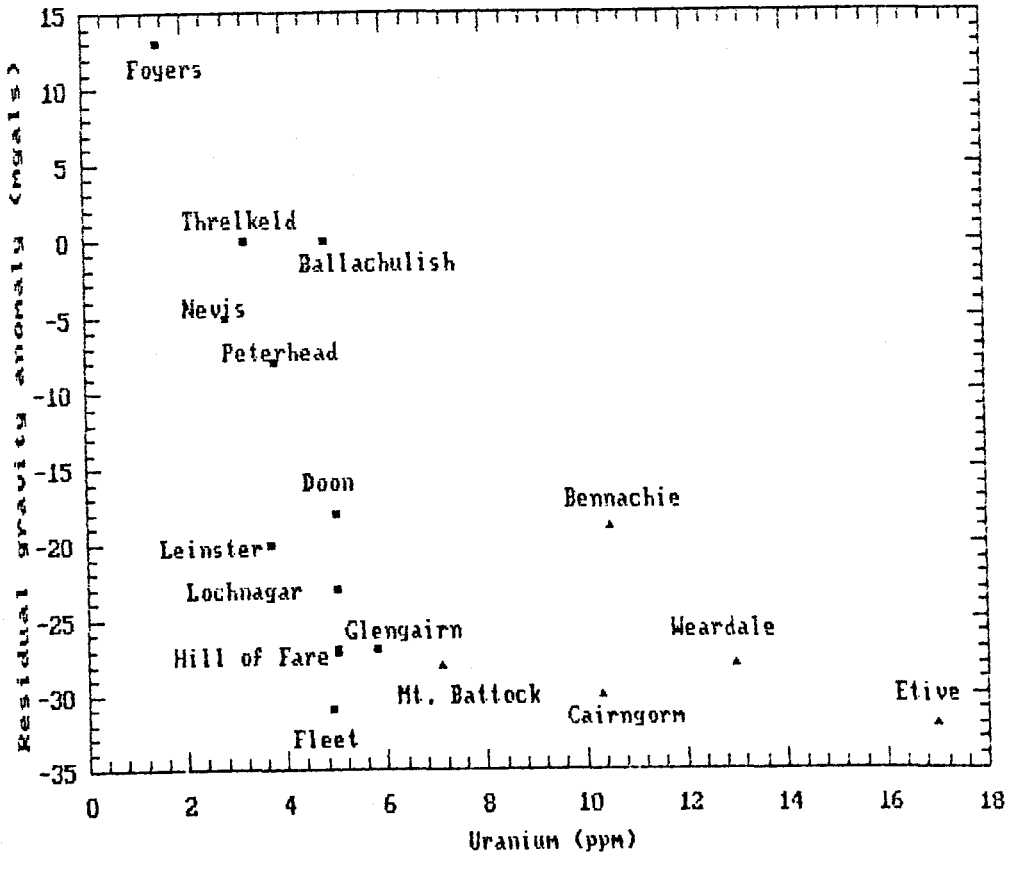

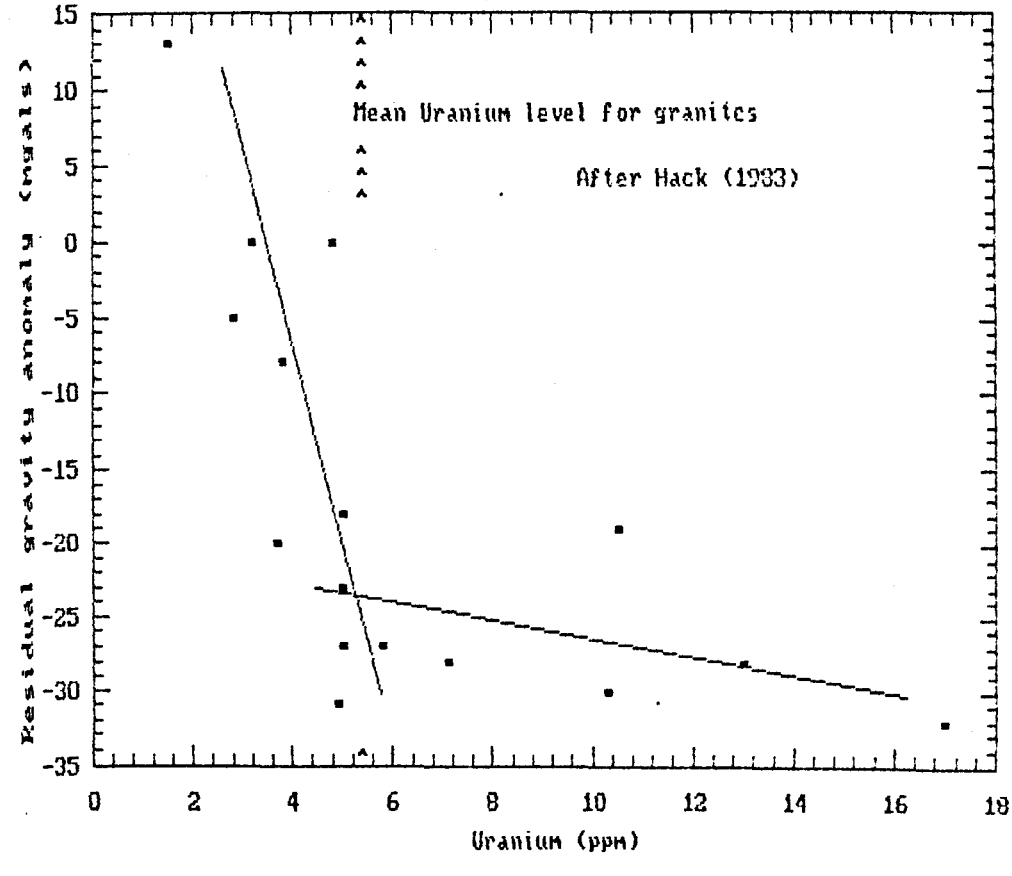

Figure 5.3.a

The aeromagnetic profile across Northern England and the Southern Uplands

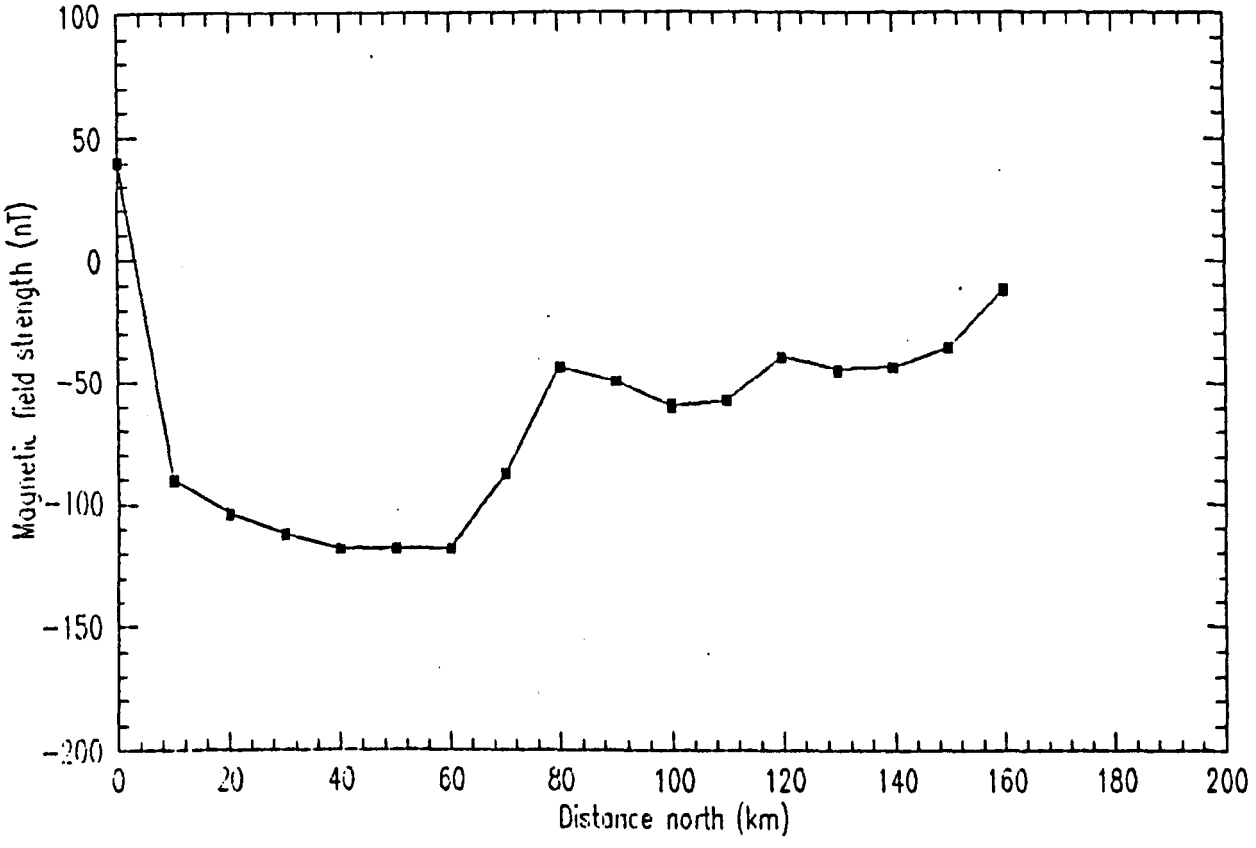

Figure 5.3.b

A slab model for the aeromagnetic profile across Northern England and the Southern Uplands

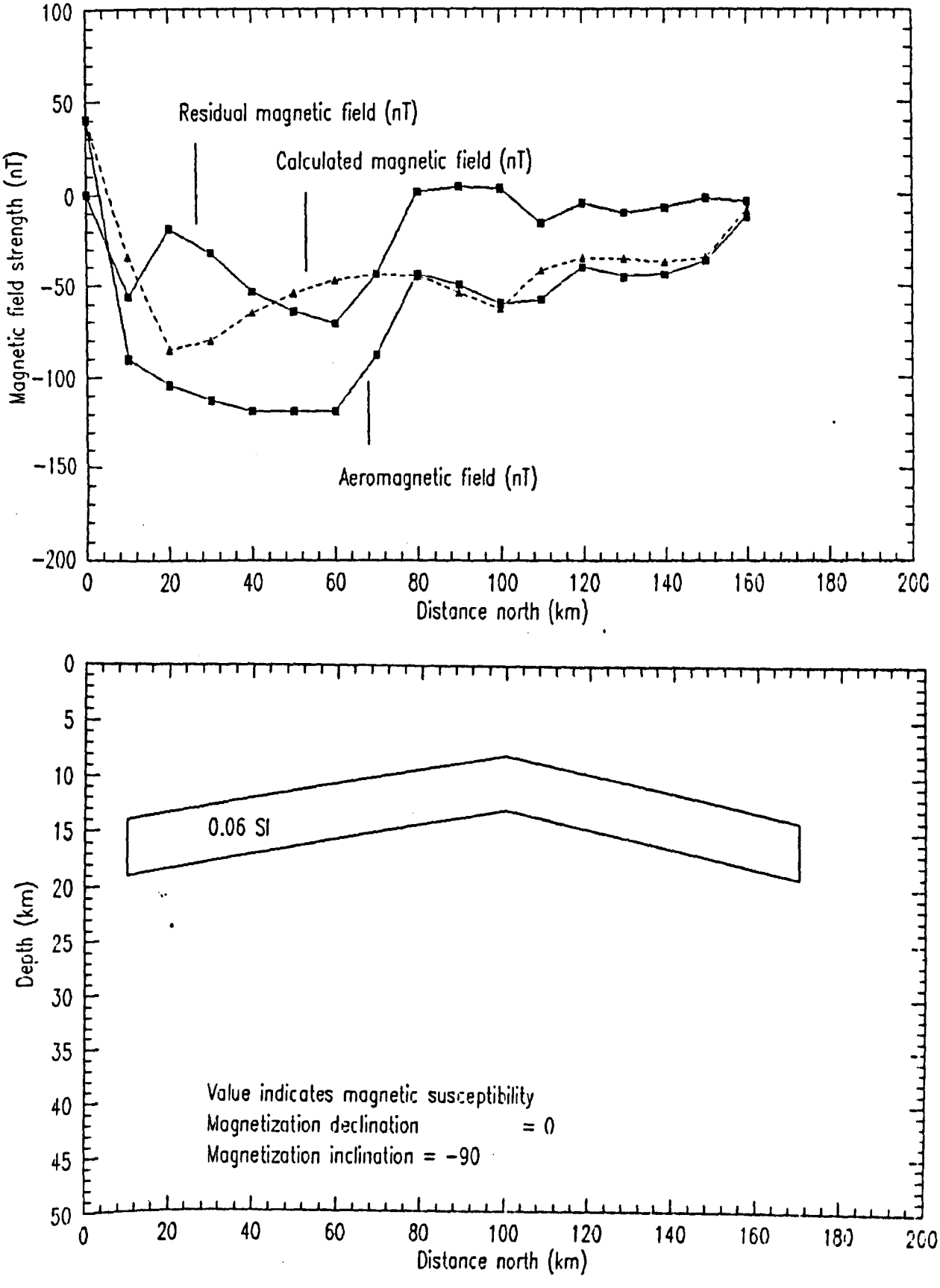

Figure 5.3.c

A slab model for the aeromagnetic profile across Northern England and the Southern Uplands

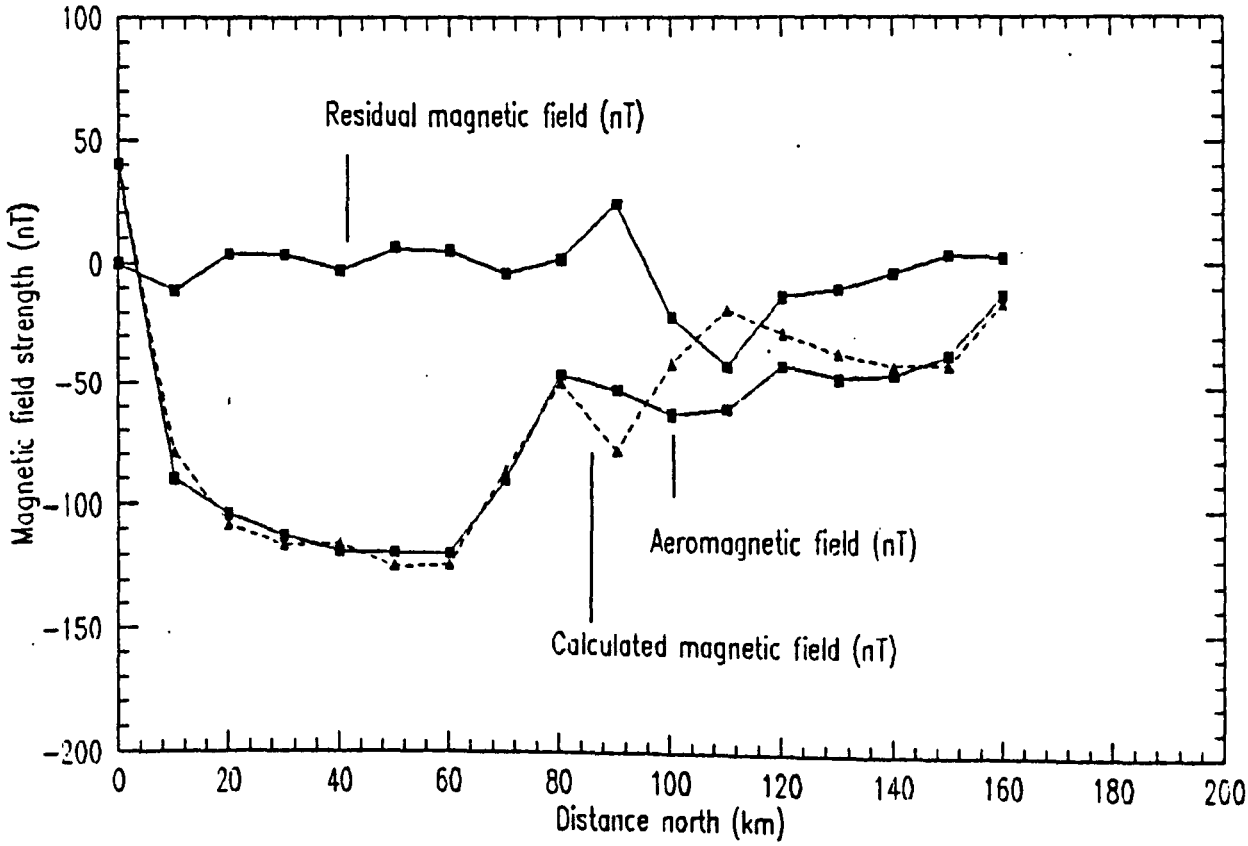

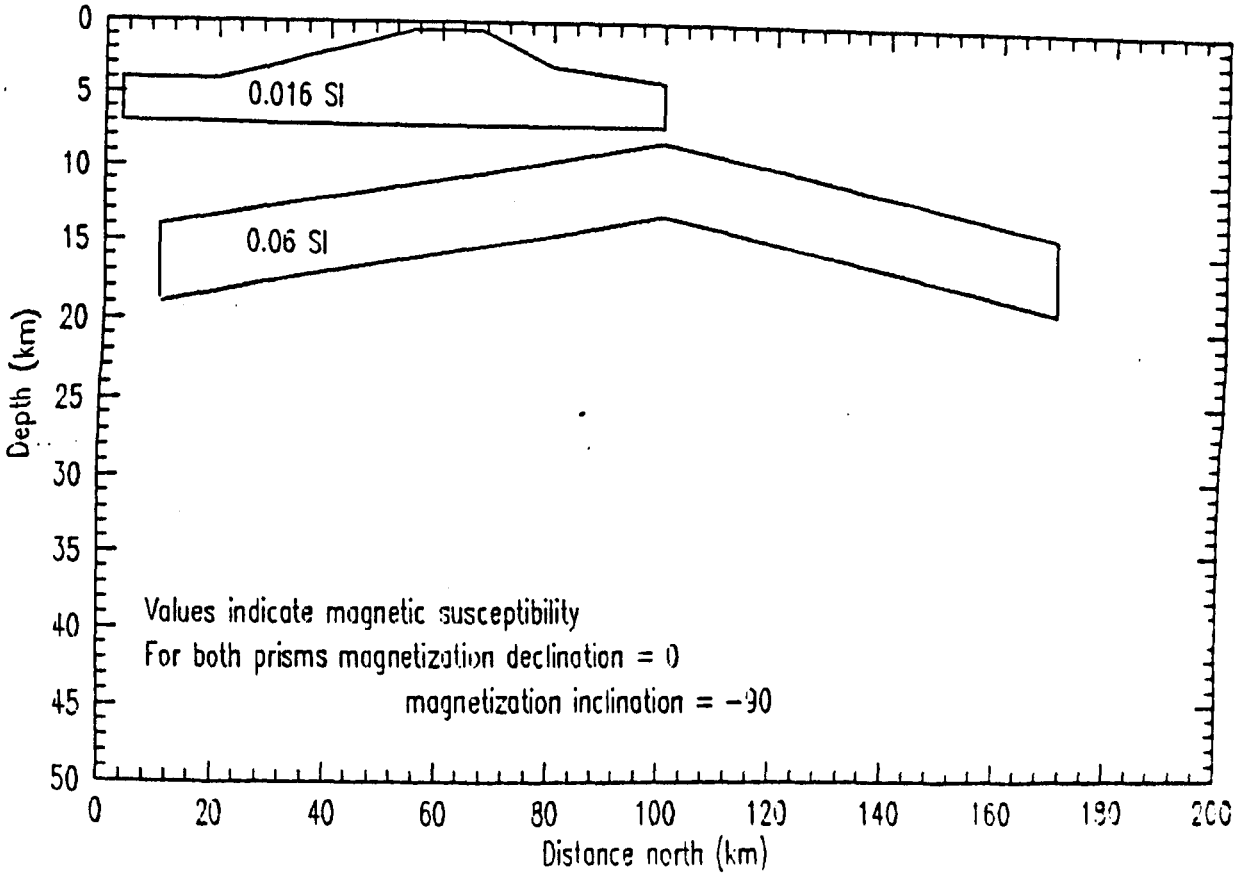

Figure 5.3.d

A model of the electrical resistivity across Northern England and the Southern Uplands

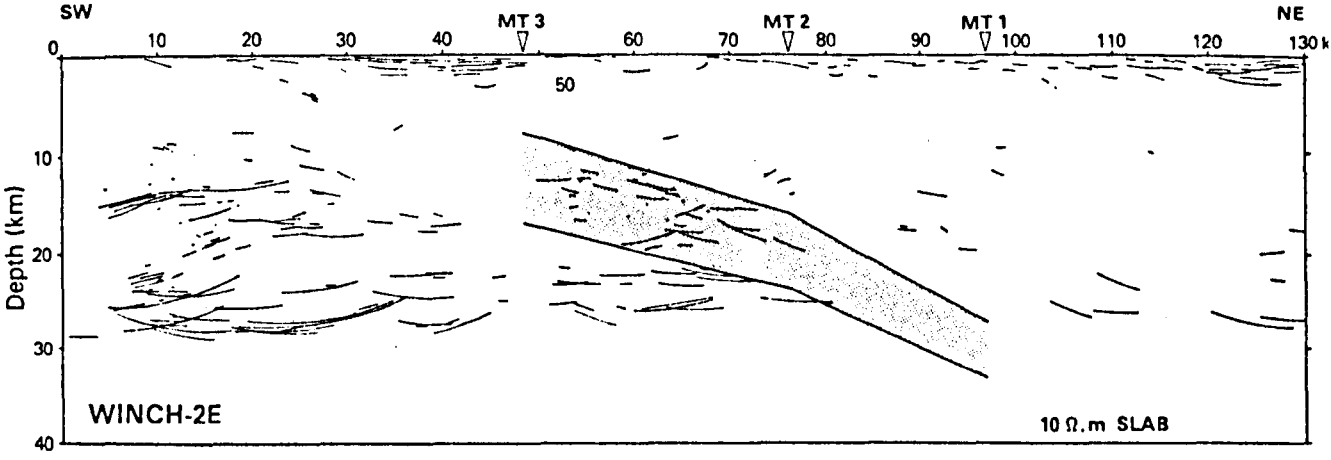

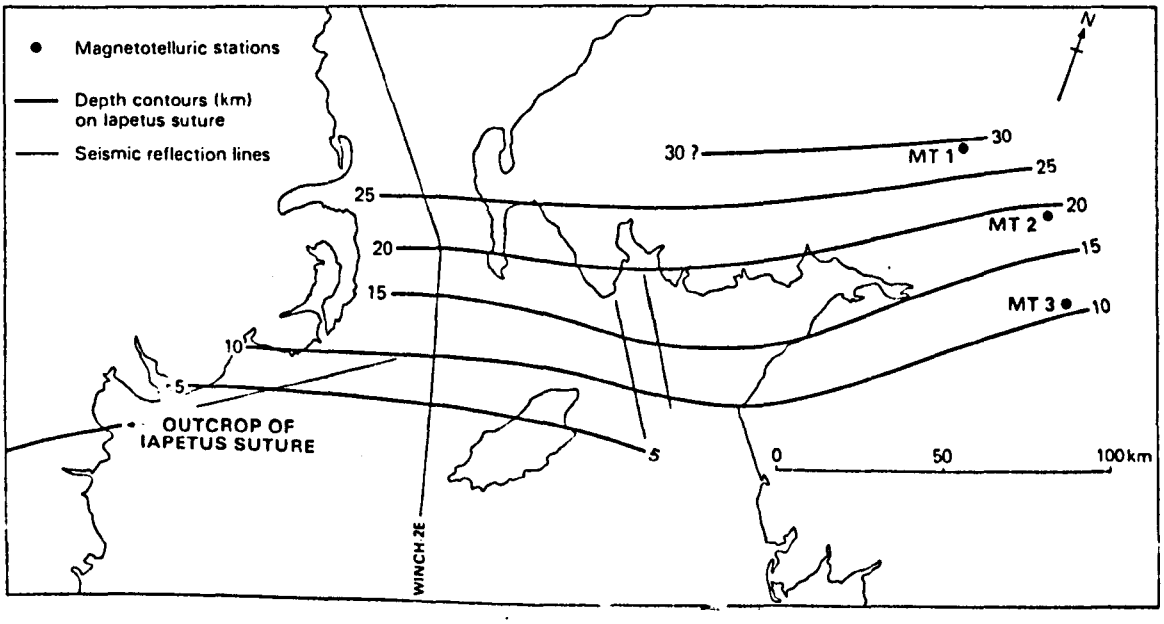

a) Electrical H^+ layer model of the 10Ω m resistivity is shown as a stippled area

b) Depth contours resulting from correlation of the seismic and electrical surfaces

After Beamish and Smythe (1986)

Figure 5.3.e

A plot of mean potassium levels against position on a profile across Northern England and the Southern Uplands

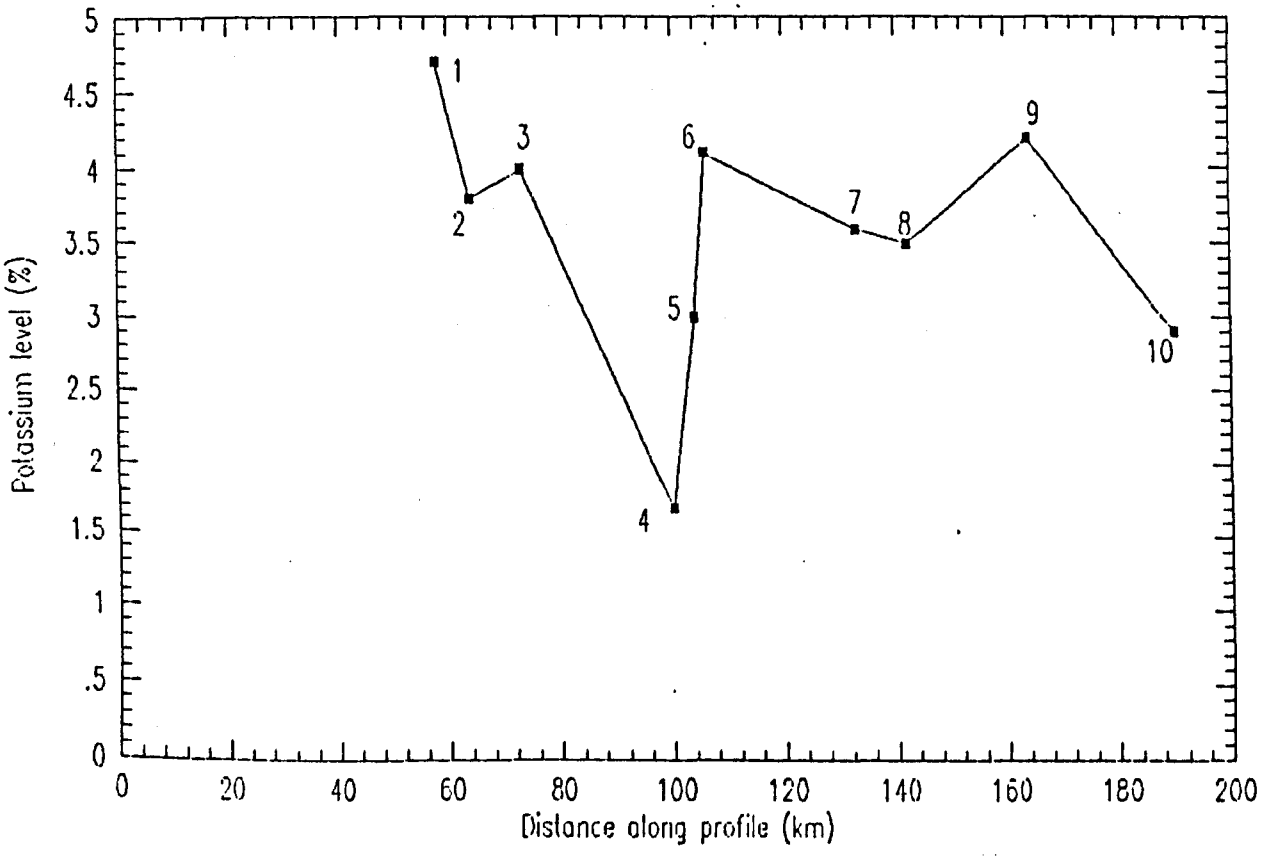

Key to granites along profile

1 Wensleydale
2 Shap
3 Eskdale
4 Ennerdale
5 Skiddaw
6 Weardale
7 Cheviot
8 Criffel
9 Fleet
10 Loch Doon